



National Library  
of Canada

Bibliothèque nationale  
du Canada

Canadian Theses Service

Service des thèses canadiennes

Ottawa, Canada  
K1A 0N4

## NOTICE

The quality of this microform is heavily dependent upon the quality of the original thesis submitted for microfilming. Every effort has been made to ensure the highest quality of reproduction possible.

If pages are missing, contact the university which granted the degree.

Some pages may have indistinct print especially if the original pages were typed with a poor typewriter ribbon or if the university sent us an inferior photocopy.

Previously copyrighted materials (journal articles, published tests, etc.) are not filmed.

Reproduction in full or in part of this microform is governed by the Canadian Copyright Act, R.S.C. 1970, c. C-30.

## AVIS

La qualité de cette microforme dépend grandement de la qualité de la thèse soumise au microfilmage. Nous avons tout fait pour assurer une qualité supérieure de reproduction.

Si manque des pages, veuillez communiquer avec l'université qui a conféré le grade.

La qualité d'impression de certaines pages peut laisser à désirer, surtout si les pages originales ont été dactylographiées à l'aide d'un ruban usé ou si l'université nous a fait parvenir une photocopie de qualité inférieure.

Les documents qui font déjà l'objet d'un droit d'auteur (articles de revue, tests publiés, etc.) ne sont pas microfilmés.

La reproduction, même partielle, de cette microforme est soumise à la Loi canadienne sur le droit d'auteur, SRC 1970, c. C-30.

THE UNIVERSITY OF ALBERTA

DIAGENESIS AND POREWATER EVOLUTION IN CRETACEOUS  
SEDIMENTARY ROCKS OF THE ALBERTA DEEP BASIN

by



Barbara J. Tilley

A THESIS


SUBMITTED TO THE FACULTY OF GRADUATE STUDIES AND RESEARCH IN PARTIAL  
FULFILMENT OF THE REQUIREMENTS FOR THE DEGREE

OF Doctor of Philosophy

Department of Geology

EDMONTON, ALBERTA

Spring, 1988



Permission has been granted to the National Library of Canada to microfilm this thesis and to lend or sell copies of the film.

The author (copyright owner) has reserved other publication rights, and neither the thesis nor extensive extracts from it may be printed or otherwise reproduced without his/her written permission.

L'autorisation a été accordée à la Bibliothèque nationale du Canada de microfilmer cette thèse et de prêter ou de vendre des exemplaires du film.

L'auteur (titulaire du droit d'auteur) se réserve les autres droits de publication; ni la thèse ni de longs extraits de celle-ci ne doivent être imprimés ou autrement reproduits sans son autorisation écrite.

ISBN 0-315-42846-5

THE UNIVERSITY OF ALBERTA

RELEASE FORM

NAME OF AUTHOR: Barbara J. Tilley

TITLE OF THESIS: Diagenesis and Porewater Evolution in Cretaceous Sedimentary  
Rocks of the Alberta Deep Basin.

DEGREE: Doctor of Philosophy

YEAR THIS DEGREE GRANTED: Spring, 1988

Permission is hereby granted to THE UNIVERSITY OF ALBERTA LIBRARY to reproduce single copies of this thesis and to lend or sell such copies for private, scholarly or scientific purposes only.

The author reserves other publication rights, and neither the thesis nor extensive extracts from it may be printed or otherwise reproduced without the author's written permission.

*Barbara J. Tilley*  
.....

University of Alberta

Department of Geology

Edmonton, Alberta

Date: *Feb 7 1988*  
.....

THE UNIVERSITY OF ALBERTA  
FACULTY OF GRADUATE STUDIES AND RESEARCH

The undersigned certify that they have read, and recommend to the Faculty of Graduate Studies and Research, for acceptance, a thesis entitled "Diagenesis and Porewater Evolution in Cretaceous Sedimentary Rocks of the Alberta Deep Basin" submitted by Barbara J. Tilley in partial fulfilment of the requirements for the degree of Doctor of Philosophy.

*Fred J. Longstaffe*  
.....  
Supervisor

*J. F. Leubeke*  
.....  
*A. Boudsgaard*  
.....  
*Kenneth W. Stewart*  
.....  
*Norman J. Dostal*  
.....

*James C. Lee*  
.....  
External Examiner

Date *January 25, 1988*

## DEDICATION

To my husband, Bruce, for his constant love, support and encouragement throughout the  
duration of this project

## ABSTRACT

The Alberta Deep Basin is the westernmost part of the Western Canadian Basin where the sedimentary section thickens towards the Cordillera. Almost the entire Mesozoic section is gas-saturated and consists of Cretaceous conglomerates, sandstones and shales, and Triassic and Permian carbonates, evaporites, and clastic rocks. Three major stages of diagenesis and porewater evolution in Cretaceous clastic rocks of the Deep Basin correspond to three different flow regimes which were controlled by geological events and maturation of organic matter. During burial in a flow regime driven by compaction and diagenetic reactions, early diagenetic hematite, siderite and chlorite were followed by later stages of chlorite, kaolinite, quartz and illite precipitation, dissolution of K-feldspar and carbonate cements, and albitization of feldspars. In most Cretaceous units, early porewaters ( $\delta^{18}\text{O}$  values = -12 to -7 ‰ SMOW) evolved to waters with  $\delta^{18}\text{O}$  values  $\pm$  3 ‰. Infiltration of saline fluids from pre-Cretaceous rocks may have produced more saline and  $^{18}\text{O}$ -rich porewaters in the Cadomin Formation.

During late stages of the Eocene Laramide Orogeny, burial depths in the Western Canadian Basin and hydraulic potentials were at their maximum. Gravity-driven meteoric water penetrated to depths where temperatures were  $>190^\circ\text{C}$ , then moved updip to the east along permeable pathways. Emplacement of these hot fluids into cooler updip rocks created a local thermal anomaly. Fluid inclusion and stable isotope analyses of quartz druse precipitated by the hot fluids, and of diagenetic dickite, ankerite and calcite precipitated during uplift, indicate the involvement of a significant fraction of meteoric water during the formation of these phases.

Subsequently, saturation of the western part of the Deep Basin by gas resulted in the interruption of both diagenesis and recharge by meteoric water originating in the west. Solutes in porewaters to the east of the gas-saturated zone were redistributed between the fluids in the various rock units. Gravity-driven meteoric fluids were redirected around the gas-saturated barrier and entered the eastern part of the Deep Basin where they mixed with older saline porewaters.

## ACKNOWLEDGEMENTS

Support by the staff of Canadian Hunter Exploration Limited was invaluable to the progress of this study. Their support included research grants, sampling permission, thin section preparation, drafting services and access to internal technical reports and maps. I would especially like to thank Bob Gies for freely discussing his observations on diagenetic features in the Deep Basin, his direction towards various Canadian Hunter resources, and his general support and interest in the project. Dr. Richard Wyman, Dr. Ray Rahmani, Howard King, Dennis Woofter and Janelle Davidson all provided information and suggestions at various stages of the project. The staff at the Grande Prairie office were particularly helpful during a visit to obtain water samples. I am also indebted to Alberta Research Council for financial support, preparation of some of the thin sections and clay mineral separations, and to Petro Canada for a research grant.

I would like to thank Dr. Fred Longstaffe for helping to ensure the high quality of the isotope data, for supervising the project and for his general support and encouragement throughout the course of the study. Drs. Fred Longstaffe, Bruce Nesbitt, and members of the supervisory committee, in particular Drs. Jim Boles and Frank Schwartz, are acknowledged for their advise and constructive criticism of various versions of the manuscript. I am especially grateful to Dr. Bruce Nesbitt for suggesting the use of fluid inclusions, helping to interpret the results and for many useful discussions.

The following people are gratefully acknowledged for their technical support: Diane Caird performed the stable isotope analyses on silicate minerals and generally kept the lab running; Bernice Young helped with the collection and preservation of water samples, and Jerry Cone and Maire Jones at Canadian Hunter did some of the drafting. Much of the drafting was done by the drafting department at Oak Ridge National Laboratory.



I wish to express my appreciation to the following people who helped at various stages of the project and to all others who helped in any way: Dr. George Beguri for use of his Raman spectroscopy equipment and his help in analysing the samples, Drs. Steve Haase, Ed Drummond, Gary Jacobs, Karen Von Damm and Dave Wyslowski for their support and advice during my stay at Oak Ridge National Laboratory, Dr. Bill Gunter for his support in the collection of water samples and for providing the chemical analyses of the water samples, Dr. Avner Ayalon for his help in setting up many of the mineral separation procedures used in this project, Dr. Jim Murowchick for his help with the fluid inclusion analyses, and Joanne Thompson for discussing her work on the present hydrogeology in the Deep Basin area.



3. DIAGÉNESIS AND ISOTOPIC EVOLUTION OF POREWATERS IN THE LOWER  
CRETACEOUS FALHER MEMBER AND CADOMIN FORMATION, ALBERTA

DEEP BASIN\_50.

INTRODUCTION	50.
DEPOSITIONAL SETTING	52.
ANALYTICAL TECHNIQUES	55.
X-ray Diffraction	55.
Isotopic Analyses	56.
Mineral Separation	57.
Carbonate Minerals	58.
Silicate Minerals	59.
2. PETROGRAPHIC AND ISOTOPIC RESULTS	60.
Detrital Minerals	60.
Diagenetic Minerals	61.
Hematite	61.
Siderite	61.
Chlorite	67.
Dolomite	71.
Pyrite	71.
Feldspar Diagenesis	71.
Illite	74.
Quartz	74.
Bitumen	75.
Kaolinite	78.
Ankerite	78.
Calcite	79.
Paragenic Sequence - Summary	80.



Fracture-Filling Diagenetic Minerals	135.
CONSTRAINTS ON POREWATER EVOLUTION	138.
CARBON-ISOTOPE COMPOSITIONS	146.
DISSOLUTION OF CARBONATE CEMENTS	148.
CROSS-FORMATIONAL FLOW	149.
CONTROLS ON DIAGENETIC PROCESSES	151.
CONCLUSIONS	153.
REFERENCES	155.
5. CHEMISTRY AND HYDROGEOLOGY OF MODERN FORMATION WATERS IN	
THE ALBERTA DEEP BASIN	157.
INTRODUCTION	157.
CHEMISTRY OF FORMATION WATERS	158.
Stable Isotope Compositions	165.
Systematic Trends in Major Ion Compositions	165.
PRESENT HYDROGEOLOGY	170.
DISCUSSION	182.
CONCLUSION	184.
REFERENCES	185.
6. GENERAL DISCUSSION AND CONCLUSIONS	186.
A MODEL FOR DIAGENESIS AND POREWATER EVOLUTION IN THE	
ALBERTA DEEP-BASIN	186.
Stage 1. Deposition and Burial	186.
Stage 2. Gravity-Driven Flow	195.
Stage 3. Redirection of Gravity-Driven Flow	196.
Difficulties with the Hydrogeological Model and Suggestions for	

Future Work .....	198
CONTROLS ON DIAGENETIC PROCESSES .....	199
MAJOR CONCLUSIONS .....	202
REFERENCES .....	204

## LIST OF TABLES

TABLE	DESCRIPTION	PAGE
2 1	Results for fluid inclusions from quartz druse.....	22
2 2	Results for fluid inclusions from calcite cement.....	23
3 1	Diagenetic phases in the Falher Member.....	62
3 2	Isotope data for the Falher Member.....	68
3 3	Isotope data for the Cadomin Formation.....	70
4 1	Isotope results for siderite.....	120
4 2	Isotope results for calcite.....	121
4 3	Isotope results for dolomite.....	125
4 4	Isotope results for authigenic quartz.....	126
4 5	Isotope results for kaolinite.....	130
4 6	Isotope results for illite.....	131
4 7	Isotope results for ankerite.....	136
4 8	Comparison of isotope values for fracture-fill and sandstone cements.....	137
5.1	X-ray diffraction data.....	160
5 2	Detailed water analyses.....	163
5.3	Mineral saturation states.....	164

## LIST OF FIGURES

FIGURE	PAGE
1 1 Location of study area.....	2
1 2 Stratigraphic section and geophysical logs for a representative well in the Alberta Deep Basin.....	4
1 3 West to east cross-section through the Western Canadian Basin showing stratigraphic nomenclature for the Alberta Deep Basin.....	5
2 1 Location of study area.....	10
2 2 West to east cross-section through the Alberta Basin showing stratigraphic nomenclature for the Deep Basin.....	11
2 3 Stratigraphic section and geophysical logs for a representative well in the Alberta Deep Basin.....	13
2 4 Thin section photomicrographs of prismatic quartz crystals and calcite cement.....	15
2 5 Geographic distribution of homogenization temperatures (°C) for fluid inclusions.....	16
2 6 Thin section photomicrographs of fluid inclusions.....	21
2 7 Raman spectra of methane in quartz druse inclusions.....	26
2 8 Data points and contours for vitrinite reflectance (Ro%) of Falher coals.....	31
2 9 Geographic distribution of maximum burial temperatures for the Falher, calculated using the Lopatin (1971)-Waples (1980) method.....	33
2 10 Geographic comparison of fluid inclusion temperatures (°C) and calculated maximum burial temperatures.....	36
2 11 Temperature versus distance plot of fluid inclusion temperatures along the line A-A' in Figure 2.10.....	37
3 1 Location of study area.....	51
3 2 Southwest to northeast cross-section extending from 93-I-15 in British Columbia to Township 74 Range 25 W5 in Alberta, through Lower Cretaceous units of the Deep	



Basin.....	53
3 3 Thin section and SEM photomicrographs of diagenetic textures in the Falher Member	65
3 4 Geographic distribution of Falher and Cadomin samples.....	66
3 5 Back-scatter electron and SEM photomicrographs showing textural relationships in the Falher Member and Cadomin Formation.....	73
3 6 Thin section and SEM photomicrographs showing textural relationships of late diagenetic phases in the Falher Member.....	77
3 7 General diagenetic sequences for the Falher Member and the Cadomin Formation.....	81
3 8 $\delta^{18}\text{O}$ of porewater versus temperature for diagenetic quartz and calcite from Falher conglomerates.....	83
3 9 Idealized porewater evolution path ( $\delta^{18}\text{O}$ of water versus temperature) for late-stage diagenesis in Falher conglomerates.....	83
3 10 Idealized porewater evolution path ( $\delta^{18}\text{O}$ of water versus temperature) for late-stage diagenesis in Falher conglomerates showing the range in conditions under which calcite precipitated.....	86
3 11 $\delta^{18}\text{O}$ of porewater versus temperature for diagenetic siderite and chlorite from Falher and Cadotte Members.....	88
3 12 Idealized porewater evolution path ( $\delta^{18}\text{O}$ of water versus temperature) for Falher conglomerates.....	91
3 13 $\delta^{18}\text{O}$ of porewater versus temperature for diagenetic minerals from Falher sandstones.....	93
3 14 Idealized porewater evolution paths ( $\delta^{18}\text{O}$ of water versus temperature) for Falher sandstones.....	93
3 15 $\delta^{18}\text{O}$ of porewater versus temperature for diagenetic minerals from the Cadomin Formation.....	95
3 16 Idealized porewater evolution path ( $\delta^{18}\text{O}$ of water versus temperature) for the Cadomin Formation.....	95
3 17 $\delta\text{D}$ versus $\delta^{18}\text{O}$ for Falher and Cadomin late-stage dickite.....	98

3.18	Idealized porewater evolution path ( $\delta^{18}\text{O}$ of porewater versus time) for Father and Cadomin sandstones and conglomerates.	101
4.1	Location of study area.	110
4.2	West to east cross-section through the Alberta Basin showing stratigraphic nomenclature for the Deep Basin.	111
4.3	Location of samples.	112
4.4	Generalized diagenetic sequences for each unit examined.	115
4.5	Thin section and SEM photomicrographs of textural relationships in the Cardium Formation.	118
4.6	Thin section and SEM photomicrographs of textural relationships in the Cardium, Paddy, and Bluesky Formations.	123
4.7	SEM photomicrographs of textural relationships in the Cardium, Paddy and Bluesky Formations.	129
4.8	Thin section photomicrographs of diagenetic textures in the Paddy Member and Bluesky Formation.	134
4.9a	$\delta^{18}\text{O}$ of porewater versus temperature for diagenetic minerals from the Cardium Formation.	139
4.9b	Idealized porewater evolution paths ( $\delta^{18}\text{O}$ of water versus temperature) for Cardium sandstones.	139
4.10a	$\delta^{18}\text{O}$ of porewater versus temperature for diagenetic minerals from the Paddy Member of the Peace River Formation.	140
4.10b	Idealized porewater evolution paths ( $\delta^{18}\text{O}$ of water versus temperature) for Paddy sandstones.	140
4.11a	$\delta^{18}\text{O}$ of porewater versus temperature for diagenetic minerals from the Bluesky Formation.	141
4.11b	Idealized porewater evolution paths ( $\delta^{18}\text{O}$ of water versus temperature) for Bluesky sandstones.	141

4.12	$\delta^{18}\text{O}$ of porewater versus temperature for diagenetic minerals from the Halfway and Belloy Formations.	145.
4.13	$\delta^{13}\text{C}$ versus $\delta^{18}\text{O}$ diagram for carbonate cements from the Alberta Deep Basin.	147.
5.1	West to east cross-section through the Alberta Basin showing stratigraphic nomenclature for the Deep Basin.	159.
5.2	Na+K/Cl versus Cl diagram.	167.
5.3	Na/Cl versus Cl diagram.	167.
5.4	Ca/Na versus Cl diagram.	168.
5.5	Ca/Cl versus Cl diagram.	168.
5.6	Mg/Cl versus Cl diagram.	169.
5.7	Ca/Mg versus Cl diagram.	169.
5.8	Geographic variation in chlorinities of Bluesky, Gething and Cadomin formation waters.	171.
5.9	Geographic variation in chlorinities of Triassic, Permian and Upper Devonian formation waters.	172.
5.10	Geographic variation in Na/Cl ratios of formation waters.	173.
5.11	Geographic variation in Ca/Na ratios of formation waters.	174.
5.12	Geographic variation in Ca/Cl ratios.	175.
5.13	Geographic variation in Mg/Cl ratios.	176.
5.14	Contours of the geographic variation in chloride content of Lower Cretaceous formation waters.	177.
5.15	Topographic map for the study area (box) and surrounding area.	179.
5.16	Map of potentiometric surface data (feet above sea level).	180.
6.1	Schematic cross-section showing fluid flow resulting from compaction during burial.	188.
6.2	Schematic cross-section showing fluid flow following maximum burial.	191.
6.3	Schematic cross-section showing fluid flow during uplift after gas saturation.	193.

## CHAPTER 1. INTRODUCTION

The Alberta Deep Basin and its extension into British Columbia (Figure 1.1) is the part of the Western Canadian Sedimentary Basin where the Mesozoic section thickens toward the Cordillera. The area is of economic interest because of large gas reserves which encompass almost the entire Mesozoic clastic section which reaches a maximum thickness of 4570 m. An understanding of diagenesis in the area is essential to the development of gas from the tightly cemented sandstones and locally permeable conglomerates.

Many of our concepts of clastic diagenesis are based on the Gulf Coast Basin of the United States. For example, the following reactions occur in sediments and sedimentary rocks of the Gulf Coast Basin as the depth of burial increases: (1) the transformation of smectitic layers in illite/smectite to illite (Perry and Hower, 1970; Hower et al., 1976; Boles and Franks, 1979); (2) the albitization of plagioclase (Boles, 1982); and (3) the progressive enrichment of Mg and Fe in carbonate cements (Boles, 1979). Smectite, K-feldspar, kaolinite and mica gradually decrease in abundance with depth, whereas illite, quartz, and chlorite increase with depth. The Gulf Coast Basin, however, represents only one type of sedimentary basin, i.e., a basin of low topographic relief, active burial and upward migration of connate and diagenetic fluids.

Because the hydrogeological setting of the Western Canadian Basin differs significantly from that of the Gulf Coast Basin, it cannot be assumed that diagenetic trends will duplicate those of the Gulf Coast Basin. The objective of this thesis is to evaluate the effect of the flow regime on the trends of clastic diagenesis and develop a geochemical model for the style of diagenesis and porewater evolution in the Deep Basin (Figure 1.1). The Western Canadian Basin is situated immediately to the east of the Cordillera mountain range, which provides sufficient hydraulic potential that meteoric water circulates through permeable units to depths on the order of at least 3000 m (Tóth, 1980). The large influx of meteoric water into the Western Canadian Basin

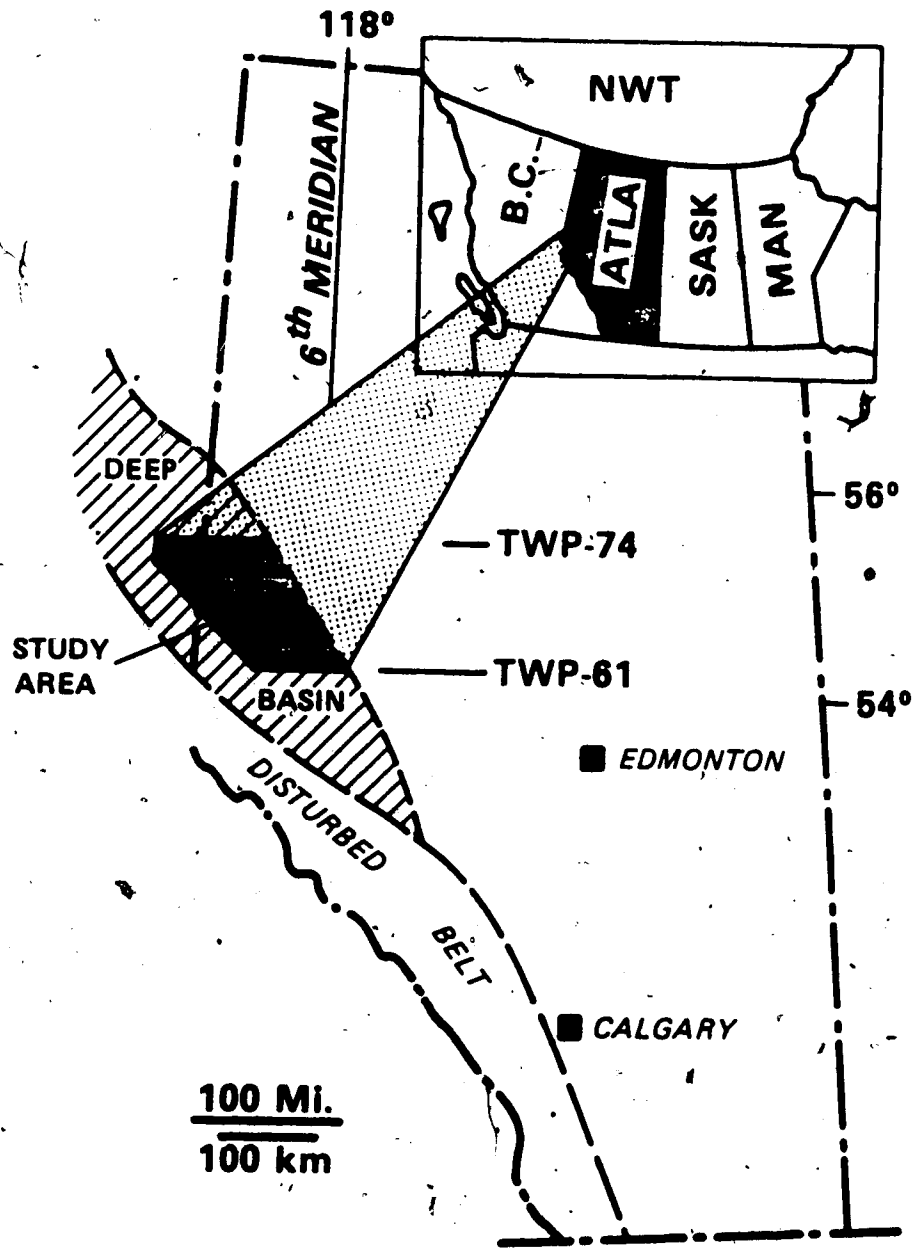


Figure 1.1 Location of study area.

significantly alters the evolution of formation waters by mixing with, and replacing earlier fluids (Clayton et al., 1966; Hitchon and Friedman, 1969). Such activity could notably affect many of the precipitation and dissolution reactions that occur in clastic rocks during diagenesis (Longstaffe, 1983). The zones of mixing may also control the location of diagenetically formed petroleum traps.

Longstaffe and Ayalon (in press) and Ayalon and Longstaffe (in press) studied diagenesis and porewater evolution in the Upper Cretaceous Belly River and the Lower Cretaceous Viking Formations in central to south-central Alberta. They concluded that meteoric water has been involved in diagenesis of both units since maximum burial and uplift (maximum relief) during or shortly after the Laramide Orogeny. This thesis aims to determine the chemical and isotopic evolution of the porewaters in a quite different part of the Western Canadian Sedimentary Basin, the Alberta Deep Basin. The Deep Basin of Alberta is of special interest because: (1) it represents a once deeply buried part of the Western Canadian Basin where maximum burial depths for Cretaceous sandstones and conglomerates (presently at depths of 2000 to 3000 m) were probably 4000 to 5000 m; (2) an understanding of diagenesis in this area is essential to the exploitation of the large gas reserves in porous conglomerates and tight sandstones; and (3) the relationship between diagenesis and the large scale production and trapping of methane gas needs to be more fully determined.

Diagenesis and porewater evolution in the Lower Cretaceous Falher Member of the Spirit River Formation, the Bluesky Formation and the Cadomin Formation (Figure 1.2) have been studied in most detail. Other units, including the Upper Cretaceous Cardium Formation, the Lower Cretaceous Paddy and Cadotte Members of the Peace River Formation, the Triassic Halfway Formation and the Permian Belloy Formation (Figure 1.3), were studied in a more cursory fashion to evaluate both vertical variations in diagenesis and the extent of cross-formational flow. Methods of study included thin section petrography, scanning electron microscopy, and electron

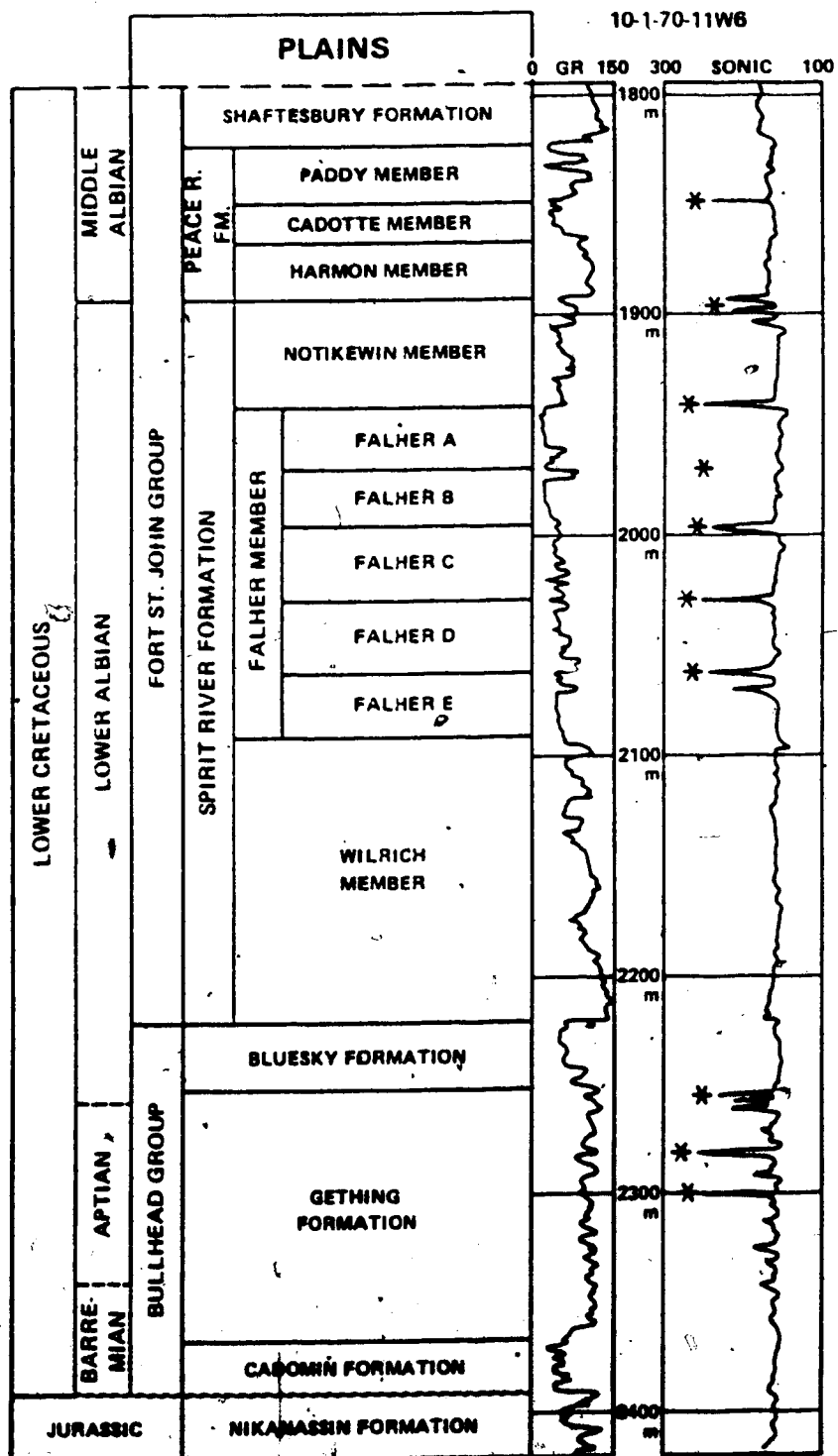
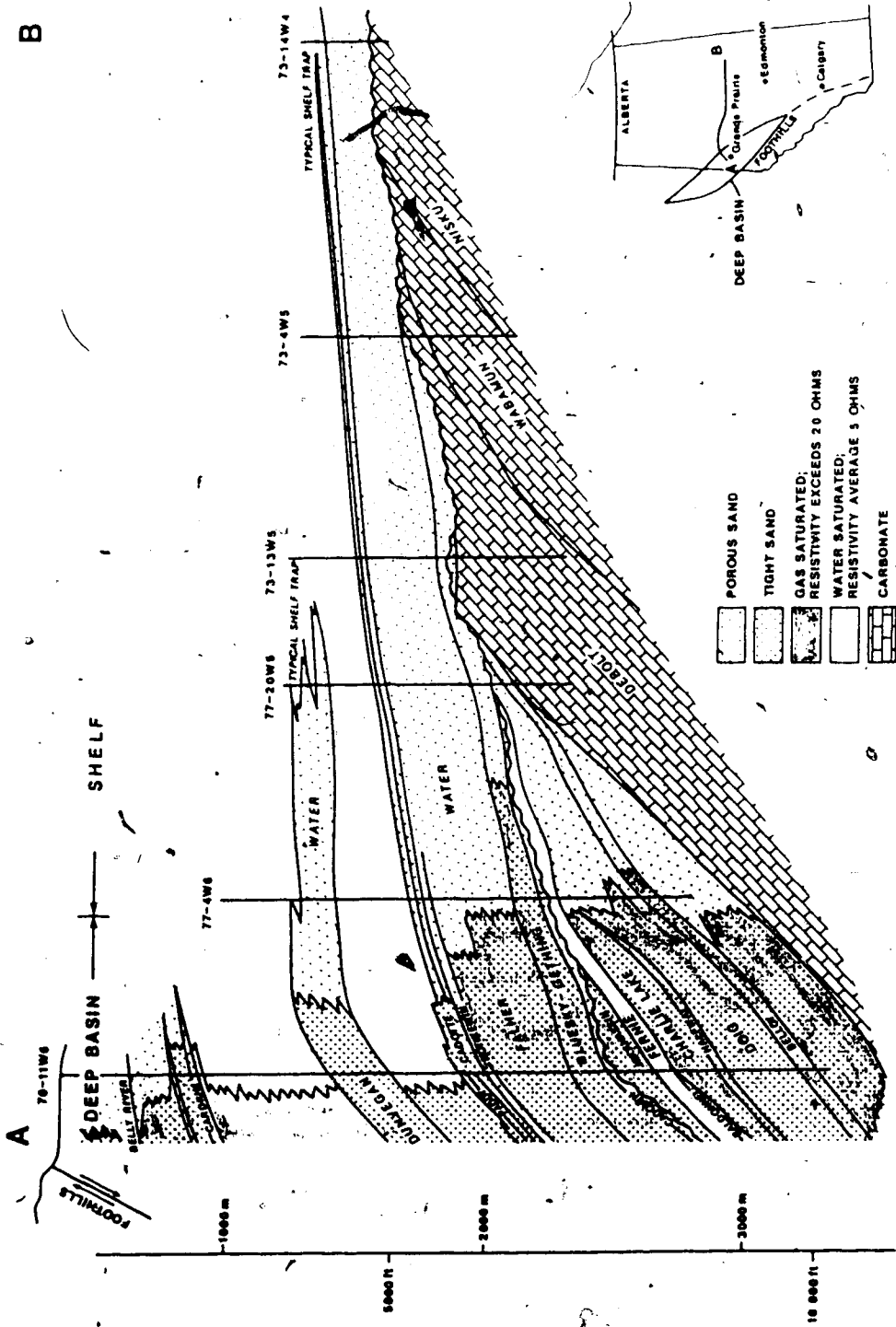


Figure 1.2 Stratigraphic section and geophysical logs for a representative well in the Alberta Deep Basin. Diagenesis and porewater evolution in the Lower Cretaceous Falher Member of the Spirit River Formation, the Bluesky Formation and the Cadomin Formation have been studied in most detail. GR-gamma ray. (modified from Smith et al., 1984).



**Figure 1.3** West to east cross-section through the Western Canadian Basin showing stratigraphic nomenclature for the Alberta Deep Basin. Almost the entire section in the western part of the Deep Basin is gas-saturated, whereas updip, to the east, the rocks are water-saturated. (modified from Masters, 1979).



microprobe, x-ray diffraction, stable isotope and fluid inclusion analyses. Chemical and isotopic compositions of existing formation waters were studied by combining information from detailed chemical and isotopic analyses of two formation waters collected for this study, with data available from the Energy Resources Conservation Board of Alberta.

The results of the thesis are presented in five sections:

Chapter 2 presents the results of fluid inclusion analyses and compares fluid inclusion temperatures with those calculated from vitrinite reflectance data using the method of Lopatin (1971) modified by Waples (1980). The comparison indicates that a thermal anomaly was present in part of the Deep Basin during maximum burial.

Chapter 3 presents results of petrographic and stable isotope analyses of the Falher and Cadomin sandstones and conglomerates. Fluid inclusion temperatures from Chapter 2 are combined with the diagenetic sequence and stable isotope data to identify temperature-dependent trends for the isotopic evolution of porewaters.

Chapter 4 examines the diagenetic sequence and porewater evolution in Cretaceous sandstones as well as Triassic and Permian sandstones with a view to understanding vertical variations in diagenetic processes in the Deep Basin.

Chapter 5 presents preliminary data on the chemistry and hydrogeology of modern formation waters in the Deep Basin. The intent of this chapter is to provide a starting point for future studies of modern hydrogeology in the study area.

Chapter 6 summarizes the results in a geochemical model for diagenesis and porewater evolution in the Alberta Deep Basin. Controls on diagenesis are examined by comparing diagenetic processes in the Alberta Deep Basin with those in the Gulf Coast Basin and Cretaceous formations of central Alberta.

REFERENCES

Ayalon, A., and Longstaffe, F.J., in press, Oxygen-isotope studies of diagenesis and porewater evolution in the western Canada sedimentary basin: evidence from the Upper Cretaceous basal Belly River sandstone: *Journal of Sedimentary Petrology*.

Boles, J.R., 1979, Active ankerite cementation in the subsurface Eocene of southwest Texas: *Contributions to Mineralogy and Petrology*, v.68, p. 13-22.

Boles, J.R., 1982, Active albittization of Gulf Coast Tertiary: *American Journal of Science*, v.282, p. 165-180.

Boles, J.R., and Franks, S.G., 1979, Clay diagenesis in Wilcox sandstones of southwest Texas: implications of smectite diagenesis on sandstone cementation: *Journal of Sedimentary Petrology*, v.49, p. 55-70.

Clayton, R.N., Friedman, I., Graf, D.L., Mayeda, T.K., Meents, W.F., and Shimp, N.F., 1966, The origin of saline formation waters: *Journal of Geophysical Research*, v.71, p. 3869-3882.

Hitchon, B. and Friedman, I., 1969, Geochemistry and origin of formation water in the western Canada sedimentary basin- I. Stable isotopes of hydrogen and oxygen: *Geochimica et Cosmochimica Acta*, v.33, p. 1321-1349.

Hower, J., Eslinger, E.V., Hower, M.E., and Perry, E.A., 1976, Mechanism of burial metamorphism of argillaceous sediments, 1, Mineralogical and chemical evidence: *Geological Society of America Bulletin*, v.87, p. 725-737.

Longstaffe, F.J., 1983, Diagenesis, IV. Stable isotope studies of diagenesis in clastic rocks: *Geoscience Canada*, v.10, p. 44-58.

Longstaffe, F.J., and Ayalon, A., in press, Oxygen-isotope studies of clastic diagenesis in the Lower Cretaceous Viking Formation, Alberta: implications for the role of meteoric water: in J.D. Marshall, ed., *The Diagenesis of Sedimentary Sequences: Geological Society Special Publication*.

Lopatin, N.V., 1971, Temperature and geologic time as factors in coalification (in Russian): *Akademiya Nauk SSSR Izvestiya, Seriya Geologicheskaya*, no. 3, p. 95-106.

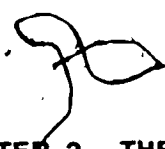
Masters, J.A., 1979, Deep Basin gas trap, Western Canada: *The American Association of Petroleum Geologists Bulletin*, v.63, p. 152-181.

Perry, E., and Hower, J., 1970, Burial diagenesis in Gulf Coast pelitic sediments: *Clays and Clay Minerals*, v.18, p. 165-177.

Smith, D.G., Zorn, C.E, and Sneider, R.M., 1984, The paleogeography of the Lower Cretaceous of western Alberta and northeastern British Columbia in and adjacent to the Deep Basin of the Elmworth area: in J.A. Masters, ed., *Elmworth Case Study of a Deep Basin Gas Field: AAPG Memoir 38*, p. 79-114.

Toth, J., 1980, Cross-formational gravity-flow of groundwater: A mechanism of the transport and accumulation of petroleum (the generalized hydraulic theory of petroleum migration): *AAPG Studies in Geology No. 10*, p. 121-167.

Waples, D., 1980, Time and temperature in-petroleum formation: Application of Lopatin's method to petroleum exploration: *The American Association of Petroleum Geologists Bulletin*, v.64, p. 916-926.

  
**CHAPTER 2. THERMAL HISTORY OF THE ALBERTA DEEP BASIN:**  
**A COMPARATIVE STUDY OF FLUID INCLUSION AND VITRINITE REFLECTANCE**  
**DATA**

**INTRODUCTION**

Locally high geothermal gradients are commonly present in oil and gas fields (Meyer and McGee, 1985), as well as Mississippi Valley-Type Pb-Zn deposits (MacQueen and Powell, 1983; White, 1968), and are believed to be produced by upward movement of high temperature basinal fluids into lower temperature sedimentary units (Meyer and McGee, 1985; Bethke, 1986; Garven, 1985; Smith and Chapman, 1983; Tóth, 1980; Roberts, 1980). In oil and gas fields, the anomalies are recognized by direct measurements of bottom-hole temperatures, although accurate temperature measurements are difficult to obtain (Ferti and Wichmann, 1976; LeBlanc et al., 1982), and even then, probably do not reflect the paleo-conditions which were responsible for diagenesis and the trapping of older oil and gas fields. In this study, local paleofluid temperatures and paleogeothermal gradients in the Alberta Deep Basin are examined by studying fluid inclusion and vitrinite reflectance data.

Organic maturity indicators such as vitrinite reflectance, thermal alteration index, and rock evaluation techniques are commonly used to determine the thermal history of sedimentary basins. More recently, stable isotope studies of diagenetic minerals have been used to trace the thermal history (Milliken et al., 1981; Longstaffe, 1983). The problem with these approaches is that they rely on accurate knowledge of the burial history, or the isotopic composition of paleo-porefluids, to indirectly determine paleotemperatures. In the case of maturity indicators, only the maximum temperature reached by the rock is recorded. In contrast, primary fluid inclusions in diagenetic minerals record the minimum temperature of the fluid which precipitated that mineral, and have potential for recording temperatures of mineral formation during cooling.

In this study, data from fluid inclusions in diagenetic quartz druse and calcite cements in Lower Cretaceous sandstones and conglomerates in the Alberta Deep Basin are used to determine minimum paleotemperatures of fluids during maximum burial and during later uplift. For comparison, maximum burial temperatures are also calculated from vitrinite reflectance data supplied by other workers (Weiss, 1985; Youn, 1983; Kalkreuth and McMechan, 1984) for the same units using the Lopatin-Waples method (Lopatin, 1971; Waples, 1980). The comparison shows that fluid inclusion temperatures for quartz druse are about 40°C higher than the calculated maximum burial temperature. The reliability of the Lopatin-Waples and other methods of translating thermal maturity to temperature data is considered in detail and deemed to be questionable. The analysis shows that fluids at higher temperatures than those suggested by maturity indicators may be common in sedimentary basins and that care should be taken in translating maturity data to paleotemperatures.

### Geological Background

Samples were collected from Lower Cretaceous conglomerates and sandstones from the Deep Basin of Alberta/British Columbia (Figure 2.1), the deepest portion of the Western Canadian Sedimentary Basin. Figure 2.2 shows a southwest to northeast cross-section through the basin. The Mesozoic section, which is 300 metres thick on the shelf in eastern Alberta, thickens westwards to over 4570 metres in the Deep Basin in front of the Foothills' overthrusts (Masters, 1979). Almost the entire western portion of the Deep Basin is gas-saturated, whereas updip, to the east, the rocks are water-saturated (Masters, 1979).

The Alberta Deep Basin is the westernmost part of a foreland basin, which formed in front of eastwardly migrating thrust sheets of the Canadian Cordillera. The eastward thrusting began in the Middle Jurassic in response to subduction and accretion of island arc terranes onto the

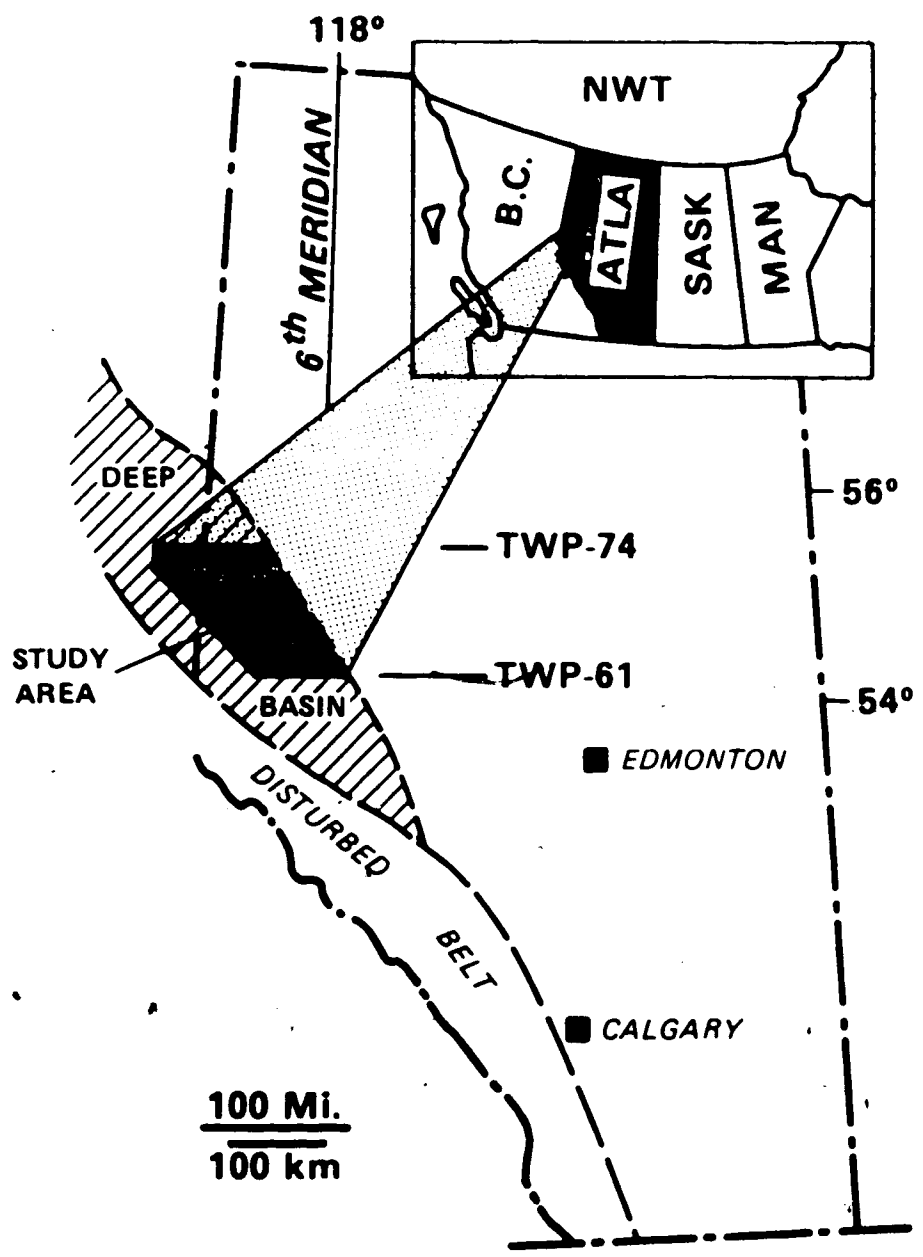


Figure 2.1 Location of study area.

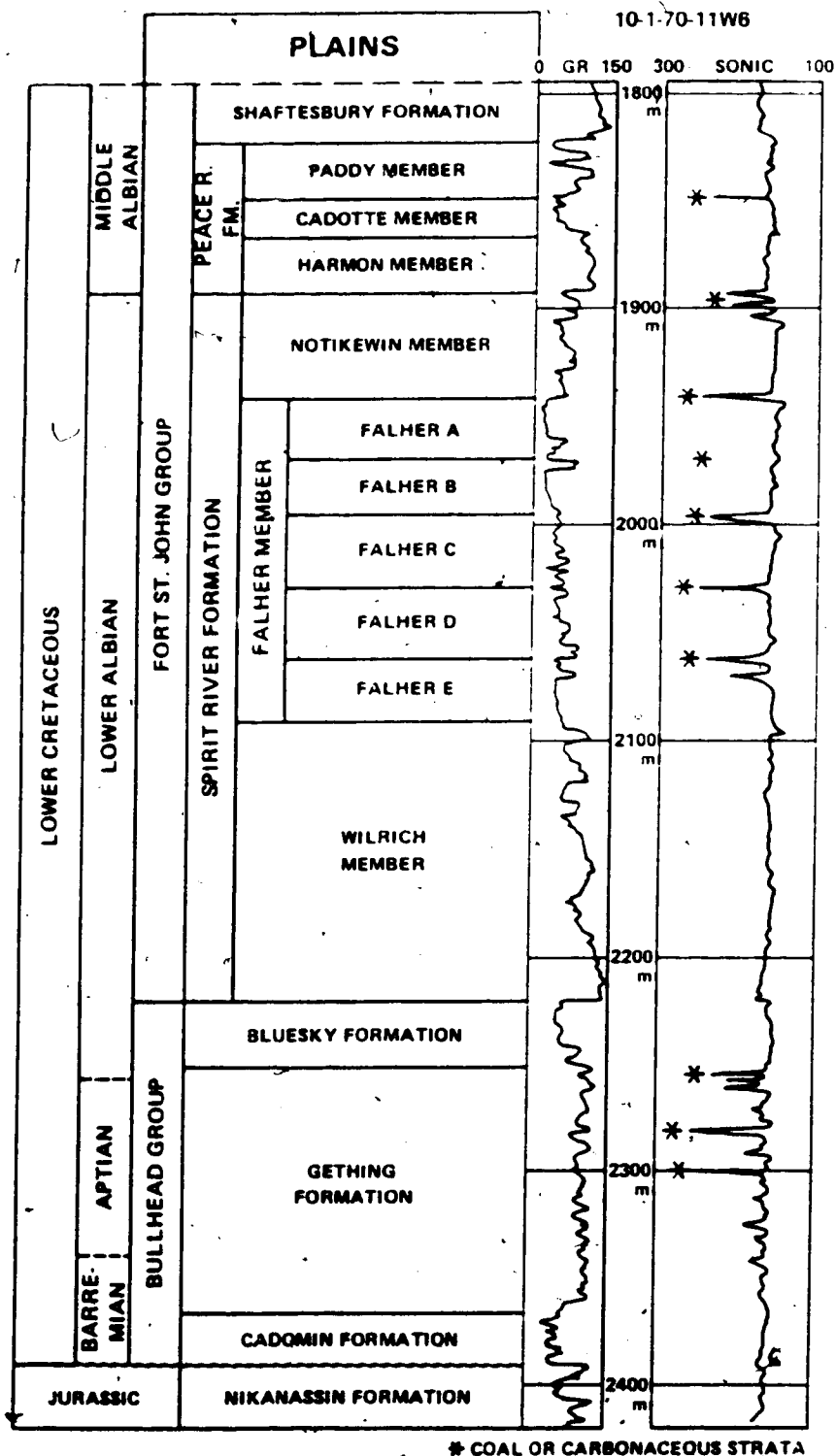


continental margin (Columbian Orogeny) (Porter et al., 1982; Monger, 1984). The emplacement of thrust sheets occurred periodically throughout the Cretaceous and resulted in the shedding of detritus eastward. Subsidence and sediment accumulation continued in the Deep Basin until the last stage of the Laramide Orogeny, which probably occurred during the Early Eocene. Maximum relief of the mountains immediately to the west of the basin and maximum burial depths within the basin occurred at this time. Uplift of the sedimentary basin and extensive erosion of the accumulated Tertiary and Upper Cretaceous rocks followed and continues at present (Beaumont, 1981; Taylor et al., 1964).

### Sample Description

Samples for this study were taken almost exclusively from the gas-saturated area. Fluid inclusions were analyzed from diagenetic quartz druse in the Cadotte Member of the Peace River Formation, the Falher Member of the Spirit River Formation, and the Bluesky and Cadomin Formations (Figure 2.3). Petrographic descriptions of these stratigraphic units in the study area are given in Chapters 3 and 4, and by Cant (1983), Cant and Ethier (1984), Gies (1984), Varley (1982), and Youn (1983).

The quartz druse occurs as prismatic crystals projecting into pore spaces of chert-pebble conglomerates (Figure 2.4a). Only those crystals that are easily visible macroscopically contain fluid inclusions that are sufficiently large for analysis. The largest and most abundant quartz druse occurs in the Cadotte and Falher conglomerates in the western portion of the study area as reflected in the geographic distribution of inclusion data (Figure 2.5). In the Cadomin Formation, quartz druse is rare, largely because in most samples, the large, open pore network, which would have provided space for quartz crystals, was filled by sandstone matrix. In the Cadotte Member, quartz druse occurs in three different settings: (1) within horizontal fractures in sandstones, (2) in vugs apparently created by partial dissolution of siderite concretions, and (3) in large pore spaces



**Figure 2.3** Stratigraphic section and geophysical logs for a representative well in the Alberta Deep Basin. The section contains the Cadotte Member of the Peace River Formation, the Falher Member of the Spirit River Formation and the Bluesky and Cadomin Formations. GR=gamma ray. (modified from Smith et al., 1984).



**Figure 2.4**

(a) Thin section photomicrograph of prismatic quartz crystals (quartz druse, Q) lining the pore (P) and partially filling a large pore space in a Falher conglomerate. The largest quartz crystal in the centre probably has fluid inclusions which are large enough for analysis. Falher Member (93-P-1, b-28-L 2348.1 m). Field of view is 3.3 mm.

(b) Thin section photomicrograph of calcite cement (CALC) filling the pore space after quartz druse (QTZ). Falher Member (11-4-70-11 W6 1999.3 m). Field of view is 2.1 mm.



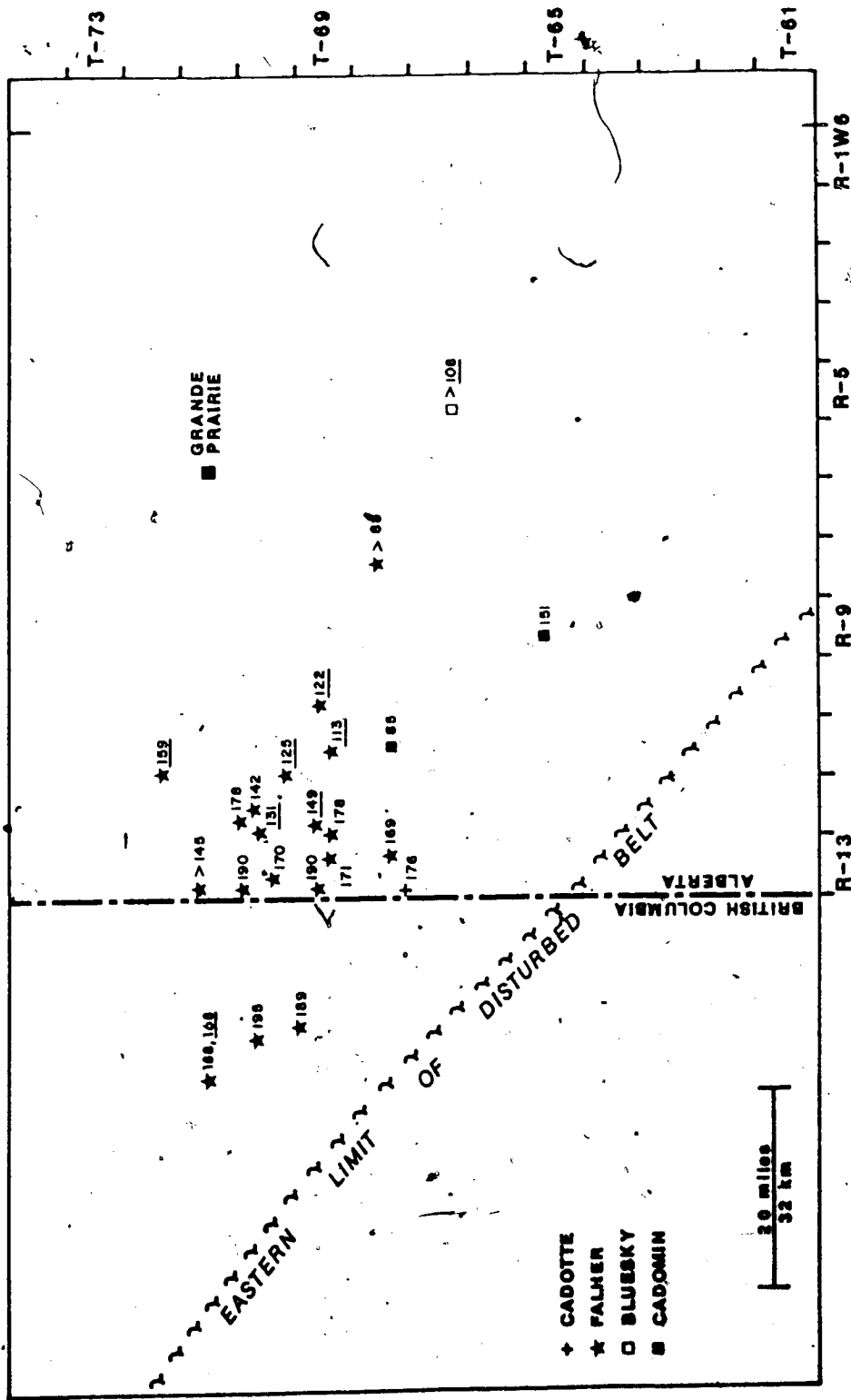


Figure 2.5 Geographic distribution of homogenization temperatures ( $^{\circ}\text{C}$ ) for fluid inclusions. Plain numbers are temperatures from quartz druse; underlined numbers are temperatures from late-stage, calcite cement. Highest temperatures ( $188^{\circ}\text{--}195^{\circ}\text{C}$ ) are in the westernmost part of the study area.

of chert-pebble conglomerates. Stable isotope data (Chapters 3 and 4) for samples of quartz druse from the Cadotte and Falher Members suggest that all three types of druse precipitated from fluids similar both in isotopic composition and temperature. Isotopic data for quartz druse from the Cadomin suggest that different fluids were involved in various stages of druse formation.

Fluid inclusions also were analyzed from macrocrystalline calcite cements in conglomerates and coarse-grained sandstones from the Falher Member and from sandstones in the underlying Bluesky Formation (Figure 2.3). Calcite-cemented zones in these sandstones or conglomerates are discontinuous and are commonly less than 1 m thick.

Diagenetic sequences for the Falher Member and Cadomin Formation are given in Chapter 3. Only the relative timing of the quartz druse and calcite cement is pertinent to this study. Quartz druse precipitated relatively late in the diagenetic sequence of the Cadotte, Falher and Cadomin, after grain fracturing. In the Falher, textural evidence shows that calcite precipitated after quartz druse (Figure 2.4b). In the Bluesky Formation, calcite also was the last diagenetic phase to precipitate.

## ANALYTICAL TECHNIQUES

Doubly polished sections for the fluid inclusion study were prepared from epoxy impregnated samples using the method of Barker and Reynolds (1984). The maximum temperature to which the samples were heated during preparation was 70°C. The data presented here are for primary inclusions from authigenic quartz druse or calcite cement unless otherwise noted. Only isolated inclusions that showed no preferred orientation or planar distribution were considered to be primary (Roedder, 1984). The following abbreviations referring to fluid inclusion properties are used here:  $T_h$ =temperature of homogenization,  $T_m$ =temperature of melting,  $T_t$ =temperature of trapping, and  $T_c$ =critical temperature.

Heating and cooling experiments were performed using a modified U.S. Geological Survey, gas flow stage developed by Fluids Incorporated (Werre et al., 1979; Woods et al., 1981). Homogenization determinations at temperatures above room temperature were made first, using the quick cycling of temperature method described by Roedder (1984). In some inclusions, sudden nucleation of the gas bubble never clearly occurred, even after cooling from 30°C over the apparent homogenization temperature. The apparent homogenization temperatures for such inclusions are recorded, but represent minimum homogenization temperatures.

Once homogenization temperatures had been determined, freezing runs were conducted using the reversal of temperature cycling method described in Roedder (1984). Samples were cooled until the fluid in two phase inclusions was frozen (-45° to -35°C). Freezing of the liquid phase was usually detected by shrinking or disappearance of the vapor phase, although the vapor phase in some inclusions only disappeared or shrank in size after reheating to a few degrees below the melting temperature.

After melting temperatures had been obtained, the sample was cooled to -190°C and then allowed to warm to 0°C to determine critical or homogenization temperatures of methane, CO<sub>2</sub> or hydrocarbon phases. Samples were then heated up to +30°C to detect the possible presence of clathrates or methane hydrates.

Measurements of homogenization and melting temperatures were repeated at least twice to test for reproducibility. Replicate measurements for T<sub>h</sub> of H<sub>2</sub>O in quartz were within ±0.5°C. The T<sub>h</sub> of H<sub>2</sub>O in some calcite samples increased by 1°C for each run, suggesting that stretching was taking place (Roedder, 1984; p. 72). In these cases, the first T<sub>h</sub> measured is recorded. The reproducibility of T<sub>m</sub> of H<sub>2</sub>O measurements was within ±0.2°C. For T<sub>c</sub> (critical temperature) of methane, reproducibility was ±1°C. The T<sub>h</sub> for inclusions which homogenized in the temperature range -40 to -10°C was difficult to determine. For some of these inclusions, the range of

temperature over which the phase change occurred is all that could be determined. Based on reproducibility and stage calibrations against standards, accuracy is estimated at  $\pm 1.5^{\circ}\text{C}$  for  $T_h$  between  $150\text{-}200^{\circ}\text{C}$  and  $\pm 0.3^{\circ}\text{C}$  for  $T_m$  of aqueous inclusions.

Some of the larger inclusions near the surface of the plate were analyzed by Raman spectroscopy. Methods for analyses of fluid inclusions using Raman spectroscopy are described by Rosasco et al. (1975), Touray et al. (1985), and Pasteris et al. (1986). In this study, Raman spectra were recorded with a Ramanor HG-2S spectrophotometer (Jobin Yvon-Instruments SA) at the Chemistry Division, Oak Ridge National Laboratory. This instrument employs a double monochromator with curved holographic gratings, cooled photoelectric detection and pulse counting electronics. A Nicolet 1170 signal averager was used to control the spectrometer and to accumulate spectra from multiple scans. Spectra were excited with the 514.5 nm line of a Spectra-Physics model 164 argon-ion laser. Spike filters were used to eliminate most of the plasma lines emitted by the laser. Using 40X and 80X objectives, methane was the only phase detectable.  $\text{H}_2\text{O}$ ,  $\text{CO}_2$ , ethane and propane were not detected but the detection limits for these phases under the conditions of this study are not known.

## RESULTS

Four types of primary inclusions are present in quartz druse and calcite cement of this study:

- (1). Aqueous inclusions; two phases present at room temperature; freezing and melting behaviour typical of aqueous inclusions.
- (2). Methane-rich inclusions; one phase at room temperature;  $T_h = -78^{\circ}$  to  $-61^{\circ}\text{C}$
- (3). Two phase inclusions with a methane-rich vapor phase; two phases present at room temperature; no visible change on cooling to  $-190^{\circ}\text{C}$ .
- (4). Hydrocarbon inclusions; one phase at room temperature;  $T_h = -40^{\circ}$  to  $-30^{\circ}\text{C}$ .

**Figure 2.6**

(a) Aqueous inclusion in quartz druse. This inclusion homogenizes to the liquid phase at 188°C. Its melting temperature is -1.8°C. Length of inclusion is 15 μm. Sample 237.

(b) and (c) Two inclusions from the same crystal of quartz druse, sample 385. (b) aqueous inclusion with  $T_h > 170^\circ\text{C}$  and  $T_m = -0.5^\circ\text{C}$ . (c) methane-rich inclusion with a critical temperature of  $-63.2^\circ\text{C}$ . The dark patch in the upper left corner of the inclusion may be trapped hydrocarbons.

(d) Two phase inclusion with a methane bubble and unidentified liquid in quartz druse. The vapor was identified as methane by Raman spectroscopy (See Figure 2.7). Sample 394.

(e) Large hydrocarbon inclusion in calcite cement. This inclusion has an homogenization temperature of approximately  $-33^\circ\text{C}$ . Sample 400.

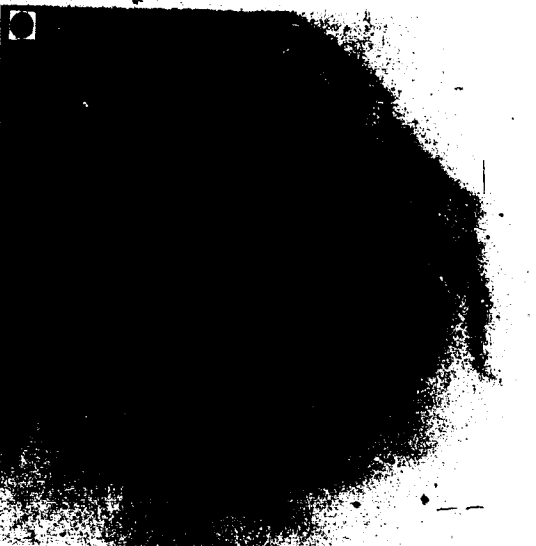
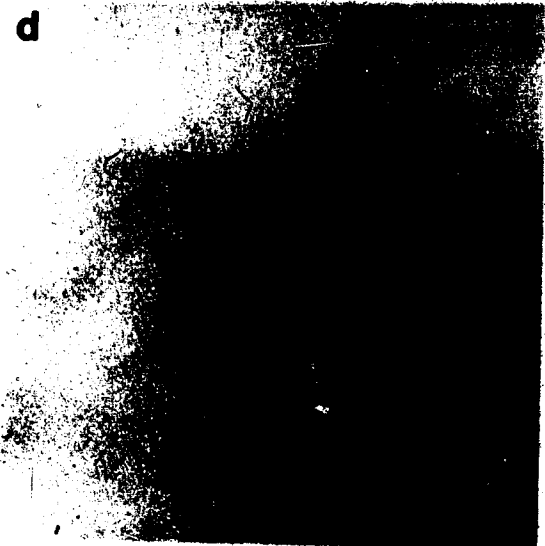




TABLE 2.1 RESULTS FOR FLUID INCLUSIONS FROM QUARTZ DRUSE

Sample No.	Heating		Melting		Range of Tm for each sample	No. of inclusions measured	No. of inclusions measured	Tc *Methane (°C)	Th Hydrocarbon (°C)
	Average Th (°C)	Range of Th for each sample	Average Tm (°C)	Range of Tm for each sample					
<b>CADOTTE</b>									
324	176	(156-193)	14	-1.6	(-1.1 to -2.0)	10	-63.3	-70 secondary	
<b>FALHER</b>									
346	>88	(>85->90)	2	+0.1		1			
367	169	(159-178)	3	-1.1	(-1.4 to -0.4)	4			
402	178	(160->195)	3	-1.2		1			
394	126	(125-144)	6	**			-43		
	171		1	**					
395	>170		1	**					
384	190		2	-1.2		2	-61		
385	>170		1	-0.5		1	-63.2 (2)		
397	142	(131-150)	4	-1.1	(-1.5 to -0.6)	2			-25 to -10
382	170	(>160-179)	7	-1.6	(-2.0 to -1.1)	4			
392	178	(160-198)	4	-1.4	(-1.4 to -1.5)	3			
380	>185		1	-1.5	(-1.6 to -1.3)	2			
290	>145		1	-1.7		1			
237	188		1	-1.8		1			
291	195	(180-211)	2	-1.3	(-1.3 to -1.2)	2			
220	189	(188-190)	2	-1.3		1			
241	>175		2	-2.3		1			
<b>CADOMIN</b>									
292	151	150-153	2	-0.1		2			
293	85	85	2	+1.5,+10			-68.8		

Abbreviations: Th=homogenization temperature, Tm=melting temperature, Tc=critical temperature

\* methane that has impurities of either propane and ethane or carbon dioxide

\*\* fluid apparently did not freeze

TABLE 2.2 RESULTS FOR FLUID INCLUSIONS FROM CALCITE CEMENT

Sample No.	Heating		Melting			No. of inclusions measured	Range of Tm for each sample	Tc Methane (°C)	Th Hydrocarbon (°C)
	Average Th (°C)	Range of Th for each sample	Average Tm (°C)	Range of Tm for each sample	No. of inclusions measured				
<b>FALHER</b>									
415	122	(97-144)	-1	(-1.7 to -0.6)	10	(-1.7 to -0.6)			
4751	113	(>96-149)	-2.2	(-2.6 to -1.8)	5	(-2.6 to -1.8)			
352	149	(146-153)	-1.1	(-1.4 to -0.7)	4	(-1.4 to -0.7)			-49
423	125	(95-140)	-1.1	(-1.4 to -0.9)	7	(-1.4 to -0.9)			
400	131	(>125-138)	-0.1	(-0.2 to +0.1)	7	(-0.2 to +0.1)			-33 -42
377	159	(159-160)	-1.5	(-1.8 to -1.3)	7	(-1.8 to -1.3)			
236	168	(161-174)	-1.1	(-1.3 to -1.1)	7	(-1.3 to -1.1)			
<b>BLUESKY</b>									
126	>108	(>100->115)	-4.5	(-4.9 to -4.2)	3	(-4.9 to -4.2)			

Abbreviations: Th=homogenization temperature, Tm=melting temperature, Tc=critical temperature

Figure 2.6 shows examples of each type of inclusion. The range and average  $T_h$  and  $T_m$  for each sample are presented in Tables 2.1 and 2.2.

### Aqueous Inclusions

Aqueous inclusions vary in size up to 15  $\mu\text{m}$  in diameter (Figure 2.6a and b). Homogenization temperatures range from 85° to 211°C for inclusions in quartz and from 95° to 174°C for inclusions in calcite (Tables 2.1 and 2.2). The majority of inclusions in quartz homogenize between 170° and 190°C and in calcite between 120° and 170°C.

The geographic distribution of  $T_h$  is shown in Figure 2.5. The highest temperatures, 188° to 195 °C, are in the westernmost part of the study area; temperatures decrease slightly to the east. Generally, calcite temperatures are lower than quartz temperatures. For example, in the westernmost well (Figure 2.5), fluid inclusions in quartz druse homogenize at 188°C (sample 237), whereas fluid inclusions in calcite cement from the same well, only 0.3m below the quartz druse, homogenize at 168°C (sample 236).

Melting temperatures for aqueous inclusions range from -2.3° to +10°C for quartz and 4.9° to +0.1°C for calcite (Tables 2.1 and 2.2). The majority of  $T_m$  values for both quartz druse and calcite cement from the Falher Member are in the range -2.3° to -0.6°C, indicating salinities of 2 to 3 NaCl eq.wt% (Roedder, 1962), i.e. slightly less than seawater (3.5 wt.%). The low melting temperatures (-4.9° to -4.2 °C) are observed in inclusions from calcite cement in one sample of the Bluesky Formation. These  $T_m$  values indicate a NaCl eq.wt% of 6.5 (Roedder, 1962). Fluid inclusions in two quartz samples have melting temperatures of about 0°C ( $\pm 0.2$ ), typical of fresh water compositions (Roedder, 1962). One sample (sample 292, Table 2.1) is quartz druse from the Cadomin Formation. Since the Cadomin was deposited in a continental depositional

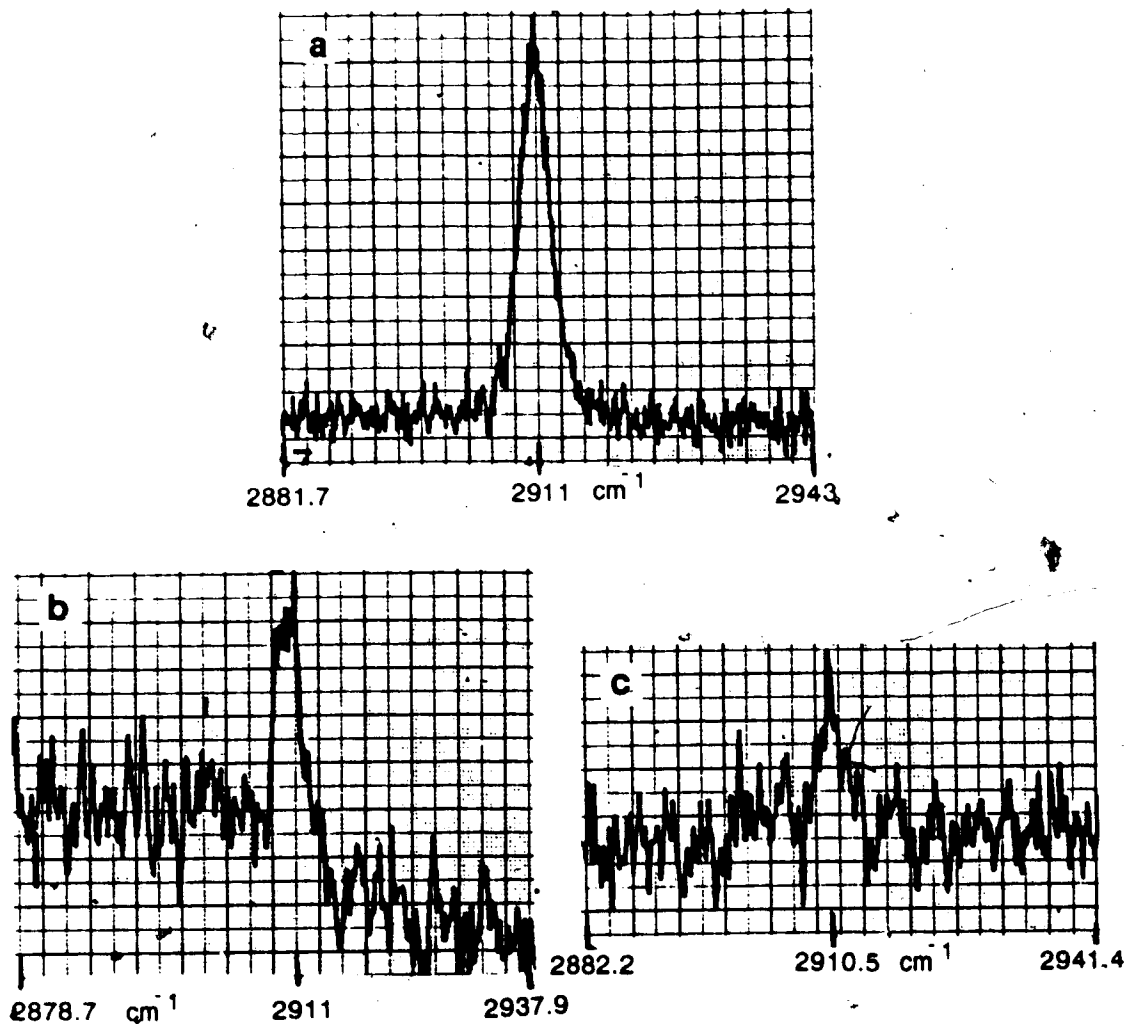
environment, the low salinity of the fluid inclusions suggests that fresh water was present during deposition and again during precipitation of late quartz druse.

The only likely interpretation of the positive  $T_m$  values for inclusions in the Cadomin sample 293 (Table 2.1) is melting of a methane hydrate (Mullis, 1979). This interpretation is supported by the coexistence of a methane-rich inclusion in the same quartz crystal. The for aqueous inclusions in this sample of quartz druse (85°C) correspond to the temperature of present formation water in the water-saturated area of the Cadomin where this well occurs. Quartz druse in this sample probably precipitated under present conditions, in contrast to quartz druse in other samples which precipitated at maximum burial temperatures.

#### Methane-Rich Inclusions

Methane-rich inclusions of this study (Figure 2.6c) separate into liquid and vapor phases when cooled below -60°C. The presence of methane is confirmed by a strong methane peak on Raman spectra (Figure 2.7a). In some of these inclusions a solid phase appears below -90°C. Homogenization temperatures generally range from -78° to -61°C, although one inclusion homogenizes at -43°C (Table 2.1). Most of these inclusions homogenize to the liquid phase, but one methane inclusion from a calcite cement (sample 236) and one from Cadomin quartz druse (sample 292) homogenize to the gaseous phase.

Homogenization temperatures for inclusions containing pure methane should be  $\leq -82.5^\circ\text{C}$ , the critical temperature for methane. Mullis (1979) measured the homogenization temperatures of methane as a function of ethane and propane content for temperatures higher than -82.5°C. According to his data, an homogenization temperature of -61°C represents approximately 8.5 mole% propane and ethane mixed with the methane. Alternatively, the critical



**Figure 2.7** Raman spectra of methane in quartz druse inclusions. (a) One-phase inclusion; Cadotte Fm. sample 324 10-7-68-13W6. (b) Two-phase inclusion, spectra on vapor phase; Falher sample 394b 7-23-69-13W6. (c) Two-phase inclusion, spectra on vapor phase; Falher sample 394b 7-23-69-13W6. Spectra were recorded with 514.5 nm excitation under the following conditions: (a) 40X objective, 100  $\text{cm}^{-1}/\text{min}$  for 22 scans, 500 mw, slit size 500  $\mu\text{m}$ ; (b) 80X objective, 100  $\text{cm}^{-1}/\text{min}$  for 32 scans, 400 mw, slit size 600  $\mu\text{m}$ ; (c) 80X objective, 100  $\text{cm}^{-1}/\text{min}$  for 32 scans, 600 mw, slit size 700  $\mu\text{m}$ .

temperature of the methane-rich inclusions could be raised by the presence of a small amount of CO<sub>2</sub> (Burruss, 1981). Our data does not permit distinction between ethane and propane or CO<sub>2</sub>.

#### **Two-Phase Inclusions with a Methane-Rich Vapor Phase**

Two-phase inclusions with a methane-rich vapor phase occur in quartz druse from only one well. They contain two phases at room temperature (Figure 2.6d) but are characterized by their lack of visible change when cooled to -190°C (Table 2.1, samples 394 and 395). Homogenization temperatures are less than or equal to those of aqueous inclusions (>170°C) in other samples. On freezing, the bubbles in some inclusions expand slightly at temperatures below -60°C. In others, there is no observable change at low temperatures but the bubble undergoes a series of rapid movements when heated from 0° to 20°C. The movement of the vapor phase may have been caused by the melting of a methane-hydrate. Methane was detected by Raman spectroscopy in the vapor phase of two inclusions of this type (Figures 2.7b and 2.7c). The liquid phase is probably water, but because the liquid phase would not stay under the laser beam during Raman spectroscopy, its composition could not be determined.

#### **Hydrocarbon Inclusions**

Hydrocarbon inclusions are relatively large (up to 40 μm in diameter) and were observed only in calcite cement (Figure 2.6e). On cooling, a fringe of liquid generally begins to form at about -40° to -30°C and gradually expands until about -90°C. On heating, the fringe of liquid gradually shrinks back to the sides until it finally disappears at temperatures between -40° and -30°C. Analyses of these inclusions by Raman spectroscopy was not possible due to the fluorescence of the sample from epoxy. The inclusions were examined under ultraviolet fluorescent light, but no fluorescence was observed. At best, these inclusions may fluoresce

weakly. They probably contain some methane with a mixture of higher hydrocarbons (R.C. Burruss, pers. comm.)

### Estimation of Formation Temperatures for Quartz Druse and Calcite Cement from Fluid Inclusions

In general, homogenization temperatures of fluid inclusions are lower than the trapping temperature (for primary inclusions, the temperature of crystallization). However, when a vapor phase can be demonstrated by fluid inclusion data to coexist in equilibrium with a liquid phase, the homogenization temperature equals the trapping temperature (Roedder, 1984; p.254). In this study, where methane-rich inclusions coexist with aqueous inclusions in quartz druse and calcite cement, the water was saturated with methane, and methane was present as a vapor phase. Under these conditions, the homogenization temperatures represent the formation temperature of the quartz druse or calcite cement in which the inclusions occur.

Although as discussed above, homogenization temperatures are generally less than or equal to the trapping temperatures, Hanor (1980) suggested two situations involving methane that could produce homogenization temperatures that are higher than the trapping temperatures. These are (1) trapping of a methane bubble with the aqueous phase in the inclusion; and (2) decarboxylation of acetate dissolved in the entrapped water, to produce methane *in situ*.

Inclusions that apparently trapped both water and a methane bubble do occur in the quartz druse and calcite cements sampled in this study, but can be distinguished and excluded from those entrapping an homogeneous fluid. Such inclusions have a larger than normal bubble at room temperature and do not homogenize at temperatures below 200°C. One such inclusion was heated to 250°C before homogenization took place. The homogenization temperatures for such inclusions were normally not determined.

It is difficult to determine whether decarboxylation of acetate and *in situ* production of methane within the inclusions has occurred. However, following the arguments presented by Hanor (1980), the maximum possible error in the homogenization temperature of inclusions examined in this study, caused by the *in situ* production of methane, is +13°C. This estimate assumes that acetate concentrations of 5000 mg/l were present in the inclusions at the time of trapping. This is the maximum concentration of acetate found in present-day sedimentary basins (Kharaka et al., 1983); concentrations of acetate in the inclusions were probably lower, causing correspondingly smaller errors in temperature. Furthermore, the kinetics of acetate decomposition are sluggish (S.E. Drummond, pers. comm.), and complete breakdown of the acetate is unlikely in the time available since its entrapment.

Another concern involving the presence of methane in inclusions is its effect on melting temperatures and calculated salinities. Hanor (1980) states that the presence of methane in an inclusion will probably lower the freezing temperature of water by less than a degree. Hedenquist and Henley (1985) calculated the effect of dissolved CO<sub>2</sub> on melting temperatures and calculated salinities. Analogous calculations for the effect of CH<sub>4</sub> on calculated salinities can be made. For our inclusions where T<sub>m</sub> = -1.7°C, the uncorrected salinity is 2.8 equiv. wt.% NaCl (Roedder, 1962). Based on the solubility of CH<sub>4</sub> at 200°C and 600 bars (0.6m CH<sub>4</sub>) (Drummond, 1981), the methane-corrected salinity is 1.7 equiv. wt.% NaCl. Therefore, the salinities reported here may be, at most, about 1 wt% too saline.

In summary, we are unaware of any likely mechanism that would produce a majority of inclusions with erroneously high homogenization temperatures. Therefore, it is concluded that the homogenization temperatures represent the temperatures of the fluids when entrapped. The temperature for quartz precipitation ranges from 195°C in the west to 142°C in the east; for calcite, temperatures range from 168°C in the west to >108°C in the east. The waters were probably as saline or slightly less saline than indicated by T<sub>m</sub> values (2-3 equiv. wt.% NaCl).



## REGIONAL BURIAL TEMPERATURES

Vitrinite reflectance data for Falher coals in the study area have been obtained by Kalkreuth and McMechan (1984), Weiss (1985), Youn (1983) and Zhu (1981). The highest vitrinite reflectance value ( $1.9 \pm 0.12\%$ ) was reported by Kalkreuth and McMechan (1984) for a Falher coal in the southwestern part of the area (Figure 2.8). Vitrinite reflectivities of Falher coal interbeds in the main area of this study gradually decrease eastwards from 1.5 to  $<0.8\%$   $R_o$  (Weiss, 1985). The vitrinite reflectance data of Youn (1983) and Zhu (1981) are consistent with those of Weiss (1985).

Many studies have attempted to define a universal correlation of coal maturity with maximum burial temperature. However, the relationship between temperature history and maturation of hydrocarbons remains a subject of considerable debate. At least three different models relating time, temperature and organic maturity have been applied (Lopatin, 1971 and Waples, 1980; Tissot and Espitalié, 1975; and Hood et al., 1975) to estimate burial temperature and organic maturity, each giving different results in some settings (Daly and Lilly, 1985), particularly for higher temperatures (ie.  $>130^\circ\text{C}$ ). The most widely used model, that of Lopatin (1971) modified by Waples (1980), has been used in this study to obtain an estimate of the maximum burial temperature.

Kalkreuth and McMechan (1984) used the Lopatin (1971)-Waples (1980) method to deduce the burial and temperature history of the sedimentary section for an area including the foothills southwest of our study area and extending eastwards to the syncline of the Western Canadian Basin. Their easternmost well falls within the southwesternmost part of our study area (Figure 2.8). In the "Lopatin-Waples method", the depositional and tectonic history of a sedimentary unit is plotted on a time-depth diagram and superimposed on a temperature grid that reflects the geothermal gradient of the area. Kalkreuth and McMechan (1984) estimated the present geothermal gradient for their study area using selected bottom-hole temperatures

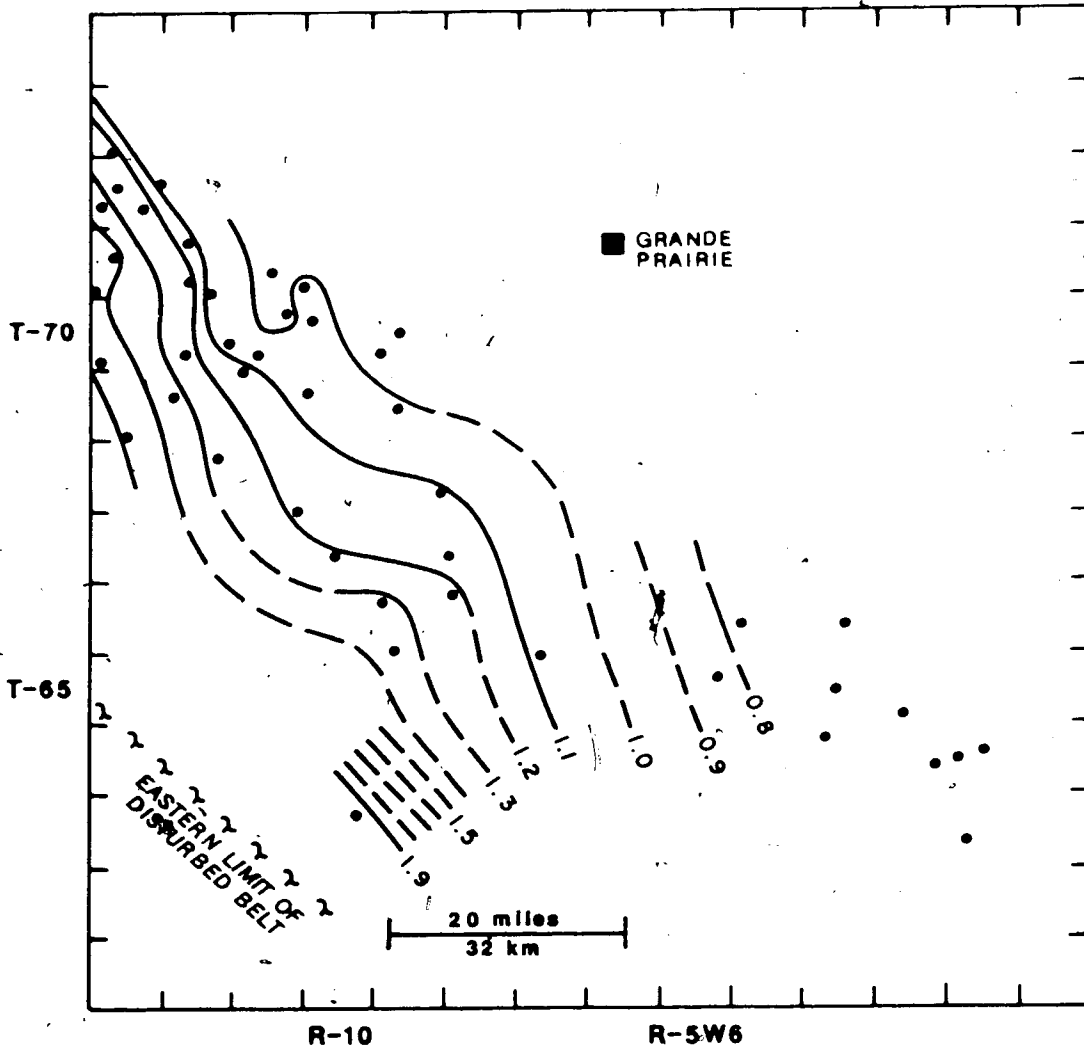


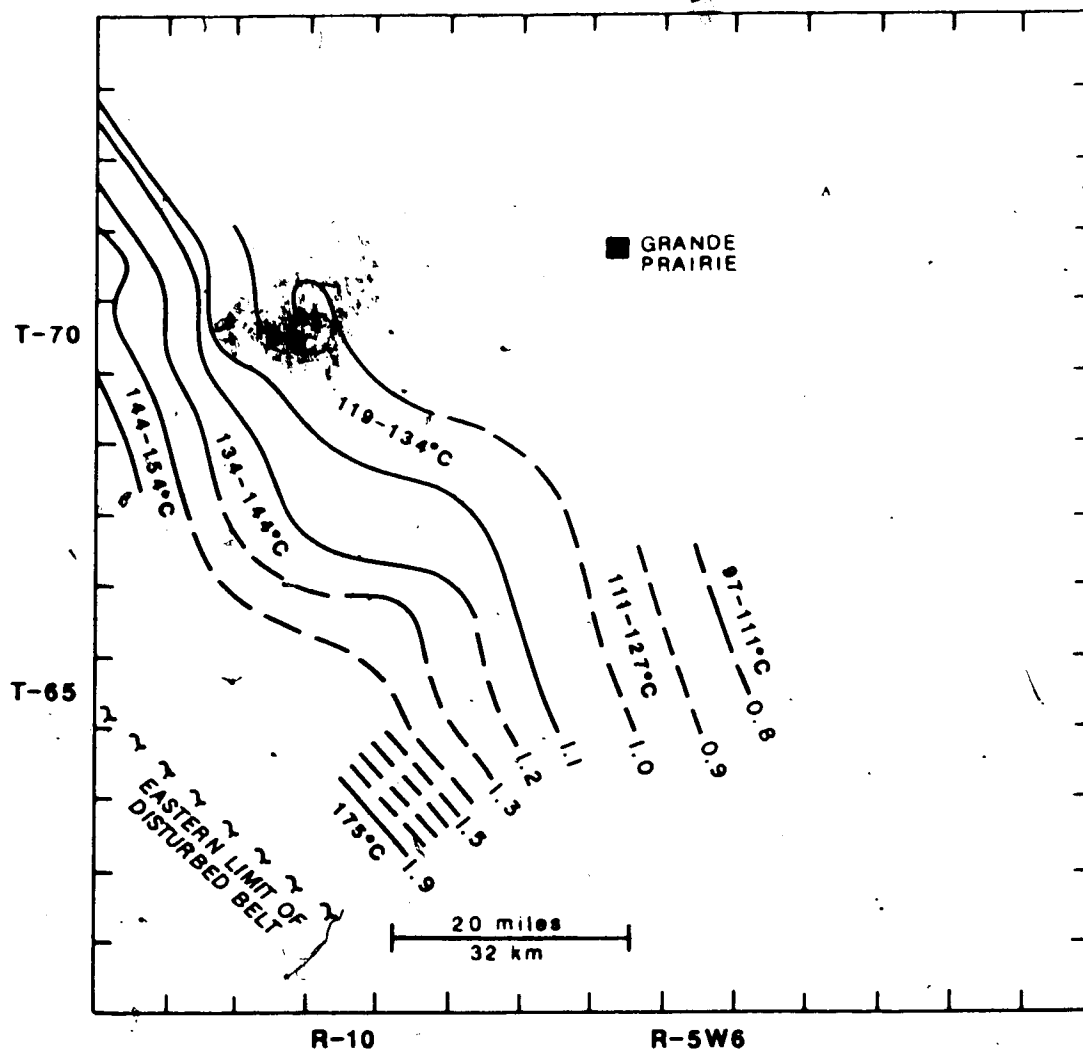
Figure 2.8 Data points and contours for vitrinite reflectance (Ro%) of Falher coals (data from Weiss, 1985). The southwesternmost point (>1.9 Ro%) is from Kalkreuth and McMechan (1984).

recorded in petroleum exploration well logs. Their data indicate a present geothermal gradient of 27°C/km, which is consistent with results for this area from other workers (Majorowicz et al., 1985a). Kalkreuth and McMechan (1984) determined the paleogeothermal gradient using the method of Buntebart (1979) in which paleogeothermal gradients are calculated on the basis of measured vitrinite reflectance and the integral of time and depth. Their data on Lower and Upper Cretaceous coals from four wells indicate a paleogeothermal gradient of 27°C/km. Time-temperature indices (TTI) were calculated from the time-depth(temperature) curves assuming a doubling of the organic reaction rate for every 10°C increase in temperature (see Kalkreuth and McMechan, 1984 and Waples, 1980 for a full description of the method). The final TTI was translated to a Ro% value using the TTI-Ro% calibration presented by Waples (1980). The close match between the calculated Ro% value and the measured Ro% value for each unit indicate that the burial history curves are approximately correct. Kalkreuth and McMechan (1984) calculated a maximum burial temperature of 175°C for the Falher in the southwestern part of this study area (Figure 2.9).

Similar calculations have been performed here to determine maximum burial temperatures across the study area. Simplified burial history curves modified from Kalkreuth and McMechan (1984), and their present and paleogeothermal gradients of 27°C/km, were used to estimate burial temperatures. Four points on the burial history (time versus depth) curves were determined:

(1) Burial of the Falher began at about 107 Ma (Kalkreuth and McMechan, 1984); Point 1 - Time=107 Ma, Depth=0 m.

(2) Burial of the Wapiti began at 75 Ma (Caldwell et al., 1978; Obradovich and Cobban, 1975). Since there is presently 1650m of sediment between the Falher and the Wapiti, the Falher was at a depth of approximately 1650m when deposition of the Wapiti began at 75 Ma; Point 2 - Time=75 Ma, Depth=1650 m.



**Figure 2.9** Geographic distribution of maximum burial temperatures for the Falher, calculated using the Lopatin (1971)-Waples (1980) method (see text). Contours, from Figure 2.8, provide boundaries for the temperature zones.

(3) Subsidence and burial were continuous from the early Cretaceous until uplift occurred during the late Paleocene-early Eocene. Maximum burial is assumed to have occurred immediately before the onset of uplift. Kalkreuth and McMechan (1984) estimated the beginning of uplift at 48 Ma based on K-Ar cooling dates in the Ominica Crystalline belt to the west (Gabrielse, 1975). Values for depth or temperature of maximum burial were varied until the calculated  $R_o$  value matched the measured  $R_o$  value. Point 3 - Time=48 Ma, Depth=variable dependent on the value of the measured  $R_o$  to be duplicated by the calculation.

(4) The final point of the curve reflects the present depth and formation temperature which decreases eastwards across the study area. Point 4 - Time=0 Ma, Depth=present burial depth.

Temperatures range from 144°-154°C where  $R_o=1.45\pm 0.1\%$ , 134°-144°C where  $R_o=1.25\pm 0.1\%$ , 119°-134°C where  $R_o=1.05\pm 0.1\%$ , 111°-127°C where  $R_o=0.95\pm 0.1\%$  and 97°-111°C where  $R_o=0.75\pm 0.1\%$  (Figure 2.9). Standard deviations on vitrinite reflectance data reported by Weiss (1985) were generally  $\pm 0.06$  to  $\pm 0.1$  for at least 50 measurements. The error range in  $R_o$  values results in a temperature range of  $<10^\circ\text{C}$ . The calculated temperatures are equivalent to maximum burial depths of 4800m, 4400m, 4000m, 3800m and 3000m.

By the Lopatin-Waples method, the time spent by the coal at the highest temperatures most affects the final maturity of the coal; time spent by the coal at lower temperatures has little effect on the final coal maturity. Hence, the maximum burial temperature is essentially independent of burial history. The geothermal gradient determines the maximum depth of burial necessary to obtain the calculated burial temperature, but does not affect the maximum burial temperature itself. Assuming the Lopatin-Waples method to be valid, the calculated temperatures presented above are the maximum possible burial temperatures which could have produced the measured vitrinite reflectance values. Further calculations indicate that an increase in temperature of a few °C results in maturities significantly higher than measured.

## COMPARISON OF FLUID INCLUSION AND CALCULATED BURIAL TEMPERATURES

In Figure 2.10, contours for maximum burial temperatures (Figure 2.9) have been superimposed on a map showing the geographic distribution of fluid inclusion temperatures (Figure 2.5). The squares and crosses on this diagram represent locations where the fluid inclusions analyzed were in formations other than the Falher. The temperature associated with each of these symbols is the temperature calculated for the Falher assuming a geothermal gradient of  $27^{\circ}\text{C}/\text{km}$ .

A difficulty in using fluid inclusion temperatures to calibrate organic maturity data is that the timing of fluid inclusion entrapment relative to maximum burial is generally not known. However, in this case, quartz homogenization temperatures are sufficiently high ( $170^{\circ}$ - $195^{\circ}\text{C}$ ) to suggest that this quartz druse precipitated near maximum burial conditions. Petrographic relationships indicate that quartz druse is a relatively late diagenetic phase, formed after compaction and grain fracturing (Chapter 3). Petrographic data also show that calcite is the latest diagenetic phase in the Falher, after quartz druse (Figure 2.4b). Figure 2.11 shows that temperatures for calcite precipitation are generally lower than temperatures for quartz druse. These facts suggest that calcite precipitated as fluids cooled during uplift. In the Cadomin, about 400m below the Falher, fluid inclusions in some quartz druse homogenize at  $151^{\circ}\text{C}$ . Whether this temperature represents the maximum burial temperature for the Cadomin at that location or whether the quartz druse precipitated during cooling cannot be ascertained. In summary, only the highest temperature quartz data were assumed to represent conditions at near maximum burial; lower quartz and calcite temperatures may represent precipitation from fluids which had cooled during uplift.

A temperature-distance plot comparing fluid inclusion temperatures with those calculated using the Lopatin-Waples, maturity-temperature calibration is shown in Figure 2.11. The

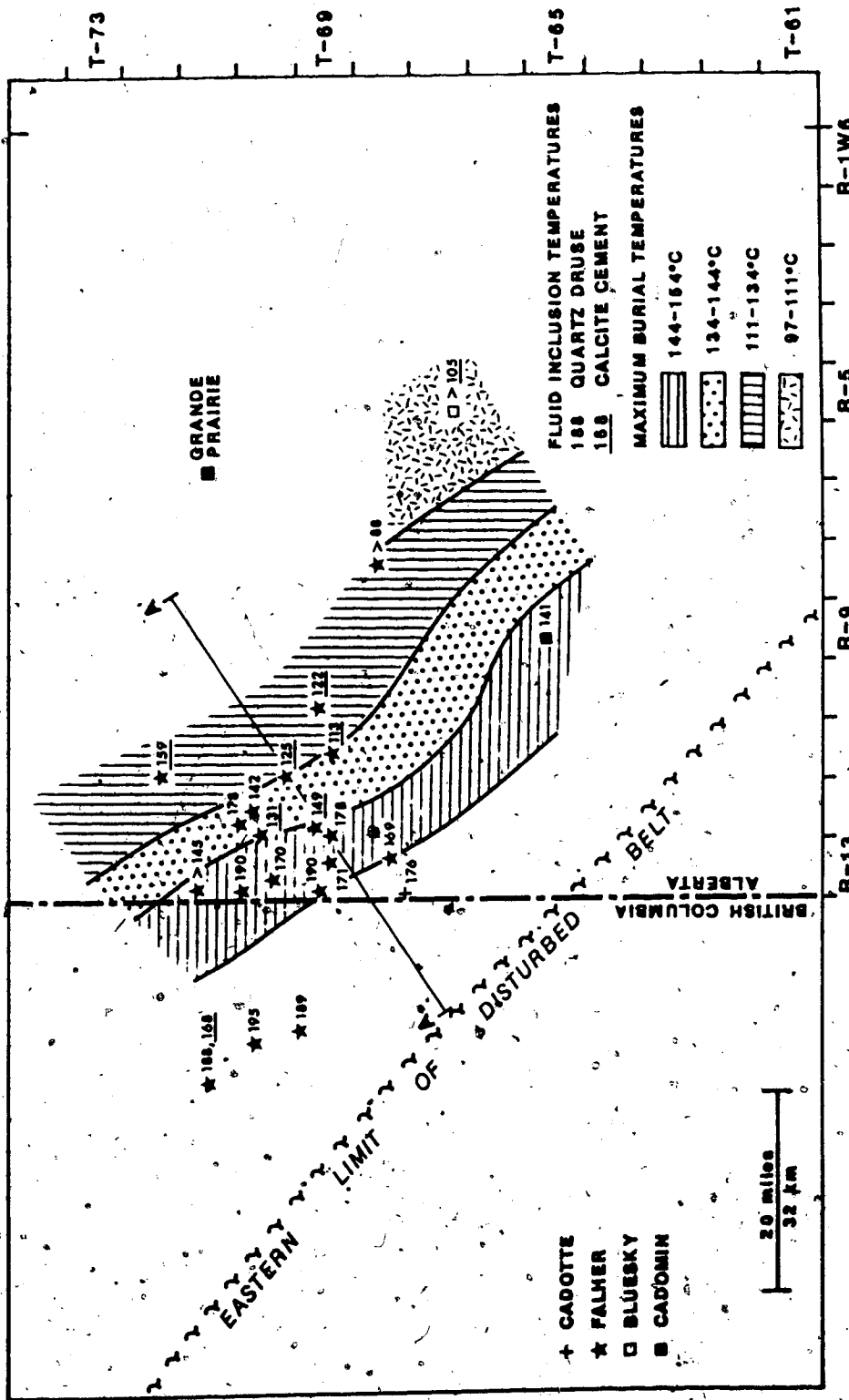
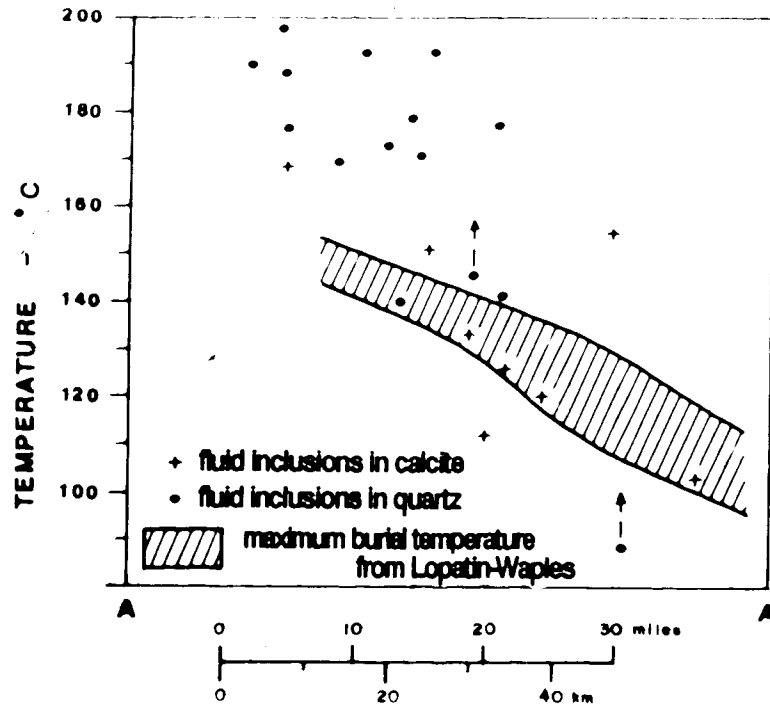


Figure 2.16 Geographic comparison of fluid inclusion temperatures (°C) and calculated maximum burial temperatures. Squares and crosses represent locations where the fluid inclusions analyzed were in formations other than the Falher. The temperature associated with each of these symbols is the temperature calculated for the Falher assuming a geothermal gradient of 27°C/km.



**Figure 2.11** Temperature versus distance plot of fluid inclusion temperatures along the line A-A' in Figure 2.10. Temperatures in Figure 2.10 are projected perpendicularly to this line to locate their position on the horizontal axis of this figure. The range of calculated maximum burial temperatures (from the Lopatin-Waples method) is shown by the diagonally striped band. Fluid inclusion temperatures for quartz druse generally lie well above this band in the western part of the area; in the east, they generally lie closer to the band of maximum burial temperatures. Fluid inclusions temperatures from calcite cements commonly lie within the maximum burial temperature range.



horizontal axis is the line A-A' on Figure 2.10. Notably, quartz temperatures are significantly higher than the calculated maturity temperatures in the western part of the area (170°-195°C versus 144°-154°C). Calcite temperatures generally fall within the range of calculated burial temperatures. In at least one western location, quartz fluid inclusions ( $T_h=190^\circ\text{C}$ ) occurred only 13m below a coal bed with  $R_o=1.43\pm 0.1$  ( $T=144^\circ\text{-}154^\circ\text{C}$ ) in a nearby well. The difference between the highest quartz temperatures (190°-195°C) and the vitrinite reflectance temperatures (144°-154°C) must be explained.

Two explanations are possible: (1) the temperatures calculated from vitrinite reflectance are inaccurate, and should be higher; (2) fluids with temperatures higher than the ambient rock temperature resided in Cadotte and Falher conglomerates, at least for a short time. In view of the uncertainty in the relationship between temperature history and maturation of hydrocarbons, neither explanation can be summarily discounted.

## EVALUATION OF TEMPERATURE-ORGANIC MATURITY RELATIONSHIPS

The most fundamental disagreement in relating temperature history and maturation of hydrocarbons is whether maturity is time- as well as temperature-dependent. The three models listed earlier (Lopatin, 1971; Tissot and Espitalié, 1975; and Hood et al., 1975) all assume some time dependence. However, Price (1983) and Barker (1983) argued that the  $R_o\%$  value is determined only by the maximum burial temperature if the time at that temperature is at least  $10^4$  to  $10^6$  years. Price (1983) presented a relationship with no time-dependence between  $R_o\%$  and temperature. Lerche et al. (1984) later tested this relationship in a number of different basins and after obtaining very poor fits with his data, he concluded that the Price relationship is a poor measure of observed  $R_o$  values. Edjedawe and Coker (1986), in turn, argued that abundant experimental and field evidence has shown that maturation is a function of both temperature and time. Altebaumer et al. (1981) demonstrated that vitrinite reflectance is strongly dependent on

the heating rate. This dependence explains why maturity values at a given temperature in geothermal fields or laboratory experiments, where heating rates are relatively rapid, are significantly lower than in burial settings where temperatures have increased slowly. At present, the most widely held view is that organic maturity is a function of time and temperature, but temperature plays the most important role, particularly at temperatures  $>130^{\circ}\text{C}$  (Gretener and Curtis, 1982).

Assuming that time is important, the kinetics of organic reactions become important. First-order kinetics are most commonly assumed (Lopatin, 1971; Tissot and Espitalie, 1975; and Hood et al., 1975). However, Price (1983) pointed out that experimental evidence shows that more rapid increase in reflectance occurs during the initial heating period (Pearson, 1981, p. 32), and the reaction, therefore, is not first-order. Tissot (1984) concluded that first-order kinetics is valid for reactions with low activation energies, such as the transformation of organic matter during the beginning stages of oil generation. However, at peak oil generation or during gas generation, activation energies are much higher and correspond to reaction rates multiplied by 4 to 10 (Tissot, 1984; instead of 2 used by Lopatin-Waples).

Several problems can be identified with the most commonly applied Lopatin-Waples model. The TTI-Ro% calibration presented by Waples (1980) combines data from Types I, II and III organic matter and as a result, underestimates maturities for Type II kerogen (Heasler and Surdam, 1985) and overestimates the maturity of Type I kerogen (Sweeney et al., 1987). This problem is probably not important for Type III kerogens that comprise the coals of this study.

More importantly for this study, Issler (1984) showed that different regression equations relate TTI to Ro% in different basins. Waples' (1980) relationship is an average TTI-Ro% equation for many different basins. At TTI values  $<10$ , the correlation between the different regression equations is good and the average relationship derived by Waples can probably be applied in

different basins. However, at higher maturities, the regression equations for different basins start to diverge. Calculations for the Alberta Deep Basin (this study) using the regression equations presented by Issler (1984) indicate that for a TTI value of 267 (maximum burial temperature = 149°C), Ro values can range from 0.91% (Grand Banks correlation; Issler, 1984) to 2.40% (Lopatin, 1971). Obviously, if the burial history curves are to be adjusted so that calculated Ro% values match the measured Ro% values, use of the correct regression equation relating TTI to Ro% is critical. The large variation in Ro% values corresponding to one TTI index is the result of underestimation of the calculated maturity (TTI) in some basins. Such underestimation results from (1) the use of present-day temperatures to reconstruct the thermal history in thermally unstable basins (eg. Labrador Shelf; Issler, 1984); and (2) underestimation of the amount of erosion that occurred (eg. Canning Basin and Lopatin's correlation; Issler, 1984). Issler (1984) believes that these errors are minimized in thermally stable basins where sediments are presently at their maximum burial depth and temperature (eg. Scotian Shelf and the Grand Banks Basins). In such basins, local calibrations of TTI will yield results closely approximating a universal TTI-Ro% relationship (Issler, 1984). This conclusion suggests that the high fluid inclusion temperatures (170-195°C) in the Alberta Deep Basin may represent the true maximum burial temperature and that these temperatures might be used to recalibrate the TTI-Ro% relationship specifically for the Alberta Deep Basin. However, due to the existing uncertainties in the calibration equation, ambient rock temperatures could have been any temperature ranging from <150°C to 190°C where fluid temperatures were 190°C.

## THERMAL ANOMALY

The fluid inclusion data show that the fluids attained temperatures much higher than previously thought for this part of the Deep Basin (Majorowicz et al., 1985b). If the calculated maximum burial temperature (150°C) is correct, the ambient rock temperature was 150°C when fluids in the porous conglomerates were 190°C, and a local thermal anomaly of limited vertical

thickness was present. Conversely, if the fluid inclusion temperatures represent the true burial temperature (i.e. calculated burial temperatures are inaccurate), a thermal anomaly on a much larger vertical scale was present. For a maximum burial temperature of 190°C, geothermal gradients must have been much higher than at present (~38°C/km instead of 27°C/km), or significantly more erosion occurred than was previously recognized. Because several studies across Alberta suggest that eroded thicknesses were in the range of 1500 to 2000m (Hacquebard, 1977; Nurkowski, 1984), higher geothermal gradients seem more probable than significantly more erosion.

In the first case (ambient rock temperature = 150°C; fluids in the porous conglomerates = 190°C), the temperature difference suggests that hot fluids were injected into conglomerates of the Cadotte and Falher Members without significantly affecting the surrounding sedimentary rocks of lower permeability. The lack of heat flow into less permeable rocks suggests that heat transfer was dominantly by convection in the permeable zones but by conduction in the units with low permeabilities. Using an intruding hot magma as an analogy, the change in temperature of the wall rock is 20% of the initial temperature difference, for a distance outward from the intrusive midplane of 2.5 times the body half-width (Norton and Cathles, 1979). In the Deep Basin, the conglomerate is 7 metres thick and the initial temperature difference was at least 40°C.

Surrounding shale for a distance up to 5.5m from the permeable conglomerate would be raised in temperature by only 8°C. The vitrinite reflectance in one particular well was measured from a coal bed 13 m above the conglomerate bed. This coal bed would not have seen any increase in temperature. Even if hot fluids did flow through the coals, time of exposure to hot fluids may have been too short to significantly alter the maturation of the coal.

In the second case, a high geothermal gradient is indicated in the western part of the study area. In the absence of tectonic or igneous activity in the immediate area, the most probable mechanism for raising geothermal gradients is fluid flow. Several authors have described or

modelled the increase in geothermal gradients in discharge areas by the upward movement of relatively hot fluids from deeper parts of the basin (Hitchon, 1984; Smith and Chapman, 1983; Bethke, 1985, 1986; Garven, 1985). The western part of the Deep Basin could be on the discharge pathway of deeper hot fluids.

Two possible pathways for the influx of hot water should be considered: (1) vertical flow from underlying formations via fractures or cross-formational flow; or (2) intra-formational flow, updip along permeable beds or bedding-plane fractures. Waters originating in or flowing through the underlying Permian-Triassic, carbonate evaporite section should have high salinities and high  $\delta^{18}\text{O}$  values ( $\sim +7$  to  $+9$  ‰ SMOW; Suchecky and Land, 1983). The Falher waters at 170-195°C have low salinities (2-3 wt %) and low  $\delta^{18}\text{O}$  values ( $+3$  ‰ SMOW, Chapter 3). Therefore, it seems unlikely that hot waters were derived from the underlying evaporite section.

The more likely alternative is that hot fluids migrated updip within conglomeratic beds and along bedding-plane fractures within the Cadotte and Falher. The present-day slope of the conglomeratic units in the Falher is about 1.6%; calculations of paleodepths using vitrinite reflectance data (Figure 2.8) suggest that the slope increased westward to about 6-7%. The coal maturity data of Kalkreuth and McMechan (1984) indicate that maximum burial depths and temperatures were attained at the synclinal axis of the basin, immediately east of the disturbed belt. The perpendicular distance from the synclinal axis to the linear zone (maximum burial temperatures  $\sim 150^\circ\text{C}$ , Figure 2.9) is about 25-30 km. Assuming a downward slope of 6.6% westwards from the  $150^\circ\text{C}$  zone, the maximum burial depth at the synclinal axis could have been 6450m with burial temperatures of  $195^\circ\text{C}$ . If the geothermal gradient increased towards the synclinal axis, then burial temperatures would be even higher. Hence, fluids with temperatures as high as  $200^\circ\text{C}$  could have migrated updip within the permeable conglomerate.

The distribution of quartz druse provides support for the model of eastwardly migrating, hot, silica-saturated fluids. Large quartz druse in the Falher and Cadotte is found only in the western part of the study area (Figure 2.5). The eastward decrease in abundance and size of quartz druse suggests that the source of silica-supersaturated water was to the west. Pressure solution of chert grains in conglomerates, which is common in the western part of the study area, provides a possible mechanism for waters to become supersaturated with respect to quartz. In the Gulf Coast, present waters are commonly supersaturated with respect to quartz by as much as 50 ppm (Kharaka et al., 1977; Morton et al., 1981). Such concentrations suggest that under reservoir conditions, a fluid can become oversaturated with respect to quartz to a limit of 50 ppm before precipitation of quartz actually occurs (Land, 1984). If each litre of water passing through conglomerate with 8.7% porosity (Cant and Ethier, 1984) precipitated 50 mg of silica, then  $26 \times 10^4$  to  $53 \times 10^4$  litres or  $3 \times 10^3$  to  $6 \times 10^3$  pore volumes of silica-supersaturated fluid must have passed through the one cubic metre of rock.

## CONCLUSIONS AND IMPLICATIONS

Burial temperatures calculated from coal vitrinite reflectance data using the Lopatin-Waples method have maximum values of 144-154°C in the western part of the study area, whereas fluid inclusions in quartz druse at the same location homogenize at 190°C. The discrepancy between the two types of temperatures can be explained in two ways: (1) fluids in conglomerates were at temperatures 40°C higher than ambient rock temperatures; or (2) the correlation of coal maturity with maximum burial temperatures in the Deep Basin is inaccurate. Both explanations are equally plausible. In the first case, where the calculated burial temperatures represent the ambient rock temperature, a thermal anomaly on a limited vertical scale was present. Hot fluids moved through these rocks at a rate fast enough such that their heat was not dissipated along the pathway. A relatively short duration of flow or its confinement to porous rocks is implied by the lack of effect on

coal maturity. In the second case, geothermal gradients of  $\sim 38^\circ\text{C}/\text{km}$  (versus  $27^\circ\text{C}/\text{km}$ ) are indicated and a thermal anomaly on an extensive vertical scale was present. A temperature for recalibration of the TTI-Ro% index (Waples, 1980) specific to the Deep Basin is available (1.4 Ro% correlates to  $190^\circ\text{C}$ ). Such recalibration may allow prediction of maximum burial temperatures throughout the Deep Basin that differ significantly from those presently assumed. Regardless of whether or not calculated burial temperatures are accurate, unexpectedly high temperatures ( $190^\circ\text{C}$ ) were present in at least the Falher Member of the Spirit River Formation and the Cadotte Member of the Peace River Formation. Either just the fluids, or the entire unit, were at these temperatures. A redistribution of heat by fluid flow is the most logical explanation for these high temperatures in the Deep Basin.

An important implication of these results pertains to the interpretation of stable isotope data. Stable isotope analyses of diagenetic minerals can be used to deduce the isotopic evolution of porewaters if the temperature of the porewater is known. The temperature of the porewater is commonly estimated from the maximum burial temperature which, in turn, is commonly calculated from maturity data. The possible difference between calculated burial temperatures and the actual fluid temperatures in this study, emphasizes the importance of knowing the actual temperature of the fluids. In this case, use of the maximum burial temperature ( $150^\circ\text{C}$ ) instead of the fluid temperature for precipitation of quartz druse ( $190^\circ\text{C}$ ) would produce calculated oxygen-isotopic compositions for the porewater of  $0\text{‰}$  versus  $+3\text{‰}$  SMOW.

## REFERENCES

- Altebaumer, F.J., Leythaeuser, D., and Schaefer, R.G., 1981, Effect of geologically rapid heating on maturation and hydrocarbon generation in Lower Jurassic shales from NW-Germany: *Advances in Organic Geochemistry*, p. 80-86.
- Barker, C.E., 1983, Influence of time on metamorphism of sedimentary organic matter in liquid-dominated geothermal systems, western North America: *Geology*, v.11, p. 384-388.
- Barker, C.E. and Reynolds, T.J., 1984, Preparing doubly polished sections of temperature sensitive sedimentary rocks: *Journal of Sedimentary Petrology*, v.54, p. 635-636.
- Beaumont, C., 1981, Foreland basins: *Geophysical Journal of the Royal Astronomical Society*, v.65, p. 291-329.
- Bethke, C.M., 1985, A numerical model of compaction-driven groundwater flow and heat transfer and its application to the paleohydrology of intracratonic sedimentary basins: *Journal of Geophysical Research*, v.90, p. 6817-6828.
- Bethke, C.M., 1986, Hydrologic constraints on the genesis of the Upper Mississippi Valley mineral district from Illinois Basin brines: *Economic Geology*, v.81, p. 233-249.
- Buntebarth, G., 1979, Eine empirische Methode zur Berechnung von palaeogeothermischen Gradienten aus dem Inkohlungsgrad organischer Einlagerungen in Sedimentgesteinen mit Anwendung auf den mittleren Oberrhein-Graben: *Fortschritte Geologie Rheinland und Westfalen*, v.27, p. 97-108.
- Burruss, R.C., 1981, Hydrocarbon fluid inclusions in studies of sedimentary diagenesis: in L.S. Hollister and M.L. Crawford, eds., *Short Course in Fluid Inclusions, applications to petrology*: Toronto, Mineralogical Association of Canada, p. 138-156.
- Caldwell, W.G.E., North, B.R., Stelk, C.R., and Wall, J.H., 1978, A foraminiferal zonal scheme for the Cretaceous system in the Interior Plains of Canada: in C.R. Stelk, and B.D.E. Chatterton, eds., *Western and Arctic-Canadian Biostratigraphy*: Geological Association of Canada, Special Paper 18, p. 495-575.
- Cant, D.J. and Ethier, V.G., 1984, Lithology-dependent diagenetic control of reservoir properties of conglomerates, Falher Member, Elmworth Field, Alberta: *The American Association of Petroleum Geologists Bulletin*, v.68, p. 1044-1054.
- Cant, D.J., 1983, Spirit River Formation - A stratigraphic-diagenetic gas trap in the Deep Basin of Alberta: *The American Association of Petroleum Geologists Bulletin*, v.67, p. 577-587.
- Daly, A.R. and Lilly, D.H., 1985, Thermal subsidence and generation of hydrocarbons in Michigan Basin: Discussion: *The American Association of Petroleum Geologists Bulletin*, v.69, p. 1181-1184.
- Drummond, S.E., 1981, Boiling and mixing of hydrothermal fluids: chemical effects on mineral precipitation: PhD dissertation, Pennsylvania State University, University Park, Pennsylvania, 380 p.
- Ejedawe, J.E. and Coker, S.J.L., 1986, Dynamic interpretation of organic-matter maturation and evolution of oil-generative window: reply: *The American Association of Petroleum Geologists Bulletin*, v.70, p. 1011-1014.
- Ferti, W.H. and Wichmann, P.A., 1976, Static formation temperatures from well logs: *Dresser Atlas Technical Memorandum*, v.7, no. 3.



- Gabrielse, H., 1975, Geology of Fort Grahame E-1/2 map-area, British Columbia: Geological Survey of Canada, Paper 75-33.
- Garven, G., 1985, The role of regional fluid flow in the genesis of the Pine Point deposit, Western Canada sedimentary basin: *Economic Geology*, v.80, p. 307-324.
- Gies, R.M., 1984, Case history for a major Alberta Deep Basin gas trap: the Cadomin Formation: *in* J.A. Masters, ed., *Elmworth case study of a Deep Basin Gas Field: American Association of Petroleum Geologists Memoir 38*, p. 115-140.
- Gretener, P.E. and Curtis, C.D., 1982, Role of temperature and time on organic metamorphism: *The American Association of Petroleum Geologists Bulletin*, v.66, p. 1124-1149.
- Hacquebard, P.A., 1977, Rank of coal as an index of organic metamorphism for oil and gas in Alberta: *in* The origin and migration of petroleum in the Western Canadian sedimentary basin, Alberta: Geological Survey of Canada Bulletin 262, p. f1-22.
- Hanor, J.S., 1980, Dissolved methane in sedimentary brines: potential effect on the PVT properties of fluid inclusions: *Economic Geology*, v.75, p. 603-617.
- Heasler, H.P. and Surdam, R.C., 1985, Thermal evolution of coastal California with application to hydrocarbon maturation: *The American Association of Petroleum Geologists Bulletin*, v.69, p. 1386-1400.
- Hedenquist, J.W., and Henley, R.W., 1985, The importance of CO<sub>2</sub> on freezing point measurements of fluid inclusions: evidence from active geothermal systems and implications for epithermal ore deposition: *Economic Geology*, v.80, p. 1379-1406.
- Hitchon, B., 1984, Geothermal gradients, hydrodynamics, and hydrocarbon occurrences, Alberta, Canada: *The American Association of Petroleum Geologists Bulletin*, v.68, p. 713-743.
- Hood, A., Gutjahr, C.M., and Heacock, R.L., 1975, Organic metamorphism and the generation of petroleum: *The American Association of Petroleum Geologists Bulletin*, v.59, p. 986-996.
- Issler, D.R., 1984, Calculation of organic maturation levels for offshore eastern Canada - implications for general application of Lopatin's method: *Canadian Journal of Earth Science*, v.21, p. 477-488.
- Kalkreuth, W. and McMechan, M.E., 1984, Regional pattern of thermal maturation as determined from coal-rank studies, Rocky Mountain foothills and front ranges north of Grande Cache, Alberta - implications for petroleum exploration: *Bulletin of Canadian Petroleum Geology*, v.32, p. 249-271.
- Kharaka, Y.K., Callender, E., and Carothers, W.W., 1977, Geochemistry of geopressured waters from the Texas Gulf Coast: *in* Proceedings of the Third Geopressured-Geothermal energy conference: University of Southwestern Louisiana, Lafayette, Louisiana, p. 121-165.
- Kharaka, Y.K., Carothers, W.W., and Rosenbauer, R.J., 1983, Thermal decarboxylation of acetic acid: implications for origin of natural gas: *Geochimica et Cosmochimica Acta*, v.47, p. 397-402.
- Land, L.S., 1984, Frio sandstone diagenesis, Texas Gulf Coast: a regional isotopic study: *in* R. Surdam and D. MacDonald, eds., *Clastic Diagenesis: American Association of Petroleum Geologists: Memoir 37*, p. 47-62.

- LeBlanc, Y., Lam, H.L., Pascoe, L.J. and Jones, F.W., 1982, A comparison of two methods of estimating static formation temperature from well logs: *Geophysical Prospecting*, v.30, p. 348-357.
- Lerche, I., Yarzab, R.F., and Kendall, C.G.St.C., 1984, Determination of paleoheat flux from vitrinite reflectance data: *The American Association of Petroleum Geologists Bulletin*, v.68, p. 1704-1717.
- Longstaffe, F.J., 1983, Diagenesis, IV. Stable isotope studies of diagenesis in clastic rocks: *Geoscience Canada*, v.10, p. 44-58.
- Lopatin, N.V., 1971, Temperature and geologic time as factors in coalification (in Russian): *Akademiya Nauk SSSR Izvestiya, Seriya Geologicheskaya*, no. 3, p. 95-106.
- Macqueen, R.W., and Powell, T.G., 1983, Organic geochemistry of the Pine Point lead-zinc ore field and region, Northwest Territories, Canada: *Economic Geology*, v.78, p. 1-25.
- Majorowicz, J.A., Jones, F.W., Lam, H.-L., and Jessop, A.M., 1985a, Terrestrial heat flow and geothermal gradients in relation to hydrodynamics: *Journal of Geodynamics*, v.4, p. 265-283.
- Majorowicz, J.A., Rahman, M., Jones, F.W. and McMillan, N.J., 1985b, The paleogeothermal and present thermal regimes of the Alberta Basin and their significance for petroleum occurrences: *Bulletin of Canadian Petroleum Geology*, v.33, p. 12-21.
- Masters, J.A., 1979, Deep Basin gas trap, Western Canada: *The American Association of Petroleum Geologists Bulletin*, v.63, p. 152-181.
- Meyer, H.J. and McGee, H.W., 1985, Oil and gas fields accompanied by geothermal anomalies in Rocky Mountain Region: *The American Association of Petroleum Geologists Bulletin*, v. 69, p. 933-945.
- Milliken, K.L., Land, L.S. and Loucks, R.G., 1981, History of burial diagenesis determined from isotopic geochemistry, Frio Formation, Brazoria County, Texas: *The American Association of Petroleum Geologists Bulletin*, v.65, p. 1397-1413.
- Monger, J.W.H., 1984, Cordilleran tectonics: a canadian perspective: *Bull. Soc. geol. France*, v.26, p. 255-278.
- Morton, R.A., Garrett, C.M.Jr., Posey, J.S., Han, J.H., and Jirik, L.A., 1981, Salinity variations and chemical compositions of waters in the Frio Formation, Texas Gulf Coast: Contract Report DOE/ET/27111-5, University of Texas Bureau of Economic Geology, 96 p.
- Mullis, J., 1979, The system methane-water as a geologic thermometer and barometer from the external part of the Central Alps: *Bull. Mineral.*, v.102, p. 526-536.
- Norton, D. and Cathles, L.M., 1979, Thermal aspects of ore deposition: in H.L. Barnes, ed., *Geochemistry of Hydrothermal Ore Deposits Second Edition*: John Wiley and Sons, p. 611-631.
- Nurkowski, J.R., 1984, Coal quality, coal rank variation and its relation to reconstructed overburden, Upper Cretaceous and Tertiary Plains coals, Alberta, Canada: *The American Association of Petroleum Geologists Bulletin*, v.68, p. 285-295.
- Obradovich, J.D., and Cobban, W.A., 1975, A time scale for the Late Cretaceous of the Western Interior of North America: in W.G.E. Caldwell, ed., *The Cretaceous System in the Western Interior of North America*: Geological Association of Canada, Special Paper 13, p. 31-54.

- Pasteris, J.D., Kuehn, C.A. and Bodnar, R.J., 1986, Applications of the laser raman microprobe Ramanor U-1000 to hydrothermal ore deposits: Carlin as an example: *Economic Geology*, v.81, p. 915-930.
- Pearson, D.B., 1981, Experimental simulation of thermal maturation in sedimentary organic matter: Ph.D. thesis, Rice University, Houston, Texas.
- Porter, J.W., Price, R.A. and McCrossan, R.G., 1982, The western Canada sedimentary basin: *Philosophical Transactions of the Royal Society of London*, v.305, p. 169-192.
- Price, L.C., 1983, Geologic time as a parameter in organic metamorphism and vitrinite reflectance as an absolute paleogeothermometer: *Journal of Petroleum Geology*, v.6, p. 5-38.
- Roberts, W.H., 1980, Design and function of oil and gas traps: in W.H. Roberts, III and R.J. Cordell eds., *Problems of Petroleum Migration: AAPG Studies in Geology No. 10*, p. 217-240.
- Roedder, E., 1984, Fluid inclusions: *Reviews in Mineralogy Volume 12*, Mineralogical Society of America, 644 p.
- Roedder, E., 1962, Studies of fluid inclusions I: Low temperature application of a dual-purpose freezing and heating stage: *Economic Geology*, v.57, p. 1045-1061.
- Rosasco, G.J., Roedder, E., and Simmons, J.H., 1975, Laser-excited raman spectroscopy for nondestructive partial analysis of individual phases in fluid inclusions in minerals: *Science*, v.190, p. 557-560.
- Smith, D.G., Zorn, C.E. and Sneider, R.M., 1984, The paleogeography of the Lower Cretaceous of western Alberta and northeastern British Columbia in and adjacent to the Deep Basin of the Elmworth area: in J.A. Masters, ed., *Elmworth Case Study of a Deep Basin Gas Field: AAPG Memoir 38*, p. 79-114.
- Smith, L. and Chapman, D.S., 1983, On the thermal effects of groundwater flow: 1. Regional scale systems: *Journal of Geophysical Research*, v.88, p. 593-608.
- Suchecky, R.K. and Land, L.S., 1983, Isotopic geochemistry of burial-metamorphosed volcanogenic sediments, Great Valley sequence, northern California: *Geochimica et Cosmochimica Acta*, v.47, p. 1487-1499.
- Sweeney, J.J., Burnham, A.K., and Braun, R.L., 1987, A model of hydrocarbon generation from type I kerogen: application to Uinta Basin, Utah: *The American Association of Petroleum Geologists Bulletin*, v.71, p. 967-985.
- Taylor, R.S., Mathews, W.H. and Kupsch, W.O., 1964, Tertiary: in R.G. McCrossan, and R.P. Glaister, eds., *Geological History of Western Canada: Alberta Society of Petroleum Geologists*, p. 190-194.
- Tissot, B., and Espitalié, J., 1975, L'évolution thermique de la matière organique des sédiments: applications d'une simulation mathématique: *Revue de l'Institut Français du Pétrole*, v.30, p. 743-777.
- Tissot, B.P., 1984, Recent advances in petroleum geochemistry applied to hydrocarbon exploration: *The American Association of Petroleum Geologists Bulletin*, v.68, p. 545-563.
- Tóth, J., 1980, Cross-formational gravity-flow of groundwater: A mechanism of the transport and accumulation of petroleum (the generalized hydraulic theory of petroleum migration): in W.H. Roberts, III and R.J. Cordell, eds., *Problems of Petroleum Migration: AAPG Studies in Geology No. 10*, p. 121-167.

- Touray, J.C., Beny-Bassez, C., Dubessy, J., and Guilhaumou, N., 1985, Microcharacterization of fluid inclusions in minerals by raman microprobe: Scanning Electron Microscopy, p. 103-118.
- Varley, C.J., 1982, The sedimentology and diagenesis of the Cadomin Formation, Elmworth area, northwestern Alberta: M.Sc thesis, University of Calgary, Calgary, Alberta, 173 p.
- Waples, D., 1980, Time and temperature in petroleum formation: application of Lopatin's method to petroleum exploration: The American Association of Petroleum Geologists Bulletin, v.64, p. 916-926.
- Weiss, H.M., 1985, Geochemische und petrographische Untersuchungen am organischen Material kretazischer Sedimentgesteine aus dem Deep Basin, Westkanada: Obergunzburg, PhD thesis, (in German), 261 p.
- Werre, Jr., R.W., Bodnar, R.J., Bethke, P.M. and Barton, P.B., Jr., 1979, A novel gas-flow fluid inclusion heating/freezing stage: Abstract, Geological Society of America Abstract Programs, v.11, p. 539.
- White, D.E., 1968, Environments of generation of some base-metal ore deposits: Economic Geology, p. 301-335.
- Woods, T.L., Bethke, P.M., Bodnar, R.J., and Werre, R.W., Jr., 1981, Supplementary components and operation of the U.S. Geological Survey gas-flow heating/freezing stage: U.S. Geological Survey Open File Report 81-954, 12 p.
- Youn, S.H., 1983, Depositional environments and their significance on diagenetic processes, Falher Member (Lower Cretaceous) Spirit River Formation, Elmworth area, Alberta: University of Calgary, unpublished report, 317 p.,
- Zhu, J., 1981, Vitrinite reflectance measurements and geothermal gradients on the Grande Prairie, northwest Alberta plains, Canada: University of Calgary, unpublished report, 79 p.

**CHAPTER 3. DIAGENESIS AND ISOTOPIC EVOLUTION OF POREWATERS IN  
THE LOWER CRETACEOUS FALHER MEMBER AND CADOMIN FORMATION.**

**ALBERTA DEEP BASIN**

**INTRODUCTION**

Stable isotope analyses of diagenetic minerals can be useful indicators of porewater evolution in sedimentary basins (Longstaffe, 1983,1987; Land,1984) and are potential indicators of regional paleoflow patterns. However, without data for the temperatures of the fluids which precipitated the diagenetic minerals, interpretation of the stable isotope data is severely limited. In some studies, the maximum burial temperature is estimated from the maturation of organic material and this temperature is used to constrain the data. Using this constraint, Longstaffe and Ayalon (in press) and Ayalon and Longstaffe (in press) demonstrated that an influx of meteoric water during uplift of the Western Canadian Basin is required to explain the isotopic results for diagenetic minerals in the Belly River and Viking Formations of central Alberta. However, they were unable to tightly constrain the changes in the  $\delta^{18}\text{O}$  value of porewater during burial, prior to the meteoric recharge event. An important complicating factor is that the maximum temperature for a fluid at a particular depth may not be the same as the maximum burial temperature calculated from maturity data. As shown in Chapter 2, thermal anomalies caused by rising, hot porefluids occur and may be quite common in sedimentary basins. In such cases, the maximum burial temperature is not a reliable constraint for interpretation of stable isotope data.

The purpose of this paper is to use the temperatures derived from fluid inclusion data presented earlier (Chapter 2) to interpret stable isotope data for diagenetic minerals in Lower Cretaceous sandstones and conglomerates in the Alberta Deep Basin (Figure 3.1). The following questions are addressed:

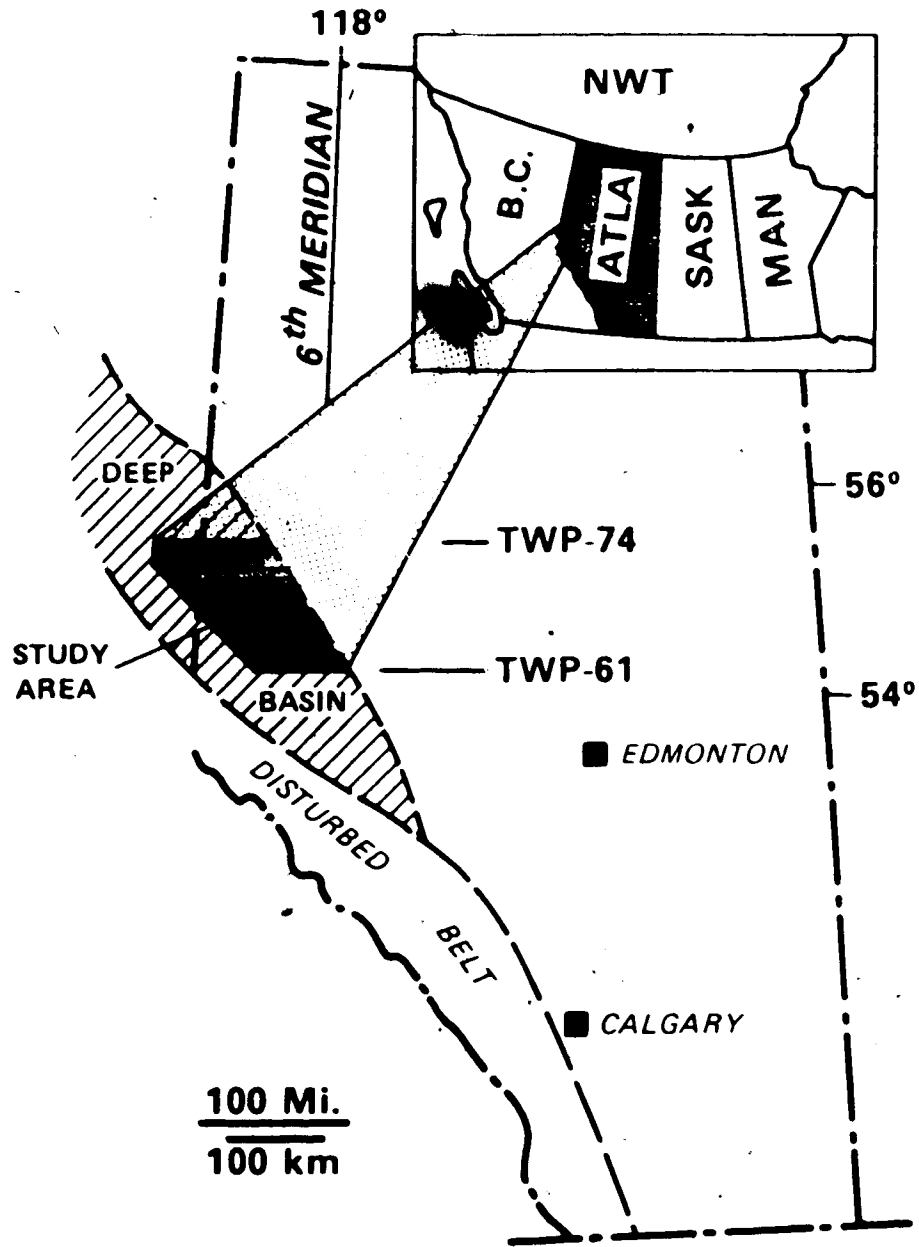


Figure 3.1 Location of study area.

1. To what extent was meteoric water involved in diagenesis on a regional scale in the Alberta Deep Basin?
2. How did the isotopic composition of porewaters vary in response to major geological events?
3. What was the relationship between diagenesis and the large scale production and trapping of methane gas?

Sandstones from the entire clastic sedimentary section in the Alberta Deep Basin have been examined; however this presentation is limited to two Lower Cretaceous units: the Falher Member of the Spirit River Formation and the Cadomin Formation (Figure 1.2). The trends in diagenesis and porewater evolution in the Falher Member are representative of most Lower and Upper Cretaceous sandstones. Late stage diagenesis and porewater evolution in the Cadomin Formation are significantly different.

### DEPOSITIONAL SETTING

Figure 3.2 is a southwest to northeast cross section through the study area showing the major facies changes in each of the Lower Cretaceous units. The Falher Member of the Spirit River Formation is composed of shoreline conglomerates, sandstones, shales and coal in the southern part of the study area, and marine coarsening-upward sequences of shale, siltstone and sandstone in the northern part (Cant, 1983; Smith et al., 1984). The Falher Member is underlain by marine shales, siltstones and sandstones of the Wilrich Member, and is overlain by the Notikewin Member which is shalier than the Falher and represents the last pulse of sedimentation before the transgression that resulted in the overlying Harmon shale (Cant, 1983).

Within the study area (Figure 3.1), the Cadomin Formation is a distal, gravel-dominated braidplain deposit (Varley, 1982, 1984; Smith et al., 1984) ranging in thickness from 1 to 19 m. It

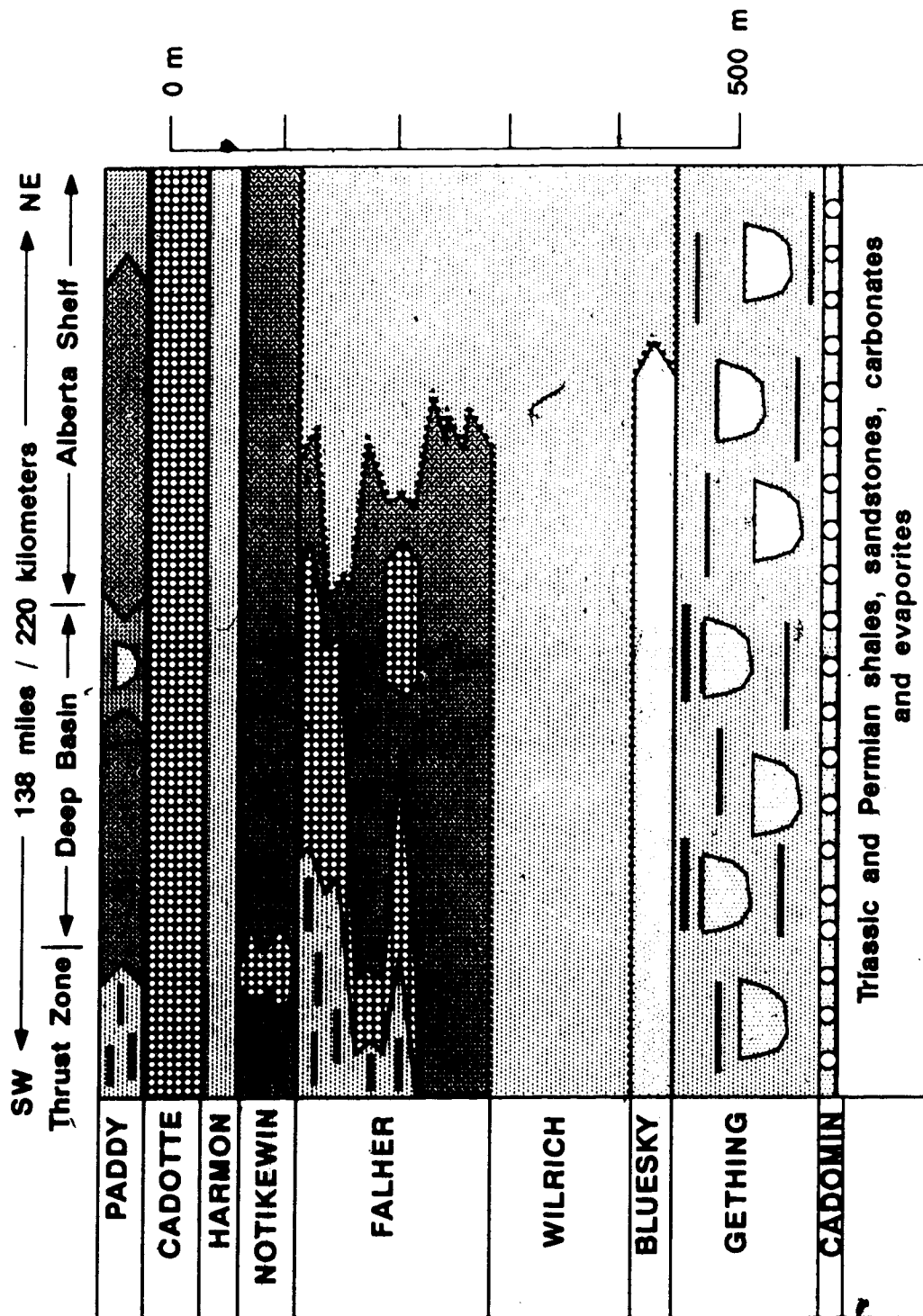


Figure 3.2 Southwest to northeast cross-section extending from 93-1-15 in British Columbia to Township 74 Range 25 W5 in Alberta, through Lower Cretaceous units of the Deep Basin. Facies and facies boundaries are taken from paleogeographic maps of Smith et al. (1984).



**LEGEND**

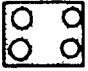


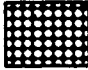
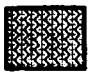
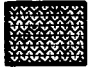
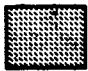
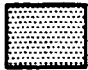

-  Alluvial plain and braid plain - conglomerates and sandstones
-  Lower delta plain - mud, silt, thin sands, coals
-  Barrier bar sands - coarsening upward sands
-  Wave dominated sand delta - conglomerates and sands
-  River dominated mud delta - muds and silts
-  Salt marsh/ mud flats - mud, silt and coal
-  Subtidal bay - mud and thin sandstones
-  Offshore silts, thin sands and marine shale
-  Conglomerate or sand-filled channel

Figure 3.2 cont. Legend for Figure 3.2.

unconformably overlies Upper Jurassic to Lower Cretaceous sandstones of the Nikanassin Formation and is overlain by continental coals and fine-grained sediments of the Gething Formation.

## ANALYTICAL TECHNIQUES

Samples of sandstones and conglomerates from the Falher Member of the Spirit River Formation and the Cadomin Formation were examined using a variety of analytical techniques: optical petrography, scanning electron microscopy (SEM), energy dispersive spectrometry (EDS), X-ray diffraction (XRD), electron microscopy and oxygen-, carbon- and hydrogen-isotope geochemistry.

### X-ray Diffraction

The mineralogy of diagenetic phases was confirmed using X-ray diffraction. For clay minerals, the  $<2 \mu\text{m}$  size-fraction was separated using standard sedimentation techniques. About 50 mg of Ca- and K-saturated portions of the  $<2 \mu\text{m}$  material were dispersed in distilled water and deposited by suction upon ceramic discs, producing a preferred orientation of platy minerals. The samples were analyzed using a Phillips X-ray diffractometer with Co K-alpha radiation (50kV, 20mA). Diffraction patterns were obtained for Ca-saturated samples at 54% relative humidity and following saturation with ethylene glycol. To confirm the identification of the clay minerals, additional diffractograms were obtained for the K-saturated samples at 0% and 54% relative humidity, and upon heating to 300°C and 550°C. The relative humidity of the samples was controlled prior to, and during analysis.

The  $<0.2 \mu\text{m}$  size-fraction was obtained by centrifugation following Jackson (1979), and examined by X-ray diffraction. Oriented mounts (glass slides) of the  $<0.2 \mu\text{m}$  material were

studied at 0% and 54% relative humidities, following solvation with ethylene glycol, and upon heating to 550°C; these procedures were used to identify the mixed-layer clays concentrated in this fraction.

Relative percentages of clay minerals were estimated from the (001) diffractions of illite, kaolinite and the 13Å diffraction for illite/smectite (ethylene-glycol solvated samples). The chlorite (001) diffraction was measured on samples heated to 550°C; appropriate corrections were applied for the overlap between the kaolinite (001) and chlorite (002) diffractions. Details of the calculations, including form factors used to account for variations in crystallinity among the clay minerals, are given in Dean (1985). Reproducibility of duplicate analyses is about  $\pm 15\%$  of the amount present. The percentage of expandable layers in illite (Table 3.2) was determined following the procedures of Srodón (1984).

Relative percentages of carbonate minerals were estimated by direct comparison of the relative peak intensities of the (104) peaks at d-spacings between 3.0 and 2.7 Å.

### Isotopic Analyses

Oxygen- and carbon-isotope data are presented in the usual  $\delta$  notation relative to Standard Mean Ocean Water (SMOW) for oxygen and hydrogen (Craig, 1961) and the *Belemnitella americana* from the Peedee Formation (PDB) for carbon (Craig, 1957). An oxygen-isotope, CO<sub>2</sub>-H<sub>2</sub>O fractionation factor of 1.0412 at 25°C has been employed in these calculations.

Oxygen was extracted from silicate minerals using the BrF<sub>5</sub> method of Clayton and Mayeda (1963), and quantitatively converted to CO<sub>2</sub> over red-hot graphite. Prior to this procedure, the 15 mg samples were dried at 105°C and maintained in a zero humidity environment for at least six

hours prior to loading in the reaction vessels. The reaction vessels and their contents were evacuated at 350°C for two hours prior to treatment with BrF<sub>5</sub>. Duplicate analyses of clays indicated that results are independent of the evacuation temperature, 350° or 160°C. Replicate analyses of unknowns were normally better than  $\pm 0.2$  ‰. During the course of these experiments, NBS-28 gave an average value of  $+9.61 \pm 0.12$  ‰.

Carbonate minerals were prepared for isotopic analysis by reacting powdered rock samples or mineral separates in anhydrous H<sub>3</sub>PO<sub>4</sub> at 25°C, following procedures described by Walters et al. (1972) and modified after McCrea (1950) and Epstein et al. (1964). CO<sub>2</sub> was extracted 1 hour after reaction at 25°C for calcite, after 10 days for ankerite or dolomite and after 21-27 days for siderite.  $\delta^{18}\text{O}$  results for replicate siderite samples treated at 50°C for 16 hours differed from the results for runs at 25°C for 21-27 days by less than  $\pm 0.4$  ‰;  $\delta^{13}\text{C}$  results differed by  $\pm 0.1$  ‰. For the 10 and 21 day reactions, the gas evolved after the first 3 hours was pumped away to avoid contamination by calcite. Where ankerite was present with minor amounts of dolomite but calcite was absent, the gas evolved after 1 hour was measured as ankerite. Analyses obtained for pure ankerite after 1 hour compare favourably with those of the 10 day runs for pure ankerite. The following total carbonate CO<sub>2</sub>-H<sub>3</sub>PO<sub>4</sub> extracted CO<sub>2</sub> fractionation factors ( $\alpha$ ) at 25°C were used: 1.01025 for calcite and 1.01110 for dolomite (modified after Sharma and Clayton, 1965), and 1.01163 for siderite (Rosenbaum and Sheppard, 1986). The dolomite  $\alpha$  was used in all calculations for ankerite; using the  $\alpha$  (25°C) for ankerite reported by Rosenbaum and Sheppard (1986) would lower the values reported here by about 0.66 ‰. During these experiments, NBS-20 gave average  $\delta^{18}\text{O}_{\text{SMOW}} = +26.50 \pm 0.02$  ‰ and  $\delta^{13}\text{C} = -1.17 \pm 0.01$  ‰.

### Mineral Separation

Mineral separates of authigenic dickite, quartz crystals and calcite cements were obtained by hand picking from pores in conglomerates. For sandstone samples, the preparation of

suitable carbonate and silicate samples for oxygen- and carbon-isotope study required a variety of physical and chemical mineral separations. The purity of all separations was verified by X-ray diffraction as well as SEM techniques (if required), prior to isotopic analysis.

### **Carbonate Minerals**

#### **Calcite**

Most isotopic analyses for calcite were made on samples where calcite was the only carbonate mineral present in more than trace amounts. For samples that contained up to 40% dolomite and 10% ankerite with the calcite, gas was extracted from the 5-45  $\mu\text{m}$  size fraction after one hour of reaction.

#### **Ankerite**

Where ankerite occurred as a cement in a sample containing grain-size dolomite, the sample was crushed and sieved to obtain the 45-75  $\mu\text{m}$  size fraction. This size fraction was put through a Franz magnetic separator to collect a pure ankerite separate which was checked by XRD. Separation of pure ankerite was not achieved in samples where calcite cement was present.

#### **Siderite**

In the Falher, only one sample had siderite present in sufficient quantities for analysis. The siderite sample from this conglomerate contained 65% siderite, 25% calcite, <5% ankerite and <5% dolomite. The gas produced after 3 hours of reaction was discarded, but there may still have been some contamination. For comparison,  $\delta^{18}\text{O}$  values of siderite samples from the Cadotte Member of the Peace River Formation are about 2 ‰ more enriched than the Falher sample. The Cadotte is located 75 metres stratigraphically above the Falher in a similar depositional setting. It is possible that, in the Falher sample, contamination is responsible for its lower  $\delta^{18}\text{O}$  value. The one analysis from the Cadotte represents a rock powder of a sandy conglomerate where siderite was the only carbonate present.

## *Silicate Minerals*

### *Authigenic quartz*

To separate the quartz overgrowths in sandstones, samples were crushed using a mortar and pestle, and disaggregated in distilled water using an ultrasonic probe at low power. The samples were then dispersed in distilled water, and the suspended fraction removed. The samples were dried and the size fractions including the majority of detrital quartz grains were obtained by sieving. Non-quartz minerals were removed from this fraction following the chemical treatments of Syers et al. (1968) and Jackson (1979). The quartz overgrowths were then isolated from the detrital quartz following the method of Lee and Savin (1985), and examined for authigenic morphology and purity using the scanning electron microscope. Only results for quartz-rich sandstones are reported. In samples where chert was abundant, the hydrofluoric etching process appeared to break up the chert particles as well as the quartz overgrowths.

### *Authigenic Illite, Illite/smectite (I/S)*

Illite and I/S were concentrated in the  $<0.2\mu\text{m}$  size fraction, which was obtained by centrifugation. No chemical treatments were used during the size separation. The  $<0.2\mu\text{m}$  samples were analyzed by X-ray diffraction prior to isotope analysis. Any samples with greater than trace amounts of quartz, kaolinite or chlorite were rejected before isotope analysis. If carbonate minerals were present in the  $<0.2\mu\text{m}$  sample, the sample was heated to  $65^\circ\text{C}$  in 10% HCl for 2-4 hours and then washed in distilled water.

### *Chlorite*

The  $\delta^{18}\text{O}$  values for a mixture of clays in the  $<2\mu\text{m}$  size-fraction were obtained, following which the chlorite was removed chemically. This procedure involved immersion in 10% HCl at  $80^\circ\text{C}$  for one hour, followed by boiling in a 3%  $\text{Na}_2\text{CO}_3$  solution for ten minutes to remove silica associated with the decomposition of the chlorite. No appreciable effect upon the oxygen-isotope composition of the remaining material (henceforth referred to as  $<2\mu\text{m-HCl}$ ) results from this treatment (Longstaffe, 1986). Examination by XRD of the  $<2\mu\text{m-HCl}$  material showed most samples to be comprised of kaolinite and illite $\pm$ I/S; a few samples comprised of only illite $\pm$ I/S. The

$\delta^{18}\text{O}$  values of these samples were measured directly. The  $\delta^{18}\text{O}$  of the chlorite was calculated (to  $\pm 1$  ‰) from the isotopic values obtained for the  $< 2 \mu\text{m}$  and  $< 2 \mu\text{m-HCl}$  samples, and chlorite abundances estimated from XRD data.

Calculated  $\delta^{18}\text{O}$  values for chlorite range from +1.8 to +7.1 ‰. However, the percentage of chlorite in each sample was determined by XRD which can underestimate the abundance of chlorite. If the percentage of chlorite in the sample is assumed to be 10% greater than measured, the  $\delta^{18}\text{O}$  values then range from 4.3 to 7.8 ‰, a much narrower range. It is possible that the  $\delta^{18}\text{O}$  values for chlorite are low by as much as 2 or 3 ‰.

## PÉTROGRAPHIC AND ISOTOPIC RESULTS

### Detrital Minerals

The Falher is composed of both unimodal and bimodal conglomerates and very fine to coarse-grained sandstones. Granules and pebble-size clasts consist mainly of chert (45%) and silicified fine-grained rock fragments, both sedimentary and volcanic (52%) (Cant and Ethier, 1984). The sand matrix consists of quartz (45%), chert (25%) and sedimentary and volcanic rock fragments (30%) with minor feldspar, mica and heavy minerals (Cant and Ethier, 1984). The majority of sandstones are composed of 50-70% quartz, 10-30% siliceous rock fragments of chert and altered grains, <2% feldspar and up to 20% detrital dolomite and dolomite-replaced grains. Rare sandstones, mostly in the northern part of the study area, are feldspar-rich with 15-35% feldspar, 10-40% siliceous rock fragments or chert, 10-20% quartz, 10-30% shale and volcanic rock fragments and 15-25% altered grains.

The Cadomin is composed dominantly of poorly-sorted, clast- and matrix-supported conglomerates, with some sandstones (Varley, 1984). Pebbles consist of mainly chert with some quartzite pebbles and sandstones are chert-rich with 10-20% quartz (Gies, 1984).

## Diagenetic Minerals

Diagenetic minerals in the Falher include hematite, siderite, chlorite, dolomite, quartz overgrowths, albite, illite, quartz druse, dickite, ankerite, calcite and minor amounts of pyrite (see Table 3.1). The diagenetic mineral assemblage in the Cadomin is more limited and includes siderite, kaolinite, quartz overgrowths, illite, quartz druse and dickite. Grain fracturing and pressure solution are common in clast-supported conglomerates, whereas grain dissolution, compaction and diagenetic mineral precipitation and dissolution are common to all the sedimentary rocks examined. In sandstones, most pore spaces have been occluded by diagenetic cements. In conglomerates, primary pore space was large enough that its reduction in size by diagenetic cementation is insignificant in some places; in some samples, however, pores are totally occluded by kaolinite or calcite.

### *Hematite*

Hematite fills some pores in one Falher conglomerate examined. Other pores in this sample have remnant traces of hematite which indicate that hematite was present before the precipitation of quartz overgrowths and calcite cement (Figure 3.3a). The traces of hematite suggest that other pore space once occupied by hematite has been replaced by siderite and then calcite.

### *Siderite*

Siderite is present in both the Falher and Cadomin, although in the Falher, siderite is usually observed only in samples south of township 71 (Figure 3.4). Siderite occurs in Falher sandstones as clusters of grain-coating rhombs which are commonly overlain by quartz overgrowths (Figure 3.3b). Detrital dolomite grains which were replaced by dolomite during early diagenesis generally comprise up to 20% of the framework grains in Falher sandstones where siderite is present and may themselves be coated by siderite. Siderite in Falher



TABLE 3.1 DIAGENETIC PHASES IN THE FALHER MEMBER

Sample	Location (W6)	Depth(m)	Rock Type*	Diagenesis*	
chlorite with quartz overgrowths					
3533	7-9-70-10	1900.0	c.g.sst.	rare chl.rims, drusy qtz, rare kaol. pore fill	
4076	7-29-71-10	1768.0	f.g.sst.	chl. embedded in qtz. o.g., qtz.o.g. after chl.	feld-rich
3685	10-28-71-11	1851.2	v.f.g.sst.	thick chl. rims, qtz.o.g. after chl.	
3686	10-28-71-11	1851.7	f.g.sst.	2 layers of chl.,pyrite & qtz.og. before 2nd layer,k-feld alt.to illite	
3687	10-28-71-11	1855.5	v.f.g.sst.	early chl. rims, qtz o.g. after rims, qtz dominates	
4039	11-5-72-12	1885.2	v.f.g.sst.	early chl. rims,qtz.o.g. after chl.,calcite replaces feld.	
4066	7-15-72-12	1817.5	v.f.g.sst.	chl.&qtz.o.g. intergrown,pyrite,kfeld alt. to ill-chl, albite	feld-rich
225	93-P-7,a-57-C	2346.2	congl.	chl., qtz. druse	
chlorite without quartz overgrowths					
3688	10-28-71-11	1858.3	m-c.g.sst.	chl.rims,feld.dissol.,illite, bitumen, calcite	feld-rich
3942	10-19-72-13	1955.3	v.f.g.sst.	chl. rims, carbonate replacing grains	feld-rich
3888	7-13-73-13	1723.2	v.f.g.sst.	chl. grain replacement	feld-rich
4046	6-32-73-13	1763.4	v.f.g.sst.	pore rimming and filling chl.	feld-rich
feldspar-rich without chlorite					
3539	7-9-70-10	1940.7	m.g.sst	kaol-filled pore, carbonate alteration	
4047	11-12-71-13	2026.6	f.g.sst.	illite-rich	
4028	11-5-72-12	1870.0	f.g.sst.	albitization, calcite cement	
4040	11-5-72-12	1890.8	m-c.g.sst.	albitization,illite pore fills and grain coating, calcite cement	
4041	11-5-72-12	1894.9	f.g.sst.	feld alt. to illite, illite pore fills	
3640	93-P-1,a-85-G	2295.0	m.g.sst.	k-feld partially alt.to albite, albite rim filled with kaol&calcite, some plag. preserved, calcite cement	
4518	93-P-1,c-16-I	2148.6	m.g.sst.	feld alt. to illite, Fe-calcite cement	
4520	93-P-1,c-16-I	2151.3	f.g.sst.	feld alt. to illite, illite pore-fill	
252	93-P-7,a-48-J	1997.9	congl.	plag. with albite rim, remnant k-feld mostly alt. to albite, Fe-calcite cement	

TABLE 3.1 cont. DIAGENETIC PHASES IN THE FALHER MEMBER

early siderite									
3772	11-30-68-8	2001.3		sid rims, qtz.og., local calcite cement, local kaol., pore-fill					dolomite-rich
3711	11-4-69-7	1870.7	1.g.sst.	sid rims, qtz og., feld to illite, sid coated by illite					dolomite-rich
351	10-33-69-10	1908.6	v.f.g.sst.	sid. rims, qtz. og.					
	6-28-69-12	2139.4	congl.	hematite, sid., calcite cement, biotite replaced by siderite					
4910	10-11-70-9	1759.3	v.f.g.sst.	thick sid. rims and large zones of siderite, qtz. og.					dolomite-rich
3700	6-5-70-10	1919.3	v.f.g.sst.	thick sid. rims, few qtz. og.					dolomite-rich
178	10-13-70-10	1769.0	v.f.g.sst.	sid. rims, qtz. o.g.					dolomite-rich
180	11-4-70-11	1988.3	v.f.g.sst.	sid. rims, qtz. og., ankerite					dolomite-rich
	11-4-70-11	2000.8	congl.	sid. rhombs before pressure sol'n, kfeld dissol, illite,					
222	93-P-7, a-57-C	2323.5	sandy	qtz. druse with embedded kaol., kaol. pore-fill					
			congl.	sid. rims, qtz. og., qtz druse					
texturally early carbonate									
202	7-30-69-11	2122.7	v.f.g.sst.	ankerite cement					
218	93-P-6, b-24-B	2282.0	siltstone	grains floating in Fe-calcite cement, no qtz.og.					

\* abbreviations: sst.=sandstone, v.f.g.=very fine grained, f.g.=fine-grained, m.g.=medium grained, c.g.=coarse-grained  
 congl.=conglomerate, chl=chlorite, qtz=quartz, kaol=kaolinite, qtz o.g.=quartz overgrowths, k.feld=k-feldspar,  
 sid=siderite, alt.=altered, dissol=dissolution, plag=plagioclase, feld-rich=abundant feldspar

### Figure 3.3

(a) Thin section photomicrograph showing remnants of hematite (Fe, arrow). Hematite was present before precipitation of quartz overgrowths occurred, which in turn, were precipitated before calcite cement. Plane polarized light. Falher (6-28-69-12 W6, 2139.4 m). Field of view is 0.83 mm.

(b) Thin section photomicrograph showing rims of siderite (arrow) coating detrital quartz grains. Siderite rims are overlain by quartz overgrowths. Plane polarized light. Falher (11-4-70-11 W6, 1988.3 m). Field of view is 0.42 mm.

(c) Thin section photomicrograph of pore-filling siderite (sid) which has been partially replaced by calcite in a conglomerate. Plane polarized light. Falher (6-28-69-12 W6, 2139.4 m). Field of view is 2.1 mm.

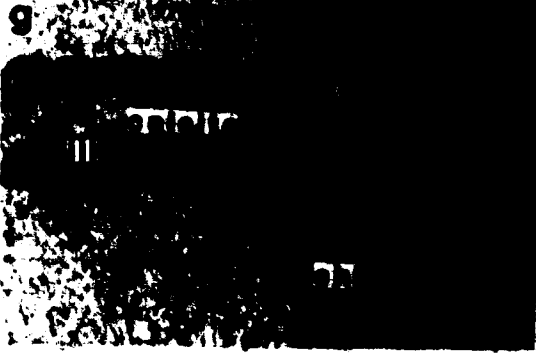
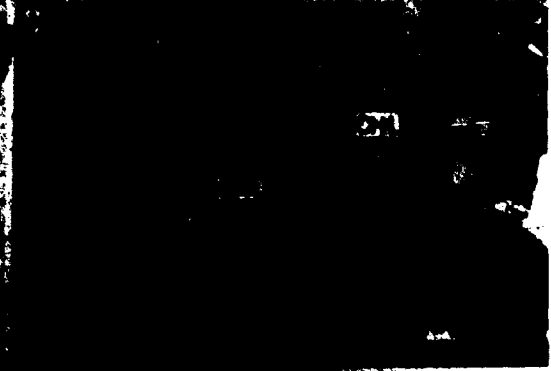
(d) SEM photomicrograph of chlorite (CHL) coating grains and filling the pore space. Falher (7-15-72-12 W6, 1817.5 m).

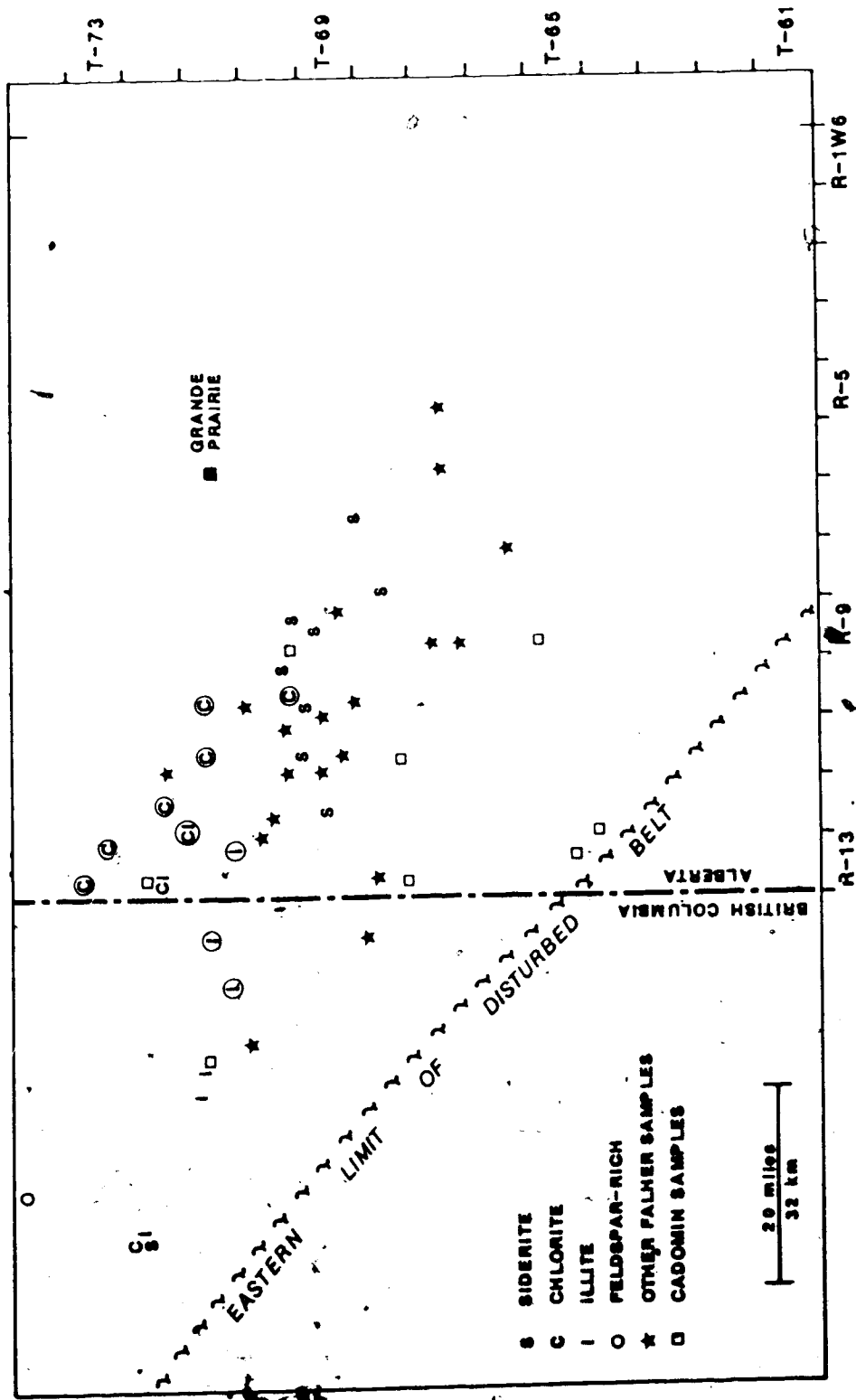
(e) Thin section photomicrograph of pore-rimming chlorite which is overlain by authigenic quartz (q, qtz). The remaining pore space is filled by calcite cement (calc). Plane polarized light. Falher (10-28-71-11 W6, 1858.3 m). Field of view is 0.42 mm.

(f) SEM photomicrograph of chlorite (CHL) partially embedded in authigenic quartz. Pyrite (PY) formed after some quartz precipitation but also inhibited its growth. Falher (10-28-71-11 W6, 1851.7 m).

(g) Thin section photomicrograph of chlorite pore rims (chl, arrow) coated by illite (ill). The remaining pore space is filled by calcite. Plane polarized light. Falher (10-28-71-11 W6, 1858.3 m). Field of view is 0.42 mm.

(h) Thin section photomicrograph showing chlorite rims (arrow), illite (ill) and calcite (calc) under crossed nicols. Falher (10-28-71-11 W6, 1858.3 m). Field of view is 0.42 mm.





**Figure 3.4** Geographic distribution of Falher and Cadomin samples. The symbols S, C, and I indicate the location of samples in which siderite, chlorite or illite, respectively, were observed. The locations of feldspar-rich samples are indicated by circles. Chlorite is commonly present in these samples.

conglomerates occurs in small clusters coated by authigenic quartz crystals and as a partially dissolved pore-filler, largely replaced by calcite (Figure 3.3c). In the Cadomin, siderite occurs as an early pore-filler in the sandy matrix of bimodal conglomerates.

Only siderite cement from one Falher conglomerate could be separated in sufficient quantities for isotopic analysis; it has  $\delta^{18}\text{O} = +16.5$  ‰ and  $\delta^{13}\text{C}_{\text{PDB}} = -0.1$  ‰ (Table 3.2). Data for siderite concretions in the Cadotte Member of the Reace River Formation suggest that  $\delta^{18}\text{O}$  for early siderite is as high as  $+19.6$  ‰. One sample of siderite from the Cadomin has a comparable  $\delta^{18}\text{O}$  value ( $+20.1$  ‰, Table 3.3).

### *Chlorite*

Chlorite was observed most often in Falher samples north of township 71 (Figure 3.4). It occurs as pore rims (Figures 3.3d,e and g) and clusters filling pores (Figure 3.3d). Chlorite is most common in feldspar-rich sandstones although it also occurs in quartz-rich samples. Trace amounts of volcanic rock fragments are preserved in most samples containing chlorite and in at least some samples chlorite has partially replaced these rock fragments. Chlorite crystallization preceded the formation of both authigenic quartz (Figures 3.3e and f) and illite (Figures 3.3g and h) which both formed before calcite cement. Pyrite formed before authigenic quartz (Figure 3.3f) at approximately the same time as chlorite.

Calculated  $\delta^{18}\text{O}$  values for chlorite range from  $+4.3$  to  $+7.8$  ‰ (Table 3.2, see analytical methods). Chlorites in samples N3888 and N4046 are the most  $^{18}\text{O}$ -enriched. Chlorite in these samples occurs as grain replacements and pore-filling clay, respectively, instead of the more common pore rims.

TABLE 3.2 ISOTOPE DATA FOR THE FALHER MEMBER

SAMPLE	LOCATION	DEPTH (m)	ROCK TYPE*	DESCRIPTION*	$\delta^{18}\text{O}$ (SMOW)	$\delta\text{D}$ (SMOW)
<b>CHLORITE</b>						
N4076	7-29-71-10W6	1768.0	f.g. sst.	55chl, 27K, 18I, 0ML	3.8	
N3687	10-28-71-11W6	1855.5	v.f.g. sst.	47chl, 26K, 24I, 3ML	1.8	
N3688	10-28-71-11W6	1858.3	m.-c.g. sst.	58chl, 26K, 14I, 3ML	3.4	
N4039	11-5-72-12W6	1885.2	v.f.g. sst.	31chl, 38K, 32I	4.9	
N3942	10-19-72-13W6	1955.3	v.f.g. sst.	59chl, 26K, 15I, 0ML	4.4	
N3888	7-13-73-13W6	1723.2	v.f.g. sst.	61chl, 0K, 27I, 12ML	7.1	
N4046	6-32-73-13W6	1763.4	v.f.g. sst.	75chl, 0K, 23I, 1ML	6.5	
<b>QUARTZ</b>						
196	7-30-69-11W6	2101.3	congl.	hand picked	16.3	
290	11-31-71-13W6	1996.0	congl.	hand picked	15.5	
237	93-P-1, b-28-L	2348.1	congl.	hand picked	15.4	
291	93-P-1, c-40-F	2414.5	congl.	hand picked	15.0	
177	11-4-70-11W6	1975.4	v.f.g. sst.	chem & sieve	16.6	
178	11-4-70-11W6	1988.3	v.f.g. sst.	chem & sieve	18.4	
n3685	10-28-71-11W6	1851.2	v.f.g. sst.	chem & sieve	15.8	
249	93-P-1, a-57-C	2301.0	v.f.g. sst.	chem & sieve	14.7	
224	93-P-1, c-12-L	2338.6	v.f.g. sst.	chem & sieve	14.5	
<b>DICKITE</b>						
348	11-5-69-7W6	1864.5	congl.	dickite	10.3	-131.0
419	11-4-69-10W6	2035.2	congl.	dickite	11.0	
196	7-30-69-11W6	2101.3	congl.	dickite	10.6	
200	7-30-69-11W6	2117.1	congl.	dickite	10.3	-104.0
188	10-1-70-11W6	1981.4	congl.	dickite		-113.0
206	7-12-70-11W6	1951.6	congl.	dickite	11.0	-115.0
182	11-4-70-11W6	2006.0	congl.	dickite	12.3	-108.0
220	93-P-7, a-57-C	2321.3	congl.	dickite	10.7	
n3535	7-9-70-10W6	1908.7	v.f.g. sst.	55K, 34I, 4C, 7ML	11.4	
n3539	7-9-70-10W6	1940.7	m.g. sst.	79K, 13I, 4C, 3ML	10.6	
n4991	6-5-71-10W6	1785.0	f.g. sst.	74K, 15I, 5C, 5ML	11.4	
<b>ILLITE</b>						
249	93-P-1, c-12-L	2301.0	f.g. sst.	I+ISII < 15% S	11.0	
251	93-P-1, c-12-L	2306.0	v.f.g. sst.	I+ISII < 15% S	11.3	
242	93-P-1, b-28-L	2353.4	v.f.g. sst.	I+IS > 15% S	10.6	
224	93-P-7, a-57-C	2338.6	v.f.g. sst.	I+IS 25% S	10.5	
n3638	93-P-1, a-85-G	2286.0		93I, 3K, 1C, 3ML	8.8	
n4520	93-P-1, c-16-I	2151.3	f.g. sst.	59I, 20K, 7C, 14ML	10.5	
n4250	93-P-16, b-28-I	2502.5		53I, 24K, 9C, 14ML	10.6	
n4047	11-12-71-13W6	2026.6	f.g. sst.	77I, 3K, 8C, 12ML	10.7	
n4030	11-5-72-12W6	1879.1	v.f.g. sst.	59I, 23K, 18C	11.4	
n4040	11-5-72-12W6	1890.8	m.-c.g. sst.	60I, 10K, 10C, 20ML	9.7	
n4041	11-5-72-12W6	1894.9	f.g. sst.	70I, 10K, 4C, 16ML	10.1	
n5095	10-19-72-13W6	1941.9		78I, 2K, 6C, 12ML	7.6	

TABLE 3.2 cont. ISOTOPE DATA FOR THE FALHER MEMBER

SAMPLE	LOCATION	DEPTH (m)	ROCK TYPE*	DESCRIPTION*	$\delta^{18}\text{O}$ (SMOW)	$\delta^{13}\text{C}$ (PDB)
<b>SIDERITE</b>						
351	6-28-69-12W6	2139.4	congl.	67S,27C,4A,2D	17.9	-0.1
Siderites from the Cadotte Formation						
298	14-18-74-12W6	1460.2	v.f.g.sst.	siderite grain rims	20.1	-2.2
301	14-18-74-12W6	1460.2	v.f.g.sst.	concretion	21.0	4.4
327	10-7-68-13W6	2487.0	v.f.g.sst.	92S,8D concretion	19.8	3.1
<b>CALCITE</b>						
218	93-P-6, b-24-B	2282.0	silt	early micro-cryst. Fe-calcite	11.2	-9.1
252	93-P-7, a-48-J	1997.9	congl.	macro-cryst. Fe-calcite	11.2	-2.2
236	93-P-1, b-28-L	2348.4	congl.	macro-cryst.	10.8	-3.1
369	6-28-68-13W6	2552.7	congl.	macro-cryst.	10.8	-7.6
414	11-30-69-10W6	1995.6	congl.	macro-cryst.	11.2	-1.9
N4751	10-16-69-11W6	2088.0	congl.	cement	11.6	-5.2
351	6-28-69-12W6	2139.4	congl.	macro-cryst.	11.2	-1.4
353	6-28-69-12W6	2141.5	congl.	cement	11.2	2.8
423	6-7-70-11W6	1981.8	congl.	macro-cryst.	12.3	7.3
424	6-7-70-11W6	1980.9	congl.	meso-cryst. after sid.	12.2	9.7
403	6-21-70-12W6	1979.4	congl.		11.8	-2.1
N4480	11-30-70-12W6	2021.5	congl.	macro-cryst.	11.8	-4.6
377	6-18-72-11W6	1782.0	congl.	macro-cryst.	12.5	-2.9
359	11-13-66-8W6	2556.0	congl.	late micro-cryst.	23.4	1.4
366	6-8-67-9W6	2389.9	congl.		23.6	1.9
N4028	11-5-72-12W6	1870.0	f.g. sst.	micro-meso	11.6	-7.1
N4518	93-P-1, c-16-l	2148.6	m.g. sst.	macro-cryst. Fe-calcite	11.5	-4.6
224	93-P-7, a-57-C	2338.6	v.f.g. sst.	meso-cryst. 54C,39D,7A	14.1	-2.6
N3640	93-P-1, a-85-G	2295.0	m.g. sst.	micro-meso	14.2	2.1
DC100	6-2-68-4W6	1707.0	m.g. sst.	72C,19D,9A	14.6	-0.3
<b>ANKERITE</b>						
202	7-30-69-11W6	2122.7	v.f.g.sst.	ankerite	14.7	-1.0
178	11-4-70-11W6	1988.3	v.f.g.sst.	73A,26D,1C	15.0	4.5
	6-2-68-4W6	1720.0	congl.sst.	79A,14S,7C	14.7	-2.8
	11-13-66-8W6	2566.0	f.g.sst.	51A,46D,3S	15.7	-0.6
<b>DOLomite</b>						
	10-20-67-5W6	1910.5	v.f.g.sst.	97D,3S	22.4	-1.7
	7-20-67-6W6	2003.6	v.f.g.sst.	68D,20A,12C	22.0	-0.9
	10-29-67-10W6	2397.0	f.g.sst.	79D,11A,10S	22.0	-1.0
	10-13-69-9W6	1867.0	v.f.g.sst.	70D,15A,15S	17.1	-0.5

Abbreviations: sst.=sandstone, v.f.g.=very fine grained, f.g.=fine-grained, m.g.=medium-grained, c.g.=coarse-grained, congl.=conglomerate  
chem& sieve = quartz separate prepared using the method of Syers et al.(1968);  
Jackson (1979) and Lee and Savin (1985)  
K=kaolinite, I=illite, C=chlorite, S=siderite, ML=mixed layer I/S



TABLE 3.3 ISOTOPE DATA FOR THE CADOMIN FORMATION

	LOCATION	DEPTH (m)	ROCK TYPE*	Th*	$\delta^{18}\text{O}$ (SMOW)	$\delta^{13}\text{C}$ (PDB)
<b>Siderite</b>						
339	10-8-70-9W6	2204.0	sandy congl.		20.1	-3.6
<b>Quartz</b>						
293	6-16-68-11W6	2631.0	congl.	85°C	18.2	
292	5-32-65-9W6	3188.0	congl.	151°C	18.9	
372	7-27-72-13W6	2298.0	congl.		18.5	
<b>Kaolinite</b>						
266	16-31-64-12W6	3316.5	congl.		14.0	$\delta\text{D}$ (SMOW) -104
292	5-32-65-9W6	3188.0	congl.		12.2	-102
267	9-11-65-13W6	3248.0	congl.		14.2	-96
293	6-16-68-11W6	2631.0	congl.		13.3	
337	10-8-70-9W6	2197.9	congl.		13.7	-93
373	7-27-72-13W6	2298.3	congl.			-93
255	93-P-1,c-12-L	2727.9	congl.		13.6	
<b>Illite</b>						
338	10-8-70-9W6	2201.6	sandstone		16.4	
318	10-7-68-13W6	2988.6	sandstone		16.0	

\*Abbreviations: congl.=conglomerate, Th=homogenization temperature of fluid inclusions.

### ***Dolomite***

Dolomite is common only in very fine grained sandstones of the Falher where it occurs as single crystal or polycrystalline grains. Remnants of silica within some grains suggest that at least some dolomite is a diagenetic grain replacement.

Most dolomite in the Falher has  $\delta^{18}\text{O} = +22$  ‰ (Table 3.2). Similar values have been reported for dolomite in the Bluesky Formation (Chapter 4) and for Lower Cretaceous diagenetic dolomite from the Viking Formation, southern Alberta (Longstaffe and Ayalon, in press). In contrast, unaltered detrital dolomite from Cretaceous sandstones in southern Alberta have higher  $\delta^{18}\text{O}$  values of +26 to +28 ‰ (Longstaffe 1983, 1984, unpublished data).

### ***Pyrite***

Pyrite is present only in minor amounts and its relative timing is difficult to determine. Its textural relationship with respect to chlorite and quartz in the Falher (Figure 3.3f) suggests that at least some pyrite formed before the cessation of quartz overgrowth formation.

### ***Feldspar Diagenesis***

The minor amount of feldspar (<2%) in the Falher occurs as skeletal K-feldspar in various stages of dissolution, and as albite. Feldspar diagenesis is important only in the rare feldspar-rich sandstones. In these, albite overgrowths have formed on partially dissolved K-feldspar (Figure 3.5a); most feldspars showing polysynthetic twinning are now albite. A few grains of plagioclase (An<sub>30</sub>), with only minor alteration to albite, are present in one sample. Secondary pore space defined by the preservation of albite rims and cleavage planes is sometimes filled by kaolinite (Figure 3.5b) followed by calcite cement. Illite commonly occurs associated with albite (Figure 3.5c).

**Figure 3.5**

(a) Back-scatter electron photomicrograph of an albite overgrowth (alb, dark grey areas) on partially dissolved K-feldspar (kfeld, medium-grey areas). The lightest grey area surrounding the feldspar grain is calcite. Falher (11-5-72-12 W6, 1890.8 m).

(b) Back-scatter electron photomicrograph of the skeletal structure of an albitized feldspar grain filled by authigenic kaolinite (kaol, k). Thin dark areas are albite (arrow). The white zones within and surrounding the feldspar grain are calcite. Falher (11-5-72-12 W6, 1890.8 m).

(c) SEM photomicrograph of albite (ALB) surrounded by illite (ILL). Falher (6-5-71-10 W6, 1795 m).

(d) SEM photomicrograph of illite (ILL) coating authigenic quartz (Q) and undifferentiated feldspar (FELD). Falher (11-4-70-11 W6, 1975.4 m).

(e) SEM photomicrograph of illite (ILL) occurring in sandstone laminae. The platy and hairlike texture of the illite appears authigenic rather than detrital. Falher (93-P-1, c-12-L, 2306 m).

(f) SEM photomicrograph of illite coating authigenic kaolinite in a Cadomin sandstone. Cadomin (10-7-68-13 W6, 1988.6 m).



### Illite

Illite occurs as an intermediate-stage diagenetic cement in minor amounts in almost all Falher samples. It is also present as an abundant pore-filling phase in some feldspar-rich sandstones. Illite occurs after chlorite but before calcite (Figures 3.3g and 3.3h) in feldspar-rich sandstones and after some authigenic quartz in quartzose sandstone (Figure 3.5d).  $\delta^{18}\text{O}$  values for Falher illite (all samples from the westernmost part of the study area; see Figure 3.4) range from +10.5 to +11.3 ‰ (Table 3.2). This illite occurs as delicate hair-like to platy masses in laminae between grains (Figure 3.5e). The data base for illite can be extended by including eight more illite-rich clay mixtures.  $\delta^{18}\text{O}$  values for these samples range from +7.6 to +11.4 ‰ (Table 3.2). Since kaolinite has a composition of +10 to +11 ‰ (Table 3.2), its inclusion in these samples does not significantly affect the illite isotope value. Some of these samples are from feldspar-rich sandstones, where illite ( $\delta^{18}\text{O}=+9.7$  to  $+10.7$  ‰) occurs as a pore-filling clay before calcite (Figure 3.3e & 3.3f). These values are in the same range as the illite occurring in laminae.

In the Cadomin, illite commonly overlies diagenetic kaolinite in sandstones (Figure 3.5f), but illite is not commonly associated with late-stage dickite in Cadomin conglomerates. This distribution of illite suggests that kaolinite in sandstones is an early phase overlain by an intermediate stage of illite precipitation. Dickite in conglomerates precipitated after illite. The  $\delta^{18}\text{O}$  value for Cadomin illite in sandstones is about +16 ‰ (Table 3.3), a value significantly more  $^{18}\text{O}$ -enriched than that of the Falher illite.

### Quartz

The formation of quartz overgrowths occurred in virtually all samples where sand-size, detrital quartz grains were present, unless the sandstone was first cemented by a very early diagenetic carbonate phase. In many quartz-rich sandstones, silica precipitation continued until the pore space became totally cemented. The  $\delta^{18}\text{O}$  value for chemically-separated quartz

overgrowths from one Falher sandstone is +18.4 ‰ (Table 3.2). Ankerite cement postdates the quartz overgrowths in this sample.

In both Falher and Cadomin samples, where chert and pore space were abundant, prismatic authigenic quartz crystals (quartz druse) (Figure 3.6a) are common. These crystals can range in size from a few micrometers up to a few millimeters in length in the coarser conglomerates. In the Falher, the largest and most abundant quartz druse is found in grain fractures and large open pores in conglomerates in the westernmost part of the study area. Towards the east, quartz druse is still present in some conglomerates but crystals are significantly

Textural relationships in both the Falher and Cadomin suggest that quartz druse precipitated relatively late during burial, after fracturing. The presence of dickite that is both embedded in the diagenetic quartz and resting on its surface (Figures 3.6b and c) suggests that dickite precipitated both before and after quartz druse.

$\delta^{18}\text{O}$  values for hand picked quartz druse from Falher and Cadomin conglomerates are significantly different: +15.0 to +16.3 ‰ (Table 3.2) for the Falher; and +18.2 to +18.9 ‰ for the Cadomin (Table 3.3). The degree of confidence for these values is high since the quartz crystals were hand picked to ensure that no detrital quartz was included.

### ***Bitumen***

Pyrobitumen fills the pore space after quartz druse in one sample (Figure 3.6b). In another sample, pores are lined by pyrobitumen and the remaining pore space is filled by calcite (Figure 3.6c).

**Figure 3.6**

(a) Thin section photomicrograph of prismatic quartz crystals (quartz druse, Q) lining the pore (P) and partially filling a large pore space in a Falher conglomerate. Plane polarized light.

Falher (93-F-1, b-28-L, 2348.1 m). Field of view is 3.3 mm.

(b) Thin section photomicrograph of quartz druse (Q) lining a pore space. The black material (BIT) filling the pore space after quartz druse is pyrobitumen. Plane polarized light. Falher (6-1-70-10 W6, 1861 m). Field of view is 0.83 mm.

(c) Thin section photomicrograph of pores lined by pyrobitumen (BIT, arrow). The pore space is filled by calcite (CALC). Plane polarized light. Falher (6-21-70-12 W6, 1977.5 m). Field of view is 3.3 mm.

(d) SEM photomicrograph of dickite (K) partially embedded in authigenic quartz (QTZ) and also resting on its surface. Falher (11-4-70-11 W6, 2000.7 m).

(e) Thin section photomicrograph of dickite embedded in authigenic quartz (QTZ). Dickite (KAOL) also fills the surrounding pore space. Plane polarized light. Falher (7-30-69-11 W6, 2113.2 m). Field of view is 0.83 mm.

(f) Thin section photomicrograph of late-stage ankerite cement (A) which fills the pore space after siderite rims (arrow) and quartz overgrowths. Plane polarized light. Falher (11-4-70-11 W6, 1988.3 m). Field of view is 0.83 mm.

(g) Thin section photomicrograph of texturally early ankerite cement (C). Quartz overgrowths are notably absent. Plane polarized light. Falher (7-30-69-11 W6, 2122.7 m). Field of view is 0.83 mm.

(h) Thin section photomicrograph of calcite cement filling the pore space after quartz druse (qtz). Plane polarized light. Falher (11-4-70-11 W6, 1999.3 m). Field of view is 2.1 mm.





### *Kaolinite*

Dickite is abundant as a late diagenetic pore-filling clay in the coarser-grained sandstones and conglomerates in both the Falher and Cadomin. It occurs together with authigenic quartz druse (Figures 3.6d and 3.6e) but more commonly fills large pores where quartz druse is absent.

$\delta^{18}\text{O}$  values for dickite, hand picked from pores in Falher conglomerates, range from +10.3 to +12.3 ‰ (Table 3.2).  $\delta^{18}\text{O}$  values for the three Falher sandstones in Table 3.2 represent clay mixtures which have a high proportion of kaolinite. These values fall within the same range as the dickite discussed above.  $\delta^{18}\text{O}$  values for dickite, hand picked from pores in Cadomin conglomerates, range from +12.2 to +14.0 ‰ (Table 3.3).  $\delta\text{D}$  values for Falher dickites range from -131 to -104 ‰ SMOW (Table 3.2);  $\delta\text{D}$  values for Cadomin dickites range from -104 to -93 ‰ SMOW (Table 3.3).

In Cadomin sandstones, kaolinite is commonly coated by illite (Figure 3.5f). The presence of illite coating kaolinite in sandstones but its absence on dickites in conglomerates suggests that there are two generations of kaolinite group minerals, early kaolinite in sandstones and dickite in porous conglomerates.  $\delta^{18}\text{O}$  values for kaolinite in Cadomin sandstones were not obtained due to separation difficulties.

### *Ankerite*

Ankerite is relatively rare in the Falher Member. It most commonly occurs as overgrowths on dolomite grains in very fine grained sandstones but also is found in sandstones as a relatively late stage cement after quartz overgrowths (Figure 3.6f) and as a texturally early cement (Figure 3.6g).

$\delta^{18}\text{O}$  values for Falher ankerite vary from +14.7 to +15.7 ‰ (Table 3.2). The composition of ankerite is  $(\text{Ca}_{1.06}\text{Mg}_{0.54}\text{Fe}_{0.29}\text{Mn}_{0.002})(\text{CO}_3)_2$  in sample 178 and

$(\text{Ca}_{1.08}\text{Mg}_{0.72}\text{Fe}_{0.19})(\text{CO}_3)_2$  in sample 202. The ankerite in sample 178 precipitated in a sandstone after both siderite and quartz overgrowths (Figure 3.6f), whereas the ankerite in sample 202 (Figure 3.6g) is texturally very early before any other authigenic phases. Both ankerites have essentially the same  $\delta^{18}\text{O}$  value but their  $\delta^{13}\text{C}$  values are significantly different (+4.5 versus -1.0 ‰ PDB, Table 3.2).

### Calcite

Calcite and Fe-rich calcite occur in the Falher most commonly as texturally late poikilotopic cements after grain fracturing, quartz druse (Figure 3.6h) and dickite. Calcite also rarely occurs as a texturally early microcrystalline cement (sample 218, Table 3.2).  $\delta^{18}\text{O}$  values for Falher calcite cements range from +10.8 to +23.7 ‰ (Table 3.2) but cluster into 3 distinct groups: (a) +10.8 to +12.3 ‰; (b) +14.1 to +14.6 ‰; and (c) +23.4 to +23.7 ‰.

The majority of Falher calcite cements fall into Group A with an average value of +10.7 ‰ for the 15 samples. Texturally, the calcite varies from macrocrystalline to microcrystalline.  $\delta^{13}\text{C}$  values vary from -9 to +9 ‰ (PDB) in Group A calcites. Texturally early calcite cement has the same  $\delta^{18}\text{O}$  value as the texturally late cement but its  $\delta^{13}\text{C}$  value is low (-9 ‰ PDB). The similarity in  $\delta^{18}\text{O}$  values suggests that texturally early calcite is actually recrystallized calcite cement or a replacement of early siderite cement with the  $\delta^{13}\text{C}$  value inherited from the precursor cement. Group B is represented by three, very fine grained and medium-grained sandstones with micro- to meso-crystalline calcite cement.  $\delta^{13}\text{C}$  values range from -2.6 to +2.1 ‰ PDB (Table 3.2). Although calcite in feldspar-rich sandstones may be related to plagioclase dissolution, their  $\delta^{18}\text{O}$  values fall into both Groups A and B. The two calcite cements comprising Group C are microcrystalline and occur in the pore space of conglomerates after quartz druse.  $\delta^{13}\text{C}$  values are +1.4 to +1.9 ‰ PDB (Table 3.2).

Calcite was found in only one Cadomin sample in insufficient quantity for isotopic analysis.

Calcite occurs in fractures within chert pebbles; the sand matrix is cemented by early siderite.

### Paragenetic Sequence - Summary

#### *Falher Member*

The general paragenetic sequence for the Falher, as determined from a compilation of all petrographic evidence for the study area, is presented in Figure 3.7a. Hematite was probably the earliest diagenetic phase formed under oxidizing conditions soon after deposition. As the sediments passed into reducing conditions, either siderite or chlorite formed depending on the local chemical environment. Siderite generally formed in the southern part of the study area and chlorite in the north. This geographic distribution of early phases corresponds to the west-east trending shoreline with the sea to the north (Rahmani, 1984; Smith et al., 1984) and implies that siderite precipitation required fresher water than chlorite precipitation. Rare, texturally early, calcite and ankerite cements may have precipitated early but may also represent recrystallized siderite. Grain replacement by dolomite, and pyrite formation also appear to have occurred during early diagenesis. The precipitation of quartz overgrowths on sand grains was probably the next diagenetic stage and continued slowly until pore space was filled. Feldspar dissolution, illite precipitation and albitization apparently took place during an intermediate stage of diagenesis and was completed at least before calcite cementation. As burial and compaction continued, chert grains fractured and pressure solution occurred in the unimodal conglomerates. The formation of authigenic quartz crystals was accompanied by the precipitation of pore-filling dickite. A rim of bitumen was deposited on quartz crystals at this stage. Petroleum which filled pore spaces at this time must have been drained, leaving only a rim of bitumen, and the reopened pore space was later filled by calcite. Dickite continued to fill pore space after precipitation of quartz druse. Finally, pure calcite and Fe-rich calcite were precipitated in local remaining pore spaces.

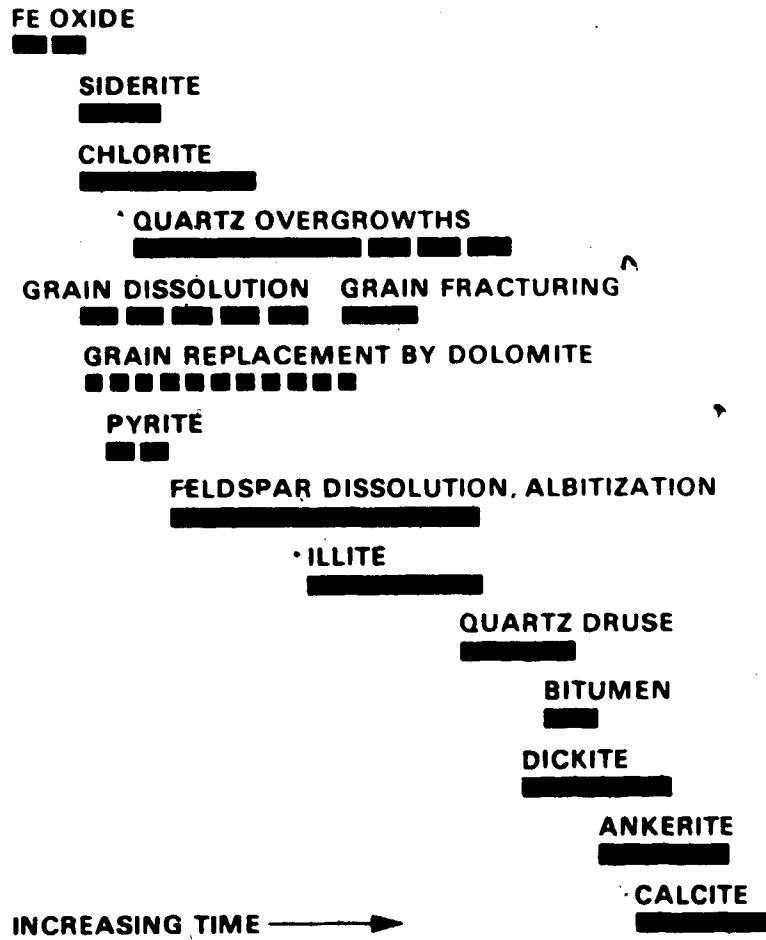


Figure 3.7 (a) General diagenetic sequence for the Falher Member.

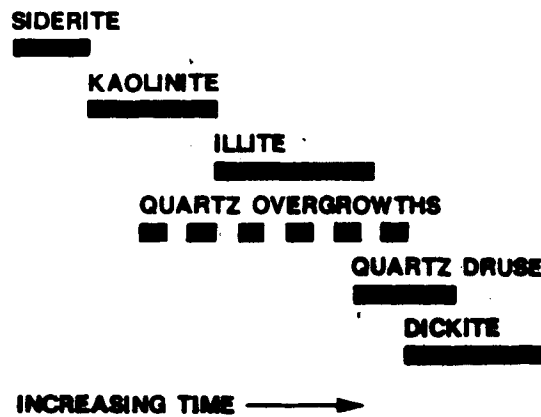


Figure 3.7 (b) General diagenetic sequence for the Cadomin Formation.

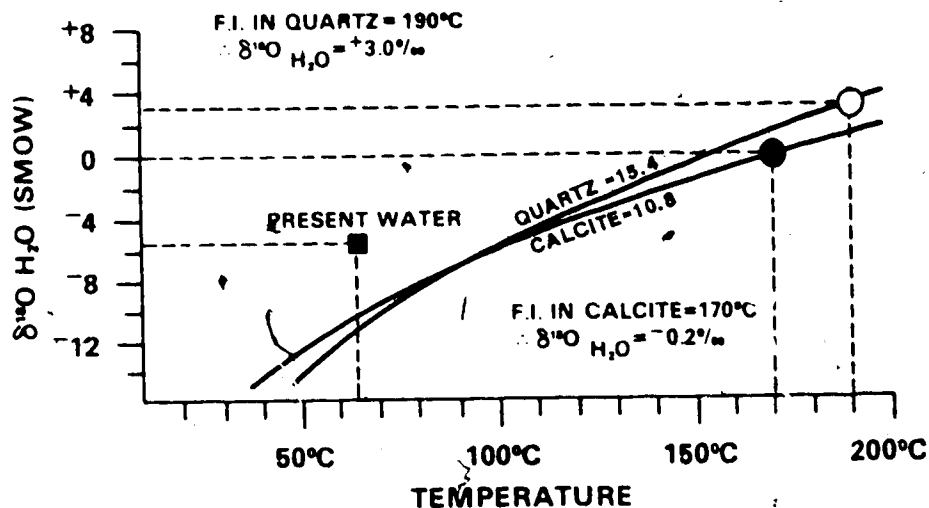
### ***Cadomin Formation***

The diagenetic sequence for the Cadomin is similar to that of the Falher in that early siderite was followed by quartz overgrowths, quartz druse and dickite (Figure 3.7b). The presence of relatively early kaolinite, rare albite, and the lack of chlorite in the Cadomin probably reflects its simpler detrital mineralogy. The major differences between the Cadomin and the Falher are: (1) in the Cadomin, kaolinite was precipitated as a relatively early diagenetic phase before illite, as well as in the form of dickite as the last diagenetic phase; (2) intermediate to late diagenetic phases in the Cadomin (i.e. illite, quartz druse, dickite,) are significantly enriched in  $^{18}\text{O}$  relative to the Falher; and (3) the last diagenetic phase in the Falher is calcite or ankerite, whereas dickite is the last diagenetic phase in the Cadomin.

## **CONSTRAINTS ON DIAGENESIS AND POREWATER EVOLUTION**

### **Constraints on Late Porewater Evolution in Falher Conglomerates**

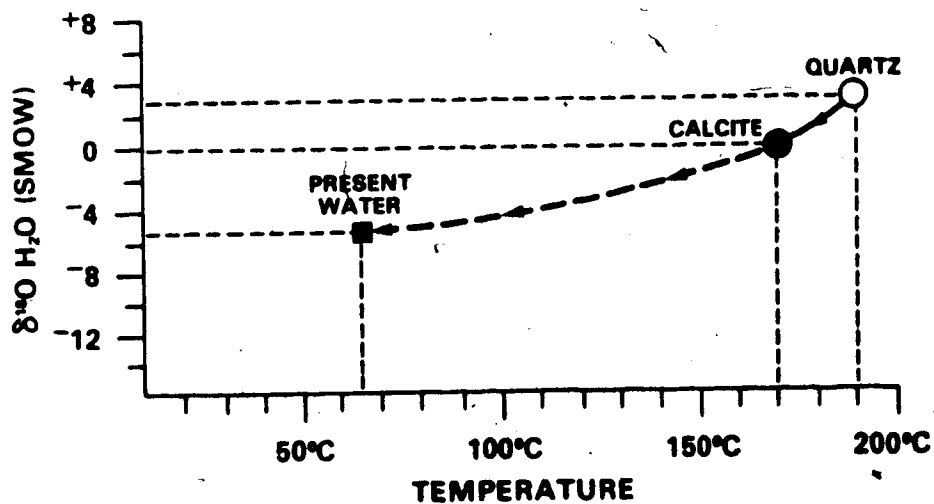
Porewater evolution during late-stage diagenesis in Falher conglomerates can be well-constrained by the data and is discussed first, in order to demonstrate the approach used to interpret the isotopic analyses of diagenetic minerals. Figure 3.8 is a plot of  $\delta^{18}\text{O}_{\text{porewater}}$  versus temperature for quartz druse with  $\delta^{18}\text{O}=15.4$  ‰ (sample 237, Table 3.2) and for calcite cement with  $\delta^{18}\text{O}=10.8$  ‰ SMOW (sample 236, Table 3.2). These  $\delta^{18}\text{O}$  values are considered here because of the availability of independent temperatures for precipitation from fluid inclusion data (Chapter 2). The two curves in Figure 3.8 represent all the possible combinations of  $\delta^{18}\text{O}$ -water compositions and temperatures which could produce diagenetic quartz or calcite with the measured  $\delta^{18}\text{O}$  values. Fluid inclusion analyses provide temperature data which can be used with the curves in Figure 3.8 to determine the  $\delta^{18}\text{O}$  value of the porewater which precipitated that mineral. Two points in the isotopic evolution of the porewater in the Falher can be determined (Figure 3.8):



**Figure 3.8**  $\delta^{18}\text{O}$  of porewater versus temperature for diagenetic quartz and calcite from Falher conglomerates. Mineral curves are shown for  $\delta^{18}\text{O}$  values of quartz and calcite from one well in the western part of the study area and the following equations ( $T = ^\circ\text{K}$ ):

- (1)  $10^3 \ln \alpha_{\text{quartz-H}_2\text{O}} = 3.38(10^6)T^{-2} - 2.90$ ; (Friedman and O'Neil, 1977; after Clayton et al., 1972)
- (2)  $10^3 \ln \alpha_{\text{calcite-H}_2\text{O}} = 2.78(10^6)T^{-2} - 2.89$ ; (Friedman and O'Neil, 1977; after O'Neil et al., 1969).

The white and black circles on the mineral curves are points in the isotopic evolution of porewaters based on fluid inclusion temperatures. The black square represents conditions of present formation waters.



**Figure 3.9** Idealized porewater evolution path ( $\delta^{18}\text{O}$  of water versus temperature) for late-stage diagenesis in Falher conglomerates. White (quartz) and black (calcite) circles are points determined using fluid inclusion temperatures. The black square represents conditions of present formation waters. The heavy dashed portion of the path represents porewater evolution in the updip water-saturated zone of the study area.

(1) Fluid inclusions from quartz druse with  $\delta^{18}\text{O}=+15.4$  ‰ SMOW (Table 3.2, sample 237) homogenize at 190°C (Chapter 2; Table 2.1). Therefore, quartz druse precipitated from porewater with  $\delta^{18}\text{O}=+3$  ‰ SMOW.

(2) Fluid inclusions in calcite cement with  $\delta^{18}\text{O}=+10.8$  ‰ SMOW (Table 3.2, sample 236) from the same locality as the quartz druse above, homogenize at 170°C (Chapter 2; Table 2.2). Therefore, this calcite precipitated from porewaters with  $\delta^{18}\text{O}=-0.2$  ‰ SMOW.

Because the diagenetic sequence (Figure 3.7a) indicates that quartz druse precipitated before calcite cement, the porewaters must have become depleted in  $^{18}\text{O}$  from  $\delta^{18}\text{O}=+3$  ‰ when quartz was formed, to  $-0.2$  ‰ when calcite precipitated. Figure 3.9 shows an idealized curve for porewater evolution during late diagenesis.

Present-day conditions provide additional constraints for late diagenesis (Figures 3.8 and 3.9). In most studies, the best known point in the evolution of porewater is its present-day composition, which can be analyzed directly. However, in this study, most wells available for sampling are gas-saturated with no moveable water. Most wells that tested positive for water during drill stem testing have been shut-in. As a consequence, the availability of water samples for isotopic analyses is very limited. This study must rely on the results of one isotopic analysis of a water sample, collected from the separator at the head of a well penetrating the Paddy Member of the Peace River Formation (Figure 3.2). This well produced 21 m<sup>3</sup> water/m<sup>3</sup> gas. The salinity of the water from this well, corrected for temperature and dilution by condensed water (Kharaka et al., 1985), is 26,989 mg/l (see Chapter 5);  $\delta^{18}\text{O}$  water =  $-5.7$  ‰ and  $\delta\text{D} = -97$  ‰. Salinities of waters from drill stem test analyses for the Falher and the Paddy are similar as are bottom hole temperatures, 60-70°C. Since the water salinities, mineralogy and diagenetic history of both the Falher and the Paddy are comparable, the isotopic composition of the analyzed Paddy water is probably representative of the Falher in water-saturated zones. The conclusion of Hitchon and Friedman (1969) that the isotopic composition of formation water in Alberta is strongly related to its

salinity supports this assumption that the  $\delta^{18}\text{O}$  value measured in the Paddy is similar to  $\delta^{18}\text{O}$  values of Falher waters with comparable salinities.

By the arguments above, the third point ( $\delta^{18}\text{O} = -5.7$  ‰ SMOW at  $65^\circ\text{C}$ ) in Figures 3.8 and 3.9 represents present-day formation water conditions in the Falher where porewater continued to be moveable. In these areas, the depletion trend continued down to the present  $\delta^{18}\text{O}$  of  $-5.7$  ‰ SMOW (Figure 3.9). In gas-saturated areas, it is probable that calcite precipitation was the last diagenetic event before water was driven out.

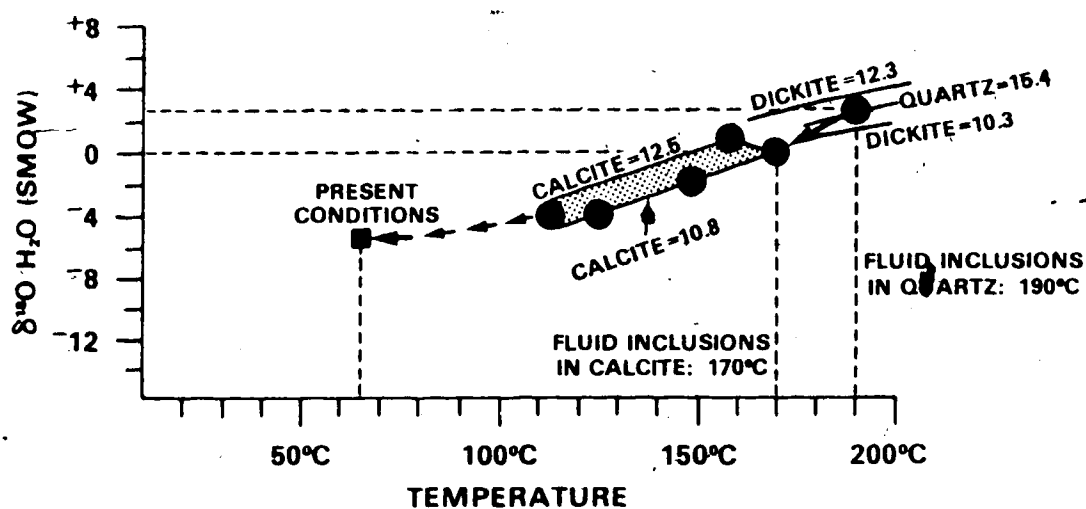
Dickite is another late diagenetic phase in the conglomerates.  $\delta^{18}\text{O}$  values for dickite range from  $+10.3$  to  $+12.3$  ‰. The high temperature portions of the dickite curves for these  $\delta^{18}\text{O}$  values are shown in Figure 3.10. The positions of the dickite curves support petrographic data which indicate that dickite formed both before and after quartz druse but before calcite cement. The  $10.3$  ‰ dickite precipitated at  $-180^\circ\text{C}$  from water lower in  $\delta^{18}\text{O}$  by at least  $2$  ‰ relative to water from which quartz druse precipitated.

The range in calcite  $\delta^{18}\text{O}$  values in Figure 3.10 is represented by the shaded band extending from  $113^\circ\text{C}$  to  $170^\circ\text{C}$ . The thickness of the band is determined by the position of the two  $\delta^{18}\text{O}$ -temperature curves defining the range of  $\delta^{18}\text{O}$  values for the majority of calcite cement. (The  $23$  ‰ calcite group is not shown here). The range of temperatures ( $113^\circ$  to  $168^\circ\text{C}$ ; Chapter 2) reflects homogenization temperatures of fluid inclusions in calcite cement. Dots within this bar represent individual samples where both stable isotopic and fluid inclusion data are available (Chapter 2, Table 2.2 and this Chapter, Table 3.2). Calcite precipitated from waters varying in  $\delta^{18}\text{O}$  from  $+1$  to  $-4$  ‰.

The data base is biased by the availability of quartz druse large enough to be hand picked in sufficient quantities. Suitable quartz druse is dominantly present in the westernmost townships



### FALHER CONGLOMERATES



**Figure 3.10** Idealized porewater evolution path ( $\delta^{18}\text{O}$  of water versus temperature) for late-stage diagenesis in Falher conglomerates. Higher temperature parts of curves are shown for maximum and minimum  $\delta^{18}\text{O}$  values of dickite and the majority of calcites using the following equations ( $T = ^\circ\text{K}$ ):

(1)  $10^3 \ln \alpha_{\text{kaolinite-H}_2\text{O}} = 2.5(10^6)T^{-2} - 2.87$ ; (Land and Dutton, 1978; Eslinger, 1971)

(2)  $10^3 \ln \alpha_{\text{calcite-H}_2\text{O}} = 2.78(10^6)T^{-2} - 2.89$ ; (Friedman and O'Neil, 1977; after O'Neil et al., 1969).

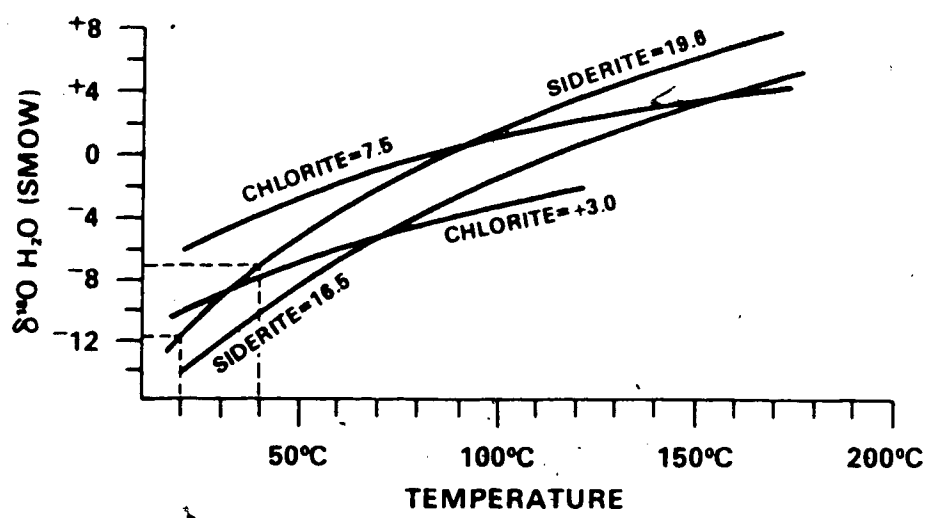
The shaded band extending from 113° to 170°C represents the range in conditions under which calcite precipitated. Dots within this band represent individual samples where both stable isotope and fluid inclusion data are available.

of Alberta and in eastern British Columbia. Sample 196 (Table 2.1, Figure 2.5 in Chapter 2) indicates that fluid temperatures in the eastern area (approx. 140°C) were lower than those in the west (approx. 170-195°C). Individual crystals of quartz druse in sample 196 (located to the east of other quartz samples) are significantly finer-grained than quartz druse in the other three samples analyzed for  $\delta^{18}\text{O}$  and this is apparently reflected in its slightly higher  $\delta^{18}\text{O}$  value (+16 ‰ in contrast to +15 ‰). The higher value and finer grain size suggest that it formed at slightly lower temperatures from less silica-enriched solutions.

### Early Diagenesis

Textural relationships in Falher sandstones and conglomerates suggest that siderite, chlorite, some calcite and some ankerite are early diagenetic phases. However, before attempting to determine the isotopic composition of early porewater from the isotopic data for diagenetic minerals, it is essential to evaluate the possibility of recrystallization or isotopic re-equilibration of the minerals with the evolving porewater (O'Neil, 1987; Longstaffe, 1987). If either late recrystallization or isotopic re-equilibration of a mineral occurred, the measured isotopic signature of that mineral is not representative of early porewaters; rather it is indicative of the later porewater involved in its alteration.

Siderite is a common, texturally early cement. Within the Falher, siderite in a conglomerate has been largely replaced by late calcite (Figure 3.3c). Dissolution of siderite from early concretions in the Cadotte created secondary porosity which was partially filled by quartz druse. The dissolution and replacement textures of siderite suggest that simple recrystallization of siderite does not occur. Instead, siderite is dissolved and a different mineral precipitates in its place. Any siderite preserved is probably original siderite that has not recrystallized. An approximation for the porewater composition during early stages of diagenesis can be made using the isotopic composition of siderite. Figure 3.11 shows the two  $\delta^{18}\text{O}_{\text{water}}$  temperature curves



**Figure 3.11**  $\delta^{18}\text{O}$  of porewater versus temperature for diagenetic siderite and chlorite from Falher and Cadotte Members. Mineral curves are shown for the maximum and minimum  $\delta^{18}\text{O}$  values of each phase using the following equations ( $T=^{\circ}\text{K}$ ):

- (1)  $10^3 \ln \alpha_{\text{siderite-H}_2\text{O}} = 2.9(10^6)T^{-2} - 2.80$ ; (Becker and Clayton, 1976);
- (2)  $\Delta^{18}\text{O}_{\text{chlorite-H}_2\text{O}} = 1.56(10^6)T^{-2} - 4.7$ ; (Wenner and Taylor, 1971).

The 16.5 ‰ value for siderite is probably low due to contamination from calcite.

for siderite,  $\delta^{18}\text{O}$  siderite = +16.5 ‰ and +19.6 ‰, representing the range of values for siderite in the Falher and Cadotte. The +16.5 ‰ value is for siderite in a Falher conglomerate where siderite is partially replaced by calcite. The measured  $\delta^{18}\text{O}$  value is probably low due to contamination from calcite. The +19.6 ‰ value for siderite is considered more reliable. Siderite commonly forms in the methanic zone during early diagenesis (Gauthier, 1983), probably in the temperature range 20-40°C. At these temperatures, the porewater composition responsible for the measured  $\delta^{18}\text{O}$  value for siderite (+19.6 ‰) must have been in the range of -12 ‰ to -7 ‰. Such low  $\delta^{18}\text{O}$  values may represent meteoric to brackish water during the Lower Cretaceous.

Texturally early ankerite and calcite cements have the same  $\delta^{18}\text{O}$  value as the texturally late cements ( $\delta^{18}\text{O}$  = +14.7 ‰ for ankerite, sample 202; and  $\delta^{18}\text{O}$  = +11.2 ‰ for calcite, sample 218, Table 3.2). These texturally early cements are microcrystalline in contrast to the late cements which are most commonly macrocrystalline. Two origins for the  $\delta^{18}\text{O}$  values of the texturally early calcite and ankerite cements are possible: (1) calcite and ankerite cements were precipitated very early at 20-40°C from porewaters with  $\delta^{18}\text{O}$  = -19 to -14 ‰ and have retained their original isotopic signatures; or (2) calcite or ankerite present now is the product of recrystallization of an earlier carbonate cement and reflects the isotopic composition of the water at the time of recrystallization. Because of these contradictory possible origins for the texturally early calcite and ankerite cements, the use of their  $\delta^{18}\text{O}$  values as an indication of early porewater composition is not reliable. The porewater composition is lower than that indicated by the siderite (-19 to -14 ‰ in contrast to -12 to -7 ‰). These calcite and ankerites may be a recrystallization product of early siderite, thus accounting for the Fe-rich nature of these cements.

Textural relationships and isotopic analyses for illite suggest that recrystallization of detrital illite or illite/smectite might have occurred. Some illite in the Falher has delicate diagenetic textures (Figure 3.5e) even though its position in laminae suggests a detrital origin. The  $\delta^{18}\text{O}$

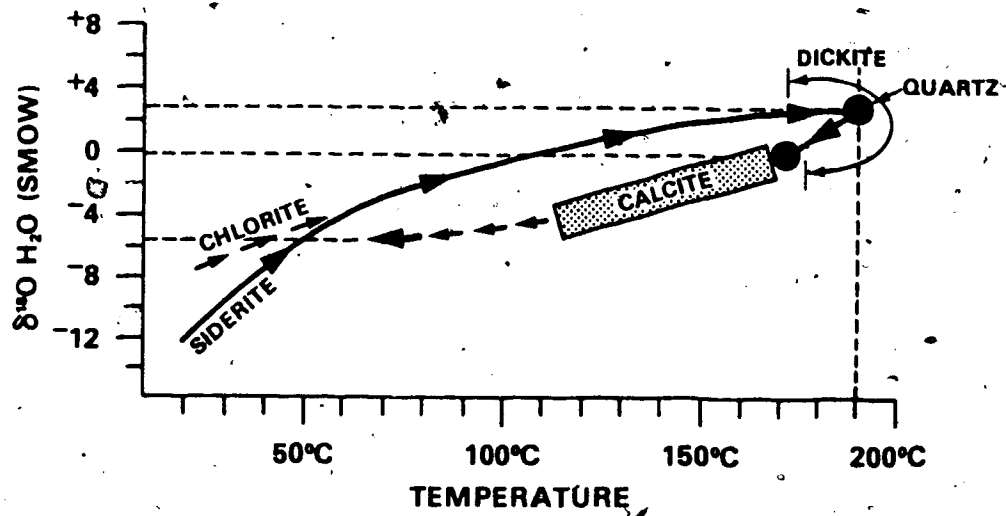
value of this illite is the same as the  $\delta^{18}\text{O}$  values of illite precipitated at an intermediate (high temperature) stage during diagenesis. This similarity in  $\delta^{18}\text{O}$  values and the petrographic relationships suggest that detrital illite was recrystallized at high temperatures, possibly as a result of a smectite to illite transition.

To summarize, calcite and ankerite, which texturally appear to be early cements, are most likely the product of recrystallization of earlier carbonate cements. Some of the illite has also been recrystallized. In contrast, siderite has retained its original isotopic composition and precipitated from porewaters with  $\delta^{18}\text{O} = -12$  to  $-7$  ‰.

The curves representing the range of  $\delta^{18}\text{O}$  values for chlorite in the Falher are also shown in Figure 3.11. Texturally early chlorite and siderite in the Falher are geographically mutually exclusive: siderite in the south, chlorite in the northern more marine setting (Figure 3.4) (Rahmani, 1984; Smith et al., 1984). This geographic relationship suggests that siderite formed from meteoric-dominated water, whereas chlorite formed from marine-dominated water. The early, grain-coating chlorite has low  $\delta^{18}\text{O}$  values (approx.  $+4$  ‰), whereas the grain-replacing and pore-filling clay, which may have precipitated during an intermediate stage of diagenesis, has higher  $\delta^{18}\text{O}$  values (up to  $+7.5$  ‰). If the data were accepted as shown in Figure 3.11, then the chlorite with the lowest  $\delta^{18}\text{O}$  values might have formed at  $20$ - $40^\circ\text{C}$  from water with  $\delta^{18}\text{O} = -9$  to  $-8$  ‰; the later, more  $\delta^{18}\text{O}$ -rich chlorite might have formed at  $100$ - $150^\circ\text{C}$  from water with  $\delta^{18}\text{O} = 0$  to  $+3$  ‰. In this case, the porewater from which early chlorite formed is not significantly more enriched in  $^{18}\text{O}$  than the porewater which precipitated siderite.

Figure 3.12 summarizes an idealized curve for porewater evolution in Falher conglomerates from the time of burial to the present. The alternative pathways shown depend on whether siderite or chlorite was the early diagenetic phase precipitated. This curve is consistent with the petrographic data, and the isotopic and fluid inclusion analyses.

### FALHER CONGLOMERATES PORE WATER EVOLUTION



**Figure 3.12** Idealized porewater evolution path ( $\delta^{18}\text{O}$  of water versus temperature) for Falher conglomerates. The discontinuous arrows at the end of the curve represent late-stage, porewater evolution in the water-saturated region of the study area.

### Constraints on Porewater Evolution In Falher Sandstones

Comparison of fluid inclusion temperatures with temperatures calculated from vitrinite reflectance data using the Lopatin (1971) - Waples (1980) method suggests that hot fluids (190°C) moved updip along permeable Falher units (Chapter 2). In areas where the hot (190°C) fluids flowed through the more permeable sandstones, the porewater evolution pathway in the sandstones would have been similar to that in the conglomerates (Figure 3.12). In zones which were not penetrated by these hot fluids, the temperature of porewaters in sandstones could have been similar to the maximum burial temperature calculated from the vitrinite reflectance data (Chapter 2) for that location. The  $\delta^{18}\text{O}_{\text{water}}$  versus temperature curves for diagenetic phases in Falher sandstones (Figure 3.13) have been interpreted accordingly, that is, assuming that maximum burial temperatures and fluid temperatures varied from 120°C in the east to 150°C in the west adjacent to the Alberta/B.C. border (Chapter 2, Figure 2.9).

Figure 3.14 shows some possible idealized pathways for porewater evolution which comply with the constraints of Figure 3.13 and the diagenetic sequence (Figure 3.7a). Siderite or chlorite precipitated early from porewaters with a  $\delta^{18}\text{O}$  value of -12 to -7 ‰. Locally, chlorite may have continued to precipitate until ~ 120°C. Data are consistent with precipitation of illite at ~ 100°C from porewaters with  $\delta^{18}\text{O} = -1$  ‰ or at the maximum burial temperature (150°C) from porewaters with  $\delta^{18}\text{O} = +2$  ‰. Quartz and 14 ‰ calcite probably precipitated at maximum burial temperatures (120°-150°C) from porewater with  $\delta^{18}\text{O} = -1$  or +2 ‰. In order to precipitate late-stage calcite and ankerite (Figure 3.7a) the porewater had to become depleted in  $^{18}\text{O}$  relative to its composition at maximum burial (Figure 3.14). Hence, the trend in porewater evolution is the same in sandstones as in conglomerates, i.e. porewaters became enriched in  $^{18}\text{O}$  during burial and depleted in  $^{18}\text{O}$  during uplift.

## FALHER SANDSTONES

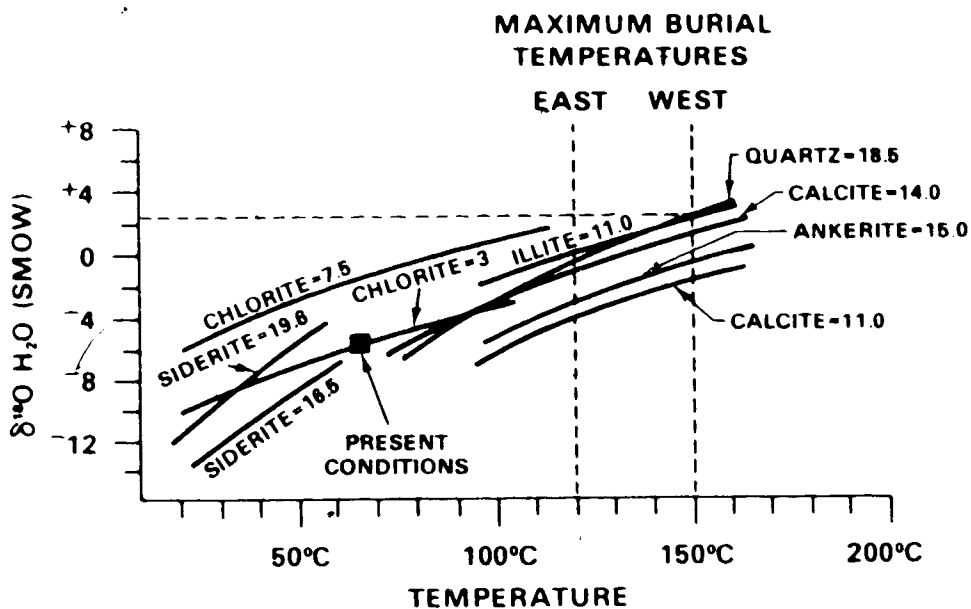


Figure 3.13  $\delta^{18}\text{O}$  of porewater versus temperature for diagenetic minerals from Falher sandstones. Equations used that are not listed in previous figure captions are the following:

- (1)  $10^3 \ln \alpha_{\text{ankerite-H}_2\text{O}} = 2.78(10^6)T^{-2} + 0.32$ ; (Dutton and Land, 1985);
- (2)  $10^3 \ln \alpha_{\text{illite-H}_2\text{O}} = 2.43(10^6)T^{-2} - 4.82$ ; (Yeh and Savin, 1977).

## FALHER SANDSTONES PORE WATER EVOLUTION PATHWAYS

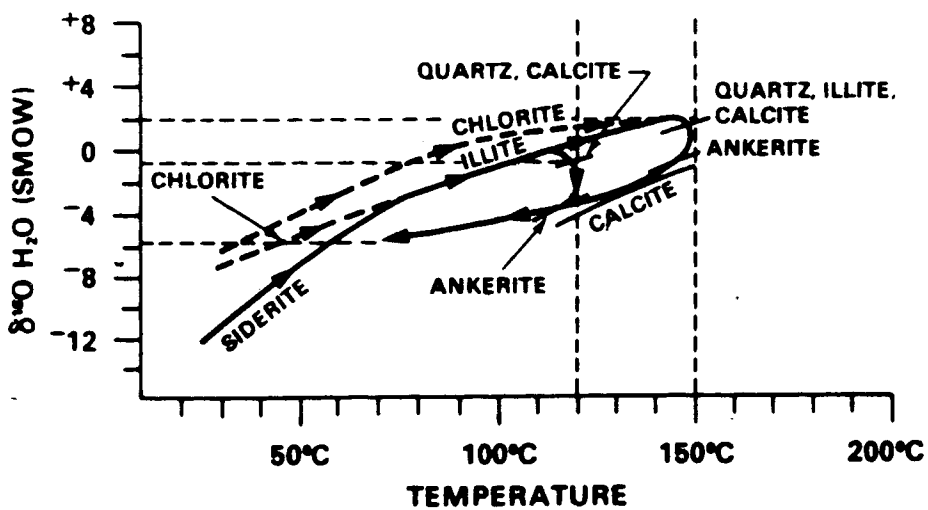


Figure 3.14 Idealized porewater evolution paths ( $\delta^{18}\text{O}$  of water versus temperature) for Falher sandstones. Each path complies with the constraints of Figure 13.



### Constraints on Porewater Evolution In the Cadomin Formation

$\delta^{18}\text{O}_{\text{water}}$  versus temperature curves for diagenetic phases in conglomerates and sandstones from the Cadomin Formation are presented in Figure 3.15. The data are constrained by:

- (1) Fluid inclusions in quartz druse (sample 292, Table 3.3) homogenize at 150°C where  $\delta^{18}\text{O}$  for quartz = +18.9 ‰.
- (2) Fluid inclusions in quartz druse (sample 293, Table 3.3) homogenize at 85°C where  $\delta^{18}\text{O}$  for quartz = +18.2 ‰; relatively pure methane inclusions are also present.
- (3) Present formation temperatures are 80-90°C.
- (4) The diagenetic sequence is: siderite, kaolinite, illite, quartz druse, dickite (Figure 3.7b).

Figure 3.16 shows idealized pathways for porewater evolution in the Cadomin. Siderite formed during early diagenesis, probably in the temperature range 20-40°C. At these temperatures, the siderite  $\delta^{18}\text{O}$  curve for the Cadomin (Figure 3.15) shows that early diagenetic porewater had an  $\delta^{18}\text{O}$  value of -11 to -6 ‰. The continental depositional environment for the Cadomin and the overlying Gething suggest that these were meteoric waters. No isotopic data is available for early kaolinite which probably also formed from meteoric water as it reacted with the rocks.

Illite which postdates kaolinite in sandstones, has an  $\delta^{18}\text{O}$  value of +16.4 ‰ (Figure 3.15). Illite can start to form from smectite at 70°C (Bruce, 1984) but the smectite/illite reaction more commonly proceeds at 100°C (Land, 1984). Alternatively, illite could be the product of K-feldspar dissolution at temperatures as high as 150°C. Using these temperatures for illite precipitation,  $\delta^{18}\text{O}$  values of porewater could vary from +2 ‰ to as high as +7 ‰. Since temperatures of 100°-150°C for precipitation of illite fit the data in the Falher, it is reasonable to use similar temperatures for the Cadomin. Although no diagenetic minerals in the Falher precipitated

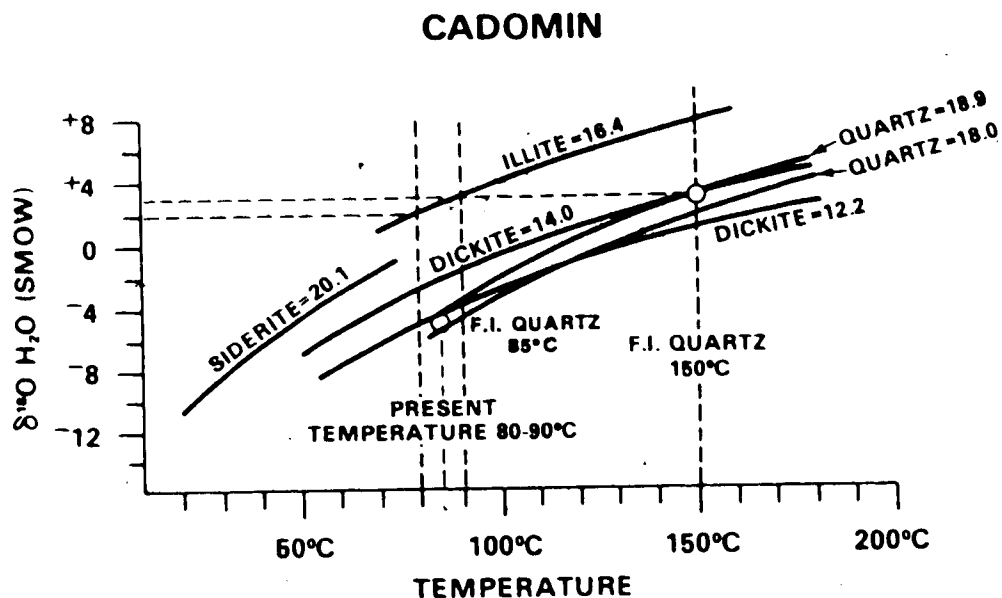


Figure 3.15  $\delta^{18}\text{O}$  of porewater versus temperature for diagenetic minerals from the Cadomin Formation. Open circles represent porewater compositions constrained by fluid inclusion temperatures and stable isotope data for quartz druse.

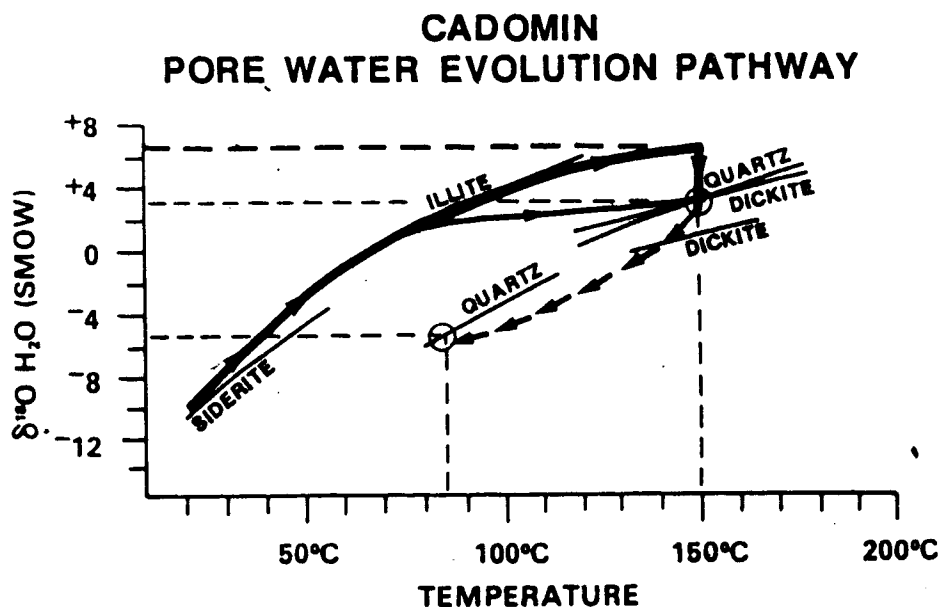


Figure 3.16 Idealized porewater evolution paths ( $\delta^{18}\text{O}$  of water versus temperature) for the Cadomin Formation. The thick curve represents porewater evolution assuming that illite formed at the maximum burial temperature; the thinner curve represents porewater evolution assuming precipitation of illite at  $80^\circ\text{C}$ , and quartz and dickite at maximum burial temperatures. Discontinuous arrows represent late-stage, porewater evolution in the water-saturated region of the study area.

from porewater more enriched in  $^{18}\text{O}$  than  $+3\text{‰}$ , it should not be assumed that porewater evolution in the Cadomin duplicated that of the Falher. The Cadomin lies unconformably above Triassic carbonates and evaporites. It is possible that during compaction  $^{18}\text{O}$ -rich porewaters migrated upwards from these units into the Cadomin, but did not migrate as far as the Falher. Hence, illite may have formed from porewater with  $\delta^{18}\text{O}$  values of  $+4$  to  $+7\text{‰}$ .

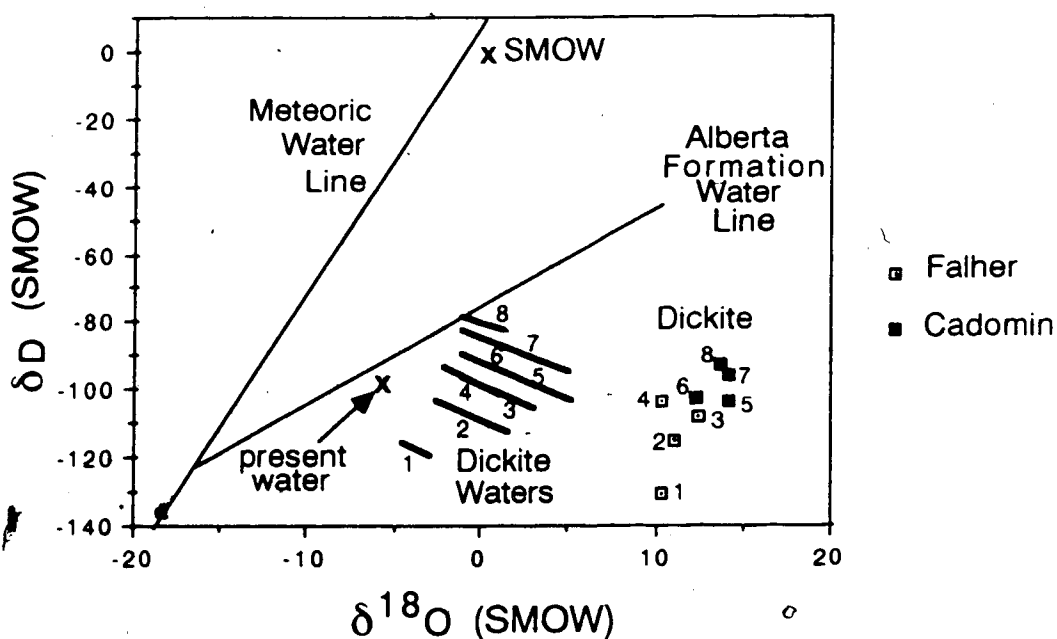
Stable isotope data and homogenization temperatures for fluid inclusions indicate that quartz druse in at least one Cadomin sample precipitated at  $150^\circ\text{C}$  from porewaters with a  $\delta^{18}\text{O}$  value of  $+3\text{‰}$  (Figure 3.15). The temperature for precipitation of quartz druse ( $150^\circ\text{C}$ ) corresponds with the maximum burial temperature calculated using vitrinite reflectance data (Chapter 2). These data suggest that if illite formed from porewater with  $\delta^{18}\text{O}$  values of  $+4$  to  $+7\text{‰}$ , porewaters had to become depleted slightly in  $^{18}\text{O}$  to precipitate quartz druse. Such a trend towards depletion of porewater in  $^{18}\text{O}$  must continue in order to precipitate dickite and a late-stage quartz druse which precipitated at  $85^\circ\text{C}$  (Figure 3.16). Alternatively, if illite formed at lower temperatures ( $70^\circ\text{--}90^\circ\text{C}$ ) from porewaters with  $\delta^{18}\text{O} = +1$  to  $+3\text{‰}$ , quartz druse at  $150^\circ\text{C}$  could have formed from porewater which had never been more enriched in  $^{18}\text{O}$  than  $+3\text{‰}$ . Very low salinities (approximately fresh, Chapter 2) of fluid inclusions in quartz druse support the former alternative (i.e. depletion of porewater in  $^{18}\text{O}$  before precipitation of quartz druse at  $150^\circ\text{C}$ ).

At township 68 range 11W6, quartz druse formed at  $85^\circ\text{C}$ , the present formation temperature. This location is situated updip from the present water-gas transition zone, on the water-saturated side. The presence of methane and aqueous inclusions in the same quartz druse at this location (Chapter 2) indicates that quartz druse formed after a significant influx of methane gas into coarse-grained sandstones and conglomerates. At  $85^\circ\text{C}$  during burial, the amount of free methane gas would have been minimal. Therefore, quartz druse at this location probably precipitated under present conditions from porewater with  $\delta^{18}\text{O} = -6\text{‰}$  (Figure 3.16).

### Constraints on Evolution of Hydrogen Isotopes in Porewaters

Deuterium analyses of diagenetic dickite in the Falher and Cadomin and of present-day water in the one Paddy sample provide some information on the hydrogen-isotope evolution of the porewaters (Figure 3.17). Kaolinite-water fractionation factors for hydrogen, determined empirically by Lambert and Epstein (1980) for temperatures less than 230°C and modified by Kyser (1987), were used to calculate the isotopic composition of waters which precipitated dickite. The compositions of these waters are shown as diagonal bars whose lengths represent the range in isotopic compositions of water assuming maximum and minimum possible temperatures for dickite precipitation. The maximum temperature for dickite precipitation in the Falher is 180°C (10°C below the maximum fluid temperature; Chapter 2) except in the eastern part of the study area which is outside the influence of the hot fluids. Here, the maximum calculated burial temperature is used (120°C). Since dickite precipitated before calcite in the Falher, minimum temperatures for dickite precipitation are slightly above the temperatures for calcite precipitation (i.e. 100-130°C). In the Cadomin, calculated maximum burial temperatures were used to estimate the maximum temperature for dickite precipitation. Minimum temperatures were estimated as 100°C (a temperature slightly above present temperatures). The range of temperatures for dickite precipitation in one Cadomin sample (292) was more tightly constrained by fluid inclusion and  $\delta^{18}\text{O}$  data (120-150°C; Figure 3.16). The correct temperatures, and  $\delta^{18}\text{O}$  and  $\delta\text{D}$  values for waters which precipitated dickite, probably lie along the bars shown in Figure 3.17.

The position of the meteoric water line, the composition of Standard Mean Ocean Water (SMOW), a line representing the isotopic composition of Alberta formation waters, and the composition of present water in the Paddy Member of the Peace River Formation in the Deep Basin (probably similar to present Falher water) are shown in Figure 3.17. The low  $\delta\text{D}$  values of the Paddy and dickite waters support a meteoric origin for these waters. The cause of enrichment in deuterium relative to meteoric water is poorly understood. Various mechanisms for D-enrichment



**Figure 3.17**  $\delta D$  versus  $\delta^{18}O$  for Falher and Cadomin late-stage dickite. Small squares represent the measured isotopic compositions of diagenetic dickite from the Falher Member and Cadomin Formation. Thick diagonal bars represent the possible range in isotopic composition of water which precipitated the dickite with the corresponding number in the diagram. The length and slope of the diagonal bars are a function of the maximum and minimum temperature possible for precipitation of the dickite. The position of the meteoric water line, the composition of SMOW, a line representing the isotopic composition of Alberta formation water, and the composition of present water in the Paddy Member in the Deep Basin are also shown.

of formation waters are: (1) isotopic exchange between meteoric water and hydrogen-bearing phases like clay minerals, hydrocarbons and H<sub>2</sub>S (Clayton et al., 1966); (2) clay dewatering during compaction and smectite/illite reactions (Yeh, 1980; Suchecki and Land, 1983); (3) isotopic fractionation due to diffusion of water through micropore systems (membrane filtration) (Graf et al., 1965; Coplen and Hanshaw, 1973); (4) mixing of meteoric water with ancient seawater that underwent evaporation (Knauth and Beeunas, 1986); or (5) mixing of meteoric water with connate water (Michon and Friedman, 1969). Because the Western Canadian Basin has been undergoing erosion and uplift for the last 50 m.y. or so, it is unlikely that compaction waters or even I/S reaction waters have been important in altering the isotopic composition of recent formation waters. Knauth and Beeunas (1986) propose that formation waters depleted in <sup>18</sup>O and D may have formed by mixing of evaporated seawater and meteoric water. Under conditions of extreme evaporation, as in the formation of halite, the residual liquids become depleted in the heavy isotopes of oxygen and hydrogen (Sofer and Gat, 1975; Holser, 1979; Pierre et al., 1984). However, mixtures of evaporated seawater and meteoric water would not produce the isotopic compositions of the waters in this study.

Mixing of meteoric water with connate water is the preferred mechanism for D and <sup>18</sup>O enrichment of formation waters in this study. Siderite data suggest that early depositional waters had  $\delta^{18}\text{O} = -12$  to  $-7$  ‰ and were probably brackish to marine waters. Such waters probably had  $\delta\text{D}$  values of  $-80$  to  $-60$  ‰ (see meteoric water line, Figure 3.17). The  $\delta\text{D}$  values of water which precipitated dickite are only slightly lower ( $-80$  to  $-120$  ‰) and can be derived by mixing with meteoric water which has been enriched in <sup>18</sup>O but not deuterium.

#### Timing of Saturation of Pores by Methane Gas

The final constraint on diagenesis and porewater evolution is the relative timing at which the water was driven from the pore space by a continuous upward-moving gas phase

(Masters, 1979). The largest quantities of gas are produced at vitrinite reflectivities between 0.9% and 1.3% (Juertgen and Klein, 1975). Weiss (1985) calculated that gas generation began in the Falher Fourth Coal at 52 Ma ( $R_o=0.9\%$ ) and was at its maximum between 49 and 38 Ma ( $R_o=1.3\%$ ). His calculation was based on estimation of the maturation level and burial history of the Falher coal using the Lopatin (1971) method as modified by Waples (1980). The results of Weiss (1985) suggest that since the maximum generation of gas occurred between 49 and 38 Ma, this is the most likely time when gas became a continuous phase capable of driving-out movable water. This period also marks the end of diagenesis in the down-dip, gas-saturated zone.

## STAGES IN THE DIAGENESIS AND POREWATER EVOLUTION OF THE FALHER AND CADOMIN: SUMMARY

The isotopic evolution of porewaters through time is illustrated for the Falher in Figure 3.18. The isotopic evolution of Cadomin porewaters follows a very similar pattern, except that porewater  $\delta^{18}O$  values during late stages of burial may have been as high as +4 to +7 ‰.

### Stage 1. Deposition and Burial

In the Falher, conglomerates, sandstones, shales and coals were deposited in a west-east-trending shoreline environment with the sea to the north. Hematite began to precipitate very early in the oxidizing zone. In the southern part of the study area, after burial moved the sediment into the reducing, methanic zone, siderite began to precipitate from meteoric or brackish porewaters ( $\delta^{18}O = -12$  to  $-7$  ‰). In the northern part of the study area, where deposition took place under marine conditions, chlorite precipitated from porewaters with  $\delta^{18}O = -9$  to  $-8$  ‰.

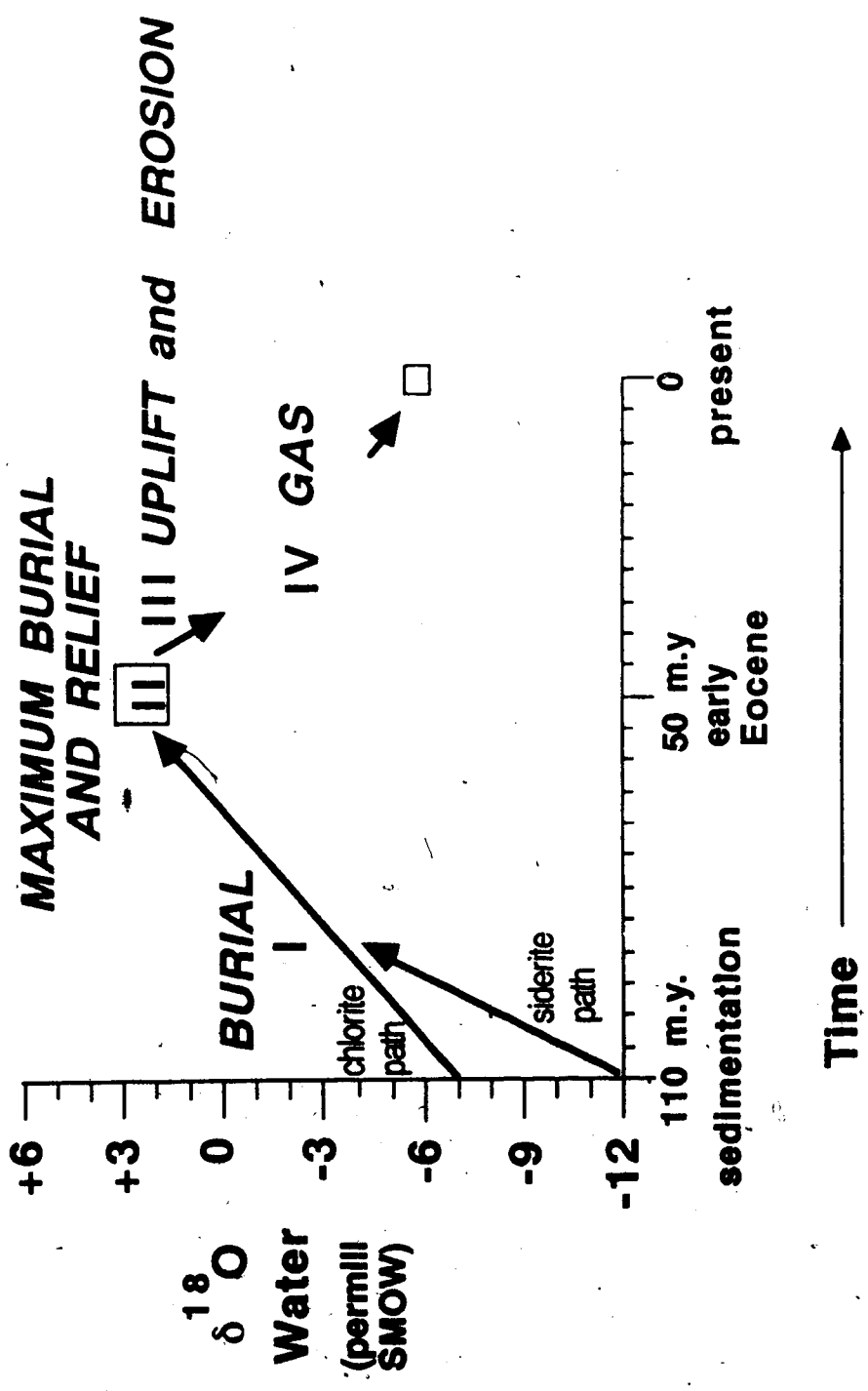


Figure 3.18 Idealized porewater evolution path ( $\delta^{18}\text{O}$  of porewater versus time) for the Falher and Cadomin sandstones and conglomerates.



Dissolution of unstable detrital grains including feldspars began early during burial and continued as temperatures and burial depths increased. Chlorite continued to precipitate locally and quartz overgrowths probably began to form on quartz sand grains at an intermediate stage of burial and continued until maximum burial. Albitization and precipitation of illite and local calcite cement occurred as the porewaters became enriched in  $^{18}\text{O}$  by limited reaction with the enclosing rocks and mixing with waters derived from shale compaction. Compaction, fracturing of detrital grains and pressure solution of chert grains became important as burial depths increased.

In the Cadomin, a mixture of unimodal, sandy conglomerates and few sandstones were deposited in a continental, alluvial floodplain. Siderite precipitated from porewaters with  $\delta^{18}\text{O} = -11$  to  $-7$  ‰, probably at temperatures between 20-40°C. Since the Cadomin is surrounded by continental sediments, there is no nearby source of marine porewater. The water which precipitated siderite had to have a low  $\delta^{18}\text{O}$  value ( $-11$  to  $-7$  ‰), that is, meteoric water. Kaolinite precipitated from the relatively fresh porewater before significant water-rock interaction had occurred. Isotopic enrichment of early porewater followed a path similar to that in the Falher, and porewater continued to react with the detrital minerals in the surrounding rock. An influx of  $^{18}\text{O}$ -rich porewaters from the underlying Triassic carbonate and evaporite section may have mixed with the porewaters to produce porewaters with  $\delta^{18}\text{O}$  values of  $+4$  to  $+7$  ‰. In the presence of these  $^{18}\text{O}$ -rich porewaters, quartz overgrowths formed on the rare quartz grains and illite began to precipitate in preference to kaolinite.

### **Stage II. Maximum Burial and Relief**

Stage II marks the end of the burial stage (1) and occurred during the early Eocene (about 50 Ma) when the last pulse of the Laramide Orogeny resulted in maximum burial of the Western Canadian Basin and maximum relief in the Cordillera. Maximum burial depths for the Falher in the study area ranged from 3000 m in the east to 4500 m in the west near the Alberta/B.C. border and

up to as much as 6300 m at the synclinal axis (Chapter 2). The Cadomin is about 400 m below the Falher. Maximum burial temperatures calculated from organic maturity data in the Falher ranged from 120°C in the east to 150°C at the Alberta/B.C border and up to 200°C at the synclinal axis. Maximum burial temperatures for Cadomin locations discussed in this study varied from 135°C to 150°C.

Updip flow of hot saline (2-3 wt%) fluid along the permeable conglomerate beds and horizontal fractures occurred in the Falher and Cadotte at this stage (Chapter 2). Horizontal fractures may have formed as a result of horizontal forces caused by the orogenic activity to the west. These hot fluids (>190°C) precipitated quartz druse in conglomerates and horizontal fractures as they cooled. The  $\delta^{18}\text{O}$  value of the hot fluid was +3 ‰ at 190°C. Methane-rich fluid inclusions trapped in quartz druse (Chapter 2) suggest that these fluids carried small bubbles of methane along their updip path.

The hot fluids were not recognized in the Cadomin where low salinity fluids at ambient temperatures (150°C) precipitated quartz druse and dickite. The  $\delta^{18}\text{O}$  value of these porewaters was +3 ‰ SMOW at 150°C. The  $\delta^{18}\text{O}$  value of illite in the Cadomin suggests that dilution of  $^{18}\text{O}$ -rich porewaters (+4 to +7 ‰) may have occurred before precipitation of this quartz druse.

### **Stage III Uplift, Erosion and Recharge by Meteoric Water**

Recharge by meteoric water occurred universally in the Falher and at least locally in the Cadomin during uplift and erosion, in response to the large hydraulic potential produced by the topographic high in the Cordillera. In the Falher, an influx of evolved-meteoric water is recorded by the low  $\delta^{18}\text{O}$  compositions of dickite, ankerite and calcite. The influx of evolved-meteoric water into the Cadomin at this stage is recorded, locally, by dickite which is depleted in  $^{18}\text{O}$  relative to quartz druse.

By the latter part of this stage, many of the pore spaces in the coarser units were probably at least partially filled by methane gas. The presence of large bubbles of methane gas may have inhibited the precipitation of late-stage diagenetic minerals, thereby producing the observed texture of some pores filled by dickite or calcite and adjacent pores apparently empty.

#### Stage IV Maximum Generation of Methane from Coals

The final stage in the diagenetic history of Lower Cretaceous sediments in the Deep Basin occurred when the interbedded coals achieved sufficient maturity to produce significant amounts of methane. Weiss (1985) calculated that this occurred between 49 and 38 Ma. The formation and upward migration of a continuous gas phase drove out the moveable formation water and caused the end of diagenesis. Recharge by meteoric water up-dip from the gas-water transition zone may have continued such that present water in the Falher has  $\delta^{18}\text{O} = -5$  to  $-6$  ‰ SMOW. Fluid inclusions in quartz druse from the Cadomin suggest that present porewater, in the updip, water-saturated areas of the Cadomin also has  $\delta^{18}\text{O} = -6$  ‰ SMOW.

## REFERENCES

- Ayalon, A., and Longstaffe, F.J., in press, Oxygen-isotope studies of diagenesis and porewater evolution in the western Canada sedimentary basin: evidence from the Upper Cretaceous basal Belly River sandstone: *Journal of Sedimentary Petrology*.
- Becker, R.N. and Clayton, R.N., 1976, Oxygen isotope study of a Precambrian banded iron-formation, Hamersley Range, Western Australia: *Geochimica et Cosmochimica Acta*, v.40, p. 1153-1165.
- Bruce, C.H., 1984, Smectite dehydration - its relation to structural development and hydrocarbon accumulation in Northern Gulf of Mexico Basin: *The American Association of Petroleum Geologists Bulletin*, v.68, p. 673-683.
- Cant, D.J., 1983, Spirit River Formation - A stratigraphic-diagenetic gas trap in the Deep Basin of Alberta: *The American Association of Petroleum Geologists Bulletin*, v.67, p. 577-587.
- Cant, D.J. and Ethier, V.G., 1984, Lithology-dependent diagenetic control of reservoir properties of conglomerates, Falher Member, Elmworth Field, Alberta: *The American Association of Petroleum Geologists Bulletin*, v.68, p. 1044-1054.
- Clayton, R.N., Friedman, I., Graf, D.L., Mayeda, T.K., Meents, W.F., and Shimp, N.F., 1966, The origin of saline formation waters: *Journal of Geophysical Research*, v.71, p. 3869-3882.
- Clayton, R.N. and Mayeda, T.K., 1963, The use of bromine pentafluoride in the extraction of oxygen from oxides and silicates for isotopic analysis: *Geochimica et Cosmochimica Acta*, v.27, p. 43-52.
- Clayton, R.N., O'Neil, J.R., and Mayeda, T.K., 1972, Oxygen isotope exchange between quartz and water: *Journal of Geophysical Research*, v.77, p. 3057-3067.
- Coplen, T.B. and Hanshaw, B.B., 1973, Ultrafiltration by a compacted clay membrane: 1. Oxygen and hydrogen isotope fractionation: *Geochimica et Cosmochimica Acta*, v.37, p. 2295-2310.
- Craig, H., 1957, Isotopic standards for carbon and oxygen and correction factors for mass-spectrometric analysis of carbon dioxide: *Geochimica et Cosmochimica Acta*, v.12, p. 133-149.
- Craig, H., 1961, Standards for reporting concentrations of deuterium and oxygen-18 in natural waters: *Science*, v.133, p. 1833-1834.
- Dean, M.E., 1965, Diagenesis of the Viking Formation, south-central Alberta: M.Sc thesis, University of Alberta, Edmonton, Alberta, 195 p.
- Dutton, S.P. and Land, L.S., 1965, Meteoric burial diagenesis of Pennsylvanian arkosic sandstones, southwestern Anadarko Basin, Texas: *The American Association of Petroleum Geologists Bulletin*, v.69, p. 22-38.
- Epstein, S., Graf, D.L. and Degens, E.T., 1964, Oxygen isotope studies on the origin of dolomite: *In* Craig et al., eds., *Isotopic and Cosmic Chemistry*: North Holland Publishing Company, Amsterdam, p. 169-180.
- Eslinger, E.V., 1971, Mineralogy and oxygen isotope ratios of hydro-thermal and low-grade metamorphic argillaceous rocks: Case Western Reserve University, 205 p.

- Friedman, I., and O'Neil, J.R., 1977, Compilation of stable isotope fractionation factors of geochemical interest: in M. Fleischer, ed., *Data of Geochemistry* (6th ed.): U.S. Geological Survey Professional Paper 440-KK, 12 p.
- Gautier, D.L., 1983, Chapter 4. Diagenesis: in *Patterns of Sedimentation, Diagenesis, and Hydrocarbon Accumulation*: in D.D. Rice and D.L. Gautier, eds., *Cretaceous Rocks of the Rocky Mountains*: SEPM Short Course No. 11, p. 4-1 to 4-29.
- Gies, R.M., 1984, Case history for a major Alberta Deep Basin gas trap: the Cadomin Formation: in J.A. Masters, ed., *Elmworth case study of a Deep Basin Gas Field*: American Association of Petroleum Geologists Memoir 38, p. 115-140.
- Graf, D.L., Friedman, I., and Meents, W.F., 1965, The origin of saline formation water: II. Isotopic fractionation by shale micropore systems: *Illinois Geological Survey Circular*, v.393, p. 32.
- Mitchon, B. and Friedman, I., 1969, Geochemistry and origin of formation water in the western Canada sedimentary basin- I. Stable isotopes of hydrogen and oxygen: *Geochimica et Cosmochimica Acta*, v.33, p. 1321-1349.
- Holser, W.T., 1979, Trace elements and isotopes in evaporites: in R.G. Burns, ed., *Marine Minerals: Reviews in Mineralogy*: Mineralogical Society of America, p. 295-346.
- Jackson, M.L., 1979, *Soil Chemical Analysis - Advanced Course*, 2nd edition: published by the author, Madison, Wis., 895 p.
- Juntgen, H., and Klein, J., 1975, Entstehung von Erdgas aus kohligen Sedimenten: *Erdol u. Kohle, Erdgas, Petrochem, Ergänzungsband*, v.1, Industrieverlag v. Hernhausen, Leinfelden bei Stuttgart, p. 52-69.
- Kharaka, Y.K., Hull, R.W. and Carothers, W.W., 1985, Water-rock interactions in sedimentary basins: in D.L. Gautier, Y.K. Kharaka, and R.C. Surdam, eds., *Relationship of Organic Matter and Mineral Diagenesis*: SEPM Short Course No. 17, p. 79-176.
- Knauth, L.P. and Beeunas, M.A., 1986, Isotope geochemistry of fluid inclusions in Permian halite with implications for the isotopic history of ocean water and the origin of saline formation waters: *Geochimica et Cosmochimica Acta*, v.50, p. 419-433.
- Kyser, T.K., 1987, Equilibrium fractionation factors for stable isotopes: in T.K. Kyser, ed., *Short Course in Stable Isotope Geochemistry of Low Temperature Fluids*: Mineralogical Association of Canada Short Course Volume 13, p. 1-84.
- Lambert, S.J., and Epstein, S., 1980, Stable isotope investigations of an active geothermal system in Valles Caldera, Jemez Mountains, New Mexico: *Journal of Volcanology and Geothermal Research*, v.8, p. 111-129.
- Land, L.S., 1984, Frio sandstone diagenesis, Texas Gulf Coast: a regional isotopic study: in R. Surdam and D. MacDonald, eds., *Clastic Diagenesis*: American Association of Petroleum Geologists, Memoir 37, p. 47-62.
- Land, L.S., and Dutton, S.P., 1978, Cementation of a Pennsylvanian deltaic sandstone: isotopic data: *Journal of Sedimentary Petrology*, v.48, p. 1167-1176.
- Lee, M and Savin, S., 1985, Isolation of diagenetic overgrowths on quartz sand grains for oxygen isotopic analysis: *Geochimica et Cosmochimica Acta*, v.49, p. 497-501.
- Longstaffe, F.J., 1983, Diagenesis, IV. Stable isotope studies of diagenesis in clastic rocks: *Geoscience Canada*, v.10, p. 44-58.

- Longstaffe, F.J., 1984, The role of meteoric water in diagenesis of shallow sandstones: stable isotope studies of the Milk River aquifer and gas pool: *in* R. Surdam and D. MacDonald, eds., *Clastic Diagenesis*: American Association of Petroleum Geologists, Memoir 37, p. 81-98.
- Longstaffe, F.J., 1986, Oxygen isotope studies of diagenesis in the basal Belly River sandstone, Pembina I-Pool, Alberta: *Journal of Sedimentary Petrology*, v. 56, p. 78-88.
- Longstaffe, F.J., 1987, Stable isotope studies of diagenetic processes: *in* T.K. Kyser, ed., *Short Course in Stable Isotope Geochemistry of Low Temperature Fluids*: Mineralogical Association of Canada Short Course Volume 13, p. 187-257.
- Longstaffe, F.J., and Ayalon, A., in press, Oxygen-isotope studies of clastic diagenesis in the Lower Cretaceous Viking Formation, Alberta: implications for the role of meteoric water: *in* J.D. Marshall, ed., *The Diagenesis of Sedimentary Sequences*: Geological Society Special Publication.
- Lopatin, N.V., 1971, Temperature and geologic time as factors in coalification (in Russian): *Akademiya Nauk SSSR Izvestiya, Seriya Geologicheskaya*, no. 3, p. 95-106.
- Masters, J.A., 1979, Deep Basin gas trap, Western Canada: *The American Association of Petroleum Geologists Bulletin*, v.63, p. 152-181.
- McCrea, J.M., 1950, On the isotopic chemistry of carbonates and a paleotemperature scale: *Journal of Chemical Physics*, v.18, p. 849-857.
- O'Neil, J.R., 1987, Preservation of H, C, and O isotopic ratios in the low temperature environment: *in* T.K. Kyser, ed., *Short Course in Stable Isotope Geochemistry of Low Temperature Fluids*: Mineralogical Association of Canada Short Course Volume 13, p. 85-128.
- O'Neil, J.R., Clayton, R.N. and Mayeda, T.K., 1969, Oxygen isotope fractionation in divalent metal carbonates: *Journal of Chemical Physics*, v.51, p. 5547-5558.
- Pierre, C., Ortlieb, L., and Person, A., 1984, Supratidal evaporitic dolomite at Ojo de Liebre lagoon: mineralogical and isotopic arguments for primary crystallization: *Journal of Sedimentary Petrology*, v.54, p. 1049-1061.
- Rahmani, R.A., 1984, Facies control of gas trapping, Lower Cretaceous Falher A cycle, Elmworth area, northwestern Alberta: *in* J.A. Masters, ed., *Elmworth Case Study of a Deep Basin Gas Field*: AAPG Memoir 38, p. 141-152.
- Rosenbaum, J. and Sheppard, S.M.F., 1986, An isotopic study of siderites, dolomites and ankerites at high temperatures: *Geochimica et Cosmochimica Acta*, v.50, p.1147-1150.
- Sharma, T. and Clayton, R.N., 1965, Measurement of  $O^{18}/O^{16}$  ratios of total oxygen of carbonates: *Geochimica et Cosmochimica Acta*, v.29, p.1347-1353.
- Smith, D.G., Zorn, C.E. and Sneider, R.M., 1984, The paleogeography of the Lower Cretaceous of western Alberta and northeastern British Columbia in and adjacent to the Deep Basin of the Elmworth area: *in* J.A. Masters, ed., *Elmworth Case Study of a Deep Basin Gas Field*: AAPG Memoir 38, p. 79-114.
- Sofer, Z. and Gat, J.R., 1975, The isotopic composition of evaporating brines: effect of the isotopic activity ratio in saline solutions: *Earth and Planetary Science Letters*, v.26, p. 179-186.
- Šrodón, J., 1984, X-ray powder diffraction identification of illitic materials: *Clays and Clay Minerals*, v.32, p. 337-349.

- Suchecki, R.K. and Land, L.S., 1983, Isotopic geochemistry of burial-metamorphosed volcanogenic sediments, Great Valley sequence, northern California: *Geochimica et Cosmochimica Acta*, v.47, p. 1487-1499.
- Syers, J.K., Chapman, S.L., Jackson, M.L. and Rex, R.W., 1968, Quartz isolation from rocks, sediments and soils for determination of oxygen isotopic composition: *Geochimica et Cosmochimica Acta*, v.32, p. 1022-1025.
- Varley, C.J., 1982, The sedimentology and diagenesis of the Cadomin Formation, Elmworth area, northwestern Alberta: M.Sc thesis, University of Calgary, Calgary, Alberta, 173 p.
- Varley, C.J., 1984, Sedimentology and hydrocarbon distribution of the Lower Cretaceous Cadomin Formation, northwest Alberta: in E.H. Koster and R.J. Steel, eds., *Sedimentology of Gravels and Conglomerates: Canadian Society of Petroleum Geologists, Memoir 10*, p. 175-187.
- Walters, L.J.Jr., Claypool, G.E. and Choquette, P.W., 1972, Reaction rates and  $\delta^{18}\text{O}$  variation for the carbonate-phosphoric acid preparation method: *Geochimica et Cosmochimica Acta*, v.36, p. 129-140.
- Waples, D., 1980, Time and temperature in petroleum formation: Application of Lopatin's method to petroleum exploration: *The American Association of Petroleum Geologists Bulletin*, v.64, p. 916-926.
- Weiss, H.M., 1985, Geochemische und petrographische Untersuchungen am organischen Material kretazischer Sedimentgesteine aus dem Deep Basin, Westkanada: Obergunzburg, PhD thesis (in German), 261 p.
- Wenner, D.L. and Taylor, H.P., 1971, Temperature of serpentinization of ultramafic rocks based on  $\text{O}^{18}/\text{O}^{16}$  fractionation between coexisting serpentine and magnetite: *Contributions to Mineralogy and Petrology*, v.32, p. 165-185.
- Yeh, H-W., 1980, D/H ratios and late-stage dehydration of shales during burial: *Geochimica et Cosmochimica Acta*, v.44, p. 341-352.
- Yeh, H., and Savin, S.M., 1977, Mechanism of burial metamorphism of argillaceous sediments, III. O-isotope evidence: *Geological Society of America Bulletin*, v.88, p. 1321-1330.

## CHAPTER 4. REGIONAL DIAGENESIS AND POREWATER EVOLUTION IN THE ALBERTA DEEP BASIN

### INTRODUCTION

Chapter 3 discussed diagenesis and porewater evolution in the Lower Cretaceous Falher and Cadomin units in the Alberta Deep Basin. Results showed that porewater evolved to a maximum  $\delta^{18}\text{O}$  value of +3 ‰ during burial and became depleted in  $^{18}\text{O}$  during uplift as a result of an influx of meteoric water. Chapter 2 showed that hot waters were involved in the diagenesis of the coarser Falher sandstones and conglomerates in the western part of the Deep Basin, whereas in the Cadomin, diagenetic minerals were precipitated from porewaters at the expected burial temperatures. This chapter examines diagenesis and porewater evolution in sandstones from several additional units in the Deep Basin (Figure 4.1) including the Upper Cretaceous Cardium, the Lower Cretaceous Paddy, Cadotte and Bluesky, the Triassic Halfway and the Permian Belloy sandstones (Figure 4.2). The objective in studying these units is to examine vertical variations in diagenetic processes. Whereas study of the Falher Member and Cadomin Formation concentrated on porewaters dominantly in conglomerates, the units examined here are predominantly very fine, fine and medium-grained sandstones. Since permeabilities in sandstones are significantly lower than those in conglomerates (0.1-1 md versus 1-1000 md; Cant and Ethier, 1984), the volumes of porefluids flowing through these sandstone units may have been significantly smaller than in the Falher or Cadomin conglomerates and the diagenetic processes may have differed.

Figure 4.3 shows the location of wells sampled in each unit. The Bluesky was studied in some detail, whereas the Cardium, Paddy, Cadotte, Halfway and Belloy were sampled on a reconnaissance basis. The Paddy well sampled is water-saturated; detailed water analyses for this well are presented in Chapter 5.



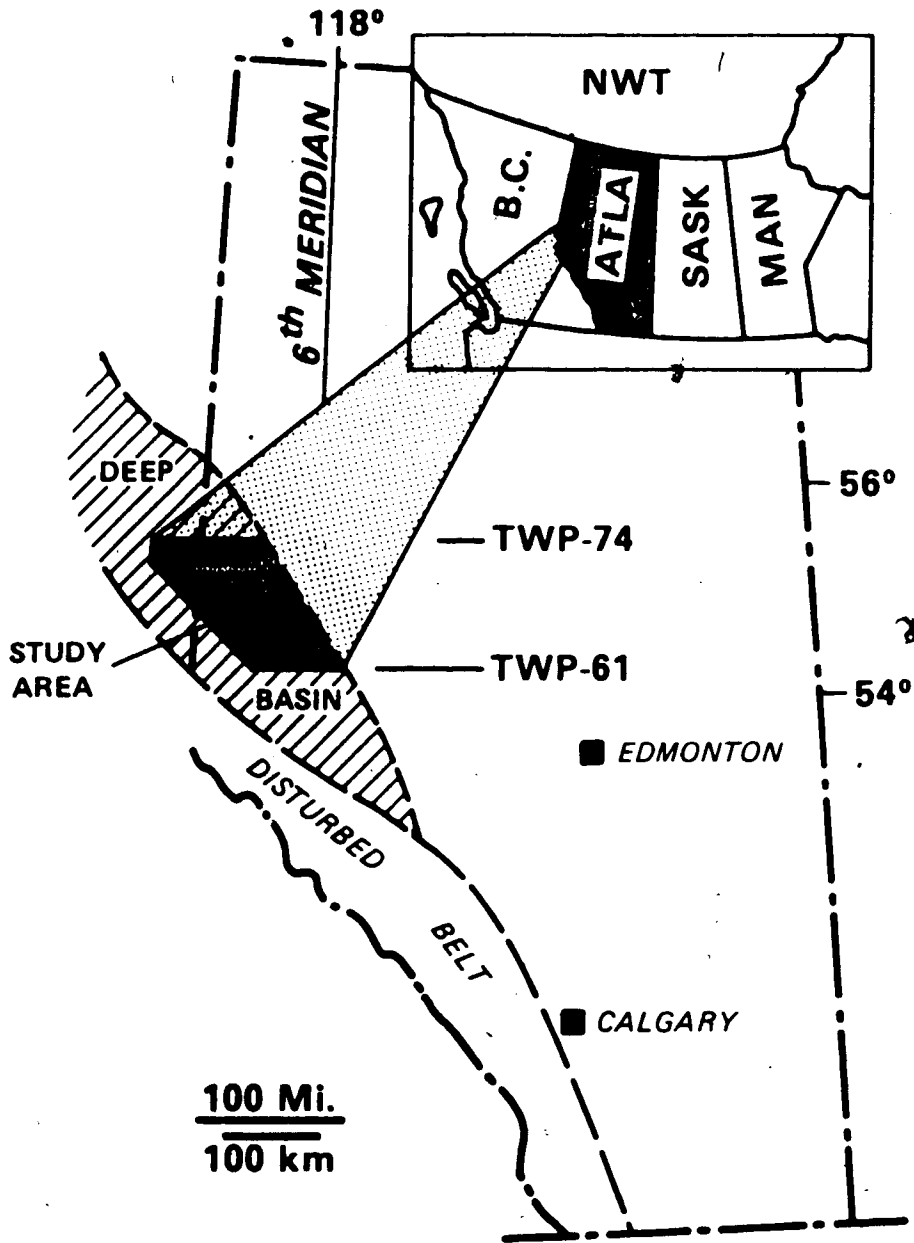


Figure 4.1 Location of study area.

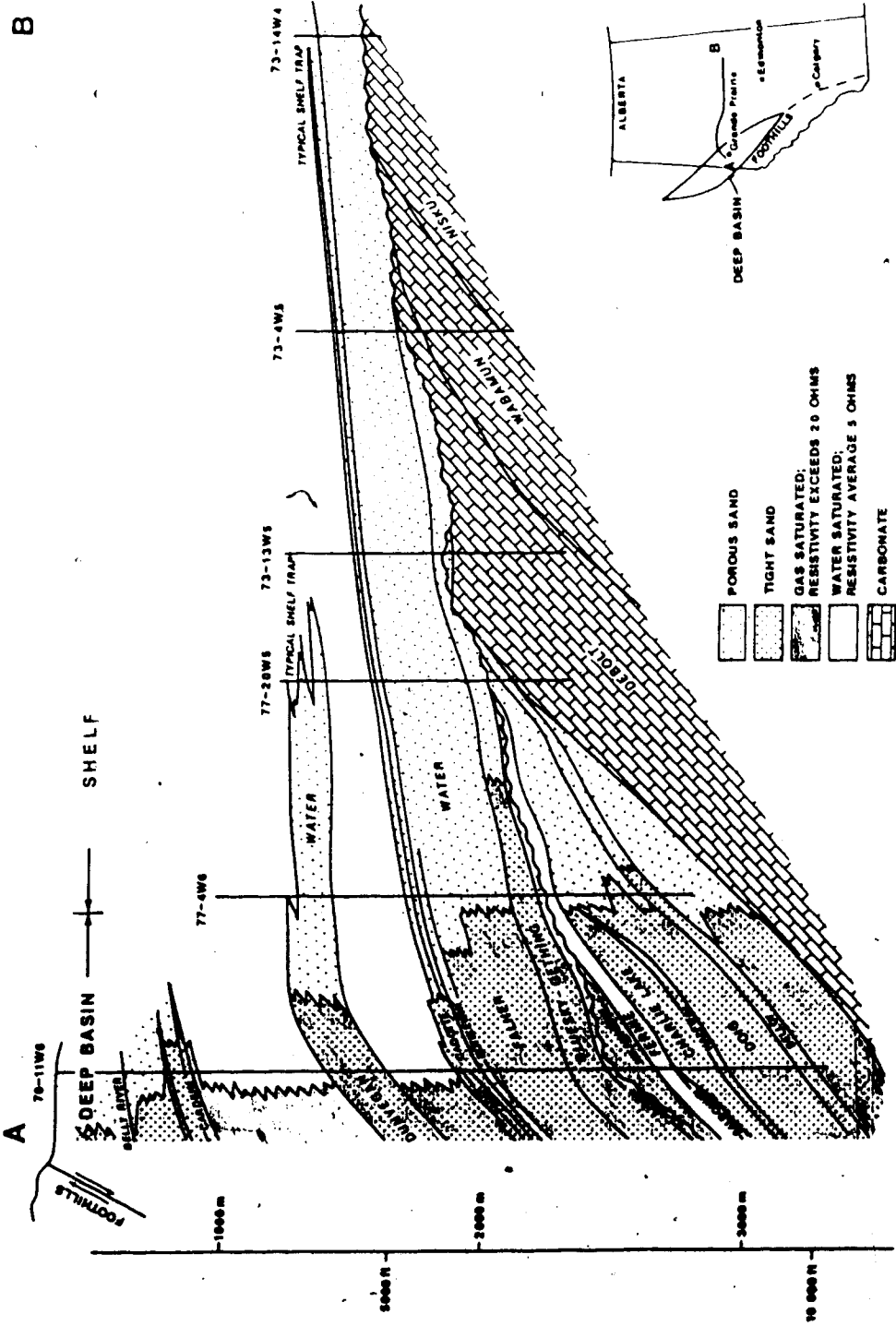


Figure 4.2 West to east cross-section through the Alberta Basin showing stratigraphic nomenclature for the Deep Basin. Almost the entire section in the western part of the Deep Basin is gas-saturated, whereas updip, to the east, the rocks are water-saturated (modified from Masters, 1979).

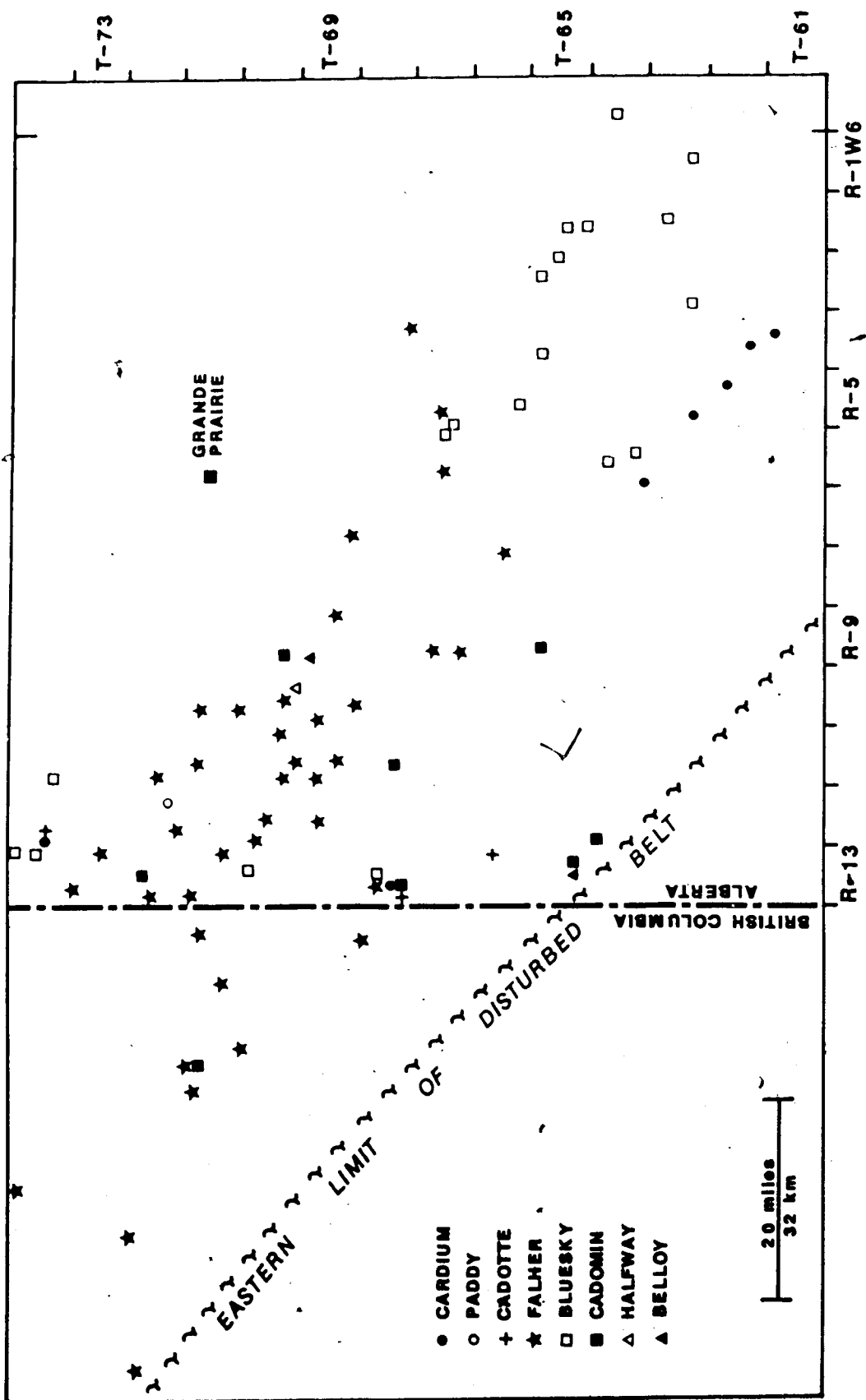


Figure 4.3 Location of samples.

## DEPOSITIONAL SETTINGS

The Cardium Formation comprises a complex suite of shelf to shoreline sediments deposited in six major coarsening-upward sequences, separated by pebble beds overlying regional erosion surfaces (Plint and Walker, 1987). The Kawka and Dismal Rat Members were sampled for this study. The Kawka Member is a very fine to medium-grained shoreline sandstone, 6-18 m thick, capped by floodplain and lagoonal deposits. The Dismal Rat Member is a ~10 m thick shallowing-upward shelf sequence of bioturbated silty and sandy mudstones containing thin stringers of pebbles. Its upper boundary is defined by a regional erosional surface (Plint et al., 1986; Plint and Walker, 1987).

The Paddy Member of the Peace River Formation, in the well sampled (Figure 4.3), is a 16 m thick sandstone which was deposited as a northwest-southeast trending tidal channel (Smith et al., 1984). The tidal channel is surrounded by subtidal bay sediments consisting of interbedded thin sandstones and shales.

The Bluesky Formation is comprised of a barrier bar/offshore bar, regressive sandstone system represented by coarsening upward sandstone. Lagoonal and bay sediments, consisting of siltstone, shale and coal, cap most of the barrier system. Low energy bay sediments predominate in the southeastern part of the study area, where the Bluesky is represented by thin, highly burrowed sandstone, siltstone and shale with occasional thin molluscan shell banks (Smith et al., 1984). The Bluesky occurs above the continental Gething Formation and below the marine Wilrich Shale.

The Triassic Halfway and Permian Belloy sandstones are surrounded by shale, limestone, dolomite and anhydrite. The Halfway Formation is interpreted by Cart (1986) as a complex of transgressive marine sands, barriers, tidal estuaries, and coquina banks which are capped by

supratidal sabkha deposits of the lower Charlie Lake Formation. No detailed sedimentological studies have been reported for the Belloy sandstone.

## PETROGRAPHIC AND ISOTOPIC RESULTS

### Detrital Minerals

Cardium sandstones examined are composed mostly of quartz with lesser amounts of chert and siliceous rock fragments. Chert-rich conglomerates are also present. The Paddy sandstone in the well examined is quartz-rich with minor amounts of rock fragments and trace amounts of mica and feldspar. Rock fragments consist of chert, shale, siltstone and possibly volcanic fragments. The Bluesky sandstones studied are composed of quartz, rock fragments (mostly chert and sedimentary rock fragments) and dolomite grains. Micas occur as a minor phase and feldspars are rare. The proportion of chert varies with grain size; medium or fine grained sandstones are dominantly chert. Glauconite is a major component in the uppermost sandstones of the Bluesky, but also occurs in minor amounts throughout. Both the Triassic Halfway and the Permian Belloy sandstones are quartz-rich.

### Diagenetic Minerals

Diagenetic minerals in Cretaceous units include siderite, chlorite, dolomite, quartz overgrowths, kaolinite, pyrite, illite, albite, calcite and ankerite. In the Triassic and Permian sandstones, the major diagenetic minerals are quartz overgrowths, calcite and anhydrite.

The general diagenetic sequence for each of the sandstone units is very similar, although a few diagenetic minerals are notably absent from some units. A summary of the diagenetic sequence in each formation is presented in Figure 4.4. Although the relative sequence of precipitation for each mineral cannot always be determined precisely, the diagenetic phases can

**STAGES OF DIAGENESIS**  
**EARLY    INTERMEDIATE    LATE**

<b>CARDIUM</b>	<u>siderite</u> <u>chlorite</u>	<u>quartz</u> <u>kaolinite</u> <u>illite</u> ? <u>siderite</u> dissolution	<u>calcite</u>
<b>PADDY</b>	<u>carbonate</u> <u>cement</u>	<u>quartz</u> <u>kaolinite</u> <u>illite</u> ? <u>carbonate</u> dissolution	<u>quartz</u> <u>ankerite</u> <u>calcite</u>
<b>FALHER</b>	<u>hematite</u> <u>dolomite</u> <u>siderite</u> <u>chlorite</u>	<u>quartz</u> <u>kaolinite</u> ? <u>siderite</u> dissolution <u>illite</u> k-feld. dissolution albitization	<u>quartz druse</u> <u>bitumen</u> <u>dickite</u> <u>ankerite</u> <u>calcite</u>
<b>BLUESKY</b>	<u>dolomite</u> <u>carbonate</u> <u>cement</u>	<u>quartz</u> <u>kaolinite</u> <u>illite</u> ? <u>carbonate</u> dissolution	<u>dickite</u> <u>ankerite</u> <u>calcite</u>
<b>CADOMIN</b>	<u>siderite</u>	<u>quartz</u> <u>kaolinite</u> <u>illite</u>	<u>quartz druse</u> <u>dickite</u>
<b>HALFWAY/ BELLOY</b>		<u>quartz</u>	<u>calcite</u> <u>anhydrite</u>

**Figure 4.4** Generalized diagenetic sequences for each unit examined.

be classified generally into early-stage, intermediate-stage, late-stage and fracture-filling cements. In this study, diagenetic minerals have been split into stages according to the following criteria: (1) Early-stage cements are the diagenetic phases which always occur immediately adjacent to detrital grains (i.e. grain coats) or they are cements which fill the pore space before any other diagenetic processes have occurred; (2) Intermediate-stage cements coat the early-stage cements and partially or completely fill the remaining pore space. They may also be phases precipitating in response to dissolution of unstable detrital grains; (3) Late-stage cements are the last phases to precipitate and fill the remaining pockets of primary pore space, as well as secondary pore space resulting from dissolution reactions. Late-stage cements precipitate after significant compaction and grain-fracturing has occurred; (4) Fracture-fill cements occur in sub-vertical or sub-horizontal fractures which cut across previously lithified sedimentary rock. A description of the diagenetic minerals, their textural relationships, and their isotopic compositions is presented below in order of early to late diagenetic stage.

### ***Early Diagenetic Minerals***

Textural relationships indicate that siderite and chlorite are the earliest diagenetic phases in the Cardium. Siderite is the most prevalent diagenetic mineral in this sandstone, whereas chlorite occurs locally in some samples where siderite is absent. Siderite can occur as: (1) isolated spherical crystals with central cores of opaque material (possibly organic matter) (Figure 4.5a); (2) pore-filling cement (Figure 4.5b); or (3) pore-lining cement coated by later pore-filling siderite (Figure 4.5c) or by later quartz overgrowths or calcite cement (Figure 4.5d). Some samples containing siderite spheres have an open pore structure (Figure 4.5a); other samples have no pore space, rather siderite spheres are squeezed between tightly compacted detrital grains (Figure 4.5e).

Two isotopic analyses for siderite give significantly different  $\delta^{18}\text{O}$  values, +22.2 ‰ for sample 310 from the Dismal Rat Member and +16.7 ‰ for sample 304 from the Kakwa Member

#### **Figure 4.5**

**(a)** Thin section photomicrograph of isolated spherical crystals of siderite (arrows) coating detrital quartz grains. Note the open pore space (P). Plane polarized light. Cardium Formation (4-6-64-6 W6, 1755.4 m). Field of view is 0.83 mm.

**(b)** Thin section photomicrograph of pore-filling siderite cement (SID). Crossed-nicols. Cardium (16-9-62-4 W6, 1835.1 m). Field of view is 0.83 mm.

**(c)** Thin section photomicrograph of pore-lining (arrow) and pore-filling (SID) siderite. Plane polarized light. Cardium (11-8-63-5 W6, 1824.1 m). Field of view is 1.34 mm.

**(d)** Thin section photomicrograph of pore-filling siderite (SID) partially replaced by calcite (CALC). Crossed-nicols. Cardium (15.16-68-13 W6, 1150.5 m). Field of view is 0.33 mm.

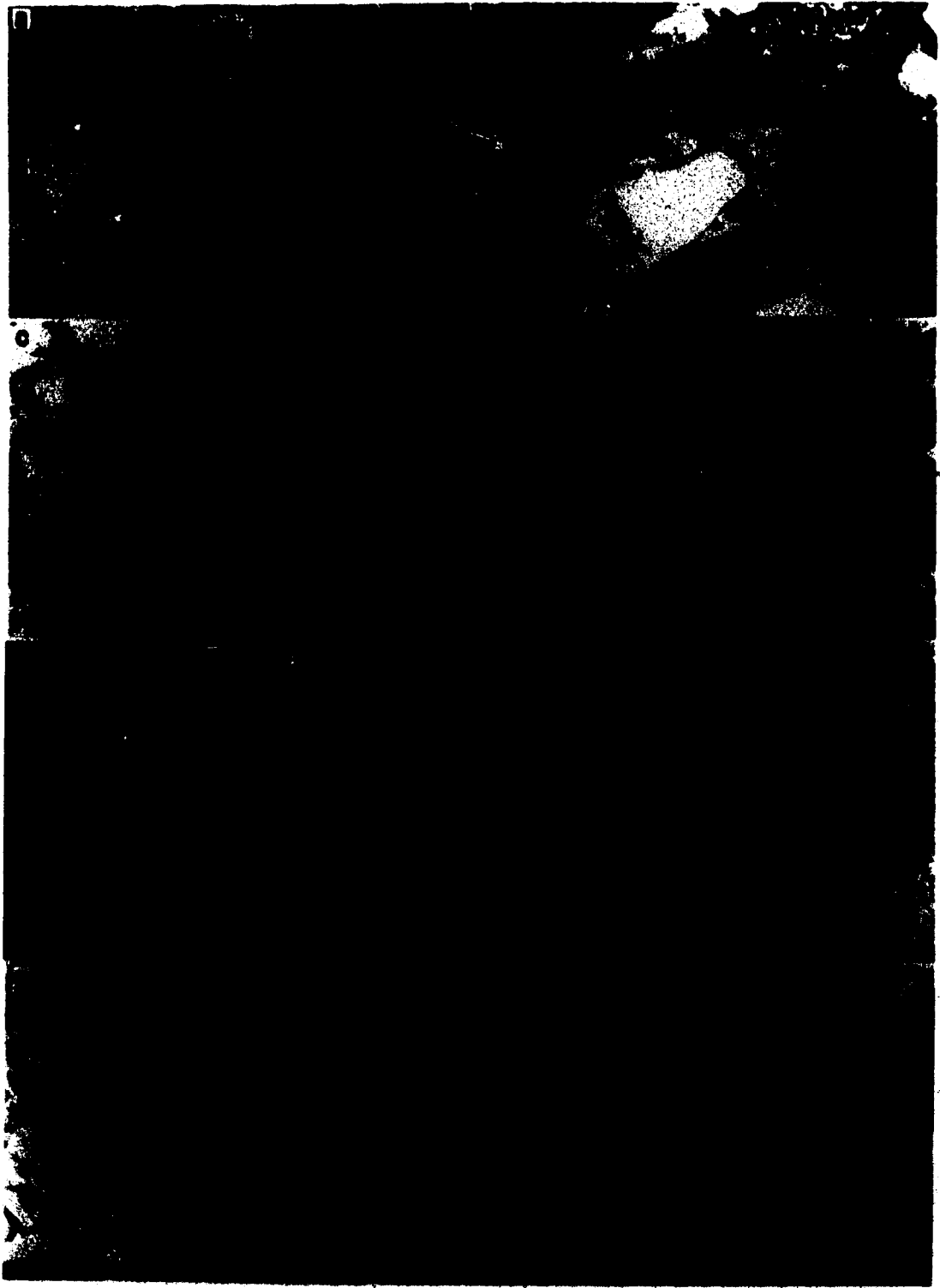
**(e)** Thin section photomicrograph of grain-coating siderite spheres (arrows) in a tightly compacted sandstone. Plane polarized light. Cardium (6-26-62-5 W6, 1860.8 m). Field of view is 0.83 mm.

**(f)** SEM photomicrograph of an authigenic quartz crystal (QTZ) overlying grain-coating chlorite (CHL). Cardium (11-8-63-5 W6, 1828.2 m).

**(g)** SEM photomicrograph of chlorite (CHL) embedded in authigenic quartz (QTZ). Chlorite precipitated before the quartz. Cardium (11-8-63-5 W6, 1828.2 m).

**(h)** SEM photomicrograph of kaolinite (KAOL) overlying grain-coating chlorite (CHL). Cardium (11-8-63-5 W6, 1828.2 m).





(Table 4.1). The +22.2 ‰ siderite in sample 310 includes both pore-lining and pore-filling siderite; in sample 304, siderite is a pore-lining phase.  $\delta^{13}\text{C}$  values are -7.7 and -8.7 ‰ PDB, respectively. Calcite occurs after siderite in both these samples.

Chlorite is present in a Cardium sample situated 4 m below the siderite-rich sample 310. Chlorite occurs as an early grain-coating phase and is coated in turn by quartz overgrowths (Figures 4.5f and 4.5g) or kaolinite (Figure 4.5h).

Neither siderite nor chlorite were observed in the Paddy or Bluesky sandstones. Rather, a texturally early calcite or ankerite cement is present in these sandstones. In the Paddy sample 233 (Table 4.2), rounded quartz grains float in calcite and ankerite cement (Figure 4.6a). Quartz overgrowths and kaolinite are absent in this sample. In the Bluesky, detrital grains float in microcrystalline Fe-calcite cement (samples 60 and 69, Table 4.2, Figure 4.6b). The  $\delta^{18}\text{O}$  composition of these apparently early calcite cements is similar to that of late-stage calcite cements in the same units, i.e. +11.7 ‰ for early Paddy calcite compared with +11.0 ‰ for late Paddy calcite, and +15 ‰ for early Bluesky calcites compared with +14 ‰ for late Bluesky calcite.  $\delta^{13}\text{C}$  values, however, from early cements in both units are significantly higher than for late stage cements (early Paddy calcite  $\delta^{13}\text{C} = -3.1$  ‰ whereas late Paddy calcite  $\delta^{13}\text{C} = -10.9$  ‰; early Bluesky calcite  $\delta^{13}\text{C} = +1.1$  to +2.2 ‰ whereas late Bluesky calcite  $\delta^{13}\text{C} = -4.0$  to -0.8 ‰ PDB).

No very early diagenetic phases were observed in the Halfway and Belloy sandstones.

### ***Intermediate-Stage Diagenetic Minerals***

Intermediate-stage diagenetic minerals include quartz overgrowths, kaolinite, illite and albite. Some replacement of unstable grains by dolomite occurred during an early to intermediate stage of diagenesis. Most of the dolomite in the Bluesky consists of detrital grains which are

TABLE 4.1 ISOTOPE RESULTS FOR SIDERITE

	LOCATION	DEPTH (m)	ROCK TYPE*	DESCRIPTION*	$\delta^{18}\text{O}$ (SMOW)	$\delta^{13}\text{C}$ (PDB)
<b>CARDIUM</b>						
	310 11-8-63-5W6	1824 10		siderite rims & pore fill, 52%C, 48%S	22.2	-7.7
	304 15-16-68-13W6	1150 50		early rims before calcite	16.7	-8.7
<b>CADOTTE</b>						
	301 14-18-74-12W6	1460 20	vfg sst	siderite concretion	19.6	4.4
	298 14-18-74-12W6	1451 75		early siderite cement	18.7	2.2
	327 10-7-68-13 W6	2487 00	vfg sst	siderite concretion, 92%S, 8%D	18.4	3.1
<b>FAHLER</b>						
	351 6-28-69-12W6	2139 40	congl	siderite cement, 67%S, 27%C, 4%A, 2%D	16.5	0.1
<b>CADOMIN</b>						
	339 10-8-70-9W6	2204 00	sandy congl	early siderite cement	20.1	3.6

\* abbreviations vfg sst very fine grained sandstone, congl -conglomerate, S-siderite, C-calcite,  
D-dolomite, A-ankerite

TABLE 4.2 ISOTOPE RESULTS FOR CALCITE

	LOCATION	DEPTH (m)	ROCK TYPE*	DESCRIPTION*	$\delta^{18}\text{O}$ (SMOW)	$\delta^{13}\text{C}$ (PDB)
<b>CARDIUM</b>						
303	15-16-68-13W6	1149.8		74%C, 26%D, late calcite cement	15.5	-4.7
310	11-8-63-5W6	1824.1		50%C, 50%S, calc. after partial siderite dissol.	12.9	-15.8
315	15-34-61-4W6	1929.0		fracture-fill calcite	13.6	-15.3
<b>PADDY</b>						
231	7-11-72-12W6	1686.2	f.g. sst.	late calcite cement	11.0	-10.9
233	7-11-72-12W6	1693.7	m.g. sst.	74C, 26A, early calcite cement	11.7	-3.1
<b>CADOTTE</b>						
323	10-7-68-13W6	2481.3	m.g. sst.	fracture-fill calcite	16.0	2.2
<b>FAHLER</b>						
218	93-P-6, b-24-B	2282.0	siltstone	early Fe-calcite cement	11.2	-9.1
217	93-P-6, b-24-B	2284.0	siltstone	fracture-fill calcite cement	17.1	-0.5
252	93-P-7, a-48-J	1997.9	congl.	Fe-calcite cement	11.2	-2.2
236	93-P-1, b-28-L	2348.4	congl.	calcite cement	10.8	-3.1
369	6-28-68-13W6	2552.7	congl.	calcite cement	10.8	-7.6
414	11-30-69-10W6	1995.6	congl.	macro-cryst. calcite cement	11.2	-1.9
4751	10-16-69-11W6	2088.0	congl.	calcite cement	11.6	-5.2
351	6-28-69-12W6	2139.4	congl.	calcite cement	11.2	-1.4
353	6-28-69-12W6	2141.5	congl.	calcite cement	11.2	2.8
423	6-7-70-11W6	1981.8	congl.	macro-cryst. calcite cement	12.3	7.3
424	6-7-70-11W6	1980.9	congl.	meso-cryst. calcite cement after siderite	12.2	9.7
403	6-21-70-12W6	1979.4	congl.	calcite cement	11.8	-2.1
4480	11-30-70-12W6	2021.5	congl.	macro-cryst. calcite	11.8	-4.6
377	6-18-72-11W6	1782.0	congl.	macro-cryst. calcite	12.5	-2.9
359	11-13-66-8W6	2556.0	congl.	late micro-cryst. calcite	23.4	1.4
366	6-8-67-9W6	2389.9	congl.	calcite cement	23.6	1.9
4028	11-5-72-12W6	1870.0	f.g. sst.	micro-meso-cryst. calcite, replaces feldspars	11.6	-7.1
4518	93-P-1, c-16-I	2148.6	m.g. sst.	macro-cryst. Fe-calcite, replaces feldspars	11.5	-4.6
224	93-P-7, a-57-C	2338.6	v.f.g. sst.	54C, 39D, 7A	14.1	-2.8
3640	93-P-1, a-85-G	2295.0	m.g. sst.	micro-meso-cryst. calcite, replaces feldspars	14.2	2.1
	6-2-68-4W6	1707.0	m.g. sst.	72C, 19D, 9A	14.6	-0.3
<b>BLUESKY</b>						
60	10-16-65-2W6	2204.7	siltstone	72C, 22D, 6A, early calcite cement	15.4	1.1
69	10-4-65-2W6	2265.1	v.f.g. sst.	55C, 16D, 29A; early calcite cement	15.1	2.2
161	6-24-65-3W6	2255.5	m.g. sst.	55C, 31D, 13A; late calcite cement	15.6	-2.7
118	11-24-67-6W6	2125.0	m.g. sst.	73C, 13D, 14A; late calcite cement	14.1	-2.6
128	7-18-67-5W6	2148.2	m.g. sst.	late calcite cement	14.4	-4.0
71	10-4-65-2W6	2269.2	f.g. sst.	late Fe-calcite cement	14.3	-3.2
156	6-24-65-3W6	2273.3	siltstone	62C, 11D, 28A; calcite shells	14.5	-2.3
429	10-34-70-13W6	2372.2	congl.	meso. to macro-cryst. calcite cement	12.0	-3.6
431	10-36-74-13W6	1829.0	congl.	macro-cryst. calcite cement	13.8	-0.8
<b>HALFWAY</b>						
274	10-3-70-10W6	2662.7		70%C, 30%D; late calcite cement	19.6	-25.7
275	10-3-70-10W6	2666.4		vug-fill calcite	18.8	-27.6
276	10-3-70-10W6	2667.0		fracture-fill calcite	19.7	-15.3
<b>BELLOY</b>						
258	11-31-69-9W6	2829.3	f.g. sst.	macro-cryst. calc. cement after authigenic qtz	21.5	-24.4

\* abbreviations: sst.=sandstone, v.f.g.=very fine grained, f.g.=fine-grained, m.g.=medium grained, congl.=conglomerate, C=calcite, D=dolomite, A=ankerite, qtz=quartz, calc.=calcite, cryst.=crystalline, dissol.=dissolution

**Figure 4.6**

**(a)** Thin section photomicrograph of rounded quartz grains surrounded by calcite and ankerite cement (C). Quartz overgrowths are notably absent. Plane polarized light. Paddy (7-11-72-12 W6, 1693.7 m). Field of view is 3.3 mm.

**(b)** Thin section photomicrograph of detrital grains floating in Fe-calcite cement. Both microcrystalline (CALC, central region) and mesocrystalline (outer regions) calcite cements are present. Plane polarized light. Bluesky (10-4-65-2 W6, 2265.1 m). Field of view is 1.34 mm.

**(c)** Thin section photomicrograph of pore space entirely filled by quartz overgrowths. Plane polarized light. Paddy (7-11-72-12 W6, 1684.4 m). Field of view is 1.34 mm.

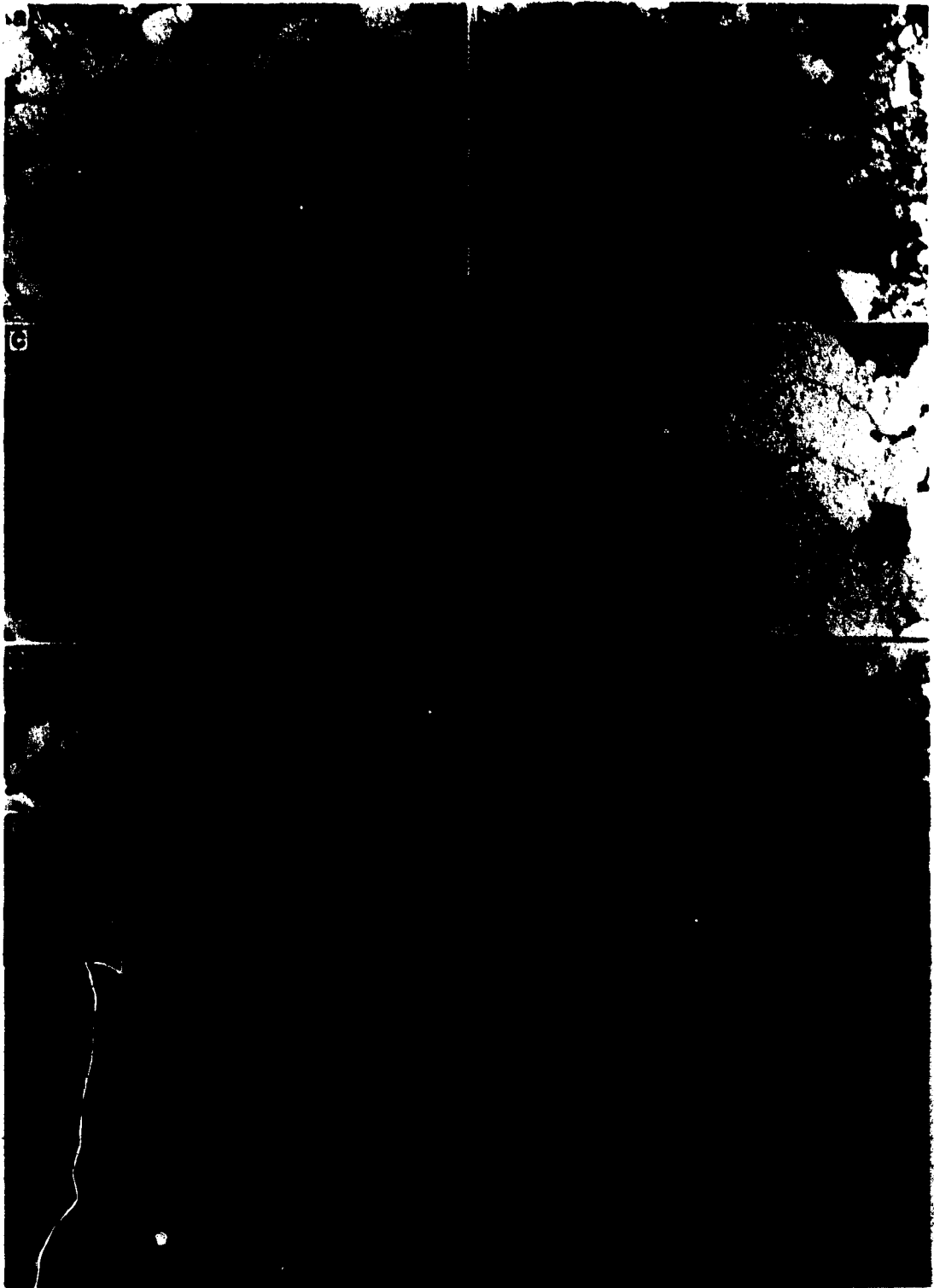
**(d)** Thin section photomicrograph of pore space (P) only partially filled by quartz overgrowths. Plane polarized light. Paddy (7-11-72-12 W6, 1697.4 m). Field of view is 3.3 mm.

**(e)** SEM photomicrograph of kaolinite (KAOL) resting on authigenic quartz (QTZ). Kaolinite has also partially inhibited the development of the quartz overgrowth. Cardium (14-18-74-12 W6, 384.9 m).

**(f)** SEM photomicrograph of kaolinite (KAOL) embedded in calcite cement (CALC). Bluesky (7-18-67-5 W6, 2148.2 m).

**(g)** SEM photomicrograph of kaolinite (KAOL) embedded in ankerite cement. Bluesky (11-24-67-6 W6, 2125.2 m).

**(h)** SEM photomicrograph of kaolinite (KAOL) embedded in authigenic quartz (QTZ). Bluesky (11-24-67-6 W6, 2125.2 m).



macrocrystalline and approximately grain size. However, dolomite overgrowths and remnants of chert mostly replaced by dolomite are present. Many of the micro- or meso-crystalline dolomite grains actually may be grain replacements.  $\delta^{18}\text{O}$  values for dolomite in the Bluesky vary from +17.5 to +23 ‰.  $\delta^{13}\text{C}$  values range from -2.5 to -0.3 ‰ (Table 4.3).

Quartz overgrowths occur in quartzose sandstones in all the Cretaceous units examined as well as in the Halfway and Belloy sandstones. In the Cardium, quartz overgrowths coat chlorite (Figure 4.5f and 4.5g) or siderite, and calcite may fill the remaining pore space. The  $\delta^{18}\text{O}$  value for quartz overgrowths in one siderite-rich Cardium sandstone is +22.5 ‰ (Table 4.4). Table 4.4 also lists  $\delta^{18}\text{O}$  values for quartz overgrowths in sandstones throughout the vertical section and for quartz druse in Cadotte, Falher and Cadomin conglomerates.  $\delta^{18}\text{O}$  values vary from +14 to +24 ‰. The Cardium, Paddy, Bluesky, Nikanassin, Halfway and Belloy sandstones all have authigenic quartz  $\delta^{18}\text{O}$  values in the range of +20 to +22.5 ‰. A quartz overgrowth in one Falher sandstone has a  $\delta^{18}\text{O}$  value of +18.4 ‰; one sample of quartz overgrowths from the Paddy has  $\delta^{18}\text{O} = +14$  ‰.  $\delta^{18}\text{O}$  values for quartz druse in the Falher are +15 to +16 ‰.

Quartz overgrowths from the Paddy have two distinctly different  $\delta^{18}\text{O}$  values, +21 to +24 ‰ and +14 ‰ (Table 4.4). The former range is similar to that of most other sandstone units. The latter value is similar to quartz druse in Falher and Cadotte conglomerates. In sample 230 ( $\delta^{18}\text{O} = +21.4$  ‰, Table 4.4), all pores that are surrounded by detrital quartz grains are completely filled by authigenic quartz (Figure 4.6c). In sample 234 ( $\delta^{18}\text{O} = +14$  ‰, Table 4.4), pore spaces that are completely surrounded by detrital quartz are only partially filled by authigenic quartz (Figure 4.6d).

Kaolinite was precipitated after chlorite in the Cardium sandstone (Figure 4.5h). It occurs partially embedded in quartz overgrowths and also sits on the surface of quartz overgrowths (Figure 4.6e). In the Paddy, kaolinite occurs in minor amounts in all samples except the calcite-

TABLE 4.3 ISOTOPE RESULTS FOR DOLOMITE

	LOCATION	DEPTH (m)	ROCK TYPE*	DESCRIPTION*	$\delta^{18}\text{O}$ (SMOW)	$\delta^{13}\text{C}$ (PDB)
<b>FALHER</b>						
	10-20-67-5W6	1910.5	v.f.g.sst.	97D,3S	22.4	-1.7
	7-20-67-6W6	2003.6	v.f.g.sst.	68D,20A,12C	22.0	-0.9
	10-29-67-10W6	2397.0	f.g.sst.	79D,11A,10S	22.0	-1.0
	10-13-69-9W6	1867.0	v.f.g.sst.	70D,15A,15S	17.1	-0.5
<b>BLUESKY</b>						
133	7-10-63-1W6	2476.1	v.f.g.sst.	dolomite	21.7	-1.0
4	4-7-63-3W6	2520.0	v.f.g.sst.	dolomite	23.0	-0.3
5	4-7-63-3W6	2523.0	v.f.g.sst.	dolomite	22.4	-0.8
19	10-10-64-6W6	2782.4	siltstone	51D,24A,25C	17.5	-2.5
137	16-28-64-6W6	2664.8	v.f.g.sst.	67D,21A,12C	18.0	-2.2
60	10-16-65-2W6	2204.7	siltstone	27D,73C	20.4	-0.7
122	11-24-67-6W6	2128.7	m.g.sst.	73D,27A	21.9	-0.9
31	5-7-74-11W6	1840.9	v.f.g.sst.	64D,11A,25C	23.0	-0.8

\* abbreviations: sst.=sandstone, v.f.g.=very fine grained, f.g.=fine-grained, m.g.=medium grained, congl.=conglomerate, C=calcite, D=dolomite, A=ankerite, S=siderite



TABLE 4.4 ISOTOPE RESULTS FOR AUTHIGENIC QUARTZ

	LOCATION	DEPTH (m)	ROCK TYPE*	DESCRIPTION*	$\delta^{18}\text{O}$ (SMOW)
<b>CARDIUM</b>					
304	15-16-68-13W6	1150.5	v.f.g. sst	chem & sieve, siderite-rich quartz before calcite cement	22.5
<b>PADDY</b>					
230	7-11-72-12W6	1684.4	f.g. sst.	chem & sieve	21.4
232	7-11-72-12W6	1689.6	m.g. sst.	chem & sieve	24.0
234	7-11-72-12W6	1697.4	m.g. sst.	chem & sieve	14.0
<b>CADOTTE</b>					
324	10-7-68-13W6	2481.0	v.f.g. sst	fracture-lining druse	16.4
324	10-7-68-13W6	2481.0	v.f.g. sst	vug-lining druse	16.0
<b>FAHLER</b>					
196	7-30-69-11W6	2101.3	congl.	hand picked	16.3
290	11-31-71-13W6	1996.0	congl.	hand picked	15.5
237	93-P-1,b-28-L	2348.1	congl.	hand picked	15.4
291	93-P-1,c-40-F	2414.5	congl.	hand picked	15.0
178	11-4-70-11W6	1988.3	v.f.g. sst.	chem & sieve	18.4
<b>BLUESKY</b>					
71	10-4-65-2W6	2269.2	v.f.g. sst.	chem & sieve, qtz before Fe-calcite cement	20.0
<b>CADOMIN</b>					
293	6-16-68-11W6	2631.0	congl.	hand picked	18.2
292	5-32-65-9W6	3188.0	congl.	hand picked	18.9
372	7-27-72-13W6	2298.0	congl.	hand picked	18.5
<b>NIKANASSIN</b>					
345	4-23-72-10W6	2127.3	m.g. sst.	chem & sieve	19.6
<b>HALFWAY</b>					
274	10-3-70-10W6	2662.7	v.f.g. sst.	chem & sieve	21.0
<b>BELLOY</b>					
258	11-31-69-9W6	2829.3	f.g. sst.	chem & sieve, qtz before calcite cement	22.7
268	9-11-65-13W6	4282.0	f.g. sst.	chem & sieve, qtz before anhydrite cement	21.2

\* abbreviations: sst.=sandstone, v.f.g.=very fine grained, f.g.=fine-grained, m.g.=medium grained, congl.=conglomerate, qtz=quartz, chem&sieve = quartz separate prepared using the method of Syers et al.,(1968); Jackson (1979) and Lee and Savin (1985).

cemented sample 233 (Figure 4.6a). This distribution suggests that most of the kaolinite is diagenetic and that early calcite cementation took place before crystallization of kaolinite. Kaolinite also occurs embedded in or resting on quartz overgrowths, and in small, secondary pore spaces created by partial dissolution of rock fragments. In the Bluesky, kaolinite is embedded in calcite (Figure 4.6f) and ankerite (Figure 4.6g) cement and in quartz overgrowths (Figure 4.6h). It also rests upon quartz overgrowth surfaces (Figure 4.7a).

Kaolinite from Falher sandstones has a  $\delta^{18}\text{O}$  value of +11 ‰ (Table 4.5), similar to dickite from Falher and Cadotte conglomerates. One sample of dickite from a Bluesky conglomerate in the northwestern part of the study area also has  $\delta^{18}\text{O}=+11.4$  ‰ (Table 4.5). However, three other samples of kaolinite from Bluesky sandstones in the southeastern part of the study area have  $\delta^{18}\text{O}$  results ranging from +10.9 to +21.6 ‰. This range supports the petrographic evidence for multiple generations of kaolinite.

Illite in the Cardium occurs as a pore-filling cement (Figure 4.7b) and as a coating on kaolinite (Figure 4.7c). In the Paddy, illite lines pore walls in some kaolinite-filled pores (Figure 4.7d); in other pores, illite forms a partial coating on kaolinite (Figure 4.7e), authigenic quartz crystals and quartz overgrowths. Illite also forms bridges between authigenic pyrite and quartz overgrowths (Figure 4.7f). In the Bluesky, illite coats pore walls and kaolinite (Figure 4.7g). Samples 52 and 147 (Table 4.6) are rich in glauconite, an Fe-rich I/S clay. This glauconite occurs as grain-size pellets of illitic clay with a fibrous texture (Figure 4.7h).

$\delta^{18}\text{O}$  values for illite are +7.6 to +11.4 ‰ in the Falher, +12.7 ‰ in the Cardium and +11.9 ‰ in the Paddy (Table 4.6).  $\delta^{18}\text{O}$  values for illite in the Bluesky, including both glauconite-rich and glauconite-poor samples, range from +13.3 to +15.1 ‰. There is no correlation between the abundance of glauconite and the  $\delta^{18}\text{O}$  value. In the Cadomin, illite has still higher  $\delta^{18}\text{O}$  values (+16.0 to +16.4 ‰).

**Figure 4.7**

(a) SEM photomicrograph of kaolinite (KAOL) filling the pore space after quartz overgrowths. Bluesky (11-24-67-6 W6, 2125.2 m).

(b) SEM photomicrograph of pore-filling illite. Cardium (15-16-68-13 W6, 1159.4 m).

(c) SEM photomicrograph of illite (ILL) coating kaolinite (K). Cardium (15-34-61-4 W6, 1929.6 m).

(d) SEM photomicrograph of pore-lining illite. Kaolinite (KAOL) formed after illite. Paddy (7-11-72-12 W6, 1684.4 m).

(e) SEM photomicrograph of illite partially coating kaolinite (KAOL). Paddy (7-11-72-12 W6, 1684.4 m).

(f) SEM photomicrograph of illite forming a bridge between authigenic quartz and pyrite. Paddy (7-11-72-12 W6, 1684.4 m).

(g) SEM photomicrograph of illite (ILL) lining the pore wall and partially coating kaolinite (KAOL). Bluesky (7-18-67-5 W6, 2151.2 m).

(h) SEM photomicrograph showing the fibrous texture on the side of a glauconite pellet. Bluesky (10-16-65-2 W6, 2195.5 m).

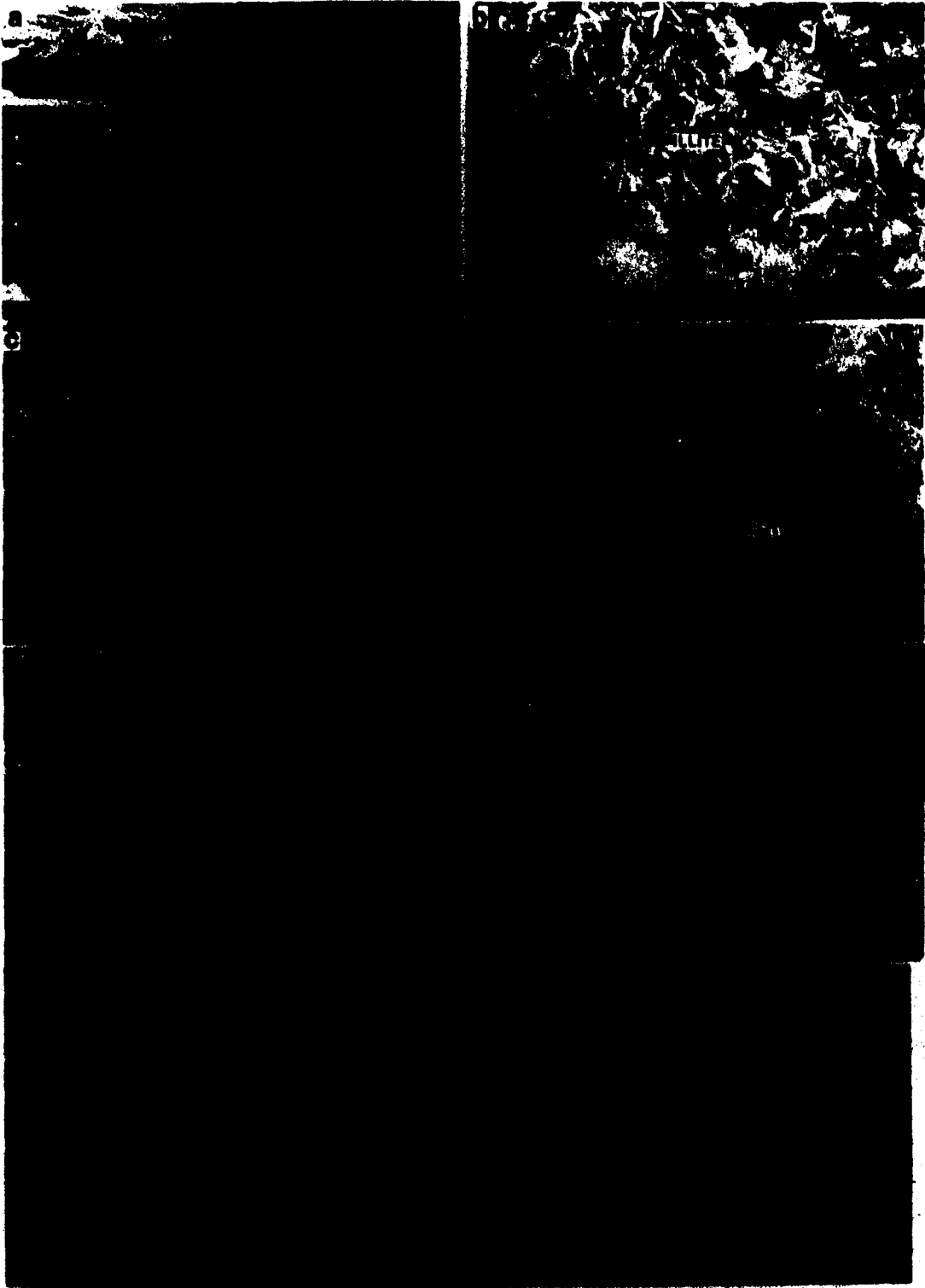


TABLE 4.5 ISOTOPE RESULTS FOR KAOLINITE

	LOCATION	DEPTH (m)	ROCK TYPE*	DESCRIPTION*	$\delta^{18}\text{O}$ (SMOW)	$\delta\text{D}$ (SMOW)
<b>CADOTTE</b>						
294	14-18-74-12W6	1437.7	fine congl.	dickite	11.3	
<b>FAHLER</b>						
348	11-5-69-7W6	1864.5	congl.	dickite	10.3	-131
419	11-4-69-10W6	2035.2	congl.	dickite	11.0	
196	7-30-69-11W6	2101.3	congl.	dickite	10.6	
200	7-30-69-11W6	2117.1	congl.	dickite	10.3	-104
206	7-12-70-11W6	1951.8	congl.	dickite	11.0	-115
182	11-4-70-11W6	2006.0	congl.	dickite	12.3	-108
220	93-P-7, a-57-C	2321.3	congl.	dickite	10.7	
3535	7-9-70-10W6	1908.7	v.f.g. sst.	55K, 34I, 4C, 7ML	11.4	
3539	7-9-70-10W6	1940.7	m.g. sst.	79K, 13I, 4C, 3ML: feldspar-rich	10.6	
4991	6-5-71-10W6	1795.0	f.g. sst.	74K, 15I, 5C, 5ML	11.4	
<b>BLUESKY</b>						
126	7-18-67-5W6	2148.2	m.g. sst.	calc. kaol.; 19% kaol. before calcite	21.6	
119	11-24-67-6W6	2125.2	m.g. sst.	calc. kaol.; 46.5% kaol.	16.7	
135	7-10-63-1W6	2481.6	f.g. sst.	calc. kaol.; 41.5% kaol.	10.9	
410	7-24-74-13W6	1848.0	congl.	dickite	11.4	
<b>CADOMIN</b>						
266	16-31-64-12W6	3316.5	congl.	dickite	14.0	-104
292	5-32-65-9W6	3188.0	congl.	dickite	12.2	-102
267	9-11-65-13W6	3248.0	congl.	dickite	14.2	-96
293	6-16-68-11W6	2631.0	congl.	dickite	13.3	
337	10-8-70-9W6	2197.9	congl.	dickite	13.7	-93
255	93-P-1, c-12-L	2727.9	congl.	dickite	13.6	
373	7-27-72-13W6	2298.3	congl.	dickite		-93

\* abbreviations: sst.=sandstone, v.f.g.=very fine grained, f.g.=fine-grained, m.g.=medium grained, congl.=conglomerate, K=kaolinite, I=illite, C=chlorite, ML=mixed layer I/S  
calc.kaol = isotopic composition of kaolinite calculated from a clay mixture

TABLE 4.6 ISOTOPE RESULTS FOR ILLITE

	LOCATION	DEPTH (m)	ROCK TYPE*	DESCRIPTION*	$\delta^{18}O$ (SMOW)
<b>CARDIUM</b>					
308	15-16-68-13W6	1159.5	v.f.g.sst.		12.7
<b>PADDY</b>					
230	7-11-72-12W6	1684.4	f.g.sst.	I+IS >15%S	11.9
<b>FAHLER</b>					
249	93-P-1,c-12-L	2301.0	f.g.sst.	I+ISII <15%S	11.0
251	93-P-1,c-12-L	2306.0	v.f.g.sst.	I+ISII <15%S	11.3
242	93-P-1,b-28-L	2353.4	v.f.g.sst.	I+IS >15%S	10.6
224	93-P-7,a-57-C	2338.6	v.f.g.sst.	I+IS 25%S	10.5
3638	93-P-1,a-85-G	2286.0		93I,3K,1C,3ML	8.8
4520	93-P-1,c-16-I	2151.3	f.g.sst.	59I,20K,7C,14ML; feldspar-rich	10.5
4250	93-P-16,b-28-I	2502.5		53I,24K,9C,14ML	10.6
4047	11-12-71-13W6	2026.6	f.g.sst.	77I,3K,8C,12ML; feldspar-rich	10.7
4030	11-5-72-12W6	1879.1	v.f.g.sst.	59I,23K,18C	11.4
4040	11-5-72-12W6	1890.8	m.-c.g.	60I,10K,10C,20ML; feldspar-rich	9.7
4041	11-5-72-12W6	1894.9	f.g.sst.	70I,10K,4C,16ML; feldspar-rich	10.1
5095	10-19-72-13W6	1941.9		78I,2K,6C,12ML	7.8
<b>BLUESKY</b>					
52	10-16-65-2W6	2195.5	m.g.sst.	I/S 11%S; glauconite-rich	14.7
133	7-10-63-1W6	2476.1	v.f.g.sst.	I+ISII <15%S	15.1
67	10-4-65-2W6	2261.9	v.f.g.sst.	I+I/S >15%S	14.6
147	11-20-64-26W5.	2214.3	m.g.sst.	I/S 15%S; glauconite-rich	13.8
130	7-18-67-5W6	2151.2	v.f.g.sst.	I with 11%S	14.3
426	10-34-70-13W6	2358.0	sandstone		13.3
416	6-28-68-13W6	2744.5	sandstone		13.6
<b>CADOMIN</b>					
338	10-8-70-9W6	2201.6	sandstone		16.4
318	10-7-68-13W6	2988.6	sandstone		16.0

\* abbreviations: sst.=sandstone, v.f.g.=very fine grained, f.g.=fine-grained, m.g.=medium grained, cong.=conglomerate, K=kaolinite, I=illite, C=chlorite, ML=mixed layer I/S, S=smectite

K-feldspar dissolution and albitization of plagioclase is evident in all units where at least minor amounts of feldspar are present. At least some illite is the result of dissolution of K-feldspar. Albite crystals are sparsely scattered throughout Cretaceous sandstones and are found in fracture-fills in the Cadomin.

### ***Late Stage Diagenetic Minerals***

Calcite and ankerite are the latest diagenetic phases that precipitated in Cretaceous units; in Triassic and Permian sandstones, late stage anhydrite is also present. Late stage ankerite occurs in the Paddy, Falher and Bluesky sandstones but is absent in the Cardium, Cadomin, Halfway and Belloy samples examined. Late stage calcite is observed in all these units except the Cadomin. In the Cadomin, the last preserved diagenetic phases are dickite and quartz druse.

Table 4.2 lists isotopic results for calcite cements. Within a particular unit, the  $\delta^{18}\text{O}$  value for calcite is the same whether the cement is texturally early or late.  $\delta^{18}\text{O}$  values for calcite in the Cardium vary from +13 to +15.5 ‰; in the Paddy and most of the Falher, calcite  $\delta^{18}\text{O} = +11$  ‰; in the Bluesky  $\delta^{18}\text{O}$  calcite = +14 to +15 ‰; and in the Halfway and Belloy calcite  $\delta^{18}\text{O}$  values are still higher, +19 ‰ and +21.5 ‰, respectively.  $\delta^{13}\text{C}$  values are highly variable, ranging from -25 ‰ in the Halfway and Belloy, to -15 ‰ in the Cardium, and from -10 to -4 ‰ up to +9 ‰ in the Paddy and Falher.

Ankerite and calcite in the Paddy replace texturally early carbonate cement in a medium-grained sandstone (Figures 4.6a and 4.8a). The ankerite and calcite have similar  $\delta^{13}\text{C}$  values. In the Bluesky, ankerite is ubiquitous as a coating on dolomite grains. In some samples, ankerite-rimmed dolomite is surrounded by later calcite cement (Figure 4.8b). In other samples, ankerite cement occurs in fine-grained sandstone whose pores are also filled by authigenic quartz and kaolinite.  $\delta^{18}\text{O}$  values for Bluesky ankerite vary from +15.9 to +17.1 ‰.  $\delta^{18}\text{O}$  values for Falher ankerite are slightly lower, about +14.7 to +15.7 ‰; those for Paddy ankerite are still lower,

**Figure 4.8**

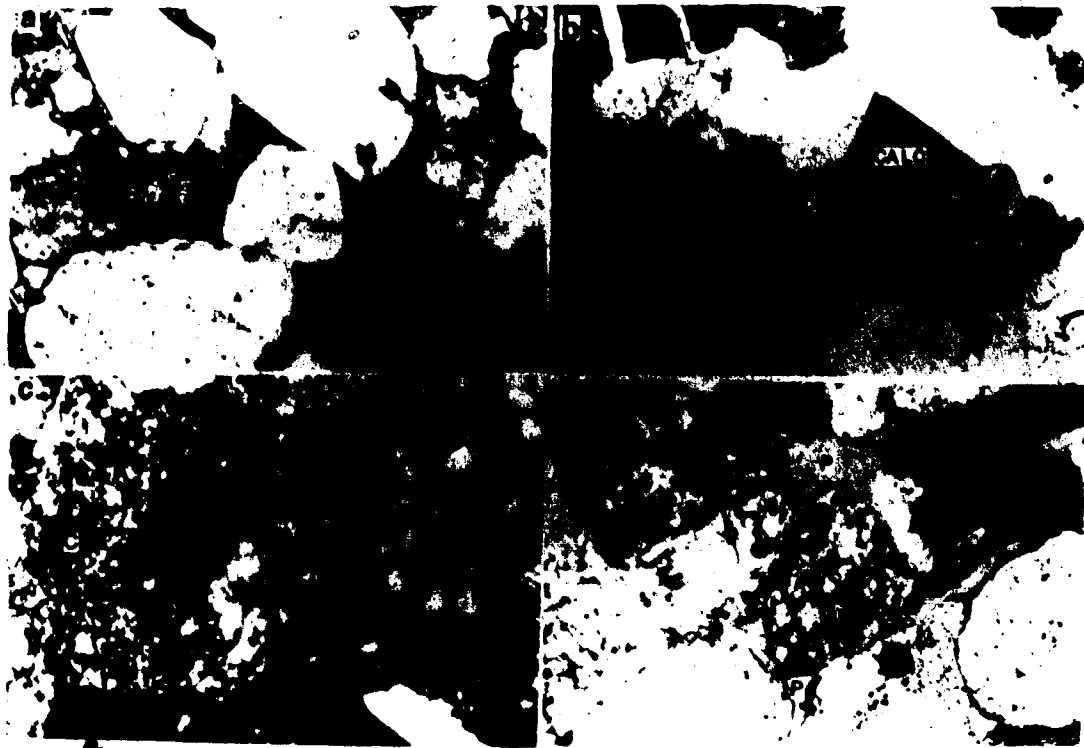
(a) Thin section photomicrograph of ankerite (arrows) and calcite cement. The cement adjacent to the ankerite crystals indicated by arrows is calcite. Plane polarized light. Paddy (7-11-72-12 W6, 1693.7m). Field of view is 1.34 mm.

(b) Thin section photomicrograph of ankerite-rimmed dolomite (D) surrounded by calcite cement (CALC). The darker rim around the dolomite grain is ankerite which was stained blue. Plane polarized light. Bluesky (11-20-64-26 W5, 2206.6m). Field of view is 1.34 mm.

(c) Thin section photomicrograph of late-stage, poiklotopic calcite cement (c). Calcite fills in a partially dissolved chert grain (centre). Crossed-polars. Bluesky (7-18-67-5 W6, 2148.2 m). Field of view is 1.34 mm.

(d) Thin section photomicrograph of a sandstone similar to that in (c), but the pore space (P) is empty. This large pore space was probably once filled by calcite cement. Plane polarized light. Bluesky (11-24-67-6 W6, 2125.0 m). Field of view is 1.34 mm.





+13.2 ‰ (Table 4.7).  $\delta^{13}\text{C}$  values for ankerite in all three units are -3 to -1 ‰ with the exception of one Falher sample with  $\delta^{13}\text{C} = +4.5$  ‰.

### *Fracture-Filling Diagenetic Minerals*

A few mineral-lined fractures were found in core during sampling. Fractures are generally sub-vertical, and are lined by calcite or Fe-dolomite (Table 4.8). One vertical fracture in the Gething contains kaolinite, barite and calcite, precipitated in that order. In one Cadotte well, a vertical fracture contains calcite, whereas an horizontal fracture is lined by authigenic quartz crystals.

Table 4.8 gives the fracture-filling cements and their isotopic compositions. For comparison, the isotopic composition of late-stage calcite cement and quartz druse are also listed. In the Cardium, calcite cement in the sandstones and fracture-filling calcite in the southeastern part of the study area have comparable  $\delta^{18}\text{O}$  and  $\delta^{13}\text{C}$  values. In the Cadotte, quartz which fills a horizontal fracture has the same  $\delta^{18}\text{O}$  value as quartz which lines a large vug created by partial dissolution of siderite. This value is also comparable to the  $\delta^{18}\text{O}$  value of quartz druse in the Falher. The similarity of the isotopic values of fracture-fill cements to the isotopic values of surrounding sandstone cements suggests that fractures were filled by minerals precipitated from the same waters as those depositing the late-stage calcite in the Cardium, and quartz druse in the Cadotte and Falher.

Isotopic values for other fracture-fill cements do not agree as closely with isotopic values of surrounding cements. In the Cadotte, vertical fractures are filled by calcite with  $\delta^{18}\text{O} = +16$  ‰ and Fe-dolomite with  $\delta^{18}\text{O} = +13.8$  ‰; vertical fractures in the Falher are filled by calcite with  $\delta^{18}\text{O} = +17$  ‰. In contrast, late-stage calcite cements in the Falher have  $\delta^{18}\text{O} = +11$  ‰. In the Nikanassin, Fe-dolomite which fills a fracture has  $\delta^{18}\text{O} = +20.5$  ‰ compared to  $\delta^{18}\text{O} = +17$  ‰

TABLE 4.7 ISOTOPE RESULTS FOR ANKERITE

	LOCATION	DEPTH (m)	ROCK TYPE*	DESCRIPTION*	$\delta^{18}\text{O}$ (SMOW)	$\delta^{13}\text{C}$ (PDB)
<b>PADDY</b>						
233	7-11-72-12W6	1693.7	m.g sst	74C,26A	13.2	-3.6
<b>FAHLER</b>						
202	7-30-69-11W6	2122.7	v.f.g sst	ankerite	14.7	-1.0
178	11-4-70-11W6	1988.3	v.f.g.sst	73A,26D,1C	15.0	4.5
	6-2-68-4W6	1720.0	congl sst	79A,14S,7C	15.4	-3.2
	11-13-66-8W6	2566.0	f.g sst	51A,46D,3S	15.7	-0.6
<b>BLUESKY</b>						
105	6-32-65-4W6	2295.3	f.g sst	63D,37A, ankerite separated	17.1	-1.1
137	16-28-64-6W6	2664.7	v.f.g.sst	12C,67D,21A, ankerite separated	17.1	-2.6
19	10-10-64-6W6	2782.4	siltstone	25C,51D,24A, ankerite separated	16.1	-3.0
81	11-27-63-2W6	2443.2	f.g sst	44D,56A, ankerite separated	15.9	-2.6
99	7-34-65-3W6	2245.2	v.f.g.sst	24D,66A, ankerite separated	17.0	-2.0
67	10-4-65-2W6	2261.9	v.f.g.sst	40D,60A	17.0	-2.3
132	7-10-63-1W6	2474.4	v.f.g.sst	2C,32D,67A	16.8	-2.2

\* abbreviations: sst = sandstone, v.f.g = very fine grained, f.g = fine-grained, m.g = medium grained, congl = conglomerate, C = calcite, D = dolomite, A = ankerite, S = siderite

TABLE 4.8 COMPARISON OF ISOTOPE VALUES FOR FRACTURE-FILL AND SANDSTONE CEMENTS

	LOCATION	DEPTH (m)	TYPE	DESCRIPTION*	$\delta^{18}\text{O}$ (SMOW)	$\delta^{13}\text{C}$ (PDB)
<b>CARDIUM</b>						
303	15-16-68-13W6	1149.8	cement	74%C,26%D	15.5	-4.7
310	11-8-63-5W6	1824.1	cement	50%C,50%S	12.9	-15.8
315	15-34-61-4W6	1929.0	fracture-fill	calcite	13.6	-15.3
<b>CADOTTE</b>						
323	10-7-68-13W6	2481.3	fracture-fill	calcite	16.0	2.2
324	10-7-68-13W6	2481.0	fracture-fill	quartz	16.4	
391	6-25-66-13W6	2504.1	fracture-fill	Fe-dolomite	13.8	-1.2
<b>FALHER</b>						
218	93-P-6,b-24-B	2282.0	cement	calcite	11.2	-9.1
217	93-P-6,b-24-B	2284.0	fracture-fill	calcite	17.1	-0.5
<b>BLUESKY</b>						
126	7-18-67-5W6	2148.2	cement	calcite	14.4	-4.0
<b>GETHING</b>						
288	6-9-66-5W6	2467.0	fracture-fill	kaol.,barite,calcite		
<b>NIKANASSIN</b>						
343	4-23-72-10W6	2124.8	fracture-fill	Fe-dolomite	20.5	-4.5
<b>HALFWAY</b>						
274	10-3-70-10W6	2662.7	cement	70%C,30%D	19.6	-25.7
275	10-3-70-10W6	2666.4	vug fill	calcite	18.8	-27.6
276	10-3-70-10W6	2667.0	fracture fill	calcite	19.7	-15.3
<b>BELLOY</b>						
258	11-31-69-9W6	2829.3	cement	calcite	21.5	-24.4

\* abbreviations: C=calcite, D=dolomite, S=siderite, kaol.=kaolinite

for late ankerite cement in the Bluesky. In the Halfway, calcite in fractures has a similar  $\delta^{18}\text{O}$  value to the calcite cement, but the  $\delta^{13}\text{C}$  value is  $-15$  ‰ instead of  $-25$  ‰.

## CONSTRAINTS ON POREWATER EVOLUTION

The evolution of porewater in the Falher and Cadomin can be well-constrained by a combination of stable isotope, petrographic, fluid inclusion and water chemistry data (Chapter 2). Data for the Cardium, Paddy, Bluesky, Halfway and Belloy Formations are much more limited. However, combined with the information for the Falher and Cadomin, some insight into porewater evolution and fluid flow throughout the entire section can be obtained. As discussed in Chapter 2 for the Falher and Cadomin, porewater  $\delta^{18}\text{O}$  values increased during burial from  $-12$  to  $-7$  ‰ during early diagenesis to  $+3$  ‰ as burial temperature rose. Even though pore fluids attained temperatures as high as  $190^\circ\text{C}$  in the Falher and at least  $150^\circ\text{C}$  in the Cadomin locality studied, porewaters with  $\delta^{18}\text{O}$  values higher than  $+3$  ‰ are indicated by existing diagenetic minerals only in the Cadomin. During uplift, an influx of meteoric water lowered the  $\delta^{18}\text{O}$  ratio of the porewater and was accompanied by precipitation of dickite in both units, and calcite and ankerite in the Falher.

Porewater evolution curves like those constructed for the Falher Member and Cadomin Formation can be sketched out for the Cardium, Paddy and Bluesky Formations. Figures 4.9a, 4.10a, and 4.11a show  $\delta^{18}\text{O}$  porewater versus temperature curves for the diagenetic minerals; Figures 4.9b, 4.10b, and 4.11b illustrate possible pathways for porewater evolution, as discussed below.

Maximum burial temperatures for each unit can be derived using the Falher temperatures, which were calculated from vitrinite reflectance data (Chapter 2; Figure 2.9) and a geothermal

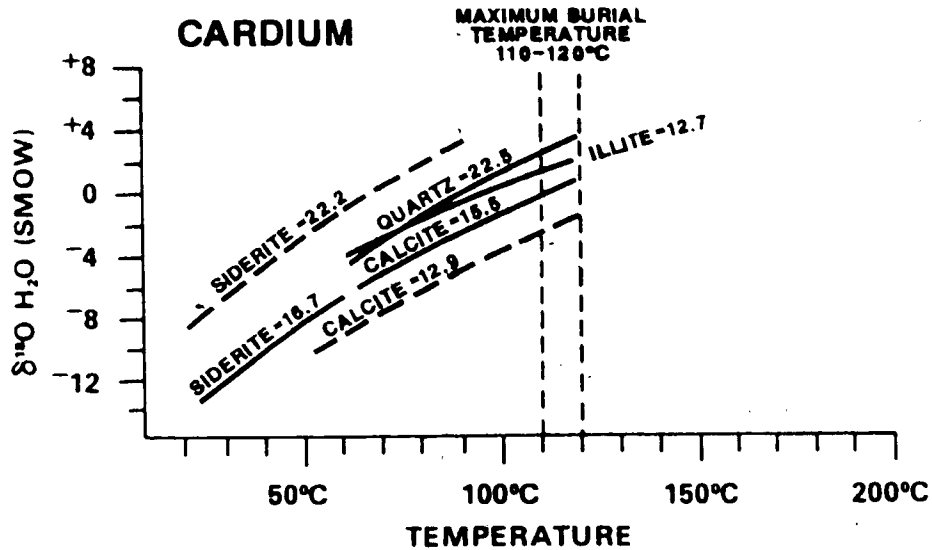


Figure 4.9a  $\delta^{18}\text{O}$  of porewater versus temperature for diagenetic minerals from the Cardium Formation. Mineral curves are shown for  $\delta^{18}\text{O}$  values of each phase using the following equations ( $T = ^\circ\text{K}$ ):

- (1)  $10^3 \ln \alpha_{\text{siderite-H}_2\text{O}} = 2.9(10^6)T^{-2} - 2.80$ ; (Becker and Clayton, 1976);
- (2)  $10^3 \ln \alpha_{\text{quartz-H}_2\text{O}} = 3.38(10^6)T^{-2} - 2.90$ ; (Friedman and O'Neil, 1977; after Clayton et al., 1972);
- (3)  $10^3 \ln \alpha_{\text{calcite-H}_2\text{O}} = 2.78(10^6)T^{-2} - 2.89$ ; (Friedman and O'Neil, 1977; after O'Neil et al., 1969);
- (4)  $10^3 \ln \alpha_{\text{illite-H}_2\text{O}} = 2.43(10^6)T^{-2} - 4.82$ ; (Yeh and Savin, 1977).

Solid curves are for diagenetic minerals from the Kakwa Member; dashed curves are for diagenetic minerals from the Dismal Rat Member.

### POREWATER EVOLUTION PATHWAYS

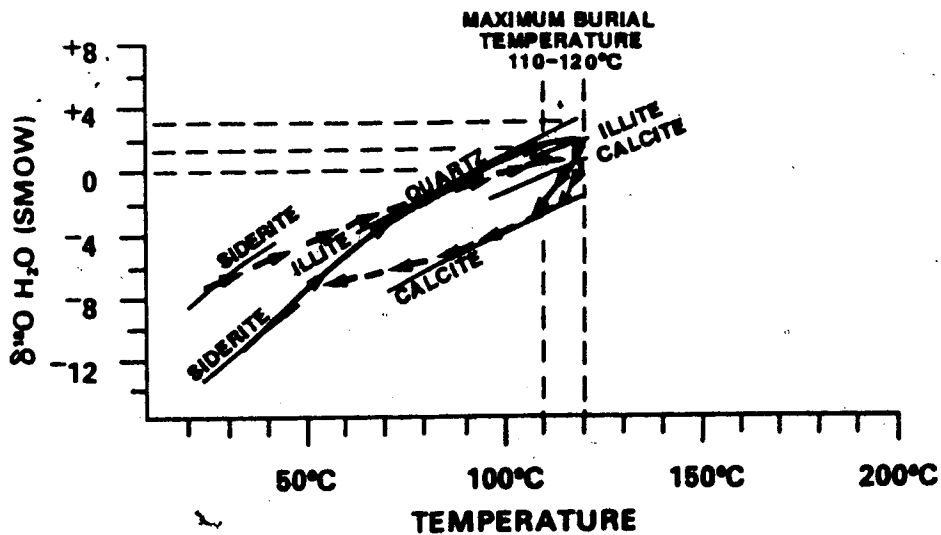


Figure 4.9b Idealized porewater evolution paths ( $\delta^{18}\text{O}$  of water versus temperature) for Cardium sandstones. Two paths are shown (1) calcite precipitated at maximum burial temperature (lower path); and (2) illite precipitated at maximum burial and calcite precipitated during cooling (upper path).

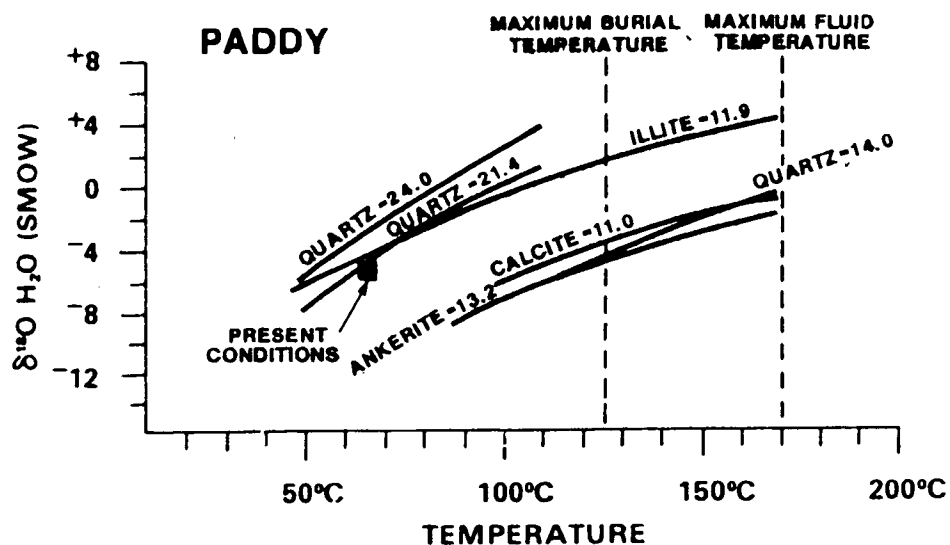


Figure 4.10a  $\delta^{18}\text{O}$  of porewater versus temperature for diagenetic minerals from the Paddy Member of the Peace River Formation. Mineral curves are shown for  $\delta^{18}\text{O}$  values of each phase using the equations listed in the figure caption for Figure 4.9a and the following equation ( $T=^{\circ}\text{K}$ ):  $10^3 \ln \alpha_{\text{ankerite-H}_2\text{O}} = 2.78(10^6)T^{-2} + 0.32$ ; (Dutton and Land, 1985).

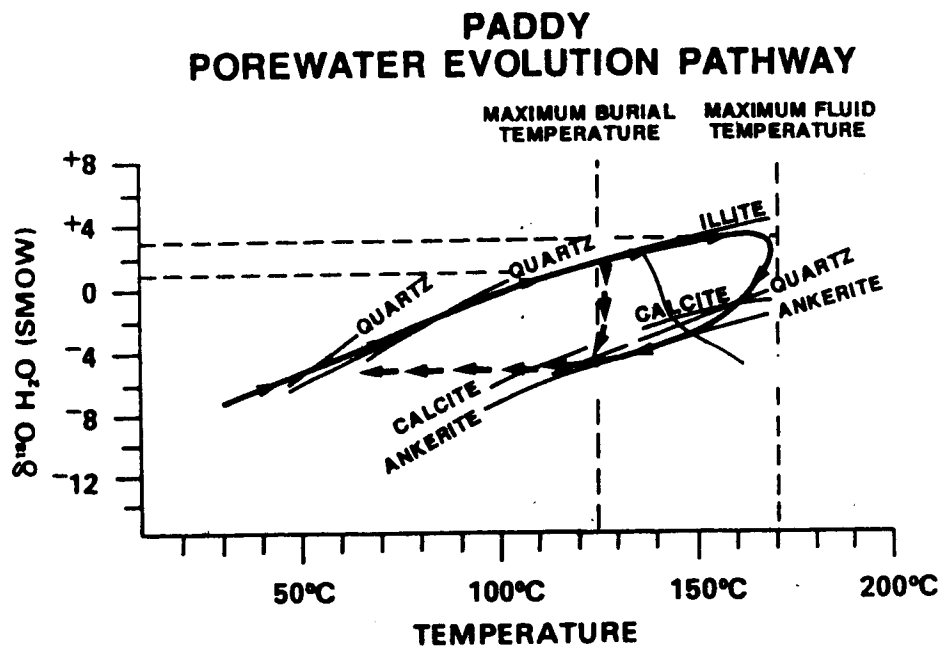
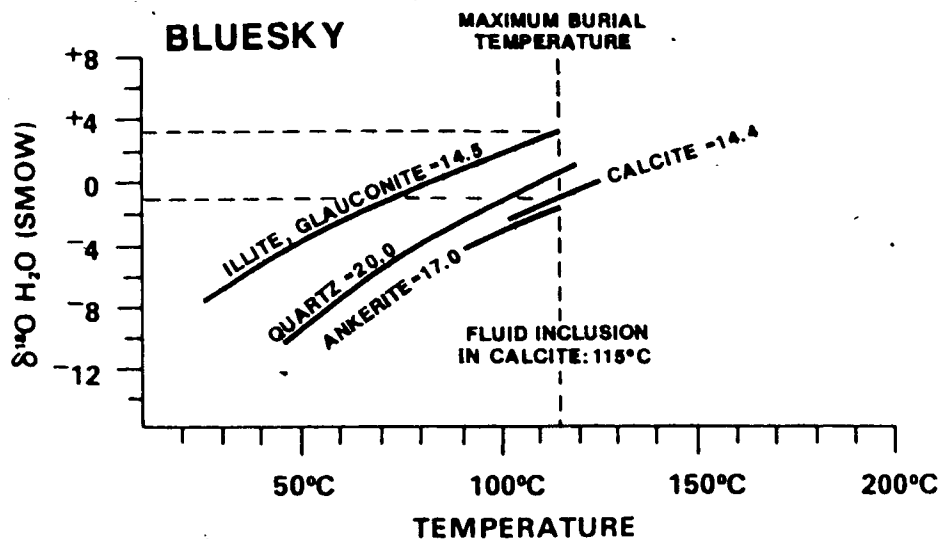
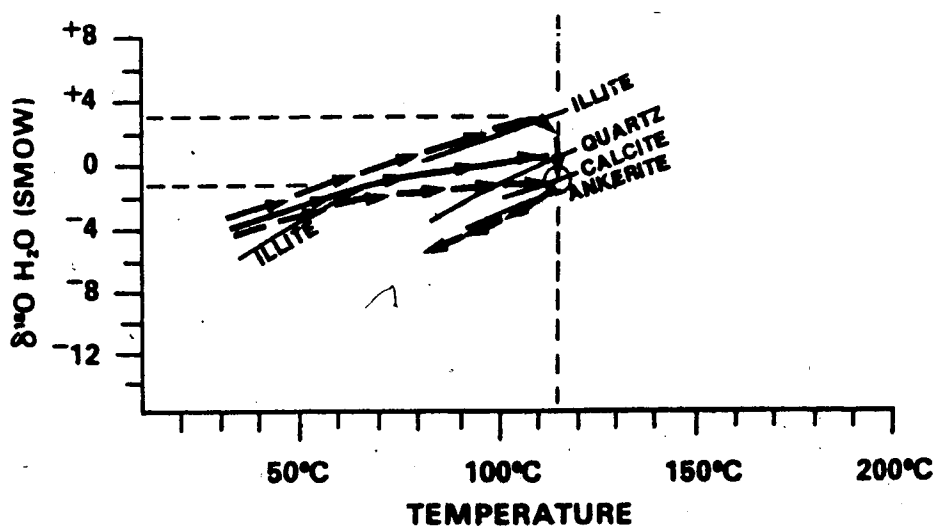


Figure 4.10b Idealized porewater evolution paths ( $\delta^{18}\text{O}$  of water versus temperature) for Paddy sandstones. The path indicated by discontinuous arrows assumes that the hot fluids from the Falher did not enter the Paddy sandstones. The solid path assumes hot fluids did enter the Paddy sandstones.



**Figure 4.11a**  $\delta^{18}\text{O}$  of porewater versus temperature for diagenetic minerals from the Bluesky Formation. Mineral curves are shown for  $\delta^{18}\text{O}$  values of each phase using the equations listed in the figure captions for Figures 4.9a and 4.10a. Fluid inclusions in calcite cement with  $\delta^{18}\text{O} = +14.4$  ‰ homogenized at  $-115^\circ\text{C}$ . These data give one control point for porewater evolution.

### BLUESKY POREWATER EVOLUTION PATHWAYS



**Figure 4.11b** Idealized porewater evolution paths ( $\delta^{18}\text{O}$  of water versus temperature) for Bluesky sandstones. Different paths are possible depending on whether illite, quartz or calcite formed at maximum burial temperatures. Open circle represents the point determined by fluid inclusion and stable isotope data.



gradient of 27°C/km. The calculated Falher burial temperatures are used here to estimate temperatures for other units, since the samples examined are located to the east of the anomalous zone defined in Chapter 2. Maximum burial temperatures versus present temperatures (in parentheses) for analyzed samples are: (i) Cardium, 110°-120°C (35°-50°C); (ii) Paddy, 125°C (65°C), (iii) Bluesky, 115°C (75°-85°C); (iv) Halfway, 145°C (75-90°C); and (v) Belloy, 150°C (80°C).

In some cases, the maximum burial temperature can be used to estimate the maximum  $\delta^{18}\text{O}$  value of the porewater from which diagenetic minerals have precipitated. For example, in the Cardium (Figure 4.9), quartz must have precipitated from porewater with  $\delta^{18}\text{O} < +3$  ‰ and illite from porewater with  $\delta^{18}\text{O} < +2$  ‰. However, this interpretation is complicated by the possibilities that: (1) pore fluid may have been hotter than the ambient rock temperature (Chapter 2) and (2) the diagenetic minerals may have precipitated at temperatures lower than the maximum burial temperature. Fluid-inclusion temperatures that could provide the additional data necessary to resolve these uncertainties are not available.

In Figure 4.9a (Cardium Formation), solid lines represent diagenetic minerals from the Kakwa Member of the Cardium Formation; dashed lines represent diagenetic minerals from the Dismal Rat Member of the Cardium Formation (Plint et al., 1986). The two different siderite values suggest that early porewaters in the Dismal Rat Member had higher  $\delta^{18}\text{O}$  values than those in the Kakwa Member. The presence of early chlorite in some Cardium samples from the Dismal Rat Member also suggests a more brackish early porewater. Since the Dismal Rat Member is a marine shelf deposit capped by a regional erosional surface, the depositional waters were marine. However, these marine waters may have been partially replaced by meteoric water during the aerial exposure represented by the erosional surface. In contrast, the Kakwa Member is a shoreline sandstone capped by lagoonal deposits. Depositional waters were probably fresh to brackish.

As porewaters evolved, kaolinite and quartz overgrowths, then illite and finally calcite were precipitated (Figure 4.4). Given the maximum burial temperature (110°-120°C), porewater  $\delta^{18}\text{O}$  values as high as 0 to +2 ‰ are possible for quartz and illite. Lower values ( $\delta^{18}\text{O} = -1$  to 0 ‰) are indicated for calcite. There is no evidence to distinguish between precipitation of calcite at maximum burial temperatures or precipitation during uplift as a result of cooling and a meteoric water influx. Both pathways are shown in Figure 4.9b. Falher data indicate that calcite precipitated during both situations. However, the 12.9 ‰ calcite in the Dismal Rat Member is a petrographically late cement. Its  $\delta^{18}\text{O}$  and  $\delta^{13}\text{C}$  values are similar to calcite cement which fills fractures in the Cardium Formation. Its lower  $\delta^{18}\text{O}$  value, relative to calcite cement in the Kakwa Member, suggests that it was precipitated as a result of the influx of meteoric water.

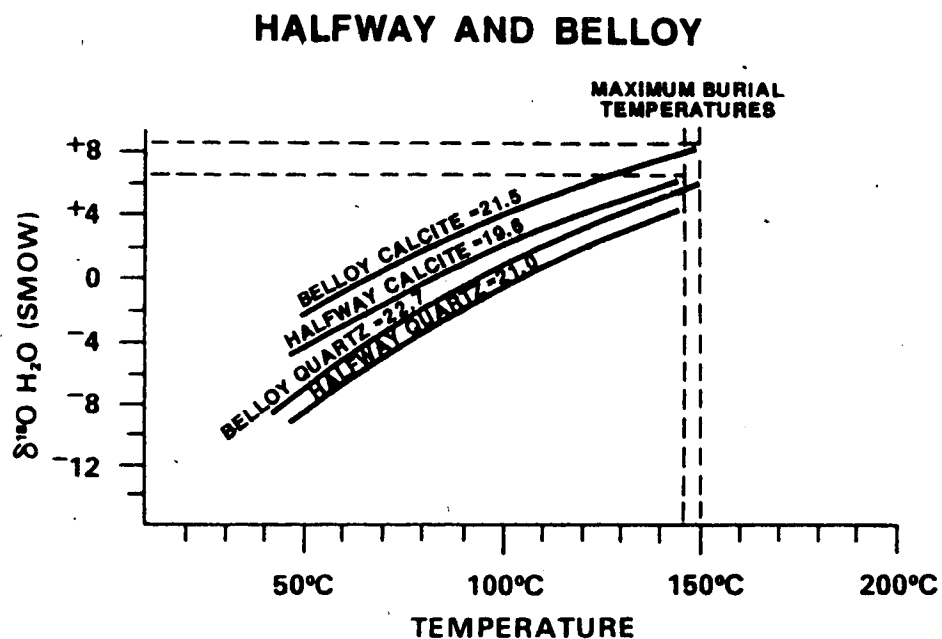
In the Paddy, if illite precipitated or recrystallized at maximum burial temperatures, porewater may have attained a maximum  $\delta^{18}\text{O}$  value of +1 ‰ at 125°C (Figure 4.10). It is also possible that the hot fluids (~170°C) from the Falher and Cadotte penetrated the Paddy. If so, maximum  $\delta^{18}\text{O}$  values for the porewater could have reached +3 ‰ (Chapter 3). In either case, the low  $\delta^{18}\text{O}$  values for late-stage calcite (+11 ‰), quartz (+14 ‰) and ankerite (+13.2 ‰) (Figures 4.10b, 4.4) suggest that the porewater became depleted in  $^{18}\text{O}$  before precipitation of these minerals. An influx of meteoric water during uplift and cooling is compatible with the Paddy data. The high  $\delta^{18}\text{O}$  quartz overgrowths (+24 ‰, +21.5 ‰) must have been precipitated during a relatively early stage of diagenesis in the temperature range of 50-90°C (Figure 4.10b). The low  $\delta^{18}\text{O}$ , late-stage quartz overgrowths (+14 ‰) were precipitated during uplift from porewater depleted in  $^{18}\text{O}$ .

In the Bluesky, fluid inclusions in late-stage calcite cement (Figure 4.4) indicate that calcite precipitated at 115°C from porewaters with  $\delta^{18}\text{O} = -1$  ‰ (Figure 4.11a). The proximity of the ankerite curve to the calcite curve suggests that ankerite precipitated under similar conditions. Some dolomite precipitation and grain replacement occurred during early to intermediate stages

of diagenesis. However, because it was not possible to separate detrital dolomite from diagenetic dolomite, the  $\delta^{18}\text{O}$  value for dolomite (+17 to +22 ‰) is probably a composite of both detrital and diagenetic forms. Dolomite isotopic data are not considered further. Glauconite and illite have the same  $\delta^{18}\text{O}$  value. Glauconite is usually precipitated under marine conditions very soon after deposition. To precipitate glauconite at 20-30°C requires porewater with  $\delta^{18}\text{O} = -9$  to  $-7$  ‰ (i.e. meteoric or brackish water) (Figure 4.11a). To form glauconite from seawater ( $\delta^{18}\text{O} = 0$  ‰), requires temperatures of  $\sim 80^\circ\text{C}$ . Therefore, the measured  $\delta^{18}\text{O}$  values for glauconite are not consistent with its precipitation during early diagenesis from marine porewaters. The fact that intermediate-stage, diagenetic illite (Figure 4.4) has a similar  $\delta^{18}\text{O}$  value suggests that the glauconite was recrystallized at higher temperatures. The fibrous or platy texture of the sides of glauconite pellets (Figure 4.7h) also suggests recrystallization. If illite precipitation and glauconite recrystallization took place at maximum burial temperatures, then the maximum enrichment of the porewaters was +3 ‰ and the porewater became depleted in  $\delta^{18}\text{O}$  as a result of a meteoric water influx before late-stage calcite and ankerite were precipitated. Alternatively, illite might have precipitated at a lower temperature (e.g. 70°C) from porewater with  $\delta^{18}\text{O} = -1$  ‰ and quartz overgrowths formed during maximum burial from porewaters with  $\delta^{18}\text{O} = 0$  ‰. The third alternative is that calcite and ankerite precipitated at maximum burial from the most highly evolved porefluids in the Bluesky (i.e. maximum enrichment of the porewaters was only  $\sim -1$  ‰).

For all except the lowermost Cretaceous unit (the Cadomin, Chapter 3), there is no evidence that porewaters became more enriched in  $\delta^{18}\text{O}$  than +3 ‰; in some units, the  $\delta^{18}\text{O}$  value of porewaters may have been no higher than  $\delta^{18}\text{O} \sim -1$  ‰. A pattern of porewater evolution including increasing  $\delta^{18}\text{O}$  during burial and decreasing  $\delta^{18}\text{O}$  during uplift is compatible with data from all the Cretaceous units studied.

$\delta^{18}\text{O}$  porewater versus temperature curves for the Triassic Halfway and the Permian Belloy diagenetic quartz and calcite are shown in Figure 4.12. Petrographic relationships indicate that



**Figure 4.12**  $\delta^{18}\text{O}$  of porewater versus temperature for diagenetic minerals from the Halfway and Belloy Formations. Mineral curves are shown for  $\delta^{18}\text{O}$  values of each phase using the equations listed in the figure caption for Figure 4.9a. If calcite precipitated or recrystallized at maximum burial temperatures, the porewater may have had an  $\delta^{18}\text{O}$  value as high as +6 ‰ in the Halfway and +8 ‰ in the Belloy Formation.

calcite is a relatively late-stage cement in both units (Figure 4.4). Calculated maximum burial temperatures are 145°C for the Halfway and 150°C for the Belloy. If calcite precipitated or recrystallized at these temperatures, the porewater may have had an  $\delta^{18}\text{O}$  value as high as +6 ‰ in the Halfway and +8 ‰ in the Belloy. Quartz overgrowths precipitated before calcite, probably at lower temperatures from less  $^{18}\text{O}$ -enriched porewaters.

### CARBON-ISOTOPE COMPOSITIONS

Carbon-isotope compositions of carbonate cements in Upper Cretaceous to Permian units vary irregularly from -27 to +9 ‰ PDB (Tables 4.2, 4.4, 4.8 and 4.9, Figure 4.13). This variation is consistent with a complex range in conditions for carbonate cementation and recrystallization throughout diagenesis. Early carbonate cements, including siderite and texturally early calcite and ankerite (recrystallization products of early carbonate cements), have  $\delta^{13}\text{C}$  values ranging from -8 ‰ to +3.5 ‰. The  $\text{CO}_2$  supply for these cements was probably a mixture of  $\text{CO}_2$  from marine carbonate ( $\approx 0$  ‰) and sulphate reduction ( $\delta^{13}\text{C} = -25$  ‰, Curtis, 1977; Irwin et al., 1977) or bacterial fermentation ( $\delta^{13}\text{C} = +15$  ‰, Curtis, 1977; Irwin et al., 1977). Detailed analyses of carbon-isotope values and chemistry of carbonate cements can reveal much about depositional waters and early porewater evolution (Curtis et al., 1986; Staley, 1986), but such work is beyond the scope of this project.

Late calcite and ankerite cements have  $\delta^{13}\text{C}$  values ranging from -27 to +9 ‰. Low values (-27 to -15 ‰) for late cements suggest that  $\text{CO}_2$  was supplied by thermal decarboxylation of organic matter ( $\delta^{13}\text{C} = -25$  to -10 ‰, Curtis, 1977; Irwin et al., 1977). Such low values occur only in late calcite cements for the Halfway and Belloy Formations. In Cretaceous units,  $\delta^{13}\text{C}$  values of carbonate cements range from -15.8 ‰ in the Cardium to +9 ‰ in the Falher. Since  $\delta^{18}\text{O}$  data suggest that late carbonate cements in Cretaceous units formed as a

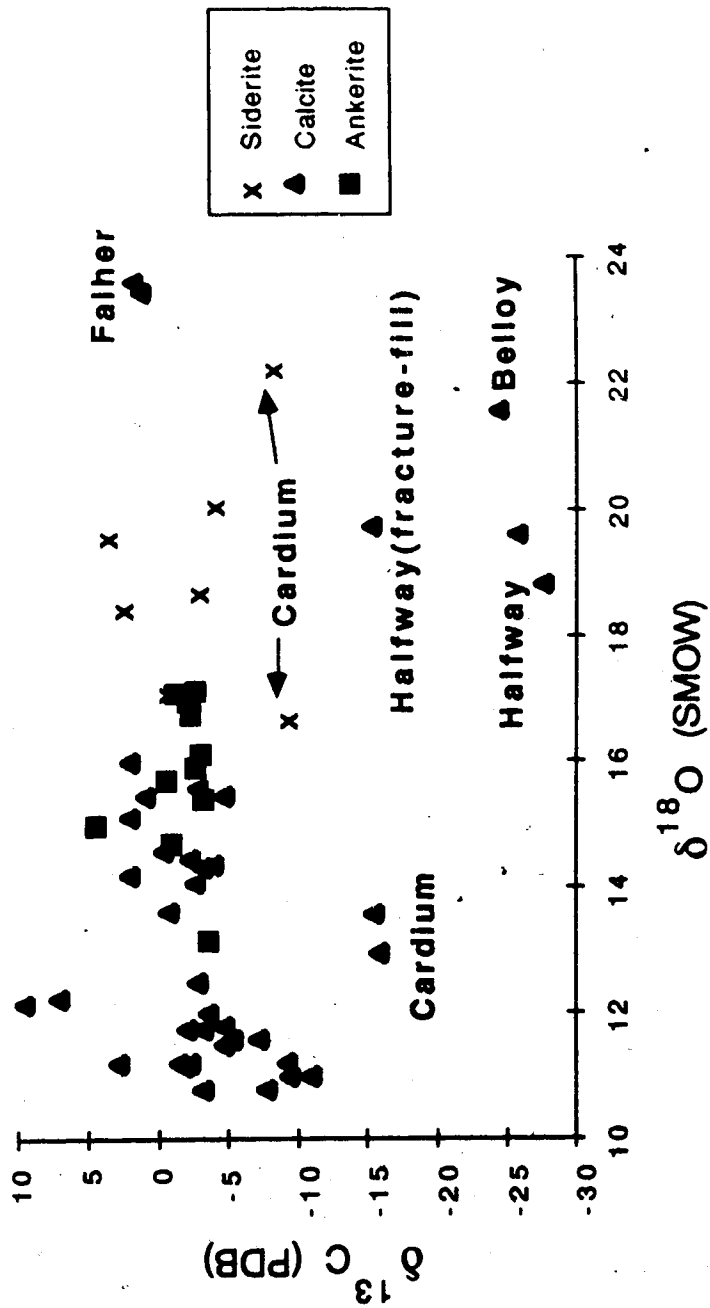


Figure 4.13  $\delta^{13}\text{C}$  versus  $\delta^{18}\text{O}$  diagram for carbonate cements from the Alberta Deep Basin.

result of the influx of meteoric water.  $\delta^{13}\text{C}$  values may reflect mixtures of *in situ* waters containing  $\text{CO}_2$  from thermal decarboxylation of organic matter, and meteoric water which may have carried  $\text{CO}_2$  from any of a number of near surface sources (eg. fermentation zone, bacterial reduction zone, soil-derived  $^{13}\text{C}$ -poor  $\text{CO}_2$ ). The restriction of very low  $\delta^{13}\text{C}$ -carbonate cements to the Halfway and Belloy Formations, suggests that these units were isolated from the influx of meteoric water when the calcite precipitated.  $\delta^{18}\text{O}$  values of their carbonate cements are consistent with this interpretation.

## DISSOLUTION CARBONATE CEMENTS

Petrographic textures suggest that dissolution of carbonate cement has occurred in several Upper and Lower Cretaceous sandstones and conglomerates. In the Cardium, some pore spaces are lined by siderite (Figure 4.5a); other samples have no pore space and siderite crystals are tightly squeezed between detrital grains (Figure 4.5e). The open pore structure of the former type of sandstone suggests that a cement was present during compaction and thus prevented grain compaction. This cement must have later dissolved away. In the Cadotte, large empty vugs in very fine grained sandstone are up to 2 cm in vertical thickness. These vugs are lined by a remnant of siderite which is overlain by quartz druse. These vugs were probably originally siderite concretions and the siderite was mostly dissolved away before precipitation of the quartz druse. In some Falher conglomerates, siderite is partially replaced by calcite cement (Chapter 3; Figure 3.3c). In these samples, at least some siderite dissolution has occurred. In the Bluesky, within a single thin section, some large pore spaces are filled by calcite cement (Figure 4.8c), whereas other large pores are empty (Figure 4.8d). Some cement must have originally been present in these large empty pores in order to prevent compaction.

Oxygen isotope data give additional evidence for dissolution of carbonate cements at an intermediate to late-stage during diagenesis. In the Paddy, two entirely different generations of

quartz overgrowths can be recognized, an early generation with  $\delta^{18}\text{O} = +21$  to  $+24$  ‰ and a late generation with  $\delta^{18}\text{O} = +14$  ‰ (Table 4.4). The pore space in the samples with early quartz overgrowths is completely filled by the authigenic quartz (Figure 4.6c) in the sample with the late quartz overgrowths, pore space has not been completely filled by quartz (Figure 4.6d). Without the isotope data, the immediate explanation for the greater porosity in the one sample compared to the other is that the sample with the greater porosity is coarser grained and original pore spaces were larger; there was insufficient time and supply of silica to completely fill these pores. However, if this were the case, the isotopic composition of diagenetic quartz in both samples should be similar. Instead, there is a difference of 7 ‰ between the  $\delta^{18}\text{O}$  values of quartz overgrowths in the two samples. Therefore, the presence of a cement must have inhibited early quartz precipitation. This cement dissolved and sometime after the initial stage of quartz precipitation, pore space became available for late quartz precipitation.

The similarity of  $\delta^{18}\text{O}$  values for both texturally early and late calcite and ankerite cements accompanied by a difference in their  $\delta^{13}\text{C}$  values suggests that dissolution of a carbonate cement and precipitation of a later carbonate cement has occurred. Original  $\delta^{13}\text{C}$  values of the earliest carbonate cement have apparently been preserved, whereas the  $\delta^{18}\text{O}$  value reflects the temperature and  $\delta^{18}\text{O}$  composition of the water involved in the re-precipitation. It seems probable that the texturally early cement in many cases was early siderite, later dissolved and replaced by calcite, Fe-calcite or ankerite.

#### CROSS-FORMATIONAL FLOW

The Cadomin Formation excluded, there is generally no evidence for extensive cross-formational flow of  $^{18}\text{O}$ -rich fluids from the Triassic and underlying units into the Cretaceous section. Isotopic analyses of Triassic and Permian calcite cements suggest that these porewaters could have  $\delta^{18}\text{O}$  values as high as  $+6$  to  $+8$  ‰. However, in most Cretaceous units, only the



rare isolated data described below suggests that porewater had  $\delta^{18}\text{O}$  values higher than +3 ‰.

Calcite cements from Falher conglomerates in township 66 range 8W6 and township 67 range 9W6 have anomalously high  $\delta^{18}\text{O}$  values (+23.4 and +23.6 ‰). To precipitate such calcite at 65-100°C requires porewater with  $\delta^{18}\text{O} = +2$  to +6.5 ‰. At higher temperatures, the required porewater is even more enriched in  $^{18}\text{O}$ . Petrographic relationships indicate that these calcites are late-stage, microcrystalline cements (Chapter 3) which probably precipitated during uplift. The data indicate that even if this calcite precipitated under present-day conditions (65°C), it must have formed from water significantly more enriched in  $^{18}\text{O}$  than the present-day regional Falher porewater ( $\delta^{18}\text{O} = +2$  ‰ compared to the regional -6 to -5 ‰). Possible explanations for this anomaly include: (1) the porewater at this locality did not experience dilution by meteoric water during uplift; or (2) an influx of ascending  $^{18}\text{O}$ -rich waters mixed with porewaters at this locality before precipitation of calcite. The present data does not allow a distinction between these two possibilities.

Although most cements filling fractures have isotopic signatures similar to the surrounding pore-filling cements, a few have anomalously high  $\delta^{18}\text{O}$  values. Calcite, which fills vertical fractures in the Cadotte and the Falher, has  $\delta^{18}\text{O}$  values of +16 ‰ and +17 ‰, respectively (Table 4.8) and represents a second locality where high  $\delta^{18}\text{O}$  fluids were probably present. The data suggest that the porefluids which precipitated these fracture-filling calcite cements may have had  $\delta^{18}\text{O}$  values of +3 ‰ when regional porefluids in the Cadotte and Falher had become depleted to -1 ‰. Possible explanations for these  $^{18}\text{O}$ -rich waters are the same as suggested above. The data are consistent with local instances of cross-formational flow but do not eliminate other explanations.

## CONTROLS ON DIA GENETIC PROCESSES

Comparison of diagenetic sequences and porewater evolution in each of the units studied suggests that in the Upper and Lower Cretaceous sediments, the major diagenetic processes are independent of actual position in the vertical section. The general diagenetic sequence is the same in each of the formations examined even though burial depths, geographic position and original depositional environment varied. The essential similarity, though, is the original detrital mineralogy. In all units the detrital mineralogy is composed dominantly of quartz and chert. As burial increased, the following diagenetic minerals precipitated: early siderite or chlorite, kaolinite, quartz overgrowths, illite and albite. Either at maximum burial or during uplift as the meteoric water influx increased, calcite and/or ankerite were precipitated. In the coarsest sandstones and conglomerates, dickite was precipitated from the evolved-meteoric water. The general pattern of porewater evolution is similar for all the Upper and Lower Cretaceous units examined.

The mechanisms which control diagenetic reactions are still not well understood, although many studies have suggested that the smectite/illite transition and organic reactions in shales play an important role. Land (1984) suggested that deeper shales that have undergone the smectite/illite transition at  $\approx 100^{\circ}\text{C}$  are the source of  $\text{SiO}_2$  and  $\text{CaCO}_3$  for quartz and calcite cements in the Frio Formation in the Gulf Coast Basin. This theory is based on evidence for precipitation of quartz at  $\approx 60^{\circ}\text{C}$  and calcite at  $\approx 80^{\circ}\text{C}$  from porewaters with  $\delta^{18}\text{O}$  values of +4 to +5 ‰. Porewaters equilibrated with shales at the temperature at which significant organic reactions and the smectite/illite transition take place ( $\approx 100^{\circ}\text{C}$ ) should have  $\delta^{18}\text{O}$  values of  $\approx +5$  ‰ (Suchecki and Land, 1983). Since diagenetic cements in the Frio Formation formed from waters with this isotopic composition, but at lower temperatures, Land (1984) concluded that calcite- and quartz-saturated porewaters were expelled from shales and moved updip in sandstones to lower temperature zones before precipitation occurred. In contrast, in the Wilcox Formation which underlies the Frio Formation, Fisher and Land (1986) noted that diagenetic quartz, kaolinite and

calcite formed at similarly low temperatures but from porewaters with  $\delta^{18}\text{O}$  values of  $\sim -3$  to  $+2$  ‰. They concluded that these relatively early diagenetic cements that formed from low  $\delta^{18}\text{O}$  porewaters were not related to organic maturation and S/I reactions.

In the Belly River Formation of the Western Canadian Basin (central and south-central Alberta), Ayalon and Longstaffe (in press) found that quartz overgrowths formed at maximum burial and during uplift at temperatures of  $100^{\circ}$ - $120^{\circ}\text{C}$ . Their data show that an influx of meteoric water played an important role in late-stage diagenesis (from the time of maximum burial to the present) and was involved in the precipitation of quartz, kaolinite, calcite, illite and illite/smectite. Because the temperature of quartz precipitation corresponds with that for organic maturation reactions and the S/I transition, they concluded that meteoric water was responsible for transporting material, produced from those reactions in shales, to sandstones where they were precipitated. Mixing of shale porewaters with meteoric water produced  $\delta^{18}\text{O}$  values of porewaters which are characteristic of isotopically evolved meteoric water.

In the Alberta Deep Basin (this study) an influx of meteoric water also controlled the late stages of diagenesis (from the time of maximum burial to the time that pores became saturated by methane gas). Evolved meteoric water was involved in the precipitation of quartz druse, dickite, calcite and ankerite in conglomerates, and calcite, ankerite and local quartz overgrowths in sandstones. In contrast to the situation in the Gulf Coast Basin, where most of the diagenetic reactions were completed relatively early during burial, the late stages of diagenesis in the Western Canadian Basin are the most significant in terms of porosity modification. As proposed by Ayalon and Longstaffe (in press), meteoric water is the transport mechanism for constituents of diagenetic cements formed during late-stage diagenesis. However, in at least the Falher Member in the Alberta Deep Basin, pressure solution of chert pebbles is common in the westernmost part of the study area. This pressure solution is probably the major source of  $\text{SiO}_2$  for quartz druse in conglomerates of the Alberta Deep Basin.

Evidence for precipitation of quartz overgrowths, kaolinite and illite, and the albitization or dissolution of feldspars during burial of Cretaceous sandstones in the Alberta Deep Basin, suggests that diagenesis during burial might have been controlled by processes similar to those in the Gulf Coast Basin. For example, the first generation of quartz overgrowths in the Paddy Member precipitated at 50°-90°C and quartz overgrowths in the Cardium Formation probably formed at 70°-90°C. In the Bluesky Formation, quartz precipitated at slightly higher temperatures (95°-115°C). The problem is that porewaters which were responsible for precipitation of the diagenetic minerals in the Deep Basin varied from -5 to +1 ‰, a range similar to that of the Wilcox Formation (Fisher and Land, 1986) but significantly lower than that of the Frio Formation (Milliken et al., 1981; Land, 1984). These low  $\delta^{18}\text{O}$  values suggest that waters derived from the S/l transition in shales may not be the dominant source of water in the Alberta Deep Basin, even during burial. However, organic maturation reactions probably are important in controlling carbonate dissolution and precipitation. Although intermediate stages of calcite cement are absent, evidence for dissolution of carbonate cements (early siderite in particular) before maximum burial suggests that precipitation and dissolution reactions similar to those described by Land (1984) may have taken place.

## CONCLUSIONS

Diagenetic processes in all the Cretaceous sandstones examined are similar. Early precipitation of siderite or chlorite was followed by intermediate stages of quartz, kaolinite, illite and albite precipitation. Calcite or ankerite precipitation was the final diagenetic event in all units except the Cadomin. In the Cadomin, there is no evidence of a late-stage carbonate phase. In most units, there is evidence for dissolution of an early carbonate phase, most commonly siderite. Diagenesis in conglomerates is distinguished from that in sandstones by the presence of quartz druse which was precipitated during maximum burial. Late-stage dickite which formed from

evolved-meteoric water is most common in conglomerates but also occurs in coarse-grained sandstones.

Data for the Cardium, Paddy and Bluesky are consistent with the porewater evolution pathways derived from Falher and Cadomin data. Porewaters began as meteoric to brackish waters, became richer in  $^{18}\text{O}$  by reaction with the rocks and/or mixing with shale compaction waters during burial, and then became depleted in  $^{18}\text{O}$  during uplift as a result of mixing with meteoric water.

Illite in the Cadomin is the only diagenetic mineral in all the Cretaceous units studied that suggests that regional porewaters ever became more  $^{18}\text{O}$ -enriched than +3 ‰; maximum  $\delta^{18}\text{O}$  values for porewater in some units possibly only reached -1 ‰. In contrast, porewaters in the Halfway and Belloy sandstones may have had  $\delta^{18}\text{O}$  values up to +6 ‰ and +8 ‰, respectively. The low  $\delta^{18}\text{O}$  values for most porewaters in the Cretaceous, relative to underlying units, suggest that cross-formational flow between the two parts of the section was limited to the basal Cretaceous unit (the Cadomin Formation).

## REFERENCES

- Ayalon, A., and Longstaffe, F.J., in press, Oxygen-isotope studies of diagenesis and porewater evolution in the western Canada sedimentary basin: evidence from the Upper Cretaceous basal Belly River sandstone: *Journal of Sedimentary Petrology*.
- Becker, R.H. and Clayton, R.N., 1976, Oxygen isotope study of a Precambrian banded iron-formation, Hamersley Range, Western Australia: *Geochimica et Cosmochimica Acta*, v.40, p. 1153-1165.
- Cant, D.J., 1986, Hydrocarbon trapping in the Halfway Formation (Triassic), Wembley Field, Alberta: *Bulletin of Canadian Petroleum Geology*, v.34, p. 329-338.
- Cant, D.J. and Ethier, V.G., 1984, Lithology-dependent diagenetic control of reservoir properties of conglomerates, Falher Member, Elmworth Field, Alberta: *The American Association of Petroleum Geologists Bulletin*, v.68, p. 1044-1054.
- Carothers, W.W., and Kharaka, J.K., 1980, Stable carbon isotopes of  $\text{HCO}_3^-$  in oil-field waters - implications for the origin of  $\text{CO}_2$ : *Geochimica et Cosmochimica Acta*, v.44, p. 323-332.
- Clayton, R.N., O'Neil, J.R., and Mayeda, T.K., 1972, Oxygen isotope exchange between quartz and water: *Journal of Geophysical Research*, v.77, p. 3057-3067.
- Curtis, C.D., 1977, Sedimentary geochemistry: environments and processes dominated by involvement of an aqueous phase: *Philosophical Transactions of the Royal Society of London*, v.268A, p. 353-372.
- Curtis, C.D., Coleman, M.L., and Love, L.G., 1986, Pore water evolution during sediment burial from isotopic and mineral chemistry of calcite, dolomite and siderite concretions: *Geochimica et Cosmochimica Acta*, v.50, p. 2321-2334.
- Dutton, S.P. and Land, L.S., 1985, Meteoric burial diagenesis of Pennsylvanian arkosic sandstones, southwestern Anadarko Basin, Texas: *The American Association of Petroleum Geologists Bulletin*, v.69, p. 22-38.
- Fisher, R.S. and Land, L.S., 1986, Diagenetic history of Eocene Wilcox sandstones, South-Central Texas: *Geochimica et Cosmochimica Acta*, v.50, p. 551-561.
- Friedman, I., and O'Neil, J.R., 1977, Compilation of stable isotope fractionation factors of geochemical interest: in M. Fleischer, ed., *Data of Geochemistry* (6th ed.): U.S. Geological Survey Professional Paper 440-KK, 12 p.
- Irwin, H., Curtis, C. and Coleman, M., 1977, Isotopic evidence for the source of diagenetic carbonates formed during burial of organic-rich sediments: *Nature*, v.269, p. 209-213.
- Jackson, M.J., 1979, *Soil Chemical Analysis - Advanced Course*, 2nd edition: published by the author, Madison, Wis., 895 p.
- Land, L.S., 1984, Frio sandstone diagenesis, Texas Gulf Coast: a regional isotopic study: in R. Surdam and D. MacDonald, eds., *Clastic Diagenesis*: American Association of Petroleum Geologists, Memoir 37, p. 47-62.
- Lee, M and Savin, S., 1985, Isolation of diagenetic overgrowths on quartz sand grains for oxygen isotopic analysis: *Geochimica et Cosmochimica Acta*, v.49, p. 497-501.
- Masters, J.A., 1979, Deep Basin gas trap, Western Canada: *The American Association of Petroleum Geologists Bulletin*, v.63, p. 152-181.

- Milliken, K.L., Land, L.S. and Loucks, R.G., 1981, History of burial diagenesis determined from isotopic geochemistry, Frio Formation, Brazoria County, Texas: *The American Association of Petroleum Geologists Bulletin*, v.65, p. 1397-1413.
- O'Neil, J.R., Clayton, R.N. and Mayeda, T.K., 1969, Oxygen isotope fractionation in divalent metal carbonates: *Journal of Chemical Physics*, v.51, p. 5547-5558.
- Plint, A.G., Walker, R.G., and Bergman, K.M., 1986, Cardium Formation 6. Stratigraphic framework of the Cardium in subsurface: *Bulletin of Canadian Petroleum Geology*, v.34, p. 213-225.
- Plint, A.G. and Walker, R.G., 1987, Cardium Formation 8. Facies and environments of the Cardium shoreline and coastal plain in the Kakwa field and adjacent areas, northwestern Alberta: *Bulletin of Canadian Petroleum Geology*, v.35, p. 48-64.
- Smith, D.G., Zorn, C.E. and Sneider, R.M., 1984, The paleogeography of the Lower Cretaceous of western Alberta and northeastern British Columbia in and adjacent to the Deep Basin of the Elmworth area: *in* J.A. Masters, ed., *Elmworth Case Study of a Deep Basin Gas Field*, AAPG Memoir 38, p. 79-114.
- Staley, G.H.S., 1986, The diagenesis of the Cretaceous Cardium and Viking Formations, Alberta Basin, Canada, (abstract): *Terra cognita*, v.6, no. 2, p. 107.
- Sucheckl, R.K. and Land, L.S., 1983, Isotopic geochemistry of burial-metamorphosed volcanogenic sediments, Great Valley sequence, northern California: *Geochimica et Cosmochimica Acta*, v.47, p. 1487-1499.
- Syers, J.K., Chapman, S.L., Jackson, M.L. and Rex, R.W., 1968, Quartz isolation from rocks, sediments and soils for determination of oxygen isotopic composition: *Geochimica et Cosmochimica Acta*, v.32, p. 1022-1025.
- Yeh, H., and Savin, S.M., 1977, Mechanism of burial metamorphism of argillaceous sediments, III. O-isotope evidence: *Geological Society of America Bulletin*, v.88, p. 1321-1330.

## CHAPTER 5. CHEMISTRY AND HYDROGEOLOGY OF MODERN FORMATION WATERS IN THE ALBERTA DEEP BASIN

### INTRODUCTION

In this thesis, the problem of elucidating the history of formation waters in the Alberta Deep Basin has been approached by examining the diagenetic minerals which precipitated from evolving porewaters. The mineral data, including textural relationships, stable isotope analyses and fluid inclusion temperatures and salinities (Chapters 2,3 and 4), permit constraints to be placed on the paleohydrogeology and ancient formation water chemistry. The next step in a study of the history of formation waters is to examine the chemistry and hydrogeology of modern formation waters. The purpose of this chapter is to present preliminary results for the detailed chemistry, geographic distribution of chemical components, and potentiometric surface data for formation waters in the Deep Basin, along with more regional chemical and flow data supplied by other workers. The intent is to present data which could form a basis for future, more extensive study of modern formation waters.

Previous studies elucidated the diagenetic and cementation history of the Western Canadian Basin by studying formation waters (e.g. Hitchon and Friedman, 1969; Hitchon et al., 1971). Such studies have provided abundant reliable data on the regional, isotopic and chemical variation of formation fluids and their hydrology (Hitchon, 1964). Hitchon et al. (1971) summarized their knowledge of the origin of formation waters in the Western Canadian Basin based on these data. They concluded that their formation waters were ancient sea water with the  $\delta D$  values altered by mixing with meteoric water and the  $\delta^{18}O$  values increased by exchange with carbonates. The work of Hitchon et al. (1971) considered an average formation water in the Western Canadian Basin rather than one particular location or formation. This thesis is concerned with the origin of formation water in Lower Cretaceous strata in the Deep Basin.



The units of major interest for this study are the Paddy and Cadotte Members of the Peace River Formation, the Falher Member of the Spirit River Formation, and the Bluesky, Gething and Cadomin Formations (Figure 5.1). These Lower Cretaceous units consist of conglomerates, sandstones, siltstones, shales and coals. Chemical analyses for waters from units underlying the Lower Cretaceous rocks are also examined. Triassic units in descending order are: (1) the carbonate-rich Baldonnel Formation; (2) the Charlie Lake Formation with mudstones and interbedded anhydrite and dolomite; and (3) sandstones, siltstones, shales and coquinas of the Halfway and Doig Formations (Figure 5.1) (Cant, 1986). The Permian Belloy Formation consists of quartzose sandstone with quartz overgrowths and anhydrite or calcite cements. Upper Devonian carbonate rocks are divided into the Wabamum, Winterburn and Woodbend Formations.

X-ray diffraction results for Cretaceous sandstones are given in Table 5.1. Kaolinite and illite are the dominant clay minerals in these sandstones as well as in the Wilrich Shale (Connolly, 1985) which underlies the Falher Member. Smectite is notably absent or is present in only trace amounts. Mixed layer illite/smectite (I/S) can comprise up to 25% of the <0.2  $\mu\text{m}$  size-fraction. Chlorite comprises <15% of the clay fraction. These data suggest that the present capacity for ion exchange in the sandstones is small, limited mostly to the smectitic component of I/S and rare smectite.

## CHEMISTRY OF FORMATION WATERS

Water samples from the Bluesky (one well) and the Paddy (one well) were collected for detailed chemical and isotopic analysis. The samples were collected from separators at the wellhead during routine production tests. Although the wells are gas producers, a significant amount of water was also produced. The amount of water condensed from the gas, thereby

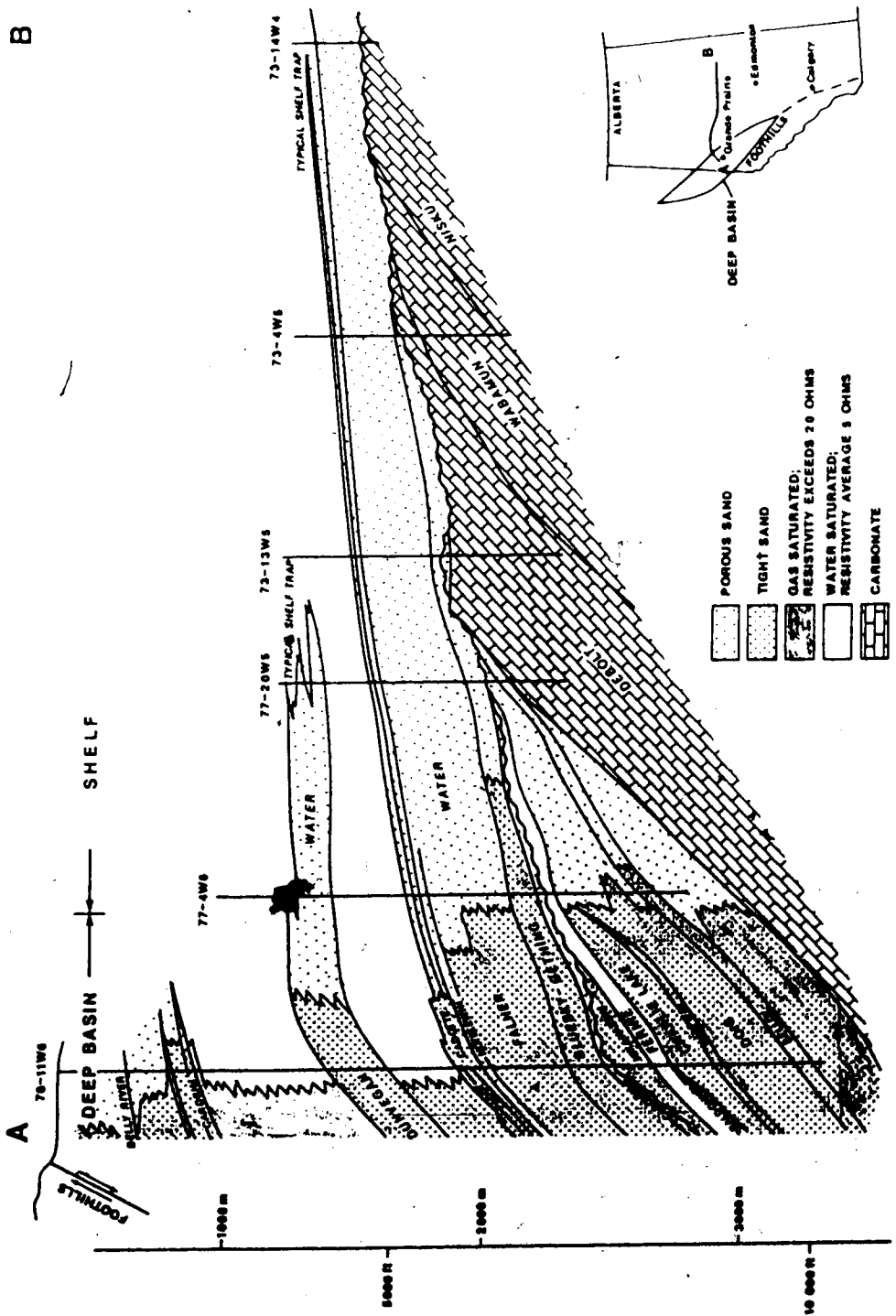


Figure 5.1 West to east cross-section through the Alberta Basin showing stratigraphic nomenclature for the Deep Basin. Almost the entire section in the western part of the Deep Basin is gas-saturated, whereas updip, to the east, the rocks are water-saturated. (modified from Masters, 1979).

TABLE 5.1 X-RAY DIFFRACTION DATA

	LOCATION	DEPTH (m)	ROCK TYPE*	SIZE FRACTION ( $\mu\text{m}$ )	K	PERCENT ILL CHL SM	M.L.	COMPOSITION OF M.L.
<b>CARDIUM</b>								
280	4-18-74-12W6	384.9		<0.2	35	60	<5	<5
				0.2-2	85	5	5	<5
308	5-16-68-13W6	1159.5	v.f.g.sst.	<0.2	0	80	<5	0 20
				0.2-2	5	90	5	<5
315	15-34-61-4W6	1929.6		<0.2	10	70	0	0 20
<b>PADDY</b>								
230	7-11-72-12W6	1684.4	f.g.sst.	<0.2	0	75	<5	20 I+I/S >15%S
232	7-11-72-12W6	1689.6	m.g.sst.	0.2-2	10	75	5	0 10
233	7-11-72-12W6	1693.7	m.g.sst.	<0.2	5	75	0	0 20
				0.2-2	<5	85	<5	0 5
<b>FALHER</b>								
	11-13-66-8W6	2576.0	v.f.g.sst.	<2	7	78	7	0 8
	11-13-66-8W6	2566.0	f.g.sst.	<2	77	17	4	0 2
	11-13-66-8W6	2562.0	congl.sst.	<2	53	31	2	0 4
	10-20-67-5W6	1905.0	ss. congl.	<2	45	37	5	5 8
	10-20-67-5W6	1910.5	v.f.g.sst.	<2	43	45	4	0 8
	7-20-67-6W6	2003.0	v.f.g.sst.	<2	21	65	2	0 11
	10-29-67-10W6	2397.0	f.g.sst.	<2	19	80	2	0 0
	10-30-67-11W6	2428.0	f.g.sst.	<2	38	39	3	0 9
	6-2-68-4W6	1707.0	m.g.sst.	<2	44	26	12	0 17
	6-2-68-4W6	1720.0	congl.sst.	<2	71	15	9	0 5
	10-13-69-9W6	1867.0	v.f.g.sst.	<2	39	44	3	0 13
	10-23-72-11W6	1770.9	f.g.sst.	<2	1	77	13	0 8
224	93-P-7,a-57-C	2338.6	v.f.g.sst.	<0.2	1	97	1	1 0 I+IS 25%S
				0.2-2	8	84	5	0 3
227	93-P-7,a-57-C	2351.1		<0.2	5	88	4	3 0 I+I/S 30%S
239	93-P-1,b-28-L	2350.2		0.2-2	19	65	14	0 2

TABLE 5.1 cont. X-RAY DIFFRACTION DATA

LOCATION	DEPTH (m)	ROCK TYPE*	SIZE FRACTION K ( $\mu$ m)	PERCENT ILL CHL SM M.L.	COMPOSITION OF M.L.
<b>FALHER cont.</b>					
242 93-P-1,b-28-L	2353.4	v.f.g.sst.	<0.2	1 97 2 0 0	I+I/S >15% S
243 93-P-1,b-28-L	2378.0		<0.2	99	
249 93-P-1,c-12-L	2301.0	f.g.sst.	<0.2	0 96 0 4 0	I+ISII <15% S
			0.2-2	6 89 2 0 2	
251 93-P-1,a-12-L	2306.0		<0.2	2 96 1 1 0	I+ISII <15% S
<b>BLUESKY</b>					
52 10-16-65-2W6	2195.5	laminated, glauc. sst.	<0.2	0 75 0 0 25	I/S 11% S
61 10-16-65-2W6	2207.1	structureless, f.g. sst.	<0.2	<5 75 5 0 20	
67 10-4-65-2W6	2261.9	laminated	0.2-2	45 40 10 0 <5	I+I/S >15% S
		f.g. sst.	<0.2	<5 75 <5 0 15	
130 7-18-67-5W6	2151.2	bioturbated f.g.sst.	0.2-2	40 45 15 0 0	
			<0.2	<5 85 0 0 10	I with 11% S
133 7-10-63-1W6	2476.1	laminated v.f.g. sst.	0.2-2	40 55 <5 0 <5	
			<0.2	0 80 0 0 20	I+ISII <15% S
140 6-9-66-5W6	2468.3	congl., clay in pores	0.2-2	30 60 10 0 <5	
		m.g. sst.	<0.2	10 65 0 0 25	
74 10-4-65-2W6	2271.2		0.2-2	55 35 10 0 0	
		m.g. sst.	<0.2	<5 70 5 0 20	
119 11-24-67-6W6	2125.2	m.g.sst.	0.2-2	35 50 10 0 5	
			<0.2	10 80 0 0 10	
135 7-10-63-1W6	2481.6	m.g.sst.	0.2-2	60 40 <5 0 <5	
			<0.2	10 60 5 0 25	
147 1-20-64-26W5	2214.3	glauc., m.g.sst.	0.2-2	65 30 5 0 0	
			<0.2	5 70 0 0 25	I/S 15% S
			0.2-2	45 45 5 0 5	

\*abbreviations: K=kaolinite, Ill=illite, CHL=chlorite, SM=smectite, M.L.=mixed layer I/S,  
glauc.=glaucousitic, v.f.g.=very fine grained, f.g.=fine grained, m.g.=medium grained,  
ss.=sandy, congl.=conglomerate

diluting the formation water, was calculated using Figure 2-14 of Kharaka et al. (1985); the ionic concentration of the formation water was corrected using this dilution factor. Table 5.2 lists the uncorrected chemical analyses at 25°C and the ionic concentrations after correction for dilution, recalculated to formation temperature and pressure using by the computer code SOLMNEQF (Aggarwal et al., in press). The sampling and analytical techniques of Gunter et al. (1985) were followed. Ph and alkalinity were measured immediately after sampling.

Chemical analyses for water from the same Paddy well, but collected and measured by industrial laboratories, are also listed in Table 5.2 for comparison. The comparison suggests that major ions are not very sensitive to the sampling and analytical techniques, but pH and  $\text{HCO}_3^-$  differ significantly. Several ion concentrations necessary for speciation and solubility calculations are not routinely analyzed by commercial laboratories, in particular, Si. The lack of these data limits the usefulness of such analyses for chemical modelling.

Dilution-corrected ionic concentrations, field measured alkalinity and pH, and organic acid concentrations for the Paddy and Bluesky waters were given as input into the computer geochemical code, SOLMNEQF (Aggarwal et al., in press) to compute ionic concentrations at subsurface conditions and the reaction states of the waters. The code calculates  $\text{HCO}_3^-$  concentration by subtracting the organic acid concentration from the field alkalinity.  $\text{Al}^{+3}$  concentration was not measured and is estimated to be 0.01 mg/l for the SOLMNEQF computations. The results in Table 5.3 indicate supersaturation with respect to an abundance of minerals. The  $\Delta G$  values close to zero indicate minerals most closely at equilibrium; positive  $\Delta G$  values indicate supersaturation and negative  $\Delta G$  values indicate undersaturation. Discrepancies between computed and observed mineral interactions result mainly from (1) errors in computed pH at subsurface conditions arising from loss of gas on production of the water; (2) errors in aluminum estimation and aluminum speciation; and (3) the presence of impurities and solid solutions in minerals (Kharaka and Spect, 1984). Both the Paddy and Bluesky waters are close to

TABLE 5.2 DETAILED WATER ANALYSES

ION	Paddy E.R.C.B.	Paddy (25°C)	Paddy (65°C)	Bluesky (25°C)	Bluesky (83°C)
mg/l	uncorrected	uncorrected	corrected	uncorrected	corrected
Na	7210	7760	9239	11500	14179
K	50	41.4	51	195	252
Li		2.9	4	3.3	4
Mg	57.6	47.2 <sup>o</sup>	51	87	104
Ca	176	175	183	335	362
Sr		60	54	140	123
Ba		150	135	315	291
SiO <sub>2</sub>		36.4	45	29.6	38
Mn		0.3	0.3	0.5	0.5
Fe	tr	23.5	25	37.5	36
NH <sub>3</sub>		2	2.5	22.9	30
Cl	11100	11400	13679	17600	21889
Br		47.3		44.8	
F		13.4	15	<0.5	
HCO <sub>3</sub> <sup>-</sup>	1130	1371	1644	1359	1618
SO <sub>4</sub>	17.1	<1		<1.0	
H <sub>2</sub> S		<0.8		<0.08	
Acetate		624	882	699	1000
Formate		12.8		4	
Propionate		97.7		86.9	
Butyrate		<1		19.5	
T.D.S.	19800	21754.4	26989	32479	42102
pH	8.4	6.9	6.77	7.06	6.79
Ionic strength		0.44	0.44	0.7	0.69
Pressure (bars)			126.8		160.7
δ <sup>18</sup> O (SMOW)		-5.7 ‰			
δD (SMOW)		-97 ‰			

TABLE 5.3 MINERAL SATURATION STATES

<b>PADDY</b>	$\Delta G$	<b>BLUESKY</b>	$\Delta G$
annite	23.472	annite	27.134
marialite	13.644	Mg-chlorite	13.305
phillipsite	12.712	phillipsite	11.581
Mg-chlorite	8.83	tremolite	10.997
muscovite	5.635	marialite	10.423
pyrophyllite	3.948	talc	6.789
kaolinite	3.914	dolomite	3.726
talc	3.578	siderite	3.343
dickite	3.21	muscovite	3.043
siderite	2.793	huntite	3.031
Na-montmorillonite	2.199	fayalite	2.08
Mg-montmorillonite	2.085	calcite	1.551
dolomite	2.084	magnesite	1.507
tremolite	2.012	aragonite	1.261
Ca-montmorillonite	1.882	kaolinite	1.192
fluorite	1.595	pyrophyllite	0.617
analcime	1.32	strontianite	0.556
albite	1.216	dickite	0.461
K-montmorillonite	1.16	analcime	0.345
illite	1.131	quartz	0.161
calcite	0.896		
aragonite	0.636		
magnesite	0.626		
quartz	0.538		
microcline	0.269		
adularia	0.265		
chalcedony	0.144		
boehmite	0.119		
strontianite	0.007		

equilibrium with respect to cristobalite, chalcedony or quartz. The departure of calcite from equilibrium in both waters is less than 2 kcal. Dolomite and siderite are both supersaturated by 2-4 kcal. Since thermodynamic data for ankerite does not exist, but late diagenetic ankerite is observed in Paddy and Bluesky sandstones, it is reasonable to assume that the waters are supersaturated with respect to ankerite and that ankerite could precipitate from present formation waters. Of the other supersaturated minerals, kaolinite, illite, and albite are observed in the rocks. SOLMNEQF results indicate that these minerals may still be precipitating from present formation waters in the Paddy and Bluesky sandstones.

### Stable Isotope Compositions

The stable isotope composition of one water sampled from the Paddy is  $\delta^{18}\text{O} = -5.7$  ‰ and  $\delta\text{D} = -97$  ‰ SMOW (Table 5.2). The  $\delta^{18}\text{O}$  composition of present formation water in the Cadomin was determined indirectly to be  $-6$  ‰ (Chapter 3). This isotopic composition was calculated by combining the  $\delta^{18}\text{O}$  value of quartz druse with the fluid inclusion data indicating that the quartz druse formed under present-day conditions.

Hitchon and Friedman (1969) analysed two Upper Devonian formation waters from the southeastern part of our study area (Simonette Field, Township 63). These waters have salinities of 278,000 and 284,000 mg/l with  $\delta^{18}\text{O}$  values of  $+3.0$  ‰ and  $+3.1$  ‰, and  $\delta\text{D}$  values of  $-51$  ‰ and  $-41$  ‰, respectively.

### Systematic Trends in Major Ion Compositions

Basic data for the ion chemistry come from analyses of formation waters gathered over the last 20-25 years by the Energy Conservation Board of Alberta. The analyses presented in this study are those surviving a rigorous qualification process to select only uncontaminated formation

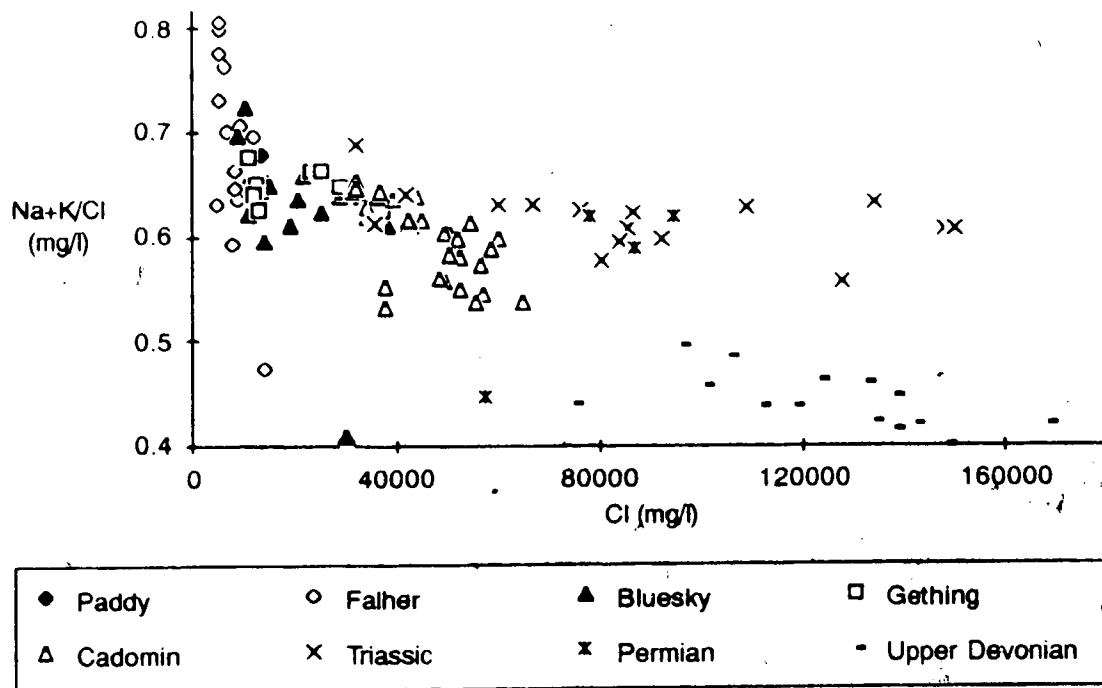


waters. Water analyses were rejected if: (1)  $\text{CO}_3^{-2}$  was present; (2)  $\text{pH} < 5.5$  or  $> 8.5$ ; (3) K concentrations were excessively high; or (4) T.D.S. contents were abnormally low for a particular unit compared to salinities in surrounding wells. The presence of  $\text{CO}_3^{-2}$  and high pH values generally indicate contamination by mud filtrate; low pH values and high K values generally indicate contamination by acid or KCl waters. The very low T.D.S. contents in some waters are the result of dilution by water condensed from the produced gas phase.

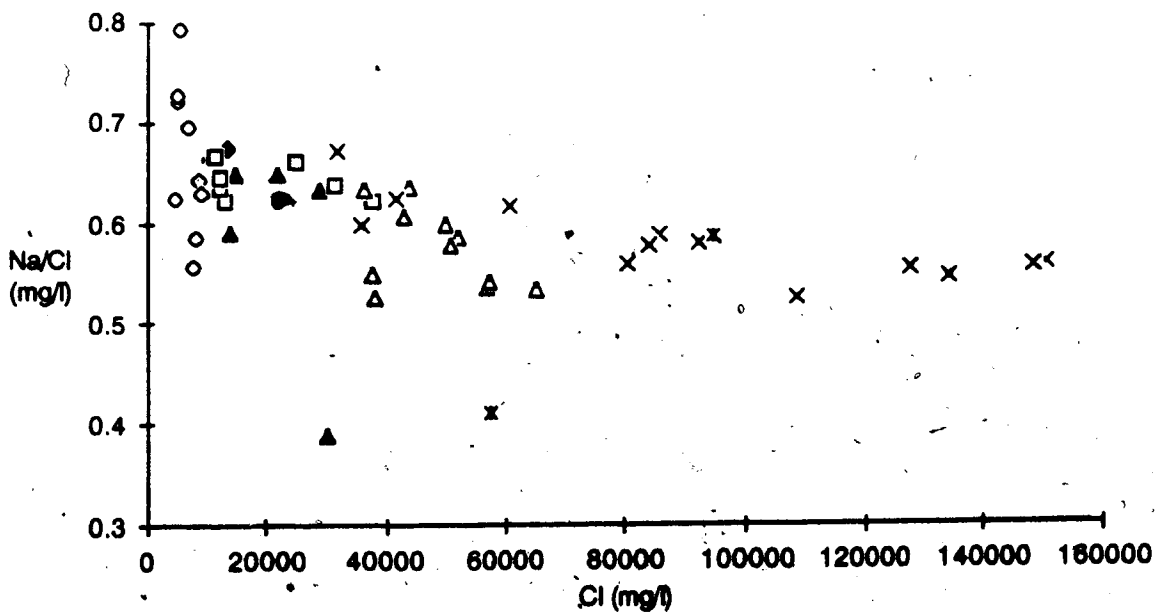
Plots of major ion/chloride ratios versus the chloride concentration (Figures 5.2-5.7) have been used to further qualify the data and to identify ionic trends associated with increasing chlorinity.  $\text{Na}+\text{K}/\text{Cl}$  and  $\text{Na}/\text{Cl}$  versus Cl diagrams (Figures 5.2 and 5.3) show decreasing  $\text{Na}+\text{K}/\text{Cl}$  and  $\text{Na}/\text{Cl}$  with increasing Cl. Older analyses of formation water do not differentiate concentrations of Na and K, thereby limiting the data for  $\text{Na}/\text{Cl}$  plots. Both plots show the same general trend.  $\text{Na}/\text{Cl}$  ratios in Cadomin waters decrease sharply with increasing salinity;  $\text{Na}/\text{Cl}$  ratios in Falher waters apparently decrease at a still greater rate. The rate of decrease in  $\text{Na}/\text{Cl}$  ratios of Triassic waters is much slower. The rate of  $\text{Na}/\text{Cl}$  decrease in Upper Devonian waters is slightly less than for Cadomin waters.

$\text{Ca}/\text{Na}$  ratios versus Cl (Figure 5.4) show definite trends for the Cadomin and Triassic data, toward increasing  $\text{Ca}/\text{Na}$  with increasing Cl. The increase is most rapid for the Cadomin waters. Amount of data for other units is insufficient and the scatter in available data is large.

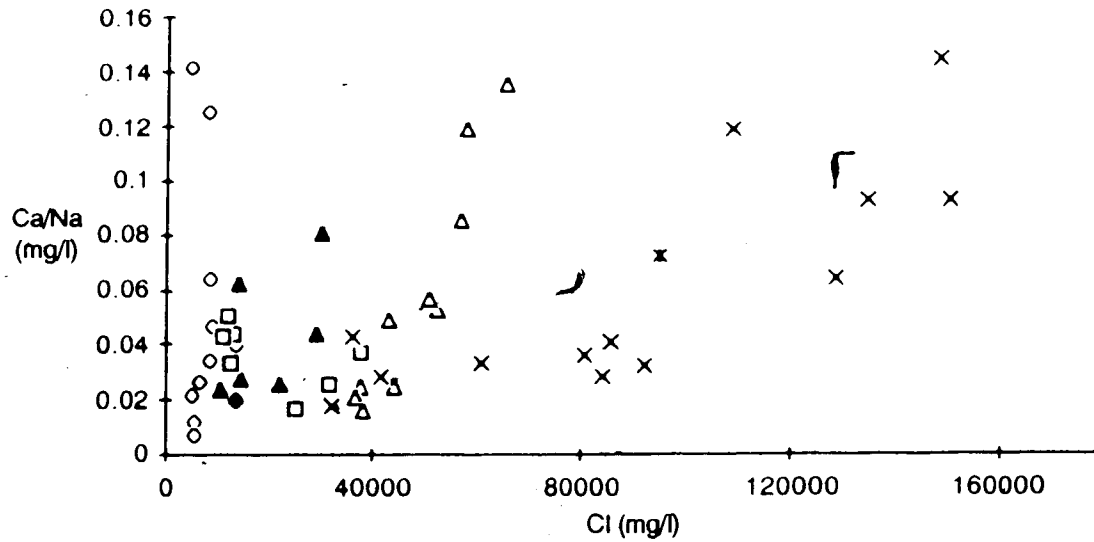
$\text{Ca}/\text{Cl}$  ratios (Figure 5.5) and  $\text{Mg}/\text{Cl}$  ratios (Figure 5.6) show a sharp increase with increasing Cl for Cadomin waters and the  $\text{Ca}/\text{Mg}$  ratio (Figure 5.7) is essentially constant.  $\text{Ca}/\text{Cl}$  and  $\text{Mg}/\text{Cl}$  are constant with a broad scatter for Falher, Paddy, Bluesky, Gething and some Triassic waters. Other Triassic waters have higher  $\text{Ca}/\text{Cl}$  ratios whose scatter encompass the range of  $\text{Ca}/\text{Cl}$  ratios in the Cadomin.



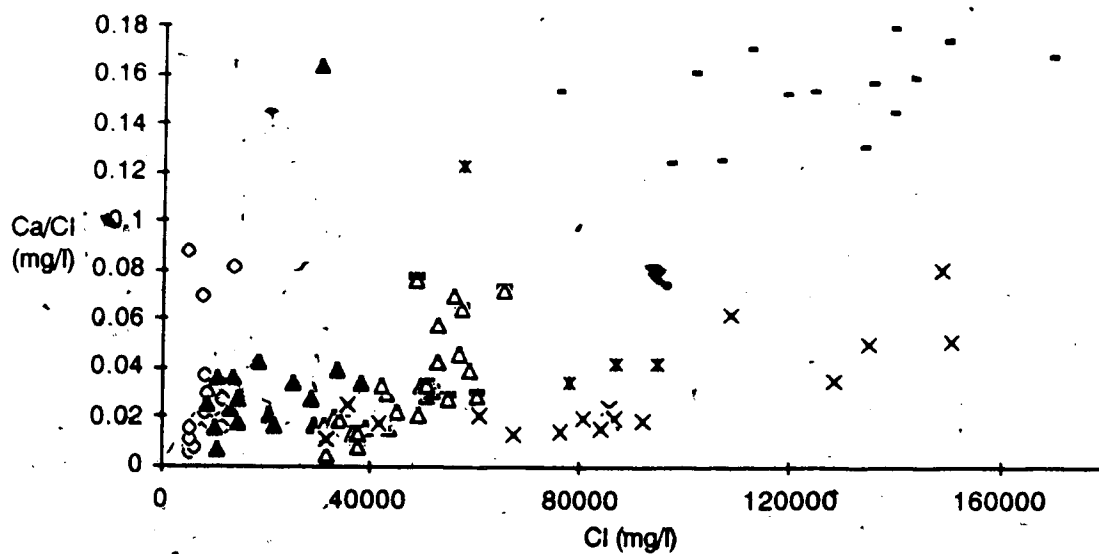
**Figure 5.2** Na+K/Cl versus Cl diagram. Na+K/Cl ratios are low in Devonian waters, and decreases with increasing chlorinity in Cadomin waters (open triangles). Legend of symbols applies to Figures 5.2 through to 5.7.



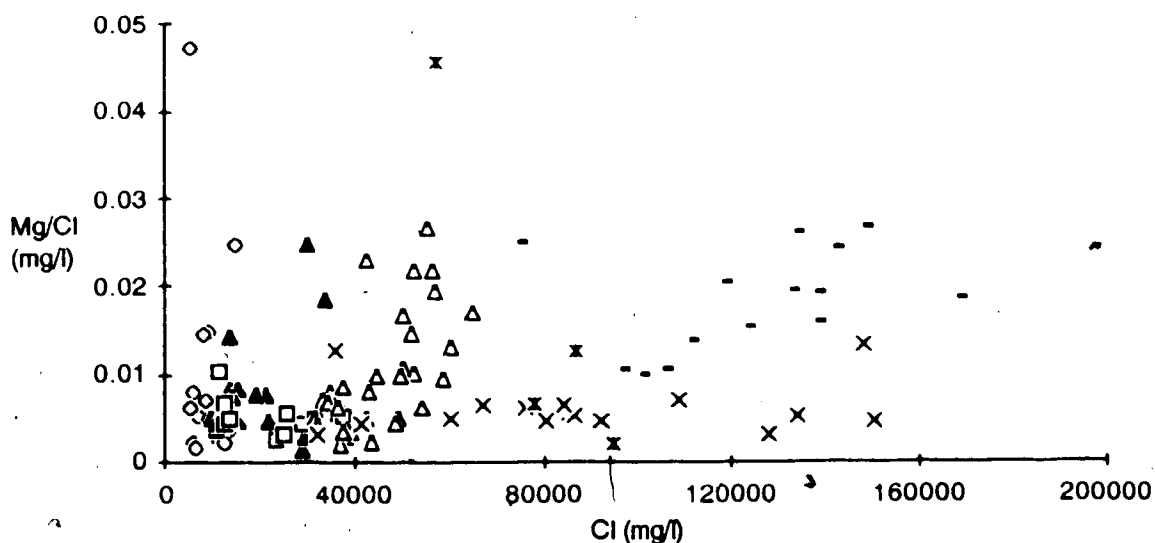
**Figure 5.3** Na/Cl versus Cl diagram. Na/Cl ratios decrease sharply with increasing chlorinity in Cadomin waters. See Figure 5.2 for legend.



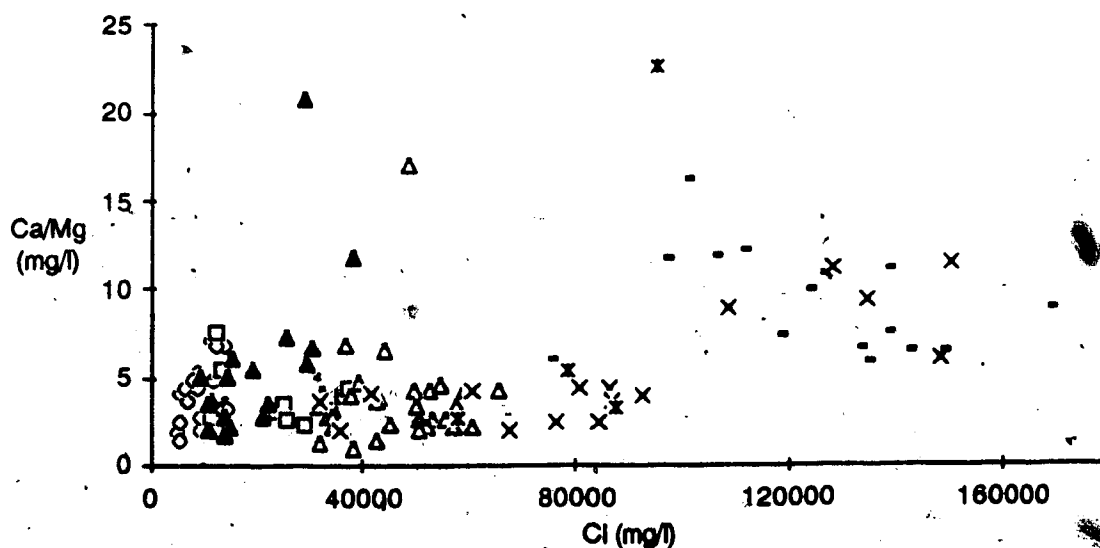
**Figure 5.4** Ca/Na versus Cl diagram. Ca/Na ratios increase with increasing chlorinity in Cadomin and Triassic waters. See Figure 5.2 for legend.



**Figure 5.5** Ca/Cl versus Cl diagram. Ca/Cl ratios sharply increase with increasing chlorinity in Cadomin waters. Ca/Cl ratios in Devonian waters are much higher than in Triassic waters with similar chlorinities. The most chloride-rich Triassic waters have Ca/Cl ratios similar to the more Ca/Cl enriched Cadomin waters. See Figure 5.2 for legend.



**Figure 5.6** Mg/Cl versus Cl diagram. Mg/Cl ratios increase sharply with increasing chlorinity in Cadomin and Devonian waters. The Mg/Cl ratio in Triassic waters remains constant with increasing chlorinity. See Figure 5.2 for legend.



**Figure 5.7** Ca/Mg versus Cl diagram. Ca/Mg ratios are constant with increasing chlorinity in Lower Cretaceous and some Triassic waters. Chloride-rich, Triassic and Devonian waters have higher Ca/Mg ratios. See Figure 5.2 for legend.

Mg/Cl ratios for all the Triassic samples are essentially constant. Upper Devonian waters have very high Ca/Cl ratios and Mg/Cl ratios which increase with chlorinity to values similar to the maximum values for Mg/Cl ratios in the Cadomin. Ca/Mg ratios show little correlation with chlorinity, although the range of Ca/Mg ratios in Lower Cretaceous and the lower chlorinity Triassic waters is generally lower than in the higher chlorinity Triassic and Lower Devonian waters.

The geographic distributions of values for those ionic ratios which show a correlation with chlorinity are shown in Figures 5.8-5.13. The Bluesky/Gething, Cadomin and Triassic units all have chlorinities which increase westwards or south-westwards across the study area (Figures 5.8 and 5.9). Permian and Upper Devonian formation waters apparently increase in chlorinity in an eastward direction (Figure 5.9).

Na/Cl ratios decrease from about 0.65 to about 0.55 towards the southwest or west in the Cadomin and Triassic units (Figure 5.10). Ca/Na ratios in the Cadomin and Triassic increase westwards (Figure 5.11) as do the Ca/Cl ratios (Figure 5.12). Mg/Cl ratios increase southwestwards in the Bluesky and Cadomin units (Figure 5.13).

## PRESENT HYDROGEOLOGY

Hitchon (1964) mapped the chloride contents of Lower Cretaceous formation waters over a region including most of Alberta. The area of interest for our study is shown in Figure 5.14. Regions of higher salinity water (18950-37900 mg/l) are divided by channels of relatively fresh water (<18950 mg/l). Hitchon (1964) concluded from this chloride distribution that recharge of meteoric water occurs in the mountains to the west. This meteoric water flows southeastwards into Alberta and then heads northeastwards to discharge in the deeply incised Peace River valley (J. Thompson, pers. comm.). The flow patterns proposed by Hitchon (1964) for Lower

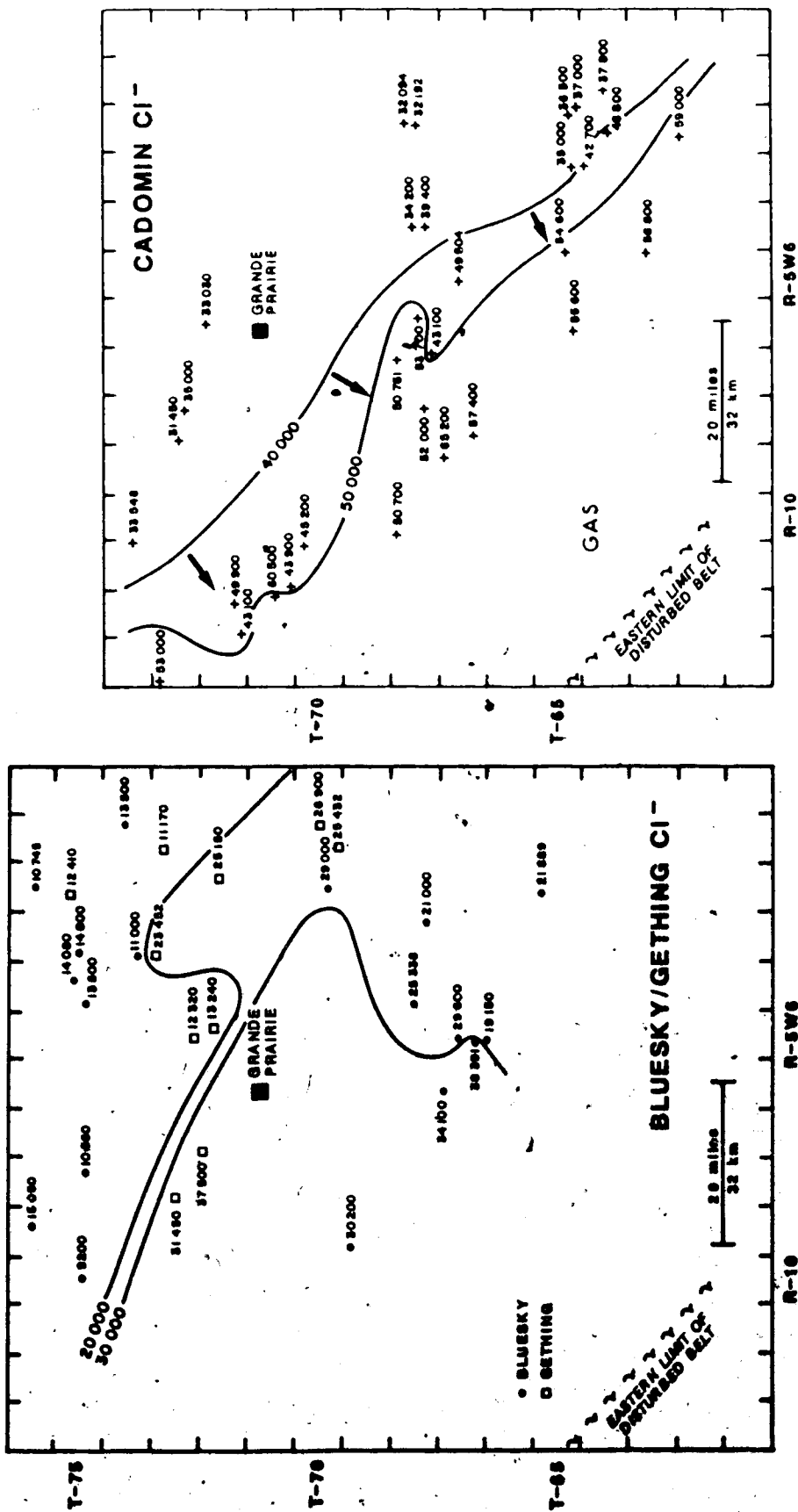


Figure 5.8 Geographic variation in chlorinities of Bluesky, Gething and Cadomin formation waters. Arrows point in the direction of increasing chlorinity.

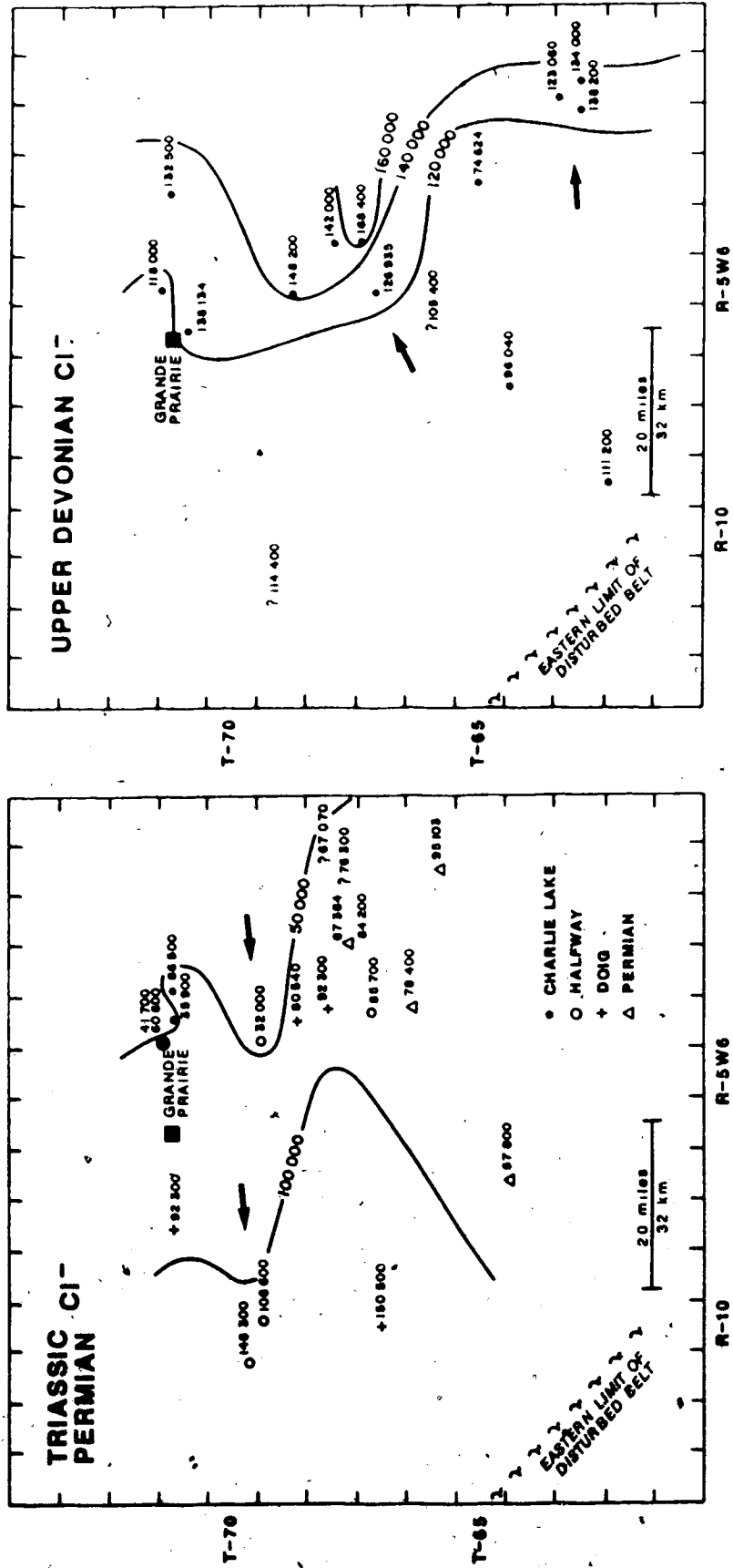


Figure 5.9 Geographic variation in chlorinities of Triassic, Permian and Upper Devonian formation waters. Arrows point in the direction of increasing chlorinity.

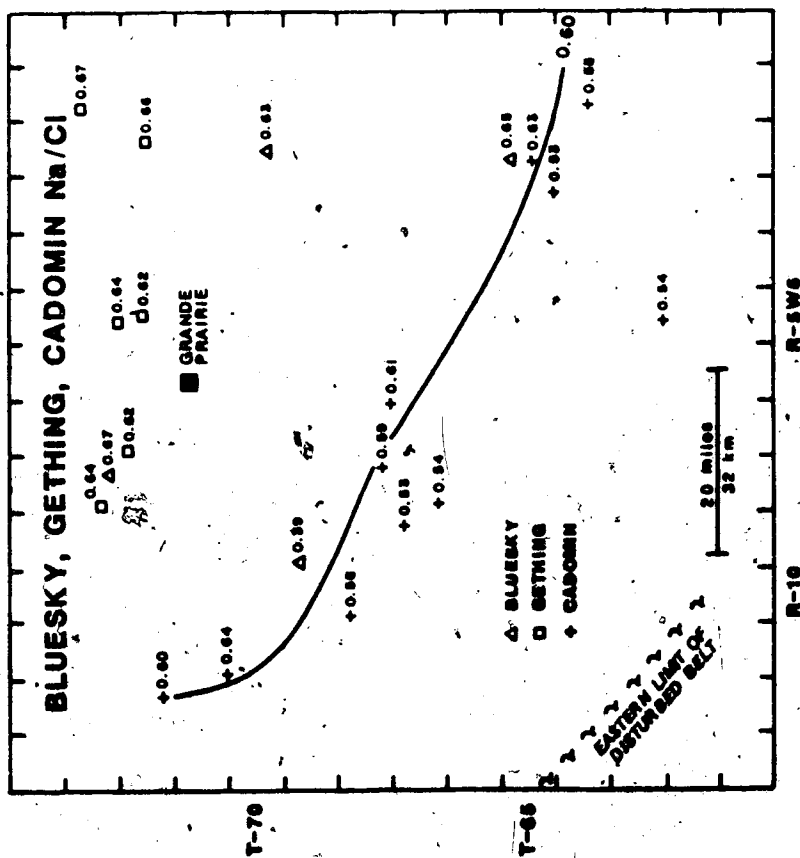
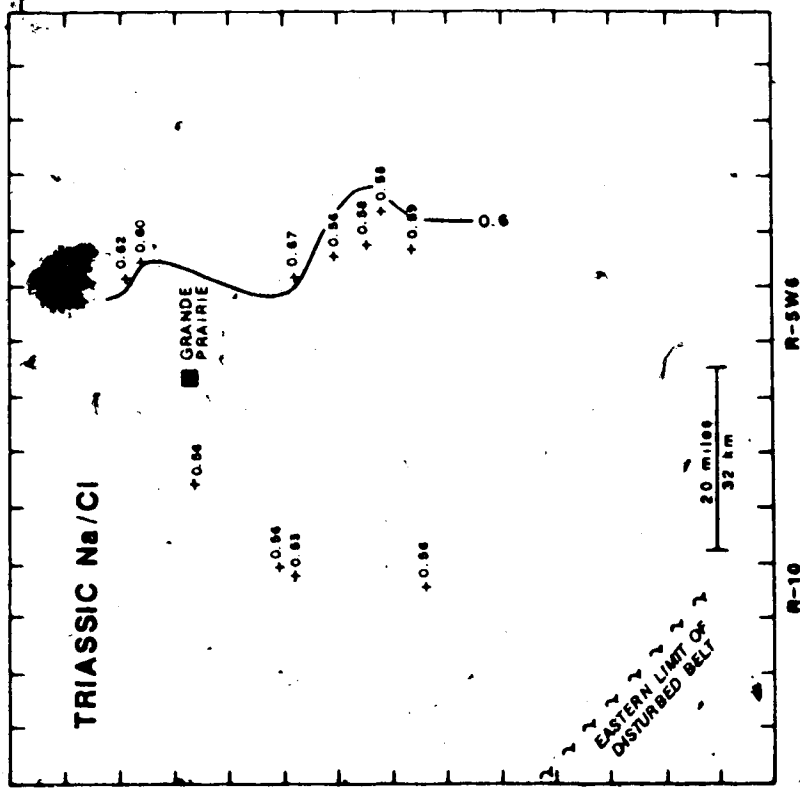


Figure 5.10 Geographic variation in Na/Cl ratios of formation waters.



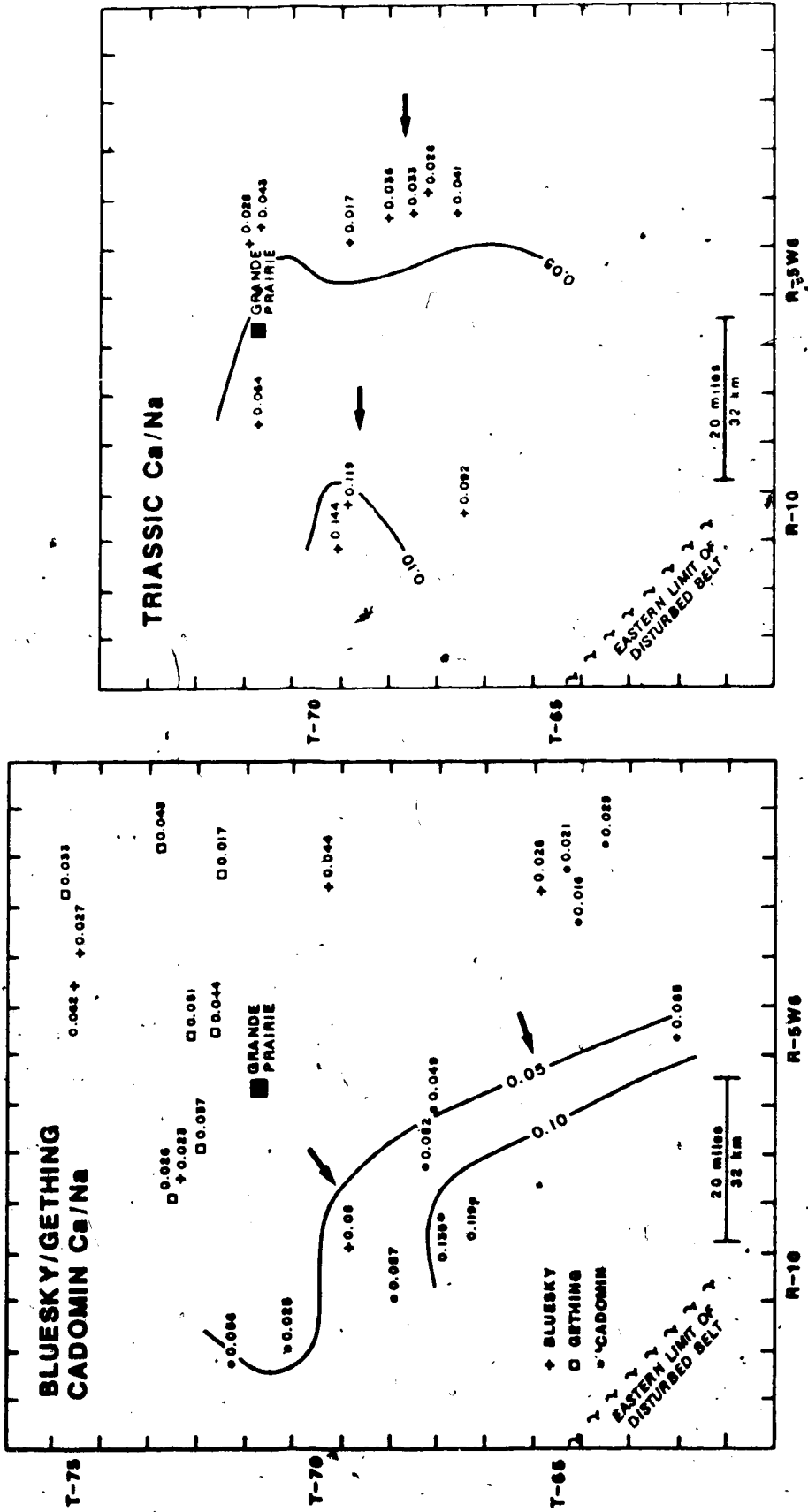


Figure 5.11 Geographic variation in Ca/Na ratios of formation waters. Arrows point in the direction of increasing Ca/Na ratios.

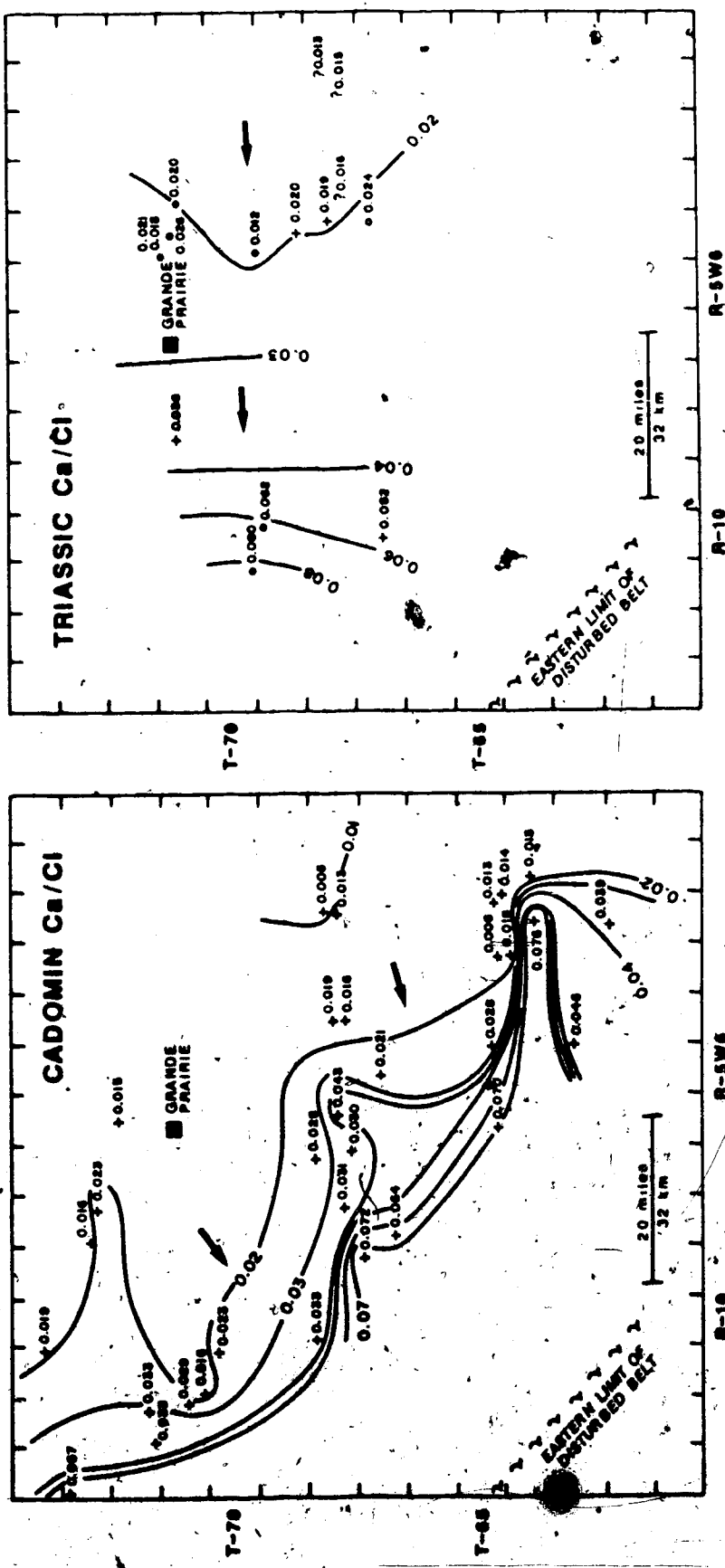


Figure 5.12 Geographic variation in Ca/Cl. Arrows point in the direction of increasing Ca/Cl ratios.

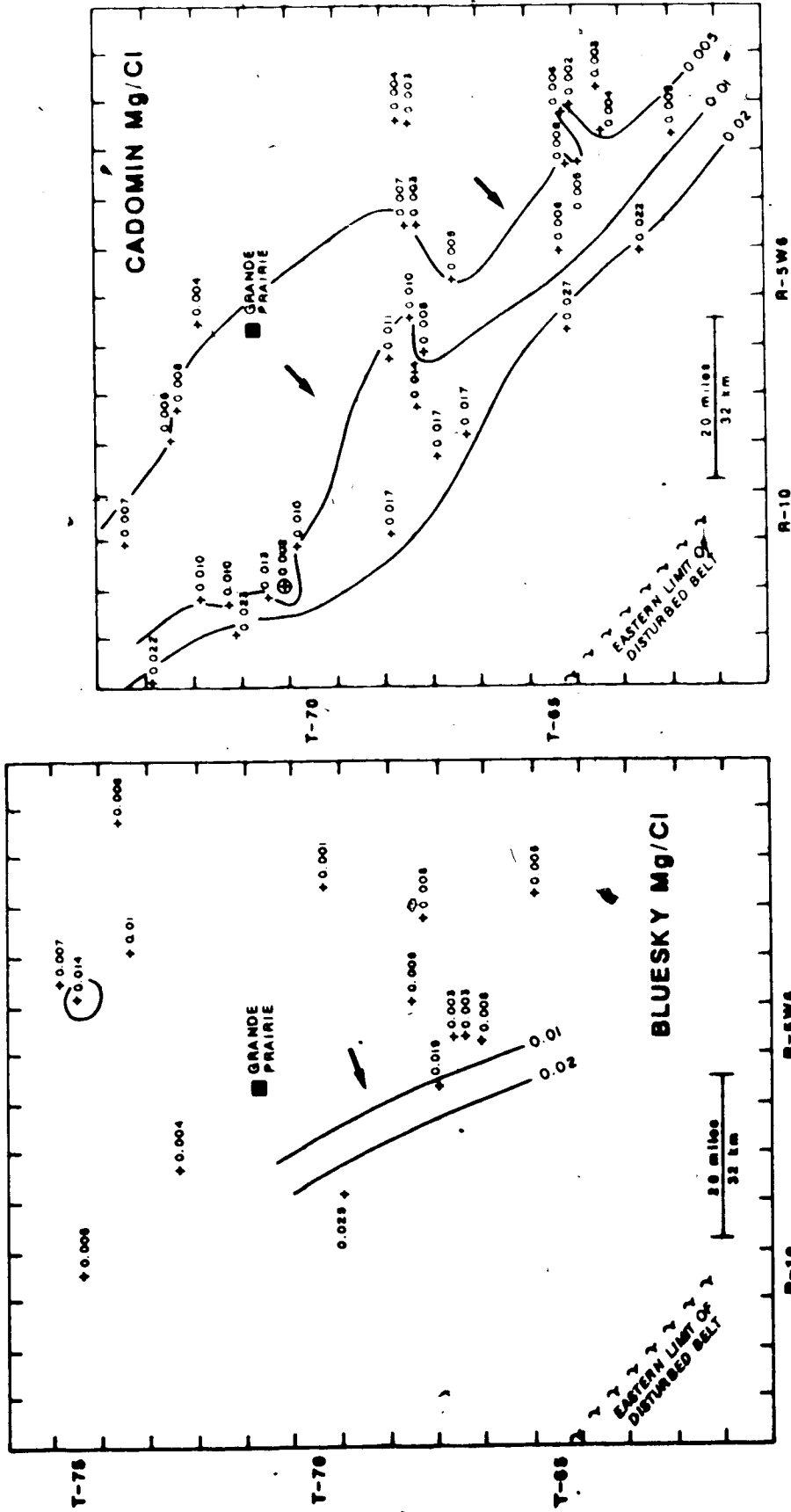
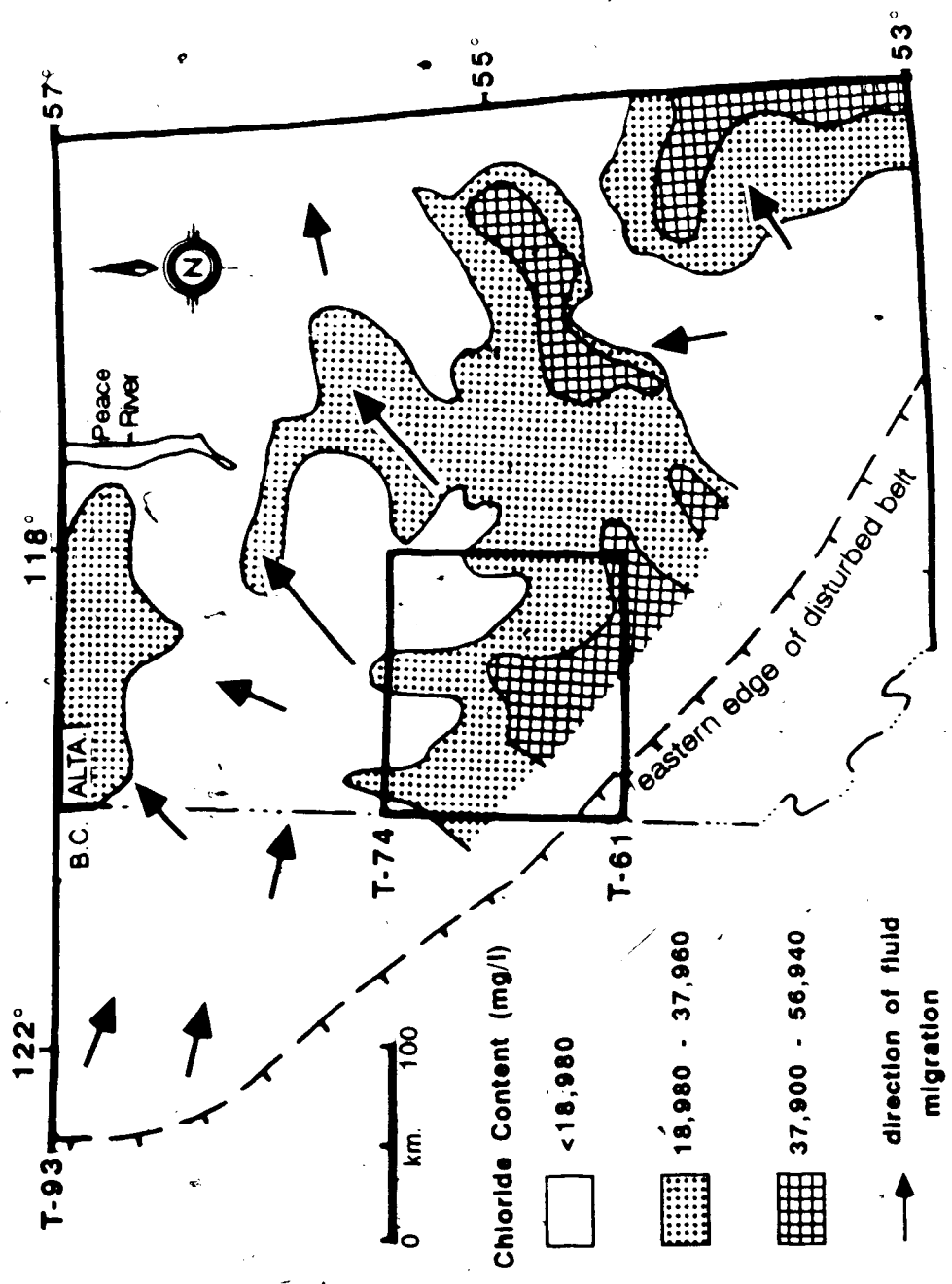


Figure 8.13 Geographic variation in Mg/Ci. Arrows point in the direction of increasing Mg/Ci ratios.



**Figure 5.14** Contours of the geographic variation in chloride content of Lower Cretaceous formation waters (modified from Hitchon, 1964). Arrows indicating flow direction are those of Hitchon (1964). The box from townships 61 to 74 is the study area detailed in earlier figures.

Cretaceous formation waters roughly correspond to surface flow controlled by topography (Figure 5.15).

More recent studies (J. Thompson, pers. comm.) of salinity distribution and potentiometric surfaces for the Cadomin Formation are confirming the regional flow pattern of Hitchon (1964), although the flow pattern differs in detail. In the Cadomin, Thompson's preliminary results indicate that fluids flow southeastwards from B.C. into Alberta, north of the study area. Flow then cuts diagonally southeastward across the study area until it turns northeastward. Northeastward flow dominates in the southern part of the study area.

A potentiometric surface map for the Cadotte Member of the Peace River Formation (Masters, 1979; his figure 12) shows flow in a southwestward direction towards the gas-water interface. However, the distribution of data points is such that the data can also be interpreted to indicate flow patterns similar to those in the Cadomin.

The limited distribution of potentiometric surface data available for the Deep Basin is shown in Figure 5.16. Hydraulic head distributions are determined from Homer-extrapolated, drill-stem pressure data and are expressed as hydraulic head in feet above sea level to permit direct comparison with the data from Masters (1979). Only analyses from drill-stem tests where chemical analyses of formation waters were also available were used. Hydraulic heads were calculated by dividing the reservoir pressure (in PSI units) by the pressure gradient and the result added to the subsea depth measured in feet. Pressure gradients were determined using the formation water salinity, reservoir pressure and temperature. Where relatively accurate reservoir temperatures were not available, temperatures were calculated based on the depth of the pressure test. The estimated error for hydraulic head values is  $\pm 100$  feet.

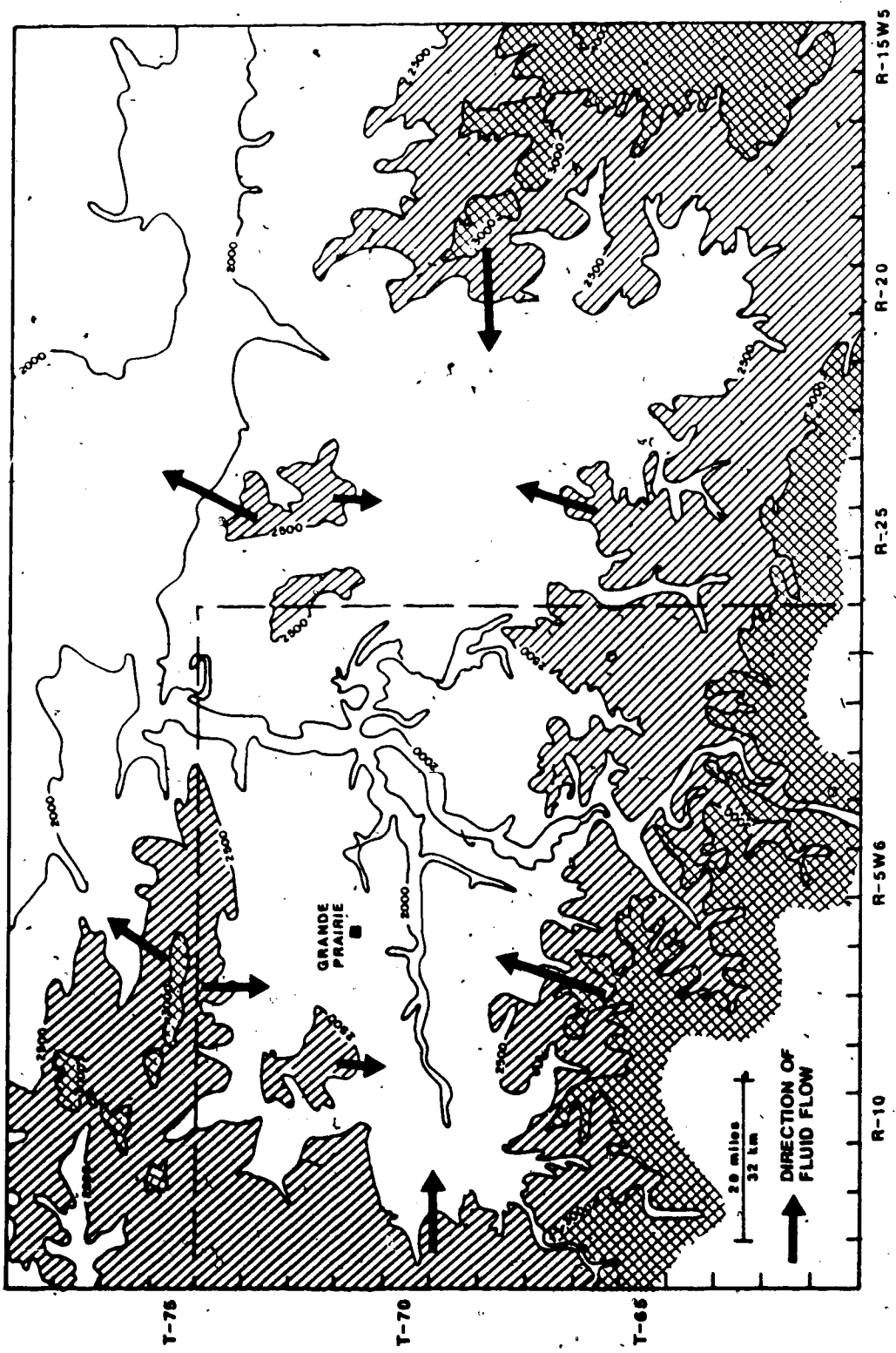


Figure 5.15 Topographic map for the study area (box) and surrounding area. Topographic highs are patterned. Arrows indicate directions of near-surface, fluid flow.

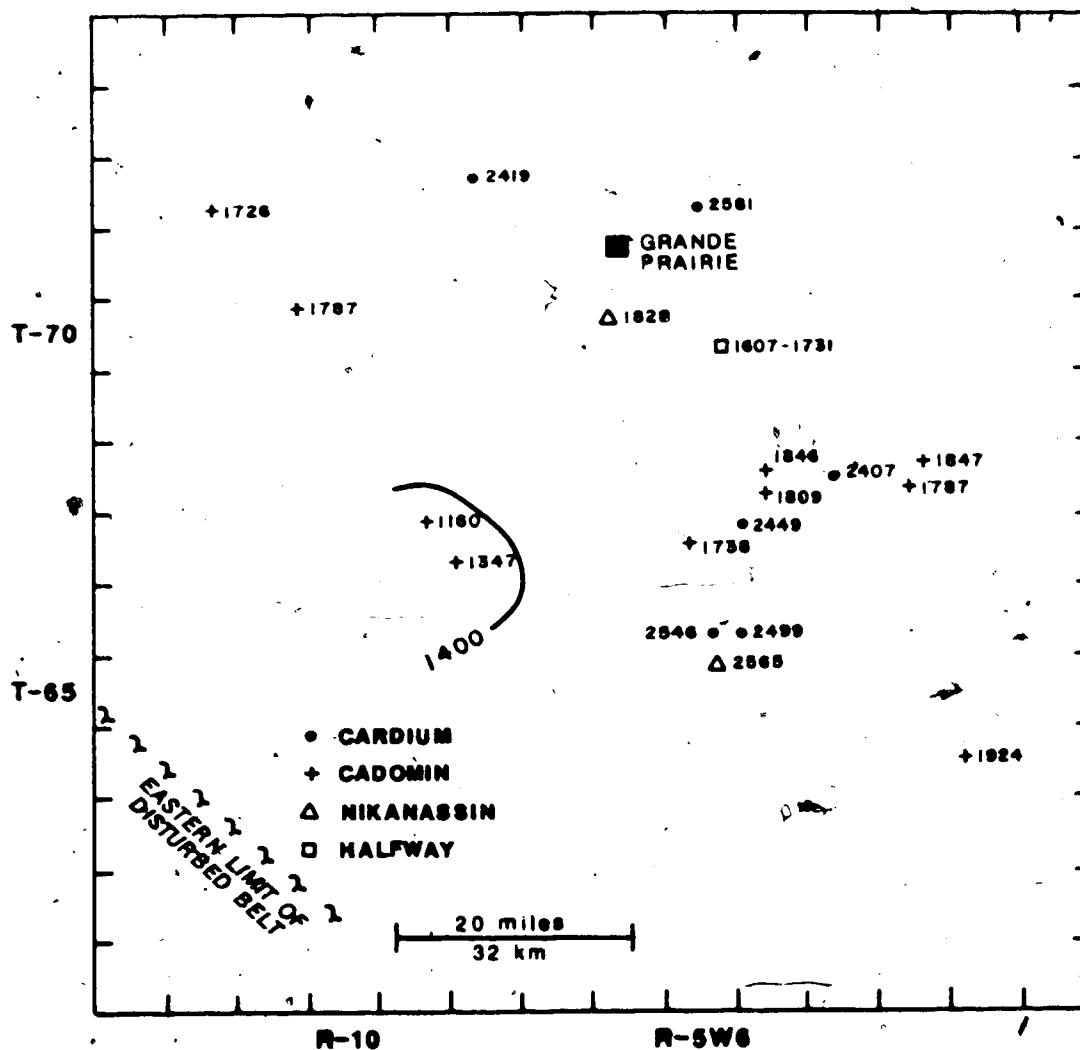


Figure 5.16 Map of potentiometric surface data (feet above sea level). Data are insufficient to determine flow directions. The 1400 ft contour in the southwest encloses two wells with anomalously low potentiometric surfaces in the Cadomin Formation. These two wells are immediately east of the gas-water contact for the Cadomin Formation.

Available data limit the distribution of hydraulic heads in the Cardium and Cadomin to the few points shown in Figure 5.16. Hydraulic heads in the Cardium range from 2419 to 2581 feet. This spread in values is probably within the range expected from inaccuracies in the data and cannot be used to reliably indicate flow directions. In the Cadomin, the distribution of hydraulic heads indicates a low about township 67-68, range 8-9 (Figure 5.16). These low potentials occur immediately adjacent to the gas zone. Gies (1984) suggested that these wells lie within an isolated reservoir which is separated from the regional flow system by a permeability barrier. The occurrence of similarly low potentials near the gas-water contact in the Cadotte (Masters, 1979; his figure 12) suggests that these potential lows may be related to dynamics of the gas-water interface.

Two hydraulic head values from the Nikanassin Formation are available (Figure 5.16). The Nikanassin consists of a quartzose sandstone immediately below the pre-Cretaceous unconformity. The potential at the northern location is comparable to that of the Cadomin, whereas the potential at the southern location is significantly higher. The southern point suggests that there is potential for upward flow from the Nikanassin into the Cadomin at that location.

Only one hydraulic head value is available for the Halfway (Figure 5.16). Within the range of errors, this value is indistinguishable from the Cadomin potentials in that area.

The similarity of potentials within each unit and the paucity of data prohibits the definition of flow directions within individual units. However, the regional flow is generally from the west or south towards the Peace River Valley to the northeast. A comparison of potentials from the different units provides clues to the potential for cross-formational flow. The data suggest that the Cadotte is a potential low (potentials vary in our study area from ~1050 to ~1250 feet), which may collect downward flow from the Cardium and upward flow from the Cadomin. Data are insufficient to postulate cross-formational flow between the Triassic units and the Cadomin.



## DISCUSSION

Within the study area, potentiometric surface data do little to aid in the determination of flow directions. The lack of significant variation in hydraulic head values within each unit suggests that lateral flow is insignificant. The low potentials characteristic of formation waters immediately adjacent to the gas zone (Cadotte and Cadomin Formations) suggest that a potentiometric sink is associated with the gas zone. However, Gies (1984) interprets the potential lows in the Cadomin Formation as representing an isolated water reservoir. Comparison of potentials from unit to unit suggest that the Cadotte Member is a potential low, which collects waters from overlying and underlying units. If so, cross-formational flow may dominate in the study area.

The vertical distribution of formation waters with chlorinities increasing down section also supports cross-formational flow. Chlorinities are lowest in the Paddy Member (13679 mg/l), increase to 65000 mg/l in the Cadomin Formation, and to 150000 mg/l in the Triassic units. All chlorinities, including those of the Paddy waters, are significantly higher than expected for the evolved meteoric water indicated by isotopic analyses (Chapters 3 and 4). Upward movement of chloride-rich waters from the evaporitic Triassic units is the most probable origin of high chloride contents.

The geographic distribution of ionic ratios is problematic. Chloride, Ca/Cl and Mg/Cl ratios increase in a southwestward direction towards the gas-water interface, whereas Na/Cl ratios decrease in this same direction. Concentration of waters by membrane filtration or by addition of solutes to the water by water-rock interaction should produce an increase in these ratios in the direction of flow. If membrane filtration or water-rock interaction are solely responsible for the observed distribution of ionic ratios, then a southwestward flow direction is indicated. However, regional studies (Hitchon, 1984; Thompson, pers. comm.) suggest that low salinity waters originating in the mountains to the northwest, flow southeastwards into Alberta north of the study

area. Work in progress by Thompson (pers. comm.) shows that the low salinity waters of Hitchon (1964), to the north of the Deep Basin, turn southeastward in the Cadomin Formation and head from the northwestern part of the study area towards the southeast before flow is redirected again towards the northeast. Thompson suggests that this flow direction in the Cadomin Formation is controlled by a barrier to flow (the Fox Creek Escarpment). A similar flow pattern in the Falher to Paddy units is suggested by the continuing low salinities and low  $\delta^{18}\text{O}$  ( $-5.7$  ‰) and  $\delta\text{D}$  ( $-97$  ‰) values in these units.

The chlorinity distribution of Hitchon (1964) (Figure 5.14) shows zones of high chlorinity waters alternating with linear trends of low chlorinity waters. This pattern suggests that high salinity zones are an artifact of paleoflow patterns; the lower salinity channels represent high salinity waters which have been diluted by modern meteoric water. In the southwestern part of the study area, high salinities are preserved because of the isolation of these waters from the influx of meteoric water. The gas-saturated zone is an effective barrier to flow from the west. Towards the eastern part of the study area, formation waters are being diluted by meteoric water derived from the northwest.

In Cadomin and Bluesky formation waters,  $\text{Ca}/\text{Cl}$ ,  $\text{Mg}/\text{Cl}$  and  $\text{Ca}/\text{Na}$  ratios increase southwestwards as salinities increase. Nesbitt (1985) demonstrated that mineral precipitation and dissolution reactions can explain systematic changes in  $\text{Ca}/\text{Na}$  ratios. In the Illinois Basin, Nesbitt (1985) showed that as salinities increase, pH decreases; the decrease in pH causes dissolution of carbonate phases and precipitation of Na-smectite. In the Lower Cretaceous section of the Deep Basin, in general, smectite is absent (Table 1) and the smectitic component of VS is probably too small to control the ionic ratios in formation water. However, diagenetic albite is observed and may be the sink for Na. The Cadomin Formation differs from other formations in the conspicuous absence of late carbonate cements (Chapter 3). The relatively high  $\text{Ca}/\text{Cl}$  and  $\text{Mg}/\text{Cl}$  ratios in the

most saline waters can be explained by dissolution, or lack of precipitation, of these carbonate cements.

### CONCLUSION

Regional flow is generally from the northwest, north of the study area, and heads southwestward across the study area until it turns northeastward to discharge in the Peace River Valley (Hitchon, 1964; Thompson, pers. comm.). Potentiometric and chemical data are too sparse in the study area to determine detailed flow directions and the extent of cross-formational flow. However, the data do suggest that cross-formational flow into the Cadotte Member may be important. Detailed chemical analyses of Paddy formation water suggest that ankerite and illite may be precipitating from present waters. Similar detailed water analyses and mineralogical study of late diagenetic phases on a regional scale within the water-saturated zone of the Deep Basin could significantly improve our understanding of present flow patterns.

## REFERENCES

- Aggarwal, P.K., Hull, R.W., Gunter, W.D., and Kharaka, Y.K., in press, SOLMNEQF: A computer code for geochemical modelling of water/rock interaction in sedimentary basins: in B. Hitchon, ed., Proceedings of the 3rd Annual Canadian/American Conference on Hydrogeology, Hydrogeology of Sedimentary Basins: Application to Exploration and Exploitation: National Water Well Association.
- Cant, D.J., 1986, Hydrocarbon trapping in the Halfway Formation (Triassic), Wembley Field, Alberta: Bulletin of Canadian Petroleum Geology, v.34, p. 329-338.
- Connolly, C., 1985, Shale diagenesis of the Wilrich Member, Spirit River Formation, northwest Alberta, Geology 507 Research Project: unpublished report, University of Alberta, Edmonton, Alberta, 36 p.
- Gies, R.M., 1984, Case history for a major Alberta Deep Basin gas trap: the Cadomin Formation: in J.A. Masters, ed., Elmworth case study of a Deep Basin Gas Field, American Association of Petroleum Geologists Memoir 38, p. 115-140.
- Gunter, W.D., Regula, D., and Young, B., 1985, Methods of collection and preservation and chemical analyses of aqueous fluids from oil sands pilots: ARC/AOSTRA Report 8586-15, 55p.
- Hitchon, B., 1964, Formation fluids: in R.G. McCrossan and R.P. Glaister, eds., Geological History of Western Canada: Alberta Society of Petroleum Geologists, Calgary, Alberta, p. 201-217.
- Hitchon, B., Billings, G.K. and Klován, J.E., 1971, Geochemistry and origin of formation waters in the western Canada sedimentary basin - III. Factors controlling chemical composition: *Geochimica et Cosmochimica Acta*, v.35, p. 567-598.
- Hitchon, B. and Friedman, I., 1969, Geochemistry and origin of formation water in the western Canada sedimentary basin- I. Stable isotopes of hydrogen and oxygen: *Geochimica et Cosmochimica Acta*, v.33, p. 1321-1349.
- Kharaka, Y.K., Hull, R.W. and Carothers, W.W., 1985, Water-rock interactions in sedimentary basins: in D.L. Gautier, Y.K. Kharaka, and R.C. Surdam, eds., Relationship of Organic Matter and Mineral Diagenesis: SEPM Short Course No. 17, p. 79-176.
- Kharaka, Y.K., and Specht, D.J., 1984, Modeling water-mineral interactions at high temperatures and pressures: in AOSTRA/ARC hydrothermal chemistry workshop, compilation of abstracts, overheads and concluding discussions, Banff, Alberta.
- Masters, J.A., 1979, Deep Basin gas trap, Western Canada: The American Association of Petroleum Geologists Bulletin, v.63, p. 152-181.
- Nesbitt, H.W., 1985, A chemical equilibrium model for the Illinois Basin formation waters: American Journal of Science, v.285, p. 436-458.
- Thompson, J., in prep., The use of hydrogeological mapping in hydrocarbon exploration, study of the early Cretaceous, Deep Basin Region, northwest Alberta: current unpublished MSc. thesis, University of Alberta.

## **CHAPTER 6. GENERAL DISCUSSION AND CONCLUSIONS**

The general purpose of this thesis was to evaluate the effect of the flow regime on clastic diagenesis and develop a geochemical model for diagenesis and porewater evolution in the Alberta Deep Basin. Specific objectives were (1) to determine the involvement of meteoric water in diagenesis of Cretaceous sedimentary rocks in the Alberta Deep Basin, (2) to determine how the isotopic and chemical composition of porewaters varied in response to major geological events, and (3) to determine the relationship between diagenesis and the production and trapping of methane gas.

A model for diagenesis and porewater evolution in the Alberta Deep Basin is described below. Three major stages in diagenesis and evolution of porewaters correspond to three different flow regimes which in turn are controlled by major geological events and maturation of organic matter. Stage 1 is diagenesis in a flow regime driven by compaction and diagenetic reactions during subsidence and burial (Figure 6.1). Stage 2 is diagenesis in a gravity-driven, meteoric water flow regime during maximum burial and relief and continuing during erosion (Figure 6.2). Stage 3 marks the end of diagenesis in a gas-saturated zone; the presence of this zone inhibited direct eastward flow of evolved meteoric water into the study area (Figure 6.3).

### **A MODEL FOR DIAGENESIS AND POREWATER EVOLUTION IN THE ALBERTA DEEP BASIN**

#### **Stage 1. Deposition and Burial**

Diagenetic minerals, precipitated during burial of Cretaceous sandstones and conglomerates in the Alberta Deep Basin include early hematite, siderite and chlorite, and later quartz, kaolinite, illite and albite. Hematite formed in the oxidized zone soon after deposition and

### Figure 6.1

Schematic cross-section showing fluid flow resulting from compaction during burial.

- Flow directions (arrows) are superimposed schematically onto a southwest to northeast cross-section extending from 93-I-15 in British Columbia to Township 74 Range 25 W5 in Alberta, through Lower Cretaceous units of the Deep Basin. Facies and facies boundaries are taken from paleogeographic maps of Smith et al. (1984). Different types of arrows distinguish between marine, brackish and fresh water based on the depositional setting of the shale.

Flow during compaction was characterized by expulsion of water from compacting shales into adjacent sandstone and conglomerate beds. Most of the coarser units probably received both marine and brackish or fresh water. Upward seepage of high salinity waters from Triassic and Permian units into the Cadomin and possibly as high as the Bluesky also occurred during burial.

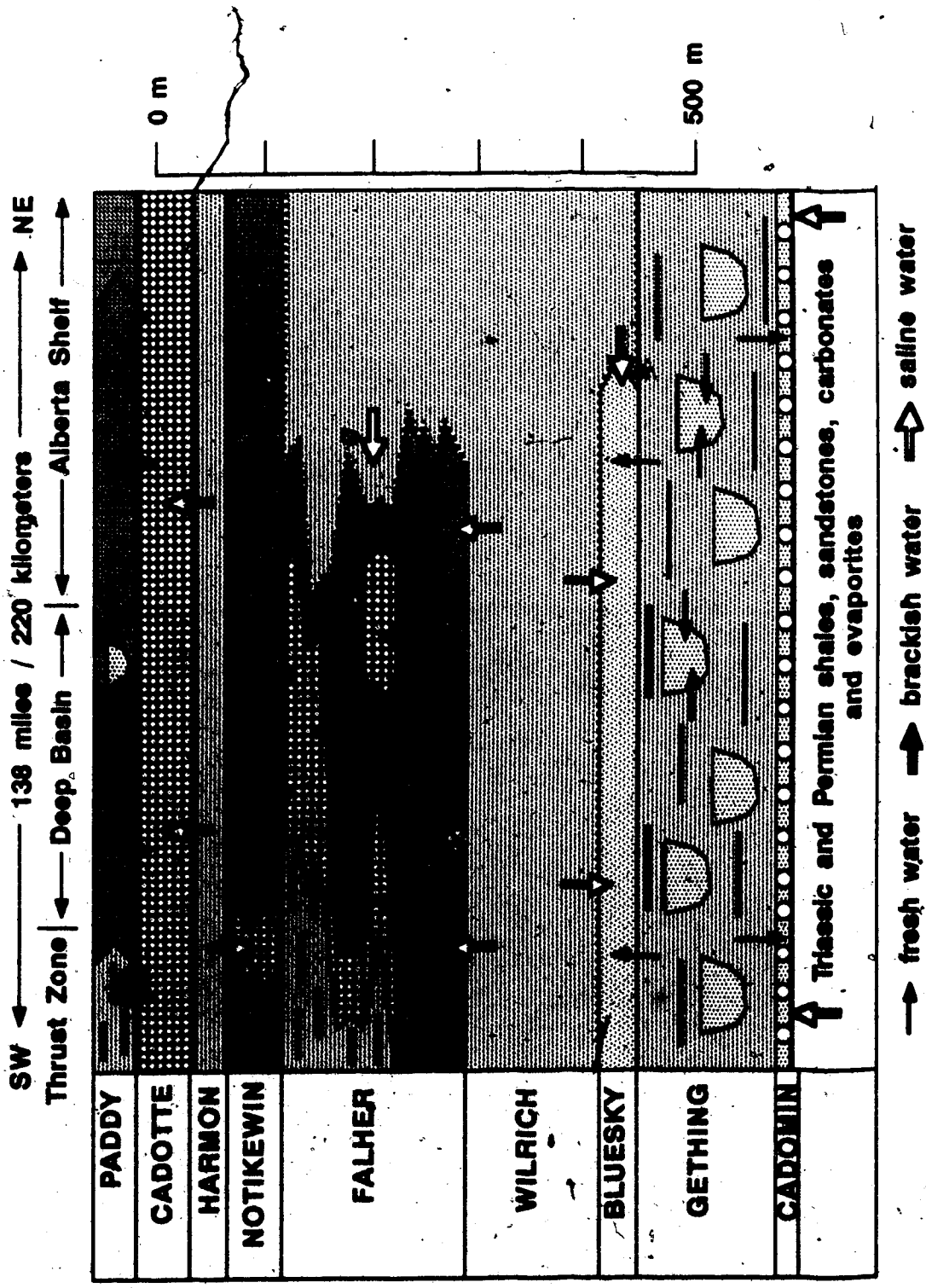
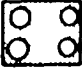
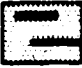

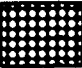

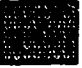

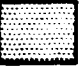



Figure 8.1

**LEGEND**

-  Alluvial plain and braid plain - conglomerates and sandstones
-  Lower delta plain - mud, silt, thin sands, coals
-  Barrier bar sands - coarsening upward sands
-  Wave dominated sand delta - conglomerates and sands
-  River dominated mud delta - muds and silts
-  Salt marsh/ mud flats - mud, silt and coal
-  Subtidal bay - mud and thin sandstones
-  Offshore silts, thin sands and marine shale
-  Conglomerate or sand-filled channel

**Figure 6.1 cont.**



**Figure 6.2**

Schematic cross section showing fluid flow following maximum burial. Present slope of Lower Cretaceous units is 1-2° to the southwest, but at maximum burial the slope may have been as high as 6-7°. By the time of maximum burial, flow of water from shales by compaction and diagenetic reactions had been exhausted. Northeastward flow (arrows) of evolved meteoric water along permeable beds or bedding plane fractures occurred. The interpretation of this flow direction is based on: (1) the high temperature (190°C) of fluids precipitating quartz druse, which suggests that waters were heated at greater depths and moved upwards; (2) isotopic compositions of these fluids which suggest that flow occurred along Cretaceous units rather than cross-formationally from underlying evaporitic and carbonate rocks; (3) precipitation of the largest and most abundant quartz druse in the west which suggests precipitation from rising, silica-saturated fluids as they cooled; (4) fluid inclusions in quartz druse which indicate that temperatures of fluids decreased eastwards; and (5) decreasing  $\delta^{18}\text{O}$  values of porewaters after precipitation of quartz druse which indicates an influx of evolved meteoric water, and low  $\delta\text{D}$  values of dickites which indicate a significant contribution of meteoric water.

The pathway for penetration of meteoric water to depths sufficient to be heated to  $>190^\circ\text{C}$  is problematic. Possible paths include fractures oriented perpendicular to the thrust sheets, or a combination of permeable near-surface sediments and eastward dipping, folded edges of Cretaceous beds in the disturbed belt east of the thrust zone. Updip flow in Cretaceous units was probably concentrated along permeable conglomerate and coarse-grained sandstone beds and bedding plane fractures.

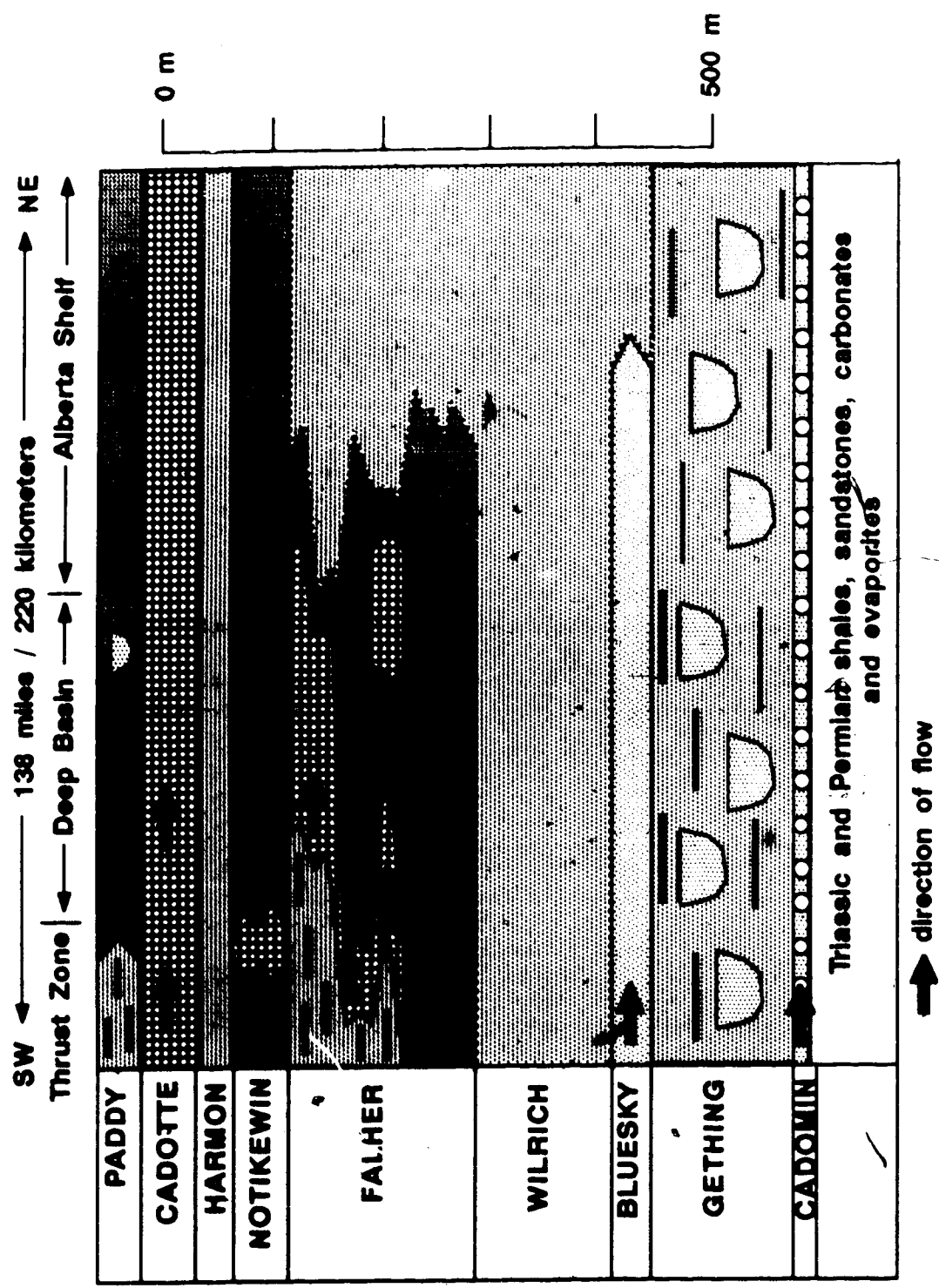


Figure 6.2

### Figure 6.3

Schematic cross-section showing fluid flow during uplift after gas saturation. Heavy vertical bars indicate the approximate gas-water interface in units where the interface was located on paleogeographic maps of Smith et al. (1984). See Figure 6.1 for legend describing facies and rock types.

The development of the gas-saturated zone created an effective block against the earlier northeastward flow shown in Figure 6.2. After the interruption of flushing by meteoric water from the southwest, redistribution of solutes occurred by mixing of low-salinity water from permeable units which had been flushed by meteoric water and of high-salinity water from less-permeable units which escaped flushing. Arrows represent this redistribution process in the lowermost formations. Upper units may have been more effectively flushed by evolved meteoric water.

Open circles enclosing dots indicate modern flow in a direction perpendicular to the cross section (southeasterly direction). Relatively low salinity, evolved meteoric water flows diagonally across the study area in a southeasterly direction in the Cadomin Formation. This modern flow pattern causes dilution of previously high-salinity formation water in the eastern part of the Deep Basin, whereas high salinities are preserved in the west, adjacent to the gas-water interface.

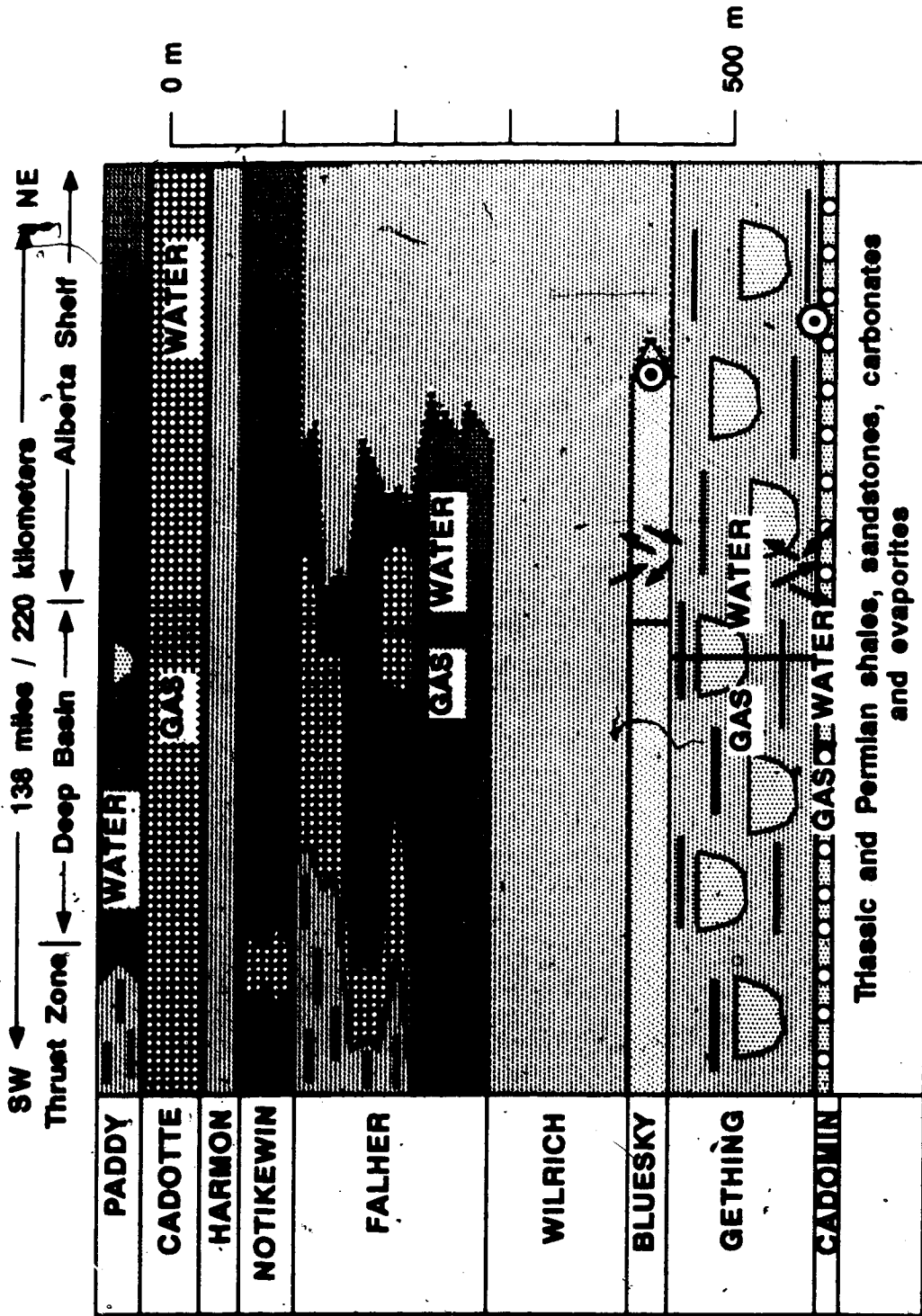


Figure 6.3

is rarely preserved. Early diagenetic siderite precipitated from low  $^{18}\text{O}$  porewaters ( $\delta^{18}\text{O} = -12$  to  $-7$  ‰ SMOW) in sediments which were deposited in continental (Cadomin Fm.), brackish (Falher Mb.) or marine (Cardium Fm.) environments. In the Cardium, a regional erosional surface which immediately overlies the sandstone in which siderite formed, provided an entrance for meteoric water. Early chlorite precipitated in sediments where penetration by meteoric water was less pervasive (for example, in the northern part of the study area in the Falher, and in the Cardium, below siderite-cemented beds in lower parts of the same sandstone unit). Chlorite grew in the Falher from porewaters with  $\delta^{18}\text{O}$  values of  $-9$  to  $-8$  ‰.

Before the Laramide Orogeny (early Eocene time), topographic relief in the Western Canadian Basin was low (Hitchon, 1984). The basin was subsiding and flow was probably predominantly driven by compaction and thermobaric reactions (Galloway, 1984). Such flow is characterized by release of water from shales into permeable sandstones (Figure 6.1). Calculations by Suchecky and Land (1983) indicate that water in isotopic equilibrium with shale (at  $100^\circ\text{C}$ ) has a  $\delta^{18}\text{O}$  value of  $\sim +5$  ‰. Porewaters which had  $\delta^{18}\text{O}$  values of  $-12$  to  $-7$  ‰ during early diagenesis in sandstones, were enriched in  $^{18}\text{O}$  during burial by reaction with the rock and by mixing with these  $^{18}\text{O}$ -rich shale waters. In most-Cretaceous sandstones, kaolinite, quartz, illite, albite and calcite precipitated from porewaters which evolved to maximum  $\delta^{18}\text{O}$  values of  $+3$  ‰. In the Cadomin Formation, illite may have precipitated from porewaters with  $\delta^{18}\text{O}$  values as high as  $+4$  to  $+7$  ‰ at  $100^\circ$ - $150^\circ\text{C}$ . Maturation of coal and other organic matter probably began to produce hydrocarbons and  $\text{CO}_2$  when burial temperatures reached  $70^\circ$ - $80^\circ\text{C}$ . A lowering of pH caused by influx of  $\text{CO}_2$  may have caused dissolution of siderite and possibly other carbonate cements.

Cross-formational flow of saline  $^{18}\text{O}$ -rich waters from the Triassic into the Cadomin during burial (Figure 6.1) is suggested by: (1) the difference in maximum  $\delta^{18}\text{O}$  values for porewaters during burial in the Cadomin and overlying units; (2) the position of the Cadomin at the base of the

Cretaceous section immediately above an unconformity which separates it from Triassic and Permian carbonate and evaporite rocks; (3) the presence of formation waters with salinities of 100,000 mg/l presently in the Cadomin whereas porewaters at the time of deposition were fresh; and (4) isotope data for diagenetic calcite which suggest that porewaters in Triassic and Permian sandstones had  $\delta^{18}\text{O}$  values of +6 to +8 ‰ during burial. To a lesser extent,  $^{18}\text{O}$ -rich, saline waters may have also infiltrated into Bluesky sandstones where fluid inclusions in late calcite cement indicate salinities of 65,000 mg/l. There is generally no evidence for  $^{18}\text{O}$ -rich fluids in the Falher or overlying units.

### Stage 2. Gravity-Driven Flow

The timing of maximum burial corresponded with maximum elevation of the mountains to the west and maximum hydraulic potential. At this time, the flow regime probably changed from compaction- and thermobaric-driven flow to gravity-driven flow of meteoric water (Hitchon, 1969; Toth, 1980). Fluid inclusion and stable isotope data indicate that quartz druse in the Falher and Cadotte conglomerates was precipitated at 190°C from porefluids with  $\delta^{18}\text{O} = +3$  ‰ and salinities of 20,000-30,000 mg/l. The relatively low  $\delta^{18}\text{O}$  value of these hot porefluids suggests that they contain a sizeable fraction of meteoric water which has mixed with connate water.

Thermobaric waters derived from smectite-illite reactions and membrane-effluent compaction waters could have low salinities, but at these high temperatures,  $\delta^{18}\text{O}$  values for porewaters equilibrated with clays should be +7 to +9 ‰ (Suchecky and Land, 1983) rather than +3 ‰.

The most likely path of the evolved meteoric waters was recharge in the mountains and seepage down through permeable rock or fractures to sufficient depths to be heated to >190°C. Since the Falher was situated at such depths near the synclinal axis of the basin, hot fluids could have migrated up permeable pathways within the Falher and Cadotte in an easterly direction (Figure 6.2), mixing with and displacing connate fluids along its path. The coexistence of methane inclusions with aqueous inclusions in quartz druse (Chapter 2), and pyrobitumen locally coating

quartz druse (Chapter 3, Figure 3.6b,c), suggest that hydrocarbons and methane gas produced from maturing coals and other organic matter migrated eastwards with the hot, evolved meteoric water.

Recharge by meteoric water in the mountains to the west continued during erosion and uplift of the sedimentary basin. Low  $\delta D$  values for late-stage dickite in both the Falher and Cadomin (-130 to -94 ‰) indicate that porewaters which precipitated dickite contained a large fraction of meteoric water. Calcite and ankerite cements were also precipitated from such waters in permeable rocks. When late-stage calcite was precipitated in the Falher (113°-170°C), fluid inclusion and stable isotope data indicate that salinities were the same as they were at 190°C (20,000-30,000 mg/l), but the  $\delta^{18}O$  value of the porewater had decreased from +3 ‰ to between 0 ‰ and -3 ‰. Salinities may have been controlled by cross-formational seepage of chloride-rich waters from the underlying Triassic evaporite and carbonate rocks.

### Stage 3. Redirection of Gravity-Driven Flow

Stage 3 began when maturing coals had produced sufficient methane such that it formed a continuous gas phase (~48-38 Ma; Weiss, 1985). This methane-rich gas phase migrated upwards and in the process drove out any moveable water; only water trapped in the micropores remained. At this time, the flow path of meteoric water must have been diverted to the north and south of the gas-plugged zone, creating the present flow path as shown by Hitchon (1984) (Figure 5.14): recharge occurs in the west and meteoric water flows eastwards in channels located to the north and south of the Deep Basin gas area. Fluids in these channels are characterized by their low salinities.

The consequences of this redirection of flow were: (1) interruption of diagenesis in the gas-saturated zone of the study area; and (2) blockage of flow of evolved meteoric water to the

eastern water-saturated part of the study area (Figure 6.3). In the water-saturated area, a redistribution of solutes took place between relatively fresh water in rocks which had been flushed by evolved meteoric water and saline water in less permeable rocks which had been bypassed during the flushing stage. Domineco and Robbins (1985) have mathematically modelled this process which is also demonstrated in the Milk River sandstone in southern Alberta (Schwartz et al., 1982). Salinities of porewaters in the Cadomin, after this redistribution of solutes, were probably similar to those of formation waters nearest the gas-water interface today (100,000 mg/l). Although fluid inclusion and stable isotope data indicate that flushing by evolved meteoric water occurred in the Cadomin, these data are limited to highly permeable conglomerates. It is possible that low permeability conglomerates and sandstones that were not flushed were just as common.

The present variation in salinities and ionic ratios in the Cadomin is controlled by the relatively recent flow pattern in the Cadomin, whereby saline formation waters in the eastern part of the study area are being diluted by relatively fresh formation waters (Figure 6.3). Work in progress by J. Thompson (pers. comm.) shows that low salinity fluids in the Cadomin Formation, to the north of the Deep Basin, cut diagonally southeastward across the study area until they are redirected towards the northeast. Thompson suggests that this flow direction in the Cadomin Formation is controlled by a barrier to flow (the Fox Creek Escarpment). A similar flow pattern in the Falher to Paddy units is suggested by the continuing low salinities and low  $\delta^{18}\text{O}$  (-5.7 ‰) and  $\delta\text{D}$  (-97 ‰) values in these units.

In Cadomin and Bluesky formation waters, Ca/Cl, Mg/Cl and Ca/Na ratios increase westwards as salinities increase. The Cadomin differs from other formations in the conspicuous absence of late carbonate cements. The relatively high Ca/Cl and Mg/Cl ratios in the most saline waters may be the result of carbonate minerals being unstable in the lower pH conditions of more saline waters (Nesbitt, 1985). Diagenetic albite is observed and may be a sink for Na.



## Difficulties with the Hydrogeological Model and Suggestions for Future Work

The above model is a simplified hydrogeological model which attempts to incorporate the observed mineralogical, isotopic and ionic chemistry data. More detailed consideration of the actual flow patterns and mechanisms reveals some problems which should be acknowledged and some possibilities for future study. During maximum burial and uplift, flow is postulated as originating in the mountains as meteoric water seeping across thrust zones via vertical fractures or porous units. However, the dominant flow direction expected in the thrust zone is to the west, parallel to the thrust planes. Whether a significant eastward flow in the Falher and Cadotte Members could be produced by water cutting across the thrust planes, via vertical fractures or permeable units, remains to be determined. Alternatively, an easier pathway for the influx of meteoric water may have been presented by upturned permeable Falher and Cadotte beds in the disturbed zone. Only combined detailed structural and hydrogeological analysis of the thrust and disturbed zones could resolve this flow problem.

The extent of flushing by evolved meteoric water has not been established. Fluid inclusions in quartz druse from one Cadomin sample indicate precipitation from fresh water, whereas fluid inclusions in calcite cement from one Bluesky sample indicate salinities of 65000 mg/l. All fluid inclusions from Falher and Cadotte samples indicate salinities of 20000-30000 ppm. These data suggest that flushing of Cretaceous units by meteoric water occurred along complicated flow paths, probably limited to the most permeable zones. Analyses of fluid inclusion salinities from quartz druse and calcite cements on a regional scale, particularly in the Cadomin and Bluesky Formations, would help evaluate the extent of flushing by evolved meteoric water.

Study of modern fluid flow patterns and the extent of cross-formational flow within the water-saturated zone of the Deep Basin is severely limited by the scarcity of reliable chemical and

potentiometric data. In addition, analyses of diagenetic minerals in this study was concentrated in the gas-saturated zone, thereby revealing little information about late diagenesis and fluid chemistry after gas saturation. The increase in salinities southwestward towards the gas-water interface suggests a southwestward flow direction. Such a flow direction is neither supported nor contradicted by the available potentiometric data. More regional studies (J. Thompson, pers. comm.) suggest a southeastward flow direction across the study area. A study of late diagenetic cements in the water-saturated zone could significantly contribute to our understanding of recent hydrogeological processes.

### CONTROLS ON DIAGENETIC PROCESSES

Comparison of diagenetic sequences and porewater evolution in each of the units studied suggests that in the Upper and Lower Cretaceous sediments, the major diagenetic processes are independent of actual position in the vertical section. The general diagenetic sequence is the same in each of the formations examined even though burial depths, geographic position and original depositional environment varied. The essential similarity, though, is the original detrital mineralogy. In all units the detrital mineralogy is composed dominantly of quartz and chert. As burial increased, the following diagenetic minerals precipitated: early siderite or chlorite, kaolinite, quartz overgrowths, illite and albite. Either at maximum burial or during uplift as the meteoric water influx increased, calcite and/or ankerite were precipitated. In the coarsest sandstones and conglomerates, dickite precipitated from the evolved meteoric water. The general pattern of porewater evolution is similar for all the Upper and Lower Cretaceous units examined.

The mechanisms which control diagenetic reactions are still not well understood, although many studies have suggested that the smectite/illite transition and organic reactions in shales play an important role. Land (1984) suggested that deeper shales that have undergone the smectite/illite transition at  $\sim 100^{\circ}\text{C}$  are the source of  $\text{SiO}_2$  and  $\text{CaCO}_3$  for quartz and calcite

cements in the Frio Formation in the Gulf Coast Basin. This theory is based on evidence for precipitation of quartz at  $\sim 60^\circ\text{C}$  and calcite at  $\sim 80^\circ\text{C}$  from porewaters with  $\delta^{18}\text{O}$  values of +4 to +5 ‰. Porewaters equilibrated with shales at the temperature at which significant organic reactions and the smectite/illite transition take place ( $\sim 100^\circ\text{C}$ ) should have  $\delta^{18}\text{O}$  values of  $\sim -5$  ‰ (Suchecki and Land, 1983). Since diagenetic cements in the Frio Formation formed from waters with this isotopic composition, but at lower temperatures, Land (1984) concluded that calcite- and quartz-saturated porewaters were expelled from shales and moved updip in sandstones to lower temperature zones before precipitation occurred. In contrast, in the Wilcox Formation which underlies the Frio Formation, Fisher and Land (1986) noted that diagenetic quartz, kaolinite and calcite formed at similarly low temperatures but from porewaters with  $\delta^{18}\text{O}$  values of  $\sim -3$  to +2 ‰. They concluded that these relatively early diagenetic cements that formed from low  $\delta^{18}\text{O}$  porewaters were not related to organic maturation and S/I reactions.

In the Belly River Formation of the Western Canadian Basin (central and south-central Alberta), Ayalon and Longstaffe (in press) found that quartz overgrowths formed at maximum burial and during uplift at temperatures of  $100^\circ\text{-}120^\circ\text{C}$ . Their data show that an influx of meteoric water played an important role in late-stage diagenesis (from the time of maximum burial to the present) and was involved in the precipitation of quartz, kaolinite, calcite, illite and illite/smectite. Because the temperature of quartz precipitation corresponds with that for organic maturation reactions and the S/I transition, they concluded that meteoric water was responsible for transporting material, produced from those reactions in shales, to sandstones where they were precipitated. Mixing of shale porewaters with meteoric water produced  $\delta^{18}\text{O}$  values of porewaters which are characteristic of isotopically-evolved meteoric water.

In the Alberta Deep Basin (this study) an influx of meteoric water also controlled the late stages of diagenesis (from the time of maximum burial to the time that pores became saturated by methane gas). Evolved meteoric water was involved in the precipitation of quartz druse, dickite,

calcite and ankerite in conglomerates, and calcite, ankerite and local quartz overgrowths in sandstones. In contrast to the situation in the Gulf Coast Basin, where most of the diagenetic reactions were completed relatively early during burial, the late stages of diagenesis in the Alberta Deep Basin are the most significant in terms of porosity modification. As proposed by Ayalon and Longstaffe (in press), meteoric water is the transport mechanism for constituents of diagenetic cements formed during late-stage diagenesis. In at least the Falher Member in the Alberta Deep Basin, pressure solution of chert pebbles is common in the westernmost part of the study area. The products of this pressure solution, transported by evolved meteoric water, are probably the major source of  $\text{SiO}_2$  for quartz druse in conglomerates of the Alberta Deep Basin.

Evidence for precipitation of quartz overgrowths, kaolinite and illite, and the albitization or dissolution of feldspars during burial of Cretaceous sandstones in the Alberta Deep Basin, suggests that diagenesis during burial might have been controlled by processes similar to those in the Gulf Coast Basin. For example, the first generation of quartz overgrowths in the Paddy Member precipitated at  $50^\circ\text{-}90^\circ\text{C}$  and quartz overgrowths in the Cardium Formation probably formed at  $70^\circ\text{-}90^\circ\text{C}$ . In the Bluesky Formation, quartz precipitated at slightly higher temperatures ( $95^\circ\text{-}115^\circ\text{C}$ ). The problem is that porewaters which were responsible for precipitation of the diagenetic minerals in the Deep Basin varied from  $-5$  to  $+1$  ‰, a range similar to that of the Wilcox Formation (Fisher and Land, 1986) but significantly lower than that of the Frio Formation (Milliken et al., 1981; Land, 1984). These low  $\delta^{18}\text{O}$  values suggest that waters derived from the S/l transition in shales may not be the dominant source of water in the Alberta Deep Basin, even during burial. However, organic maturation reactions probably are important in controlling carbonate dissolution and precipitation. Although intermediate stages of calcite cement are absent, evidence for dissolution of carbonate cements (early siderite in particular) before maximum burial suggests that precipitation and dissolution reactions similar to those described by Land (1984) may have taken place.

## MAJOR CONCLUSIONS

1. An influx of meteoric water, which began when burial and relief were at a maximum (Laramide Orogeny), had a major influence on late-stage diagenesis in Cretaceous sandstones and conglomerates. Quartz druse, dickite, ankerite and calcite were precipitated in the Alberta Deep Basin from porewater containing a significant fraction of meteoric water. The style of diagenesis during burial in the Alberta Deep Basin is comparable to that of the Gulf Coast Basin. However, because of the influx of meteoric water, late-stages of diagenesis in the Alberta Deep Basin are the most significant in terms of porosity modification. In contrast, most diagenetic reactions in the Gulf Coast Basin are completed relatively early at temperatures  $<120^{\circ}\text{C}$ . Meteoric water obviously provides a mechanism for renewed transport of ions after compaction and diagenetic waters are exhausted.

2. A thermal anomaly was created in the Falher and Cadotte Members by the influx of hot, methane-saturated, meteoric water which followed a permeable pathway updip from the west. These fluids ( $190^{\circ}\text{C}$ ) were up to  $40^{\circ}\text{C}$  higher than the maximum burial temperatures calculated from vitrinite reflectance data using the method of Lopatin (1971) modified by Waples (1980). The discrepancy between the two types of temperatures can be explained in one of two ways: (1) fluids in conglomerates were at temperatures  $40^{\circ}\text{C}$  higher than ambient rock temperatures; or (2) the correlation of coal maturity with maximum burial temperatures in the Deep Basin is inaccurate. Each explanation is equally plausible. In the first case, where the calculated burial temperatures represent the ambient rock temperature, a thermal anomaly on a limited vertical scale was present. Hot fluids moved through these rocks at a rate fast enough such that their heat was not dissipated along the pathway. A relatively short duration of flow or its confinement to porous rocks is implied by the lack of effect on coal maturity. In the second case, geothermal gradients of  $\sim 38^{\circ}\text{C}/\text{km}$  (versus  $27^{\circ}\text{C}/\text{km}$ ) are indicated and a thermal anomaly on an extensive

Vertical scale was present. A temperature for recalibration of the TTI-Ro% index (Waples, 1980) specific to the Deep Basin is available (1.4 Ro% correlates to 190°C)

3. Methane, generated by maturation of coals, was carried updip by eastward flowing meteoric water. Eventually methane accumulated and formed a continuous gas phase which drove any moveable water eastwards. The gas phase formed a barrier to eastward flow of meteoric water which was being recharged in the mountains to the west, and forced the redirection of flow to the south and north around the gas barrier. Directly to the east of the gas barrier, mixing occurred between meteoric water which had flushed the permeable units and connate water which was preserved in the low permeability units. This mixing resulted in waters with a uniform salinity. Recent flushing by meteoric water from the north has created the present trend in decreasing salinities towards the east from the gas-water interface.

## REFERENCES

- Ayalon, A., and Longstaffe, F.J., in press, Oxygen-isotope studies of diagenesis and porewater evolution in the western Canada sedimentary basin: evidence from the Upper Cretaceous basal Belly River sandstone: *Journal of Sedimentary Petrology*.
- Domenico, P.A., and Robbins, G.A., 1985, The displacement of connate water from aquifers: *Geological Society of America Bulletin*, v.96, p. 328-335.
- Fisher, R.S. and Land, L.S., 1986, Diagenetic history of Eocene Wilcox sandstones, South-Central Texas: *Geochimica et Cosmochimica Acta*, v.50, p. 551-561.
- Galloway, W.E., 1984, Hydrogeologic regimes of sandstone diagenesis: in R. Surdam and D. MacDonald, eds., *Clastic Diagenesis: American Association of Petroleum Geologists, Memoir 37*, p. 3-13.
- Hitchon, B., 1964, Formation fluids: in R.G. McCrossan and R.P. Glaister, eds., *Geological History of Western Canada: Alberta Society of Petroleum Geologists, Calgary, Alberta*, p. 201-217.
- Hitchon, B., 1969, Fluid flow in the western Canada sedimentary basin. 1. Effect of topography: *Water Resources Research*, v.5, p. 186-195.
- Hitchon, B., 1984, Geothermal gradients, hydrodynamics, and hydrocarbon occurrences, Alberta, Canada: *The American Association of Petroleum Geologists Bulletin*, v.68, p. 713-743.
- Land, L.S., 1984, Frio sandstone diagenesis, Texas Gulf Coast: a regional isotopic study: in R. Surdam and D. MacDonald, eds., *Clastic Diagenesis: American Association of Petroleum Geologists, Memoir 37*, p. 47-62.
- Lopatin, N.V., 1971, Temperature and geologic time as factors in coalification (in Russian): *Akademiya Nauk SSSR Izvestiya, Seriya Geologicheskaya*, no. 3, p. 95-106.
- Milliken, K.L., Land, L.S. and Loucks, R.G., 1981, History of burial diagenesis determined from isotopic geochemistry, Frio Formation, Brazoria County, Texas: *The American Association of Petroleum Geologists Bulletin*, v.65, p. 1397-1413.
- Nesbitt, H.W., 1985, A chemical equilibrium model for the Illinois Basin formation waters: *American Journal of Science*, v.285, p. 436-458.
- Schwartz, F.W., Muehlenbachs, K., and Chorley, D.W., 1982, Flow system controls on the chemical evolution of groundwater: in W. Back and R. Letolle, eds., *Developments in Water Science: Symposium on Geochemistry of Groundwater: New York, Elsevier*, p. 225-243.
- Suchecki, R.K. and Land, L.S., 1983, Isotopic geochemistry of burial-metamorphosed volcanogenic sediments, Great Valley sequence, northern California: *Geochimica et Cosmochimica Acta*, v.47, p. 1487-1499.
- Tóth, J., 1980, Cross-formational gravity-flow of groundwater: A mechanism of the transport and accumulation of petroleum (the generalized hydraulic theory of petroleum migration): *AAPG Studies in Geology No. 10*, p. 121-167.
- Waples, D., 1980, Time and temperature in petroleum formation: Application of Lopatin's method to petroleum exploration: *The American Association of Petroleum Geologists Bulletin*, v.64, p. 916-926.

Weiss, H.M., 1985, Geochemische und petrographische Untersuchungen am organischen Material kretazischer Sedimentgesteine aus dem Deep Basin, Westkanada: Obergunzburg, PhD thesis (in German), 261 p.